FUNCTIONAL ANALYSIS OF *DROSOPHILA* KEKKON RECEPTORS AT THE NEUROMUSCULAR JUNCTION OF *DROSOPHILA*

by

JACOB HASENAUER

A thesis submitted to the University of Birmingham for the degree of

DOCTOR OF PHILOSOPHY

School of Biosciences

College of Life and Environmental Sciences

University of Birmingham

July 2023

UNIVERSITY OF
BIRMINGHAM

University of Birmingham Research Archive

e-theses repository

This unpublished thesis/dissertation is copyright of the author and/or third parties. The intellectual property rights of the author or third parties in respect of this work are as defined by The Copyright Designs and Patents Act 1988 or as modified by any successor legislation.

Any use made of information contained in this thesis/dissertation must be in accordance with that legislation and must be properly acknowledged. Further distribution or reproduction in any format is prohibited without the permission of the copyright holder.

ABSTRACT

Neurotrophin ligands signalling via Trk receptors are key regulators of activity-dependent structural plasticity and neuronal function in vertebrates. In *Drosophila*, conserved neurotrophins (DNTs) are encoded by the *spaetzle* genes. The six Kekkon receptors (Keks) are the fly homologs of the Trk family. DNT signalling can also be mediated by Toll receptors. *kek6* can regulate synaptic plasticity in Drosophila by increasing Ca^{2+} levels and activating CaMKII. However, it was unknown if the other five Keks function similarly. Here, I investigated the Keks by asking: where are they expressed in the nervous system? Can they all regulate calcium? And what their impact is in activity-dependent structural plasticity?

Using RT-PCR I showed that all *keks* were expressed in the central nervous system (CNS), with only *kek1* and *kek5* being expressed in the periphery. I visualised the distribution of overexpressed Kek-RFP protein fusions and endogenous CRISPR/Cas9 knock-ins showing that Keks had overlapping subcellular localisations, with Kek2 being dendritic, Kek5 and -6 being presynaptic, and Kek3 and -4 localising throughout the neuron. Using Western blot I demonstrated that *kek* overexpression altered the abundance of CaMKII, with *kek3* differentially regulating alternate CaMKII isoforms. Using live Ca^{2+} imaging, I demonstrated that overexpression of all *keks*, except *kek5*, sustained Ca^{2+} levels following stimulation, with *kek2* and *-4* also lowering the amplitude of Ca^{2+} influx. Focusing on *kek4* and *6*, I show with endogenously tagged protein fusions that Kek6 colocalised with the voltage-gated Ca^{2+} channel Cacophony, and that *kek4* and *6* overexpression led to the clustering of Cacophony channels. Using optogenetics to induce activity-dependent plasticity, I demonstrated that *kek4* and *6* were required for the activity-dependent synaptic growth following activity, with immunofluorescent stainings of synaptic markers Bruchpilot (Brp) and Discs-large (Dlg) at neuromuscular junction (NMJ) 6/7.

Altogether, these data have revealed that Keks have distinct but overlapping spatial distributions and functional properties in the nervous system. *kek4* and *-6* can alter Cacophony distribution and may physically associate with active zones, indicating that Keks may act via conserved Ca^{2+}-dependent pathways to regulate activity-dependent synaptic plasticity. This work highlights the Kek receptor family as an emerging class of regulators of synaptic plasticity and neuronal function in *Drosophila*.

For my fiancée Georgi and for our cats, friends and family for the love, encouragement, support, and inspiration through the challenges of the last few years, who have made this journey possible.

ACKNOWLEDGEMENTS

I would like to thank my supervisor Alicia Hidalgo for her guidance and support throughout this project, without whom it would not have been possible. I would also like to thank the other members of the Hidalgo Lab and the 6th floor, past and present, for their friendship, advice and support throughout the years, Suzana Ulian-Benitez, Elizabeth Connolly, Guiyi Li, Marta Moreira, Maria-Dolores Sanchez-Perez, Jun Sun, Deepanshu Singh, Naser Alshamsi and Anna Parsons. I'd also like to thank Alessandro di Maio and the Birmingham Advanced Light Microscopy facility for the training and support with confocal microscopy which was essential to the project. I'd like to also thank Laurie Cazale-Debat for her assistance and guidance in the design of the optogenetics set up implemented in Chapter 5, and Andy Loat for assisting in its engineering.

TABLE OF CONTENTS

1 Introduction 13
1.1 Overview of introductory content 13
1.2 Neurotrophin signalling in mammals 14
1.2.1 Neurotrophins 14
1.2.2 Trk signalling 20
1.2.3 Truncated Trks 22
1.3 The *Drosophila* neurotrophin system 25
1.3.1 The *spaetzle* family 26
1.3.2 Toll receptors 31
1.3.3 Kekkon receptors 34
1.4 Ca^{2+} signalling in neurons 42
1.4.1 Intracellular stores of Ca^{2+} 43
1.4.2 Entry of extracellular Ca^{2+} 43
1.4.3 CaMKII: a major effector of Ca^{2+} signalling 47
1.5 Plasticity 50
1.5.1 Experience dependent structural plasticity in mammals 51
1.5.2 Experience dependent structural plasticity in insects 53
1.6 The Model system 57
1.6.1 *Drosophila* melanogaster: an overview 57
1.6.2 The central nervous system 59
1.6.3 The neuromuscular junction 60
1.7 Aims and Objectives 68
2 Methods 70
2.1 Fly Husbandry 70
2.1.1 Preparation of fly food for Ca^{2+} imaging 70

2.1.2 Preparation of fly food for optogenetic plasticity experiments 76
2.1.3 Preparation of grape juice plates 78
2.2 Genetics 78
2.3 CNS Dissections 81
2.4 Body Wall Dissections 81
2.5 Immunostaining 82
2.6 Microscopy 83
2.7 Molecular biology 85
2.7.1 Kek-5 GAL4 cloning strategy 85
2.7.2 Kek6 T-STEP cloning strategy 87
2.7.3 Genomic DNA extraction 89
2.7.4 PCR 90
2.7.5 Colony PCR 93
2.7.6 Gel electrophoresis 93
2.7.7 Eckhardt gels 94
2.7.8 Gel purification 94
2.7.9 Spin/PCR purification 96
2.7.10 Restriction digests 97
2.7.11 Transformation 97
2.7.12 Miniprep 99
2.7.13 Midiprep 100
2.7.14 DNA ligation 101
2.7.15 Gibson cloning 101
2.7.16 gRNA cloning 103
2.7.17 RNA extraction from larval tissues 105
2.7.18 cDNA synthesis 107

2.7.19 Analysis of RT-PCR data....109
2.7.20 Western Blot....110
2.8 Calcium imaging....114
2.8.1 Dissection of larvae....114
2.8.2 Live Ca^{2+} imaging microscopy....115
2.8.3 Data analysis of bouton intensity....116
2.9 Optogenetics and Activity Experiments....117
2.9.1 Staging of larvae....117
2.9.2 Optogenetic stimulation....118
2.9.3 Data analysis of NMJ morphology....123
3 Results - Spatial distribution of the Keks....124
3.1 Introduction....124
3.2 Results....124
3.2.1 All *keks* are expressed in the larval nervous system....124
3.2.2 Generation of *kek5-GAL4* constructs....125
3.2.3 Localisation of *kek5-GAL4* driven membrane-tethered fluorescent proteins 133
3.2.4 Subcellular distribution of Keks in the larval VNC....143
3.2.5 Peripheral nervous system expression of Kek proteins....146
3.2.6 Keks localised to axonal terminals of motoneurons....158
3.2.7 Generation of *kek6-TSTEP*....161
3.2.8 Localisation of Kek6-TSTEP....171
3.3 Discussion....178
4 Results - Differential regulation of calcium signalling by Keks....179
4.1 Introduction....179
4.2 *kek*s differentially regulate CaMKII isoform abundance....180

4.3 *kek*s modulate pre-synaptic Ca^{2+} dynamics at the NMJ 183
4.3.1 Ca^{2+} dynamics *kek* overexpression larvae 188
4.4 Kek6-TSTEP colocalises with Cacophony 201
4.5 *kek4* and *kek6* enhance Cacophony channel clustering 201
4.5.1 *kek4* can modulate Cac distribution 208
4.5.2 *kek6* can modulate Cac distribution 209
4.6 Discussion 209
5 Results - Keks modulate NMJ morphology and activity-dependent structural plasticity 211
5.1 Introduction 211
5.2 The effect of *kek4* misexpression on synaptic morphology 213
5.3 *kek6* regulates mature bouton number 218
5.4 Optogenetically induced activity modifies NMJ morphology 223
5.5 *kek4* is required for activity-dependent structural plasticity 228
5.6 *kek6* is required for activity-dependent structural plasticity 242
5.7 Discussion 256
6 Discussion 257
6.1 Summary of findings 257
6.2 *kek1* 258
6.3 *kek2* 261
6.4 *kek3* 262
6.5 *kek4* 264
6.6 *kek5* 267
6.7 *kek6* 268
6.8 *keks* as regulators of synaptic plasticity 274
6.9 Limitations of experimental approach 277

6.9.1 Regulation of *keks* by activity 277
6.9.2 Overexpression of protein fusions 277
6.9.3 Kek6-TSTEP 279
6.9.4 *kek4* and Ca^{2+} signalling 280
6.9.5 Ca^{2+} imaging 282
6.9.6 Western blots for CaMKII abundance 283
6.9.7 Kek misexpression and activity-dependent structural plasticity 284
6.10 Future directions 286
7 Bibliography 290

Appendix I: Basic genetics protocols

Appendix II: Statistical information

List of abbreviations used

AMPA	amino-3-hydroxy-5-methyl-4-isoxazolepropionic acid
AMPAR	AMPA receptor
ATL	Axonal terminal length
ATP	Adenosine triphosphate
ATR	All-trans retinal
AZ	Active zone
BALM	Birmingham Advanced Light Microscopy
BDNF	Brain-derived neurotrophic factor
BMP	Bone-morphogenetic protein
Brp	Bruchpilot
BW	Body wall
Cac	Cacophony
Cac-sfGFP	Cacophony endogenously tagged with superfolder GFP
CaM	Calcium-calmodulin
CaMKII	CaM-dependent protein kinase II
cAMP	Cyclic adenosine monophosphate
Carb	Carbenicillin
ChR	Channelrhodopsin
ChR-2	Channelrhodopsin-2
CNS	Central nervous system
co-IP	Co-immunoprecipitation
CREB	cAMP response element-binding protein
CRISPR	Clustered regularly interspaced short palindromic repeats
Cys-knot	Cysteine knot
DAG	Diacylglycerol
Dlg	Discs large
DNT	Drosophila Neurotrophin
DRG	Dorsal root ganglia
EGF	Epidermal growth factor

EGFR	EGF receptor
ER	Endoplasmic reticulum
ERK	Extracellular signal-regulated kinase
FIJI	FIJI is just ImageJ
FMRP	Fragile X mental retardation protein
Gbb	Glass Bottom Boat
GDP	Guanosine diphosphate
GPCR	G-protein coupled receptor
gRNA	Guide RNA
HDR	Homology directed repair
Hiw	Highwire
HR	Homologous region
HRP	Horseradish peroxidase
iGluR	Ionotropic glutamate receptor
IntDen	Integrated Density
IP3	Inositol trisphosphate
IP3R	IP3 receptor
ISN	Intersegmental nerve
JNK	c-Jun N-terminal Kinase
Kek	Kekkon
L3	Larval third instar
LIG	LRRs and immunoglobulin
LoF	Loss of function
LRR	Leucine-rich repeat
LTD	Long-term depression
LTP	Long-term potentiation
LUT	Look-up table
MAGUK	Membrane-associated guanylate kinase
MAP2	MT associated protein 2
MAPK	Mitogen activated protein kinase
MAPKKK	Mitogen-activating protein kinase kinase kinase

MAPs	Microtubule associated proteins
MB	Mushroom body
mda	Multiple dendritic arbours
MSA	Muscle surface area
MT	Microtubule
MyD88	Myeloid differentiation primary response 88
NFκB	Nuclear factor kappa-light-chain-enhancer of activated B cells
NGF	Nerve growth factor
NGS	Normal Goat Serum
NMDA	N-methyl-d-aspartate
NMDAR	NMDA receptor
NMJ	Neuromuscular junction
NT	Neurotrophin
NT-3	Neurotrophin-3
NT-4	Neurotrophin-4
NURF-38	Nucleosome remodelling factor – 38kD
OE	Overexpression
p75NTR	p75 Neurotrophin receptor
PAK	p21-activated kinase
PBS	Phosphate Buffer Saline
PDZ	Post-synaptic density-95, discs large and zona occludens-1
PHP	Presynaptic homeostatic potentiation
PI3K	Phosphoinositide 3-kinase
PIP2	Phosphatidylinositol 4,5-bisphosphate
PKC	Protein kinase C
PLC-γ1	Phospholipase C gamma 1
PNS	Peripheral nervous system
P_r	Probability of neurotransmitter release
PSD	Post-synaptic density
RBP	RIM-binding protein
ReaChR	Red activated channelrhodopsin

RFP	Red fluorescent protein
RhoGDPI1	Rho GDP Dissociation inhibitor 1
RNAi	RNA interference
ROCK	Rho-associated kinase
ROI	Region of Interest
ROS	Reactive Oxygen Species
RT-PCR	Reverse-transcriptase polymerase chain reaction
RyR	Ryanodine receptor
Shc	Src homology and Collagen
SN	Segmental nerve
SPE	Spz processing enzyme
Spz	Spätzle
SR	Sarcoplasmic reticulum
SV	Synaptic Vesicle
TIR	Toll/Interleukin-1 Receptor
TLR	Toll-like receptor
TN	Transverse nerve
Trk	Tropomyosin receptor kinase
TrkB-FL	Full length TrkB
TRP	Transient receptor potential
TRPV1	Transient receptor potential vanilloid 1
TSTEP	Tissue specific tagging of endogenous proteins
TyrK	Tyrosine kinase
VGCC	Voltage-gated Ca2+ channel
VNC	Ventral nerve cord
Wek	Weckle
Wnd	Wallenda

1 INTRODUCTION

1.1 Overview of introductory content

Alterations to the structure and function of synapses, synaptic plasticity, is a widely conserved process in animals (Abrraham et al., 2019). This conservation is indicative of the importance of synaptic plasticity in the function of nervous systems, and has been theorised to underlie learning and memory (Nicoll 2017).

Many forms of plasticity are dependent on the influx of Ca^{2+} ions into the cytoplasm, indeed Calcium-calmodulin (CaM)-dependent protein kinase II (CaMKII) has been known for decades as a vital mediator of synaptic plasticity (Lisman et al., 2002). Ca^{2+} signalling is important, as it connects neuronal activity to structural and functional changes at the synapse (Lisman et al., 2002).

In mammals, neurotrophins and their receptors are known to be key mediators of synaptic plasticity (Kowiański et al., 2018). Much of this research has investigated the neurotrophin Brain-derived neurotrophic factor (BDNF) and its receptor Tropomyosin receptor kinase (Trk) B (TrkB) (Kowiański et al., 2018). The disruption of BDNF/TrkB signalling may underlie several psychiatric and neurodegenerative diseases, and they are drug targets for the treatment of some of these diseases, such as depression and schizophrenia (Saarlainen et al., 2003, Gideons et al., 2017, Autry and Monteggia 2012, Ma et al., 2017).

Previously, neurotrophins were found to exist in *Drosophila* fruit flies (Zhu et al., 2008). *Drosophila melanogaster* is an excellent model organism for neuroscience, as they have small but complex brains, powerful genetics and over 100 years of history as a tool for fundamental research (Bellen et al., 2010). Additionally, *Drosophila* has a

genome with ~60% homology with humans (Ugur et al., 2016, Mirzoyan et al., 2019). Furthermore, ~75% of all genes known to cause disease in humans have been found to have homologs in flies (Ugur et al., 2016, Mirzoyan et al., 2019).

Drosophila neurotrophins (DNTs) were found to be structural and functional homologs of those found in vertebrates (Zhu et al., 2008). A conserved form of Trk receptors also exist in flies: the Kek receptor family (MacLaren et al., 2004). Fascinatingly, Keks lack the tyrosine kinase (TyrK) domain found in full-length vertebrate Trks that has been thought to mediate signalling via phosphorylation of downstream targets (MacLaren et al., 2004, Huang and Reichardt 2006). Truncated Trks that lack this TyrK are expressed in mammalian brains and have functions distinct from their full-length counterparts (Yacoubian and Lo 2000). It is curious that the conserved form of these receptors between flies and mammals lack this apparently critical kinase domain. The functions of the six members of the Kek receptor family are not well understood, but may offer great insight into nervous system function, including synaptic plasticity.

1.2 Neurotrophin signalling in mammals

1.2.1 Neurotrophins

Neurotrophic factors or Neurotrophins (NTs) are a conserved family of neuronal growth factors (Zhu et al., 2008). NTs are secreted protein ligands that mediate the regulation of neuronal survival, proliferation, structural plasticity, and axon guidance in target cells (Reichardt 2006, Shimazu et al., 2006). The mammalian NT family consists of Nerve Growth Factor (NGF), Brain Derived Neurotrophic Factor (BDNF), Neurotrophin-3 (NT-3) and Neurotrophin-4 (NT-4) (Cohen and Levi-Montalcini 1956, Barde et al., 1978, Maisonpierre et al., 1990, Ip et al., 1992).

The canonical receptors for the vertebrate NTs are the Trk receptor family (Huang and Reichardt 2003). There are three members of the Trk receptor family in mammals: TrkA, TrkB and TrkC (Huang and Reichardt 2003). Full-length Trks display preferential binding to different NTs, with TrkA binding NGF, TrkB with BDNF and NT-4, and TrkC to NT-3 (Huang and Reichardt 2003). Additionally, all three Trks are weakly activated by NT-3, and all NTs can weakly bind p75 neurotrophin receptor (p75NTR) (Huang and Reichardt, 2003, Skaper et al., 2012) (Fig. 1.1 A).

Of all the neurotrophins BDNF is especially relevant to the study of plasticity and synapse development (Kowiański et al., 2018, Leal et al., 2017). BDNF plays a critical role in multiple forms of plasticity in vertebrates (Lu 2003, Park and Poo 2013, Kowiański et al., 2018). BDNF was the second neurotrophin to be discovered, is highly conserved across vertebrate species and is widely expressed in the brain (Barde et al., 1978, Barde et al., 1982, Yeh et al., 2015, Hofer et al., 1990, Yan et al., 1997).

BDNF/TrkB signalling is known to promote growth and maintenance of synapses in both instructive and permissive roles depending on the context (Rutherford et al., 1998, Lin et al., 2018). Conversely, BDNF/p75NTR signalling is antagonistic to BDNF/TrkB signalling (Lee et al., 2001).

BDNF and TrkB are widely expressed in the brain and signalling via the ligand/receptor pair is required in a critical period in mammalian brain development (Hofer et al., 1990, Yan et al., 1997, Luikart et al., 2005). BDNF/TrkB signalling is required on both sides of the synapse for the proper development of each sides synaptic specialization (Luikart et al., 2005, Lin et al., 2018).

BDNF/TrkB signalling pathways are targeted in the treatment of psychiatric diseases (Saarlainen et al., 2003, Gideons et al., 2017, Autry and Monteggia 2012). Anti-

Figure 1.1 - Neurotrophins in Mammals and *Drosophila*

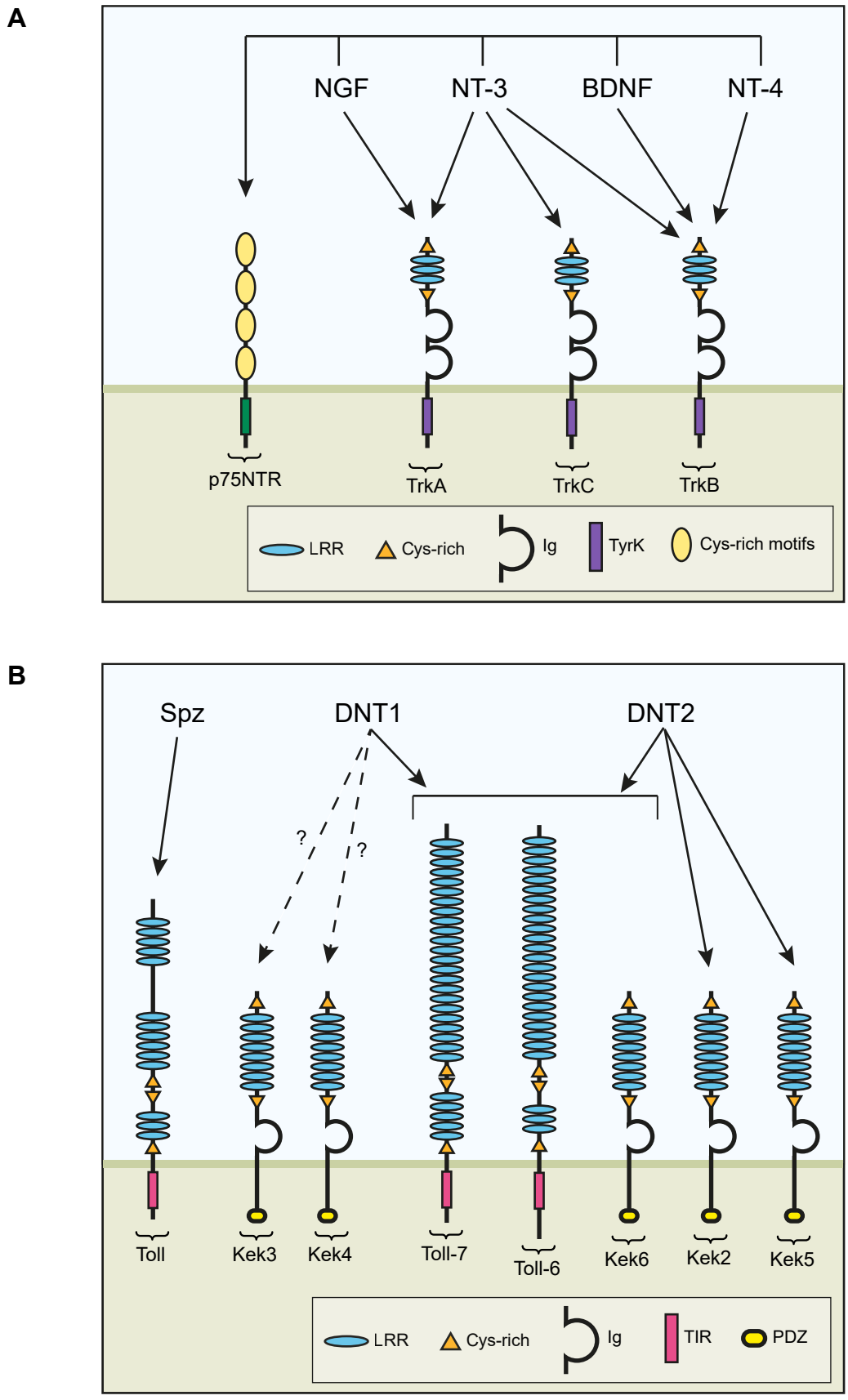


Figure 1.1 – Neurotrophins in Mammals and *Drosophila*

Schematic of mammalian and *Drosophila* neurotrophins and their receptors. **A**: In mammals, all NTs can bind to p75NTR, NGF binds to TrkA, BDNF and NT-4 to TrkB, and NT-3 binding to each Trk, with a preference for TrkC (Huang and Reichardt, 2003, Skaper et al., 2012). **B:** In Drosophila, DNT signalling is mediated by Keks and Tolls. Spz binds to Toll. DNT1 and DNT2 can promiscuously mediate signalling via Toll-6, Toll-7 and Kek6 (McIlroy et al., 2013, Ulian-Benitez et al., 2017). Kek2 and -5 can bind DNT2 in co-IP assays (Ulian-Benitez et al., 2017), and *kek3* and *-4* genetically interact with *DNT1* (Bishop, 2014). (Adapted from Anthoney et al., 2018, MacLaren et., al 2004, Skaper 2012) Key: LRR – Leucine-rich repeat, Cys-rich – Cysteine-rich domain, Ig – Immunoglobulin domain, TIR – TIR domain, TyrK – Tyrosine Kinase domain, PDZ – PDZ domain binding motif, Cys-rich motif – Cysteine-rich motif.

depressants and mood regulators such as ketamine and lithium increase BDNF levels (Fukumoto et al., 2001, Autry et al., 2011). In mouse models, it has been shown that the anti-depressant effect of ketamine and the anti-mania effect of lithium require BDNF/TrkB signalling (Ma et al., 2017, Saarlainen et al., 2003, Gideons et al., 2017).

In humans the *BDNF* gene encodes 11 isoforms which vary based on the inclusion or exclusion of untranslated regions in the mRNA transcript (Pruunsild et al., 2007). When translated all isoforms produce identical proteins (Timmusk et al., 1993, Liu et al., 2005, Aid et al., 2007, Pruunsild et al., 2007). The variation of *BDNF* isoforms may underpin a complex expression profile (Timmusk et al., 1993, Liu et al., 2005, Aid et al., 2007, Pruunsild et al., 2007), for example mice lacking an isoform of *BDNF* with the long-form 3'UTR have reduced dendritic growth in hippocampal neurons (An et al., 2008).

Structurally, NTs consist of a signal peptide, a pro-domain and a highly conserved cystine-knot domain (Lu et al., 2005, Schweigreiter 2006). The cystine-knot domain, on the C-terminal end of the protein is enriched with cysteine residues and plays a significant role in signalling and dimerization of the NTs (Schweigreiter 2006). The pro-domain is thought to be necessary for the correct folding of the cystine-knot and trafficking through vesicles, and thereby which pathway the NT is secreted by and further downstream signalling (Rattenholl et al., 2001, Lu et al., 2005, Schweigreiter 2006). The signal peptide at the N-terminal end of the protein instructs the intracellular transport machinery to secrete the NT (Schweigreiter 2006).

NTs may be secreted constitutively or in an alternate, activity-dependent manner (Lu et al., 2005). The secretory pathway that a NT travels through is dependent on the furin endoprotease cleavage of the pro-domain (Lu et al., 2005). In mouse

hippocampal neurons pro-NGF is cleaved readily by furins in the trans-Golgi network and is secreted constitutively. In contrast pro-BDNF is cleaved inefficiently by furin proteases and is consequently secreted via an activity-dependent pathway. (Lu et al., 2005).

Upon cleavage, the cysteine knot (cys-knot) domain is then able to form homodimers (Schweigreiter 2006) and are considered to be the mature form of a NT and has distinct signalling properties from the immature pro-form (Lu et al., 2005, Schweigreiter 2006). NTs can induce signalling in either the immature pro-NT form or in the mature cys-knot dimer form (Lu et al., 2005). Pro-NTs induce cell death by binding Sortilin and p75NTR receptors and signalling via the c-Jun N-terminal Kinase (JNK) pathway (Roux and Barker 2002). Mature NTs induce cell survival by binding to p75NTR and Trk receptors and signalling via the Nuclear factor kappa-light-chain-enhancer of activated B cells (NFκB) and Extracellular signal-regulated kinase (ERK) pathways, respectively (Lu et al., 2005, Huang and Reichardt 2003).

BDNF binds to TrkB receptors with high affinity, and to p75NTR receptors with low affinity (Dechant et al., 1993, Rodriguez-Tebar 1990). Although BDNF is a secreted protein it diffuses poorly and activates TrkB signalling local to the release site (Park and Poo 2013, Horch and Katz 2002). BDNF is synthesized in a pre-pro-form and the signal peptide is cleaved in the Golgi apparatus to produce the pro form of the neurotrophin (Rosenthal et al., 1991, Mowla et al., 2001).

When and where pro-BDNF is cleaved to produce mature BDNF is thought to be instructive to downstream signalling (Mowla et al., 2001, Lee et al., 2001, Matsumoto et al., 2008). BDNF can be cleaved intracellularly, whereupon it follows an activity-dependent release pathway (Mowla et al., 2001). Pro-BDNF can also be cleaved

extracellularly in a process that is thought to primarily activate p75NTR signalling (Lee et al., 2001).

1.2.2 Trk signalling

In vertebrates the canonical signalling pathway for neurotrophins is via Trk receptors. Trk signalling is implicated in cell proliferation and survival, growth and remodelling of neurites, assembly and remodelling of the cytoskeleton, synapse formation and plasticity (Huang and Reichardt 2003). Transport of Trks to the synaptic membrane is activity-dependent (Huang and Reichardt 2003). In cell culture Trks have been observed to be stored within intracellular vesicles which fuse with the synaptic membrane upon depolarisation and induction of calcium and cyclic adenosine monophosphate (cAMP) signalling (Huang and Reichardt 2003).

Upon ligand binding Trks dimerise and are then endocytosed (Huang and Reichardt 2003). Internalisation of Trk receptors is dependent on the function of the intracellular TyrK domain. Upon dimerization, conserved tyrosine residues in the intracellular portion of the Trk receptor are autophosphorylated and become the binding sites of scaffold and adaptor proteins. Signal transduction occurs while the Trk/ligand complex is in early endosomes and continues until the complex is ubiquitinated, marking the endosome for degradation (Huang and Reichardt 2003).

The downstream effectors of Trk signalling are the Ras-Mitogen activated protein kinase (MAPK)/ERK, Phospholipase C gamma 1 (PLC-γ1) and Phosphoinositide 3-kinase (PI3K) pathways (Huang and Reichardt 2003). These pathways are initiated in a phosphorylation cascade following the phosphorylation of Trk adaptor proteins, such as Src homology and Collagen (Shc). In this way Ras is activated and activates

multiple signalling pathways including MAPK pathways that lead to transient ERK signalling (Huang and Reichardt 2003).

The active kinase domain of Trks is able to activate PLC-γ1. Trk-dependent activation of PLC has been proposed as a mechanism for neurotrophin-induced depolarisation of the cell membrane (Matsumoto et al., 2001). Application of NGF potentiates the TRPV1 channel to become more active, this is dependent on PLC-γ (Jordt, 2007). TrkA forms a complex with the cation channel Transient receptor potential vanilloid 1 (TRPV1) and PLC-γ and activates TRPV1 in a PLC-γ-dependent manner (Jordt 2007).

Activated PLC-γ also promotes the conversion of Phosphatidylinositol 4,5-bisphosphate (PIP2) into diacylglycerol (DAG) and Inositol trisphosphate (IP_3) (Huang and Reichardt 2003). IP_3 subsequently initiates the release of Ca2+ from intracellular stores, thus activating Ca2+ signalling pathways.

TrkB may have a third, non-canonical function, independent of its tyrosine kinase ability in the rapid depolarization of the neuron (Kafitz et al., 1999, Blum et al., 2002). Application of low concentrations of BDNF or NT-4 is sufficient to depolarise the neuronal cell membrane in milliseconds, a timescale comparable to glutamate (Kafitz et al., 1999). This rapid response is reversibly blocked by the application of a TrkB inhibitor, indicating that TrkB signalling is capable of rapidly opening cation channels (Kafitz et al., 1999). $Na_v1.9$, a voltage-gated Na+ channel was identified as mediating the rapid influx of Na^+ after BDNF application (Blum et al., 2002). Due to speed of the response, it is possible that TrkB may form a complex with $Na_v1.9$ (Blum et al., 2002).

This process may be independent of TrkB's tyrosine kinase activity as at the neurotrophin concentrations sufficient to induce depolarisation the effects of kinase activity are too slow, occurring on the scale of minutes (Kafitz et al., 1999). It has been

proposed that TrkB forms a complex with cation channels and the conformation change in TrkB upon ligand binding causes the opening of the adjacent channel (Blum et al., 2002).

1.2.3 Truncated Trks

Truncated Trk isoforms appear to be the conserved form of neurotrophin receptor between mammals and flies (MacLaren et al., 2004, Mandai et al., 2009, Ulian-Benitez et al., 2017). Splicing of Trk receptor mRNA can produce truncated Trks that lack the characteristic kinase domain (Klein et al., 1990, Barbacid 1994, Shelton et al., 1995, Stoilov et al., 2002). Truncated Trks have been demonstrated to act as as dominant-negative regulators of full-length Trk function (Eide et al., 1996, Palko et al., 1999) and to signal independently and downstream of NTs via non-canonical pathways (Yacobian and Lo 2000, Holt et al., 2019, Rose et al., 2003, Dorsey et al., 2006, Matyas et al., 2017).

Overexpression of a truncated isoform of TrkC, TrkC-T1, was found to result in the loss of neurons in the mouse hippocampus, a phenotype that resembles NT-3 loss-of-function mutants (Palko et al., 1999). This indicated that TrkC-T1 behaves as a dominant-negative form of TrkC.

As a truncated isoform of TrkB, TrkB-T1 bears 100% homology to the full length TrkB (TrkB-FL) isoform in the extracellular domain, however TrkB-T1 lacks the cytoplasmic binding sites for adaptor protein Shc, PLC-γ1 and crucially the kinase domain, thereby making TrkB-T1 kinase-dead (Klein et al., 1990). Nonetheless, TrkB-T1 is expressed abundantly in the mammalian central nervous system and has been found to be capable of regulating the abundance of extracellular BDNF (Alderson et al., 2000),

inducing cytoskeletal changes in neurons and glia (Yacobian and Lo 2000, Holt et al., 2019) and activating intracellular signalling pathways, all of which independently of TrkB-FL (Rose et al., 2003, Cheng et al., 2007, Ohira et al., 2006).

Protein kinase C (PKC) has been found to be activated upon the application of BDNF to cortical neural stem cells in a G-protein and TrkB-T1 dependent manner (Cheng et al., 2007). This pathway promotes differentiation into astrocytes (Cheng et al., 2007). This indicates that TrkB-T1 can facilitate BDNF signalling by recruiting G-proteins that can activate downstream messengers such as PKC (Cheng et al., 2007).

Rho Guanosine diphosphate (GDP) dissociation inhibitor (RhoGDPI1) is a RhoGTPase inhibitor that binds to the intracellular tail of TrkB-T1 (Ohira et al., 2006). Upon BDNF binding, TrkB-T1 releases RhoGDPI1, due to a conformation change (Ohira et al., 2006). RhoGDPI1 is then free to inhibit Rho GTPases, supressing the activity of downstream signalling molecules including ERK, p21-activated kinase (PAK) and Rho-associated kinase (ROCK) (Ohira et al., 2006). These pathways are responsible for remodelling of the actin cytoskeleton (Ohira et al., 2006). Rho GTPases are implicated in structural synaptic plasticity as regulators of the actin cytoskeleton and are required for dendritic spine development and formation (Ohira et al., 2006).

Additionally, TrkB-T1 is capable of altering neurite and filopodia outgrowth independently of BDNF (Yacobian and Lo 2000, Holt et al., 2019). These cytoskeletal alterations have been observed in astrocytes and neurons (Yacobian and Lo 2000, Holt et al., 2019).

TrkB-T1 and TrkB-FL, differentially regulate dendritic outgrowth in cortical neurons (Yacobian and Lo 2000). Overexpression of TrkB-FL leads to the outgrowth of

dendrites proximal to the cell body, conversely TrkB-T1 overexpression leads to the outgrowth of dendrites distal to the cell body (Yacobian and Lo 2000). Interestingly these two effects are mutually exclusive, as TrkB-T1 dendritic outgrowth is inhibited by BDNF/TrkB-FL signalling (Yacobian and Lo 2000). These phenotypes are also reflected in mice lacking TrkB-T1, whose dendritic arbours lack length and complexity at distances far from the cell body (>90 μm) (Yacobian and Lo 2000).

TrkB-T1 is the only TrkB isoform expressed in astrocytes, making them a good model for dissecting potential signalling pathways that are independent of TrkB-FL (Rose et al., 2003, Dorsey et al., 2006, Matyas et al., 2017). TrkB-T1/BDNF signalling is necessary for astrocyte morphological development, as when it is knocked-out astrocytes remain in an immature state with lower volume and projection complexity (Holt et al., 2019). This further supports the idea that TrkB-T1 signalling can regulate cytoskeletal remodelling.

PLC-γ-dependent Ca^{2+} currents can be elicited by applying BDNF to astrocytes (Rose et al., 2003). These Ca^{2+} currents persist in mutants that lack TrkB-T1 but are significantly reduced when TrkB-T1 is knocked-down with RNA interference (RNAi) (Rose et al., 2003). This indicates that BDNF/TrkB-T1 can activate PLC-γ, despite the apparent lack of a binding site, which in turn triggers the release of Ca^{2+} from intracellular stores via IP_3 receptors (IP_3Rs) (Klein et al., 1990, Rose et al., 2003).

In astrocytes, TrkB-T1 can sequester extracellular BDNF levels by binding BDNF and becoming endocytosed (Alderson et al., 2000). The TrkB-T1/BDNF complex-bearing vesicles may then be transported and sorted into distinct pathways (Alderson et al., 2000). BDNF may be released from the glia if the transport vesicle fuses to the cell membrane or may be degraded if sorted into the late endosome pathway (Alderson et

al., 2000). In either case the extracellular BDNF availability is decreased, if only transiently. TrkB-T1 may also reduce the pool of available BDNF by behaving as a dominant-negative suppressor of TrkB-FL signalling (Eide et al., 1996). TrkB-T1 is thought to execute this function by forming non-productive heterodimers with TrkB-FL, thus obstructing signalling (Eide et al., 1996).

Trks and their truncated isoforms can mediate NT signalling via a variety of canonical and non-canonical pathways. For example, TrkB-FL can initiate phosphorylation cascades via its adaptor proteins activating ERK signalling and raising intracellular Ca^{2+} levels. TrkB-T1 can signal despite the truncation, being able to activate PKC, PLC-γ, and RhoGDPI1 in a BDNF-dependent manner in different contexts, and appears to influence the cytoskeleton and neurite outgrowth in a BDNF-independent manner.

1.3 The *Drosophila* neurotrophin system

Due to the experimental power provided by *Drosophila* genetics, short life-cycle, conserved genes and small yet complex brain, Drosophila melanogaster is an excellent model organism for the study of neurotrophin biology. Furthermore, the *Drosophila* neurotrophin system is fundamentally similar to that of vertebrates, and the two are likely linked by common descent (Zhu et al., 2008). The *Drosophila* neurotrophins (DNTs) are encoded by the *spätzle* (*spz*) gene family, of which there are 6 members in *Drosophila melanogaster* (Parker et al., 2001). Spätzle, DNT1 (Spz2) and DNT2 (Spz5) are structurally and functionally homologous to the vertebrate neurotrophins (Zhu et al., 2008).

A key difference between the vertebrate and *Drosophila* neurotrophic systems is that there are no full-length homologs of the vertebrate neurotrophin receptors. Instead, neurotrophic signalling can be mediated by Toll family receptors in *Drosophila* (Foldi et al., 2017) and the Kekkon (Kek) family of receptors (Fig. 1.1 B, Fig. 1.2). The Kek receptor family are kinase-less homologs of Trk receptors, similar to truncated Trk isoforms (MacLaren et al., 2004) (Fig. 1.2). Kek6 was reported to function as a neurotrophin receptor at the larval neuromuscular junction (NMJ), being required for normal DNT2 signalling and homeostatic plasticity (Ulian-Benitez et al., 2017).

1.3.1 The *spaetzle* family

As BDNF is an important neurotrophin in vertebrates, it was important to find a homologue in flies. A bioinformatics search for a structural homologue of BDNF in *Drosophila* identified DNT1 as sharing structural homology with BDNF despite sequence variance (Zhu et al., 2008). Like the mammalian NTs, all members of the *spz* family consist of a cysteine-rich domain (cys-knot) and an unstructured pro-domain. Analysis of the predicted protein structures of the neurotrophin superfamily placed Spz1, DNT1 and DNT2 in one group with the vertebrate neurotrophins, and Spz3, -4 and -6 in another, more divergent group (Zhu et al., 2008). In the group containing Spz1, DNT1 and DNT2, the cys-knot of these proteins was well conserved between vertebrates and *Drosophila*, indicating possible functional conservation (Zhu et al., 2008).

The key characteristics of vertebrate neurotrophins are their ability to regulate neuronal survival, synaptic structural plasticity, and axon guidance. DNTs in addition

Figure 1.2 - Domain and motif structure of Trks, Keks and Tolls

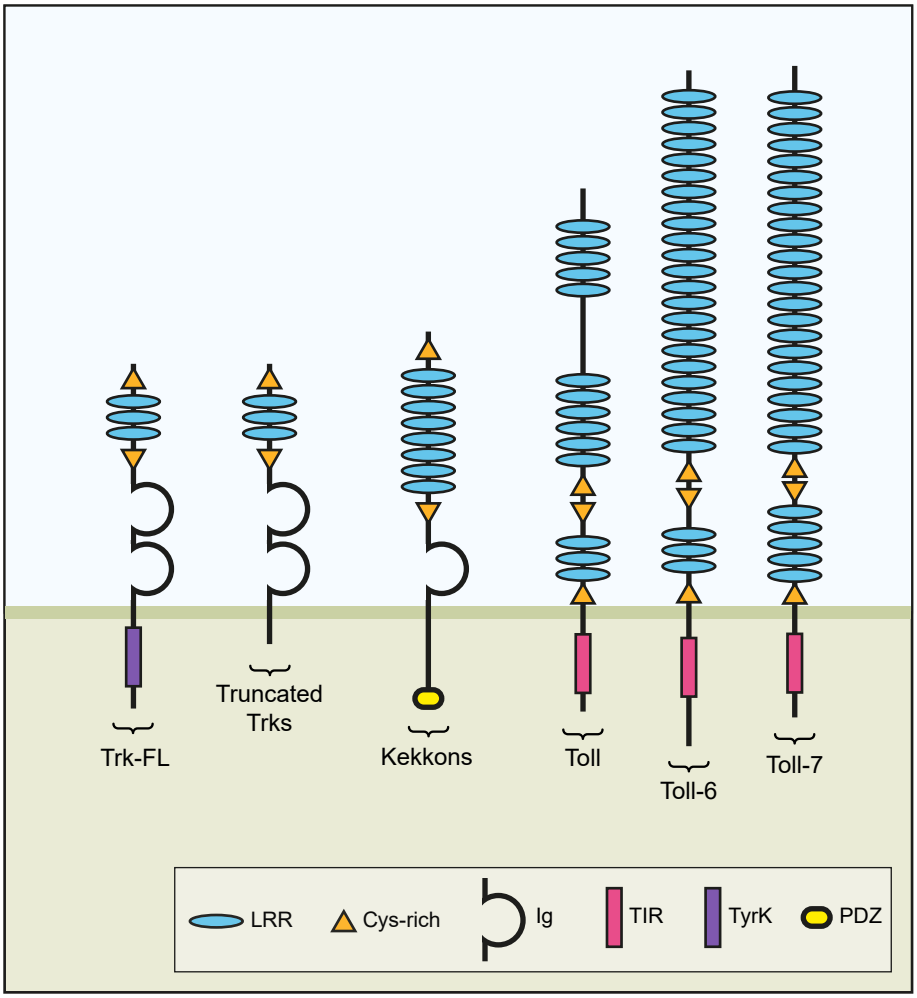


Figure 1.2 – Domain and motif structure of Trks, Keks and Tolls

Comparison of mammalian and *Drosophila* neurotrophin receptors. Full-length and Truncated Trks isoforms have identical extracellular domains but vary intracellularly. Keks have homologs of the Trks, resembling the truncated isoforms. Individual family members of Trks and Keks are structured similarly to other Trk/Kek family members, the structures shown here are representative of each family. There are 9 Tolls in *Drosophila*, Toll, Toll-6 and -7 are shown here to provide a representative sample of Tolls demonstrated to mediate DNT signalling. (Adapted from Anthoney et al., 2018, MacLaren et., al 2004, Skaper 2012, Ulian-Benitez et al., 2017). Key: LRR – Leucine-rich repeat, Cys-rich – Cysteine-rich domain, Ig – Immunoglobulin domain, TIR – TIR domain, TyrK – Tyrosine Kinase domain, PDZ – PDZ domain binding motif.

to being structurally homologous to vertebrate neurotrophins also possess these conserved functions (Zhu et al., 2008, McIlroy et al., 2013, Ulian-Benitez et al., 2017).

In *Drosophila* the loss-of-function of *spz*, *DNT1* and *DNT2* result in increased apoptosis and neuronal loss in the embryonic CNS (Zhu et al., 2008). This phenotype could be rescued by the overexpression of mature forms of the DNTs (Zhu et al., 2008). Rescue experiments also demonstrate that *DNT* function is necessary for viability, and that *DNT*s are functionally redundant, with overexpression of one active *DNT* rescuing loss of another (Zhu et al., 2008). Thus, DNTs can regulate cell number plasticity, a hallmark of vertebrate NTs.

At the larval NMJ DNT2 is an important regulator of synaptic structural plasticity (Ulian-Benitez et al., 2017, Sutcliffe et al., 2013). In situ hybridizations have shown that the *DNT*s are expressed in the muscles of the larval body wall (Zhu et al., 2008, Sutcliffe et al., 2013). This would indicate that DNTs are secreted from the muscle cells and function as retrograde signals to the pre-synaptic cell, in this case a motoneuron (Sutcliffe et al., 2013). Consistent with this model are findings that disruption of DNT function leads to changes in the structure of the axonal terminal, including changes to bouton size, bouton morphology, the length of the axonal terminal and number of active zones (Ulian-Benitez et al., 2017, Zhu et al., 2008).

Additionally, loss of *DNT* function is associated with the presence of ghost boutons and other synaptic debris, which are indicative of disrupted synapse formation (Ulian-Benitez et al., 2017). This is observable on a behavioural level, while the *DNT2* mutant larvae could achieve the same speeds of the wildtype controls, *DNT2* mutants spent longer at lower speeds or not moving at all (Ulian-Benitez et al., 2017).

Post-translational processing of neurotrophins and subsequent signalling is also markedly similar in vertebrates and *Drosophila*. In both cases neurotrophins are first expressed in an immature pro-protein form and are subsequently cleaved to produce the mature form of the neurotrophin by exposing the cystine-knot (Foldi et al., 2017). The cystine-knot dimerises and is then able to bind to a receptor.

Similar to mammalian pro-NTs, pro-DNT1 can promote apoptosis via JNK signalling, while mature forms of DNT1 and 2 were found to promote cell survival via NFκB and ERK signalling (Foldi et al., 2017). In vivo, the mammalian NTs, DNT1, and DNT2 are cleaved intracellularly before being secreted in a mature form (Foldi et al., 2017). In contrast, the full-length pro-form of Spz is secreted and then cleaved extracellularly. The pro-form of DNT1 is more common in vivo than mature DNT1, while mature DNT2 is more common than pro-DNT2, which may or may not be capable of eliciting signalling itself (Foldi et al., 2017).

Mammalian NTs are cleaved by furin proteases, this is conserved in *Drosophila*, as DNT1 and 2 have been found to be cleaved by conserved furin proteases (Lu et al., 2005, Foldi et al., 2017). Within the context of activity-dependant release, BDNF is cleaved extracellularly at the end of a serine protease cascade (Lu et al., 2005). In a similar manner, Spz1 has been found to be cleaved at the end of a serine protease cascade, albeit within the context of development and in the context of immunity, wherein Spz1 is cleaved by Easter and Spz processing enzyme (SPE), respectively (Hoffman and Riechardt 2002).

1.3.2 Toll receptors

The canonical receptor for Spz in *Drosophila* is the Toll (Toll-1) receptor (Anderson et al., 1985). Toll-6 has previously been reported to function in concert with Kek6 to mediate homeostatic plasticity at the NMJ (Ulian-Benitez et al., 2017). Tolls are an evolutionarily conserved family of type I transmembrane receptors. Toll-1 was initially discovered for its role in dorso-ventral patterning in development (Anderson et al., 1985). In mammals Toll-like receptors (TLRs) have a well-documented role in innate immunity (Fitzgerald and Kagan 2020).

The *Drosophila* Toll gene family play important roles in the development and function of the nervous system (Zhu et al., 2008, McIlroy et al., 2013), and some evidence suggests TLRs may possess similar roles in the nervous systems of mammals (Rolls et al., 2007).

There are 9 known members of the *toll* gene family in *Drosophila* (Tauszig et al., 2000, Du et al., 2000). Different names for these genes can be found in the literature but are here referred to by number: *toll-1* (*toll*), *toll-2* (*18-wheeler*), *toll-3* (*MstProx*), *toll-4*, *toll-5* (*tehao*), *toll-6*, *toll-7*, *toll-8* (*tollo*) and *toll-9* (Anderson et al., 1985, Eldon et al., 1994, Tauszig et al., 2000, Ooi et al., 2001).

Of the 9 *Drosophila* Tolls, only *toll-1* has been demonstrated to play a role in innate immunity, wherein it mediates an anti-fungal response (Lemaitre et al., 1996). There is some evidence of *toll-7* playing a role in anti-viral immunity (Nakamoto et al., 2012). *toll-9* is the most similar to mammalian TLRs (Du et al., 2000).

Structurally, the extracellular domain of Tolls consist of a signal peptide, marking the protein for transport the membrane, and a series extracellular leucine-rich repeats (LRRs) flanked by cysteine-rich regions (Tauszig et al., 2000, Gay and Gangloff 2007).

Structural analysis of TLRs indicate that the extracellular domains of TLRs fold into horseshoe-shaped structures (Botos et al., 2011). Intracellularly Tolls and TLRs possess a conserved Toll/Interleukin-1 Receptor (TIR) domain, a hallmark of the Toll receptor family (Gay and Gangloff 2007, Botos et al., 2011).

In *Drosophila* Toll-family receptors behave as receptors for the DNTs (McIlroy et al., 2013, Ulian-Benitez et al., 2017). Co-immunoprecipitations (co-IPs) from cells culture and adult fly heads revealed that Toll-6 and Toll-7 are capable of binding DNT1 and DNT2, with Toll-6 and DNT2, and Toll-7 and DNT1 likely forming ligand/receptor pairs (McIlroy et al., 2013). Ligand binding is promiscuous as DNT2 can also bind Toll-6 (McIlroy et al., 2013). Furthermore, constitutively active mutant forms of Toll-6 and -7 are capable of rescuing *DNT1* and *DNT2* mutant phenotypes, indicating a genetic and functional interaction (McIlroy et al., 2013). Additionally, disturbing *toll-6/7* function by overexpression or mutation recapitulate the corresponding phenotypes seen for *DNT2/1* mutants, indicating the Tolls are downstream of DNTs (Zhu et al., 2008, McIlroy 2013).

In mammals, the mature form of a neurotrophin elicits pro-survival signalling via Trk-receptors and cell death via Sortilin and the p75NTR receptors. In *Drosophila* Tolls are able to signal through both pathways in a context dependent manner (Foldi et al., 2017). As previously discussed, the cleavage state of DNTs influences downstream signalling, with cleaved mature forms inducing cell survival, with immature pro-forms inducing cell death (Foldi et al., 2017).

Toll-receptors have an inherent preference for either survival or cell death (Foldi et al., 2017). This may reflect preferential binding to ligands and/or downstream adaptors. Toll-2, 6 and 7 are neuroprotective and can promote increases in cell number (Foldi

et al., 2017, Li et al., 2020). Toll-1 is mostly pro-apoptotic (Foldi et al., 2017). Furthermore, different Toll homodimers, Toll-Toll heterodimers and heterodimers between Toll and other receptors may have different binding affinities to the ligands and subsequently lead to alternate signalling between death and survival (Foldi et al., 2017).

In addition to the state of ligands, the direction of Toll signalling is also dependent on the availability of intracellular downstream adaptor molecules (Foldi et al., 2017). The adaptor protein Weckle (Wek) can recruit Myeloid differentiation primary response 88 (MyD88) and Sarm to Toll receptors (Foldi et al., 2017). If MyD88 is recruited to the Toll-adaptor complex cell survival is promoted via the NF-KB and ERK pathways. Alternatively, if Sarm is recruited to the adaptor complex cell death is promoted via JNK signalling (Foldi et al., 2017). Sarm is an inhibitor of MyD88 and can hence override pro-survival signalling. MyD88 can bind Tolls independently of Wek. In this respect, Wek functions as switch between the death or survival of the cell (Foldi et al., 2017).

This is further compounded by the fact that adaptor protein abundance change throughout development (Foldi et al., 2017). Wek is scarce during early development, thereby promoting cell survival, only to become more abundant later in third larval instar and pupal phases allowing for the recruitment of Sarm and the inhibition of MyD88, hence promoting cell death (Foldi et al., 2017).

toll-6, -7 and *-8* are expressed in motoneurons (McIlroy et al., 2013, Ballard et al., 2014). *toll-6* and *-7* are expressed in the embryonic ventral nerve cord (VNC) within components of the locomotor circuitry and the central brain (McIlroy et al., 2013). *toll-1, -6* and *-7* are required for motor axon guidance during development (Halfon et al.,

1995, McIlroy et al., 2013). *toll-6, -7* and *-8* have been demonstrated to play a role NMJ growth, with *toll-6* being a regulator of activity-dependent structural plasticity (Ballard et al., 2014, McLaughlin et al., 2016, Ulian-Benitez et al., 2017).

Overexpression of *toll-6* and *toll-7* leads to increased bouton number at the NMJ (McLaughlin et al., 2016). Curiously this overgrowth is dependent on the transcription factor FoxO in the case of *toll-6* but not for *toll-7* (McLaughlin et al., 2016). Toll-6-dependent overgrowth is also dependent on the adaptor protein Sarm (McLaughlin et al., 2016). The Toll-6/Sarm/FoxO pathway drives instability of the microtubule (MT) network in motoneuron axonal terminals and promotes MT dynamics, leading to NMJ growth (McLaughlin et al., 2016).

Neurotrophic signalling downstream from Tolls in *Drosophila* is markedly similar to the processes that occur in mammals downstream of neurotrophic signalling. Trk signalling promotes cell survival and growth via ERK similarly to the Toll/MyD88 pathway (Foldi et al., 2017). p75NTR and Toll/Wek/dSarm promote cell death via JNK signalling (Foldi et al., 2017).

1.3.3 Kekkon receptors

Keks are the *Drosophila* homologs of the vertebrate Trk receptors (Mandai et al., 2009). Trk receptors belong to a family of proteins characterised by the presence of extracellular LRRs and immunoglobulin (Ig) (LIG) domains, the LIG family (Mandai et al., 2009). A phylogenetic study of LIG proteins revealed that a family of six LIG genes in *Drosophila*, the *kek* family, form a distinct clade with vertebrate *trk*s (Mandai et al., 2009).

Full length vertebrate Trks possess a Tyrosine Kinase domain that is thought to mediate signalling, Keks lack this TyrK domain and instead have more divergent cytoplasmic domains (Huang and Reichardt 2003, MacLaren et al., 2004). The Kek family more accurately resemble the truncated isoforms of Trk receptors in this regard. However, Keks possess longer intracellular domains than truncated Trk isoforms such as TrkB-T1 which possess short intracellular domains (MacLaren et al., 2004, Allendoerfer et al., 1994).

There are six known members of the Kek family in *Drosophila* (MacLaren et al., 2004). Phylogenetic analysis revealed that *kek1*, *-2*, *-5* and *-6* were well conserved between *Anopheles gambiae* (mosquito), *Apis mellifera* (European honeybee) and *Drosophila melanogaster*. Conversely *kek3* and *kek4* orthologs were not found in *A. gambiae* and *A. mellifera* indicating potentially novel roles in *Drosophila* (MacLaren et al., 2004).

The extracellular domain of Keks are particularly well conserved in insects (MacLaren et al., 2004). This is in contrast to the intracellular domains, which lack conservation with the exception of a few sites, including Post-synaptic density-95, discs large and zona occludens-1 (PDZ)-ligand motifs (MacLaren et al., 2004). These conserved sites in the in the C-terminal tail may be important for the recruitment of adaptor proteins and co-factors (MacLaren et al., 2004).

Keks 1, 2, 5 and 6 are known to possess PDZ ligand motifs at their cytosolic C-terminals (MacLaren et al., 2004). Proteins with PDZ domains and proteins bearing PDZ-binding domains (PDZ ligand motifs) can bind together forming a structurally linked complex (Kim et al., 2004).

Some PDZ domain proteins, such as Dlg, possess both the PDZ domain and ligand, allowing them to assemble into networks of PDZ proteins, forming a scaffold (Kim et

al., 2004). PDZ scaffold proteins can aid in the translocation of membrane-bound proteins that possess a PDZ ligand domain (Kim et al., 2004), and are important for the organisation and clustering of cell adhesion molecules and ion channels at the presynapse (Thomas et al., 1997).

The activity and abundance of PDZ-ligand-bearing proteins can be regulated by the phosphorylation of their PDZ ligands (Kim et al., 2004). Phosphorylation of PDZ ligand sequences prevents the binding of PDZ domains (Kim et al., 2004). PDZ scaffold proteins allow for the modular assembly of dynamic protein assemblies (Kim et al., 2004). As several members of the Kek family possess PDZ ligand domains (MacLaren et al., 2004), it is possible that they associate with a PDZ scaffold in neurons.

Co-immunoprecipitation experiments indicate that Keks are able to bind to each other (MacLaren et al., 2004). Individual Keks bind strongly in a homophillic manner and seem to be capable of binding other Keks to varying degrees of affinity (MacLaren et al., 2004).

Kek2 and Kek6 possess a strong affinity to each other, indicating that they may form a complex *in vivo* (MacLaren et al., 2004). Keks may bind each other as trans-synaptic cell adhesion molecules, or possibly as heterodimers (MacLaren et al., 2004). It is unknown which domains are important for dimerization.

The *kek* gene family is expressed in the *Drosophila* nervous system: *kek1* and *-2* are highly expressed in the embryonic CNS (Musacchio et al., 1996), *kek5* (Evans et al., 2009) and *-6* are highly expressed in the larval CNS, and *kek2, 5* and *6* are known to be expressed in motoneurons (Ulian-Benitez et al., 2017, Ulian-Benitez 2018).

At least some members of the Kek family may be *Drosophila* neurotrophin receptors. Co-immunoprecipitation experiments revealed that DNT2 can be promiscuously

bound by Kek2, 5 and 6 (Ulian-Benitez et al., 2017). Kek6 is also able to bind DNT1 (Ulian-Benitez et al., 2017).

Kek6 can bind DNT2 in vivo at the NMJ, where DNT2 is released from the post-synaptic muscle as a retrograde signal (Ulian-Benitez et al., 2017). Overexpression of *kek6* leads to an increased number of active zones at the NMJ (Ulian-Benitez et al., 2017). Additionally, an NMJ undergrowth phenotype stemming from loss of *DNT2* function can be partially rescued by *kek6* overexpression, consistent with a model where Kek6 is downstream of DNT2 (Ulian-Benitez et al., 2017).

Kek6 has been demonstrated to physically interact with Toll-6 at the larval NMJ to co-operatively mediate synaptic structural plasticity (Ulian-Benitez et al., 2017) (Fig. 1.3). This is in contrast to the relationship of full-length Trk receptors and truncated Trks, wherein TrkB-T1 can behave as a ligand-sink and an unproductive binding partner, and thus an inhibitor of TrkB-FL (Eide et al., 1996).

Overexpression of *DNT2* did lead to an overgrowth phenotype characterised by increase in axonal terminal length, branching and active zone number (Ulian-Benitez et al., 2017). However, overexpression of either *kek6* or *toll-6* did not lead to significant overall NMJ growth, but overexpression of both receptors did produce an overgrowth phenotype, mimicking *DNT2* overexpression. This indicates that Kek6 and Toll-6 may work synergistically to regulate synaptic plasticity (Ulian-Benitez et al., 2017) (Fig. 1.3).

toll-6 and *kek6* appear to have independent functions as overexpression of either in the mutant background of the other can lead to increases in active zone formation (Ulian-Benitez et al., 2017). In a *toll-6/kek6* double mutant background active zone number is decreased (Ulian-Benitez et al., 2017). This phenotype is recapitulated in

Figure 1.3 - Toll-6 and Kek6 synergistically mediate DNT2 signalling

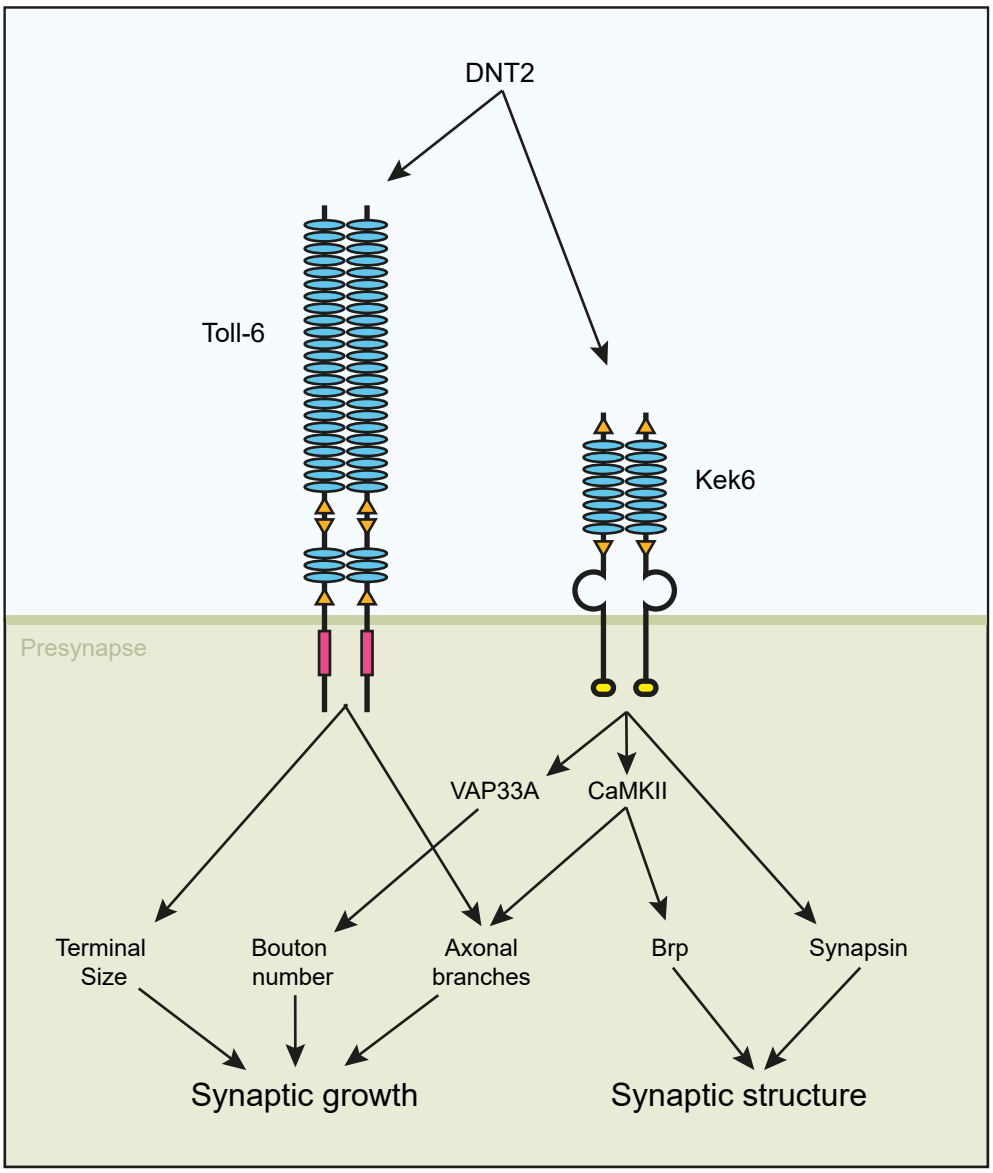


Figure 1.3 – Toll-6 and Kek6 synergistically mediate DNT2 signalling

Toll-6 and Kek6 are both required the transmission of retrograde DNT2 signalling at the larval NMJ (Ulian-Benitez et al., 2017). Toll-6 and Kek6 have overlapping and distinct functions at the NMJ to mediate the effect of DNT2 on synaptic growth and structure, with signalling via Toll-6 being required for normal axonal terminal size in a *DNT2*-dependent manner, and *kek6* being necessary for the normal number of boutons, Brp and Synapsin in a *DNT2*-dependent manner. Toll-6 and Kek6 function together to regulate axonal branching in a *DNT2*-dependent manner. Kek6 interacts with CaMKII and VAP33A to mediate the effects of DNT2. Figure adapted from (Ulian-Benitez et al., 2017).

DNT2 mutants, indicating that DNT2 exercises control over synaptic growth via these two receptors (Ulian-Benitez et al., 2017).

Kek6 is capable of binding CaMKII via its intracellular domain (Ulian-Benitez et al., 2017). Knock-down of *CaMKII* rescues the synaptic overgrowth phenotype observed under *kek6* overexpression, additionally in *DNT2* and *kek6* single null mutants, the levels of activated CaMKII is significantly reduced (Ulian-Benitez et al., 2017). This indicates that CaMKII functions downstream of Kek6 and DNT2. Similarly, Kek6 can bind and, along with DNT2, is upstream of the exocytosis regulator VAP33A (Ulian-Benitez et al., 2017). The mechanism of how Kek6 activates CaMKII is unclear (Ulian-Benitez et al., 2017).

While Kek1 has not yet been demonstrated to bind a DNT yet, it has been demonstrated to inhibit signalling via the epidermal growth factor receptor (EGFR) (Alvarado et al., 2004a). Kek2, -4, -5 and -6 were not found to inhibit EGFR activity. Supporting this, the G160 residue in LRR2 of Kek1 was found to confer the binding specificity of Kek1 to EGFR, this residue is absent in all other Kek family members indicating EGFR inhibition is unique to Kek1 (Alvarado et al., 2004b). EGFR signalling plays a key role in embryogenesis in both vertebrates and *Drosophila* (Chia et al., 1995, Lusk et al., 2017). Notably, EGFR is upstream of the PI3K/Akt and Ras/MAPK/ERK pathways, a feature shared with mammalian Trk receptors (Lusk et al., 2017).

Kek5 has also been reported to have an inhibitory function, blocking bone-morphogenetic protein (BMP) signalling in the wing disc (Evans et al., 2009). Loss of the extracellular LRR domains of Kek5 disrupts this inhibitory effect on BMP signalling (Evans et al., 2009). Furthermore, the PDZ-binding site of Kek5 is required for

inhibition of BMP signalling. The PDZ-binding site may co-ordinate the localisation of Kek5 to the cell membrane and bring it within proximity to relevant co-factors (Evans et al., 2009). This is supported by the fact that localisation of Kek5 to the membrane is also required for BMP inhibition (Evans et al., 2009).

Kek5 may act in a complex way to regulate the extracellular distribution or activity of BMP ligands (Evans et al., 2009). *kek5* genetically interacts with the BMP ligand *glass bottom boat* (*gbb*) in the wing disc (Evans et al., 2009). Gbb is also known to regulate synapse structure and growth (McCabe et al., 2003).

Interestingly, the abundance of mRNA for *kek5* and *-2* is altered in mutants with defective neuronal activity (Guan et al., 2005). In K^+ channel mutants with hyperexcitable neurons, *kek2* is upregulated, but *kek5* is downregulated (Guan et al., 2005). Conversely, in reduced excitability mutants *kek2* is downregulated, but *kek5* transcripts are unaffected relative to wildtype controls (Guan et al., 2005). *kek2* and *-5* expression is regulated by neuronal activity.

As *kek5* transcript levels were found to change following neural activity (Guan et al., 2005), *kek5* may behave as an activity-regulated inhibitor of BMP signalling at the NMJ. Interestingly, overexpression of *kek2* driven by the motoneuron driver elavC155-GAL4 lead to a reduction in bouton number by ~30%, as did loss of *kek2* expression via RNAi (Guan et al., 2005). This indicates that the precise level of Kek2 abundance is important for regulating axonal terminal structure (Guan et al., 2005).

kek2 is expressed in motoneurons and appears to cluster into puncta along the axon (Guan et al., 2005). Kek2 puncta appear with greater density in boutons but do not appear to be present in active zones (Guan et al., 2005). Kek2 is localised near FasII-

marked periactive zones. Periactive zones have been demonstrated to be locations of importance for the regulation of synaptic growth (Sone et al., 2000).

The Kek family has been demonstrated to interact with the EGFR (Alvarado et al., 2004a and b), BMP (Evans et al., 2009) and neurotrophin signalling pathways (Ulian-Benitez et al., 2017), some are known to be regulated by neuronal activity (Guan et al., 2005), and some have been demonstrated to have an impact on synapse morphology (Guan et al., 2005, Ulian-Benitez et al., 2017). Altogether this makes the Kek family an interesting target for studying structural plasticity in *Drosophila*.

1.4 Ca^{2+} signalling in neurons

Kek6 has been demonstrated to regulate presynaptic Ca^{2+} levels (Ulian-Benitez 2018). Furthermore, Kek6 was found to physically associate with CaMKII and promote its phosphorylation (Ulian-Benitez et al., 2017). As this is canonically a Ca^{2+}-dependent process, this suggests that Kek6 somehow increases Ca^{2+} levels in the cytosol (Ulian-Benitez et al., 2017, Ulian-Benitez 2018). This is important as BDNF/TrkB signalling in vertebrates also raises intracellular Ca^{2+} levels and can promote plasticity in a Ca^{2+}-dependent manner (Huang and Reichardt, 2003). This indicates that Keks and Trks may have conserved functions in plasticity.

At the *Drosophila* presynapse, Ca^{2+} can enter the cytosol from intracellular stores via the intracellular calcium channels Ryanodine receptor (RyR) and IP_3R, and from outside the cell via cation channels (Kawasaki et al., 2000, Hasan and Rosbash 1992).

1.4.1 Intracellular stores of Ca^{2+}

It was suspected that Kek6 may alter Ca^{2+} signalling neurons via triggering the release of Ca^{2+} from intracellular stores. The endoplasmic reticulum (ER) is an intracellular Ca^{2+} store and Ca^{2+} can be released from this store by the opening of RyR or IP_3R, which both localise to the ER (sarcoplasmic reticulum (SR) in muscles) (Woll and Petegem 2022). Both the RyR and IP_3 receptors and their signalling pathways are conserved between flies and mammals (Woll and Petegem 2022).

RyRs are large tetrameric Ca^{2+} channels (Lai et al., 1988). RyR permeability is influenced by a plethora of factors, including cytosolic $Ca^{2+,}$ Mg^{+}, $Ca^{2+/}$CaM, calsequestrin, adenosine triphosphate (ATP), CaMKII, reactive oxygen species (ROS), and small peptides (Petegem 2012, Donoso et al., 2011, Beard et al., 2005). Release of Ca^{2+} from intracellular stores via RyR is important for muscle contraction in *Drosophila* and in mammalian skeletal muscle (Sullivan et al., 2000, Takeshima et al., 1994).

IP_3Rs open upon binding of their ligand, IP_3 (Prole and Taylor 2019). IP_3 is synthesized from PIP2, a minor component of cell membranes. IP_3 synthesis from PIP2 is mediated by PLC activity. PLC itself can be activated by an active G-protein coupled receptor (GPCR) (Prole and Taylor 2019).

1.4.2 Entry of extracellular Ca^{2+}

1.4.2.1 Voltage-gated cation channels

During evoked synaptic transmission when an action potential reaches the axonal terminal voltage-gated calcium channels are opened, flooding Ca^{2+} into the presynapse (Katz and Miledi 1965). Ca^{2+} ions interact with calcium-sensing proteins

such as synaptotagmin to trigger fusion of vesicles to the cell membrane and the subsequent neurotransmitter release (Südhof 2012). The presence of Ca^{2+} ions within the presynapse is a direct signal of activity. Ca^{2+} signalling is therefore important for transducing neuronal activity into structural change (Lisman et al., 2002).

Voltage-gated Ca^{2+} channels (VGCCs) are heteromeric complexes canonically composed of five subunits: α_1, α_2, δ, ß and Γ. In *Drosophila*, there are three genes that encode the pore-forming α_1 subunits: *Ca-α1D*, *cacophony* (*cac*) and *Ca-α1T* (Chorna and Hasan, 2012). In vertebrates there are a plethora of voltage-gated Ca^{2+} channels and have been characterized by their functional properties (Chorna and Hasan, 2012). The three *Drosophila* α_1 subunits fit into the three categories of vertebrate α_1 subunits, with *Ca-α1D* being a Ca_v1-type, *cac* a Ca_v2-type, and *Ca-α1T* a Ca_v3-type channel (Chorna and Hasan, 2012).

In *Drosophila*, Cacophony voltage-gated Ca^{2+} channels are the primary point of entry into the neuron for Ca^{2+} following an action potential (Kawasaki et al., 2000). Cac channels are the only voltage-gated Ca^{2+} channel in *Drosophila melanogaster* that has been demonstrated to mediate synaptic transmission and localises to the active zones (AZs) at presynaptic sites (Smith et al., 1996, Vactor and Sigrist 2017). Cac channels sit in a central position in AZs and are surrounded by Brp scaffolds (Vactor and Sigrist 2017).

The probability of neurotransmitter release (P_r), a Ca^{2+}-dependent process, is proportional to the abundance of Cac at a synapse (Gratz et al., 2019). Interestingly, it has been found that only a small portion of AZs have high levels of Cac and a corresponding high P_r, and there are many low Cac/P_r AZs at the NMJ of single motoneurons (Gratz et al., 2019).

Cac levels are altered in models of homeostatic plasticity at the *Drosophila* NMJ (Gratz et al., 2019). In *GluRIIA* mutants, where the receptivity of the post-synaptic density (PSD) to glutamate is reduced, Cac levels increase at AZs, raising P_r, to compensate for the reduction in synaptic transmission (Gratz et al., 2019).

1.4.2.2 Ligand-gated cation channels

Ca^{2+} can also enter the post-synaptic cell via ligand-gated cation channels. In glutamatergic neurons two important types of ionotropic glutamate receptors (iGluRs) are α-amino-3-hydroxy-5-methyl-4-isoxazolepropionic acid (AMPA) receptors (AMPARs) and N-methyl-d-aspartate (NMDA) receptors (NMDARs) (Marrus et al., 2004, Ultsch et al., 1993, McBain and Mayer 1994, Xia et al., 2005).

AMPARs are an important family of glutamate-gated cation channels in mammals and flies, are an essential component of the post-synaptic density and are necessary for the induction of action potentials in the post-synaptic cell (Marrus et al., 2004). AMPARs are tetrameric and the electrophysiological properties of the channel can be altered by altering the composition of the subunits (Marrus et al., 2004). In *Drosophila*, 3 subunits are necessary for function (GluR-III, GluR-IID, GluR-IIE), with the fourth subunit being variable (GluRII-A or GluRII-B) (Qin et al., 2005). Consequently, AMPARs at the *Drosophila* NMJ may either be A-Type (possessing the GluRII-A subunit) or B-Type (possessing the GluRII-B subunit) (Qin et al., 2005).

A and B-type AMPARs are functionally redundant as knock-out of one does not lead to lethality, as is this case if both *GluRII-A* and *GlurRII-B* (or any of the obligate subunits) are knocked out (Marrus et al., 2004, Qin et al., 2005). A-type receptors appear to be anchored to the actin cytoskeleton by the protein Coracle, whereas B-

type receptors are dependent upon Dlg for their abundance at the PSD (Chen et al., 2005, Chen and Featherstone 2005).

A-Type AMPARs produce a greater quantal size upon stimulation and possess slower desensitisation kinetics than B-type AMPARs (Harris and Littleton 2015). Furthermore, AMPARs clusters in recently formed postsynaptic densities (PSDs) are primarily formed of A-type receptors, although the ratio of A to B type receptors becomes more balanced as the PSD matures (Harris and Littleton 2015).

NMDARs are glutamate-gated cation channels found in both mammals and *Drosophila* (Ultsch et al., 1993, McBain and Mayer 1994, Xia et al., 2005) and are structurally well conserved and have similar functional properties (Ultsch et al., 1993, Xia et al., 2005).

NMDARs are coincidence detectors as cation (Ca^{2+} and N^{+}) permeability is dependent on glutamate binding and membrane depolarisation (Nowak et al., 1984, McBain and Mayer 1994). High levels of synaptic transmission are typically sufficient to satisfy these conditions, by providing glutamate in the synaptic cleft during post-synaptic depolarisation (Nowak et al., 1984, McBain and Mayer 1994).

NMDAR activation elicits the growth and stabilisation of dendritic spines and mediates synaptogenesis (Ultanir et al., 2007, Merriam et al., 2011). NMDAR-mediated synaptogenesis is CaMKII-dependent (Barria and Malinow 2005, Zhou et al., 2007). Additionally, in mammals NMDARs can become phosphorylated themselves following BDNF/TrkB signalling, making them more permeable (Minichiello 2009).

1.4.3 CaMKII: a major effector of Ca^{2+} signalling

Kek6 was found to function upstream of CaMKII, an important effector of Ca^{2+} signalling (Lisman et al., 2002). CaMKII is well conserved across the animal kingdom and is a key driver of synaptic plasticity and is one of the few known molecules to mediate plasticity (Lisman et al., 2002, Tombes et al., 2003, Chao et al., 2011, Nairn and Picciotto 1994, Colbran 1992). In vertebrates and *Drosophila*, *CaMKII* is required for structural and functional plasticity, and learning and memory (Silva et al., 1992a, Silva et al., 1992b, Griffith et al., 1993, Griffith et al., 1994, Wang et al., 1994).

CaMKII activation is canonically dependent on the binding of Ca^{2+}/Calmodulin (CaM) complexes. CaM is a highly conserved Ca^{2+} sensor (Chin and Means 2000). CaM can bind up to four Ca^{2+} ions and undergoes a conformational change upon doing so (Chin and Means 2000). This conformational change releases free energy and allows CaM to activate the effectors of Ca^{2+} signalling (Chin and Means 2000). CaMKII binds Ca^{2+}/Calmodulin complexes, auto-phosphorylates and becomes active as a kinase (Miller and Kennedy 1986). Due to the initial dependency on Ca^{2+} ions, and its importance mediating Ca^{2+} signalling, the phosphorylation state of CaMKII can be used as a readout for Ca^{2+} signalling (Ulian-Benitez et al., 2017)

A *CaMKII* gene encodes one subunit of the dodecameric CaMKII holoenzyme (Morris and Török 2001). The CaMKII holoenzyme can be homomeric or heteromeric, by virtue of being able of being composed of different combinations of paralogs and isoforms produced by alternative splicing (Morris and Török 2001, Brocke et al., 1999). Vertebrates have multiple paralogs of *CaMKII*, for example: *Xenopus* has three, *Homo sapiens* has four (Tombes et al., 2003).

Drosophila has only one *CaMKII* gene, which is predicted to produce up to 18 isoforms via alternative splicing (Cho et al., 1991, Griffith and Greenspan 1993). The isoforms of the *Drosophila CaMKII* are generated by splicing in the region of the protein joining the regulatory domain with the association domain (Ohsako et al., 1993, Griffith and Greenspan 1993). Multiple isoforms of *Drosophila* CaMKII have the identical molecular weights and can be grouped accordingly into three groups with the weights: 60, 58 and 55 kDa (Ohsako et al., 1993).

Different paralogs and splice isoforms of CaMKII vary in structure and have different properties including being more or less sensitive to Ca^{2+}/CAM (GuptaRoy et al., 1996, Chao et al., 2011), having different subcellular localisations, and have different affinities for binding other proteins (Srinivarsan et al., 1994, Brocke et al., 1999). The CaMKII holoenzyme can therefore have a wide range of different properties based on the composition of its subunits (Brocke et al., 1999).

The subcellular localisation of CaMKII is important for its signalling, as it can promote different effects depending on its position, e.g., in the nucleus it can alter the activity of transcription factors, or when associated with the cytoskeleton it can affect actin polymerisation (Brocke et al., 1999, Andersen et al., 2005).

CaMKII can regulate protein synthesis by activating the transcription factors such as cAMP response element-binding protein (CREB) (Sheng et al., 1991). Downstream targets CREB include several proteins required for synaptic growth and development including BDNF and TrkB (Alberini 2009, Yan et al., 2016, Tao et al., 1998, Impey et al., 2004).

In addition to being a kinase, CaMKII is an important scaffolding protein in the neurons of mammals and flies (Andersen et al., 2005). CaMKII alone reportedly makes up 2%

of the protein in the brain by mass (Lisman et al., 2002). In flies and mammals CaMKII associates with the actin cytoskeleton and when in the active phosphorylated state CaMKII can promote f-actin remodelling via phosphorylation of small GTPases Rac1 and RhoA (Andersen et al., 2005, Yasuda et al., 2022). Remodelling of the actin cytoskeleton is necessary for the activity-dependent growth of neurites (Andersen et al., 2005).

CaMKII has different functions on either side of the synaptic cleft, although its function is required on both sides for plasticity (Wang, 2009, Yasuda et al., 2022). Presynaptic CaMKII can elevate cytosolic Ca^{2+} levels once activated by phosphorylating RyRs, triggering the release of Ca^{2+} from intracellular stores, or by delaying the inactivation of Ca_V2 voltage-gated Ca^{2+} channels via a kinase-independent interaction (Wang, 2009).

In addition to promoting vesicle release via elevated Ca^{2+} levels, presynaptic CaMKII can interact with Synapsin (Wang, 2009). In its unphosphorylated state Synapsin is responsible for anchoring synaptic vesicles (SVs) to the actin cytoskeleton. Phosphorylation of Synapsin by CaMKII releases SVs liberating them into the pool of available SVs for SV exocytosis (Wang, 2009).

On the postsynaptic side, CaMKII is required for normal synaptic transmission via AMPARs and for long-term potentiation of the post-synapse in a NMDAR-dependent manner (Yasuda et al., 2022). CaMKII can recruit AMPARs to the post-synaptic density independently of kinase function and can modulate their function via phosphorylation (Yasude et al., 2022).

1.5 Plasticity

Plasticity is a quality of neurons that describes their ability to alter their structure and function over time (Griffith and Budnik 2006). Activity-dependent structural plasticity has been reported to be necessary for learning and memory formation to occur and may be critical to understanding how the brain stores information (Takeuchi et al., 2014). Aberrant activity-dependent structural plasticity has been associated with neurological and psychological disorders (Applebaum et al., 2022). Consequently, activity-dependent structural plasticity is an important area of research in fundamental and translational contexts.

The study of functional plasticity of neurons is concerned with the short-term modulation of the electrical activity of neurons during synaptic transmission not typically associated with structural change (Griffith and Budnik 2006). The study of structural plasticity, on the other hand, is concerned with alterations to the neuronal cell structure, but also the networks they contribute to, all the way up to brain plasticity (Griffith and Budnik 2006).

In 1949 it was postulated by Donald Hebb that experience alters the strength of synaptic weight, or probability of transmission, between neurons (Hebb 1949). This associative form of plasticity is called ‘Hebbian plasticity’ and conceptually has been summarised as: “Neurons that fire together wire together” (Hebb 1949). Hebbian plasticity has been generally regarded as a positive-feedback loop form of plasticity, wherein high levels of neuronal activity increases the strength of a synapse leading to firing in the future to be more likely and of a greater magnitude (Hebb 1949). Hebbian plasticity also includes forms of plasticity like long-term depression (LTD) where

synaptic weight decreases in response to a particular frequency of activity (Wang et al., 2021).

Non-Hebbian activity-dependent plasticity includes homeostatic forms of plasticity where the synapse may alter its structure and/or function following activity in order to maintain a consistent synaptic weight (Wang et al., 2021). Homeostatic plasticity is important for constraining activity-dependent growth in the nervous system, for ensuring the functionality of networks and the coherency of behaviour (Wang et al., 2021). Homeostatic plasticity is also important for avoiding excitotoxicity, wherein sustained activity of a neuron can induce cell death (Dong et al., 2009). Excitotoxicity may result from elevated levels of Ca^{2+} ions in the cytoplasm as a consequence of sustained neuronal electrical activity (Dong et al., 2009).

1.5.1 Experience dependent structural plasticity in mammals

Direct evidence of Hebbian synaptic plasticity was first found in 1973 by Bliss and Lomo in the rabbit hippocampus and was called Long-term potentiation (LTP) (Bliss and Lomo 1973). High-frequency trains of stimulation were found to potentiate the synapses in the hippocampus, and that this potentiation was stable over time (Bliss and Lomo 1973). LTP has since been discovered in many parts of the brain and in a multitude of forms. LTP has been observed to occur pre- and post-synaptically (Nicoll 2017).

Structural and functional LTP in the hippocampus has been found to be dependent on neurotrophic signalling, namely via BDNF/TrkB signalling (An et al., 2008, Pang et al., 2004). Pre-synaptic BDNF is thought to initiate LTP by being released and binding to post-synaptic TrkB receptors, and post-synaptic BDNF is thought to maintain LTP by

binding to and activating TrkB receptors on pre-synaptic side of the synaptic cleft (Lin et al., 2018).

With TrkB's kinase domain active, it phosphorylates and activates Shc, MAPK and PLC-γ (Minichiello 2009). The Shc and MAPK pathways then modulate the synthesis of proteins required for synaptic development. Protein synthesis is required for late LTP in a BDNF-dependant manner (Minichiello 2009). Both MAPK and PLC-γ pathways raise intracellular Ca^{2+} levels, activating CaMKII. The heightened level of Ca^{2+} may also be important for the activation of NMDARs (Baltaci et al., 2019).

BDNF/TrkB signalling has also been found to be important for homeostatic plasticity (Wang et al., 2021). The dual nature of BDNF as a regulator of Hebbian and homeostatic plasticity may be mediated by the complex manner of its release (Wang et al., 2021). Brief, activity-dependent, Ca^{2+}-dependent release of BDNF is important for Hebbian forms of plasticity, but constitutive release can regulate homeostatic plasticity (Wang et al., 2021).

In addition to synaptic plasticity, BDNF/TrkB signalling has been found to be important for learning and memory in mammals. BDNF mutant mice perform poorly in the Morris water maze test and BDNF was found to be necessary for fear conditioning (Linnarsson et al., 1997, Hall et al., 2000, Liu et al., 2004).

In humans, people who carry an allele of BDNF (val66met), which has been found to have impaired release from neurons in vitro, have been found to also perform less well in memory tests than non-carriers of this allele (Egan et al., 2003). Additionally, BDNF has been found to be upregulated in rat hippocampi during learning tasks (Hall et al., 2000).

1.5.2 Experience dependent structural plasticity in insects

1.5.2.1 Brain plasticity

Following its discovery in vertebrates, activity-dependent structural plasticity has been since found to occur in the brain of adult insects and is observable as changes to brain volume and circuit structure (Hourcade et al., 2010). The mushroom bodies (MBs) are considered to be the centres for learning and memory within the insect brain and have been implicated in the integration of sensory information, particularly olfactory signals (Hourcade et al., 2010).

Activity has been demonstrated to regulate the maturation of the MBs and the visual and olfactory systems (Heisenberg and Barth 1997, Golovin et al., 2019). When reared under constant light for four days, the volumes of optic lobes, central complex and the calyces of the mushroom bodies are increased compared to flies reared in total darkness (Heisenberg and Barth 1997).

Furthermore, when blinded in one eye flies have a reduced volume in the optic lobes, MBs, and central complex on the same side as the blinded eye (Barth et al., 1997). The substantial increase in optic lobe laminae volume seen in the non-blinded side is caused by growth of the axonal branches of photoreceptor neurons (Barth et al., 1997), indicating that Hebbian synaptic plasticity is taking place.

1.5.2.2 NMJ plasticity

Much research into synaptic structural plasticity in *Drosophila* comes from investigation of the larval neuromuscular junction (NMJ) (Harris and Littleton 2015). Early studies of plasticity at the larval NMJ investigated loss of function mutations in the *Shaker* (*Sh*) and *ether-a-go-go* (*eag*) genes, which result in a hyperexcitability

phenotype where neuronal activity is increased (Budnik et al., 1990). Sh and Eag encode voltage-gated K^+ channels that are responsible for hyperpolarising the neuron following depolarisation, thus ending the action potential (Budnik et al., 1990).

Larvae with loss-of-function mutations in *Sh* and *eag* possess greater numbers of boutons and more complex axon arbours, which possess more branches (Budnik et al., 1990). Additionally, mutations resulting in reduced neuronal activity, such as the no action potential mutation in *maleless*, supress the overgrowth phenotype of *Sh* and *eag* mutants (Budnik et al., 1990).

Structural plasticity can be induced in motoneurons by rearing larvae in a liquid slurry food and then transferring them to harder food media (Sigrist et al., 2000). In slurry media larval locomotion isn't required for feeding, whereas in firmer media locomotion is required to overcome the physical resistance of the media (Sigrist et al., 2000). Transfer of slurry-reared larvae to firm media induces axonal terminal growth within a few hours (Sigrist et al., 2000).

Rearing larvae at a higher temperature has also been found to induce structural plasticity. Compared to larvae reared at 25^{o}C, larvae reared at 29^{o}C are more mobile and consequently have a greater number of axonal boutons and active zones (Sigrist et al., 2003). This form NMJ growth is demonstrably due to activity and not another temperature sensitive factor as growth is block when activity is blocked via a temperature sensitive allele of the Na+ channel *paralytic* (Sigrist et al., 2003). Interestingly, when larvae are reared at 32^{o}C axonal terminals develop with more boutons, but have fewer active zones, perhaps to compensate for the high level of activity (Oswald et al., 2018

Besides the DNTs, a number of molecular mechanisms have been discovered to play a role in synaptic plasticity at the larval NMJ (Harris and Littleton, 2015). For example, the mutation of translational repressors has been found to alter the size and morphology of the larval NMJ (Zhang et al., 2001). For example, Fragile X mental retardation protein (FMRP) is an RNA-binding protein that acts as repressor of translation that is conserved between flies and humans (Brown et al., 2001, Zhang et al., 2001). In FMRP loss-of-function mutants *Drosophila* the larval NMJ is overgrown and has an increased probability to fire (Zhang et al., 2001). mRNA transcripts that FMRP is known to target include several proteins important for synaptic structure and function including iGluRs, microtubule associated proteins (MAPs) (Zhang et al., 2001, Pan and Broadie 2007). FMRP selectively binds mRNA transcripts and sequesters them from ribosomes (Darnell et al., 2011).

In addition to the regulation of protein synthesis, synapse morphology can also be altered by the regulation of protein degradation. At the *Drosophila* larval NMJ, activity-dependent axonal terminal growth is constrained by the expression of the gene *highwire* (hiw) (Collins et al., 2006). Highwire is a large (566kDa) E3 ubiquitin ligase. Highwire is highly conserved between *Drosophila, C.elegans* and zebrafish, suggesting an evolutionarily important function (Collins et al., 2006).

Highwire, as a ubiquitin ligase, promotes the degradation of the mitogen-activating protein kinase kinase kinase (MAPKKK) Wallenda (Wnd) (Collins et al., 2006). Loss of hiw function results in overgrown axonal terminals, smaller boutons and reduced quantal size and content (Wan et al., 2000). Mutations in *wnd* completely supress the phenotypes observed in *highwire* mutants and larvae with *wnd* overexpression possess an overgrown synapses not unlike those of *highwire* mutants (Collins et al., 2006).

Wallenda can activate JNK signalling, which is necessary for the synaptic overgrowth phenotype of *highwire* loss-of-function mutants (Collins et al., 2006). JNK signalling can modulate transcription by activating the transcription factor Fos, which is essential for the synaptic overgrowth of highwire mutants. In *Drosophila* Fos can dimerise with itself and with fellow leucine zipper Jun to form the transcription factor AP-1 (Ciapponi and Bohmann 2002). In flies and mammals AP-1 functions downstream of JNK and can upregulate synaptic growth (Sanyal et al., 2002).

JNK has also been found to regulate MT dynamics via activating MT associated protein 2 (MAP2), an activator of MT assembly (Chang et al., 2003). Additionally, MT stability is an important factor in JNK signalling in the Unc-dependent transport of synaptic proteins to the synapse (Voelzmann et al., 2016). Unc mediates the transport of synaptic proteins to the axonal terminal and its inhibition by JNK may cause the release of the transported proteins. Consequently, the subcellular localisation of JNK activation is important in this process as JNK activation in the soma or throughout the neuron blocks the normal transport of synaptic proteins, possibly due to premature release by Unc (Voelzmann et al., 2016).

Highwire may interact with the Gbb/BMP/TGF-ß signalling pathway by degrading Medea, a co-Smad responsible for translocating a transcription factor to the nucleus upon reception of the BMP ligand (McCabe et al., 2004). BMPs make up a family of ligands within the TGF-ß superfamily. Members of the TGF-ß superfamily are conserved secreted differentiation and growth factors vital for development in metazoans (Harris and Littleton 2015). BMPs are expressed throughout the *Drosophila* nervous system during development and are known to mediate activity-dependant structural plasticity in the *Drosophila* embryonic NMJ (McCabe et al., 2003, McCabe et al., 2004). Larvae with mutations in the BMP pathway have small synaptic

terminals and reduced synaptic transmission phenotypes at the NMJ (McCabe et al., 2003, McCabe et al., 2004).

BMP ligand Glass Bottom Boat has been demonstrated to be required for a critical period in the first larval instar NMJ (Berke et al., 2013). A transient BMP signal in this period is required for synaptic growth and is necessary for activity-dependant structural plasticity during this growth (Berke et al., 2013).

1.6 The Model system

1.6.1 *Drosophila* melanogaster: an overview

Examining the role of the Keks in structural plasticity in *Drosophila* requires a working knowledge of the biology of the model organism. *Drosophila melanogaster* is a cosmopolitan species of fruit fly, also known as vinegar flies, in the insect Order *Diptera*. *Drosophila melanogaster* an excellent model organism due to its small size and low upkeep costs (Roote and Prokop 2013). *Drosophila melanogaster* has a short generation time, being 10 days long at 25^{o}C reaching the wandering third instar stage after 5 days. Additionally, *Drosophila* development is temperature sensitive, and the generation time can be extended to 20 days by rearing the flies at 18^{o}C (Roote and Prokop 2013, Budnik et al., 2006).

Having been used as a model organism for well over one hundred years there is a is great wealth of knowledge about *Drosophila* biology (Bellen et al., 2010, Roote and Prokop 2013). The *Drosophila* genome consists of ~17,800 genes (as of the latest genome assembly release), split between 4 pairs of chromosomes (less than the 20-25,000 genes across 23 pairs for humans and 20 for mice). This relative simplicity and

the high degree of annotation the *Drosophila* genome has, in addition to the development of genetic tools, makes the fruit fly a powerful system for genetic analysis and manipulation (Bellen et al., 2010, Roote and Prokop 2013).

Despite their size *Drosophila* possess a sophisticated centralised nervous system (Bellen et al., 2010). The *Drosophila* nervous system is plastic yet stereotypic, allowing for reproducible observations of activity-dependant plasticity (Harris and Littleton 2015). Additionally, *Drosophila* larvae and adults have a repertoire of quantifiable behaviours, allowing for genetic screens and epistatic analysis of the genes that underlie behaviour (Bellen et al., 2010).

An important tool to understand when working with *Drosophila* is the GAL4/UAS binary expression system. The GAL4/UAS system is a transcription factor/enhancer pair originally derived from *Saccharomyces cerevisiae* (Fischer et al., 1988). By inserting the GAL4 coding sequence downstream of a gene's promoter GAL4 will become under the influence of the promoter of the gene of interest (Brand and Perrimon 1993). In doing so one can link the expression of a gene of interest to a reporter whose expression is activated by the binding of GAL4 to an upstream UAS sequence (Brand and Perrimon 1993).

Genes can be over-expressed by placing the gene, or a copy of it, under the influence of the UAS promotor sequence and expressing a tissue or cell-type specific GAL4, thereby driving expression of the gene of interest specifically in expression pattern of the GAL4 (Brand and Perrimon 1993).

Gene editing is an important technique in fundamental research for expanding the toolkit for research. Clustered regularly interspaced palindromic repeats (CRISPR)/Cas9 tools have been developed for use in *Drosophila* (Yu et al., 2013,

Bassett et al., 2013, Gratz et al., 2013). When accompanied with a locus-specific guide RNA (gRNA) molecule Cas9 creates double strand breaks in DNA (Sapranauskas et al., 2011). Insertions can be precisely made into the *Drosophila* genome using CRISPR-cas9 to trigger homology directed repair (HDR) (Gratz et al., 2014). CRISPR/Cas9-catalyzed HDR and other CRISPR technologies greatly expands the available toolkit to *Drosophila* researchers *Drosophila* (Yu et al., 2013, Bassett et al., 2013, Gratz et al., 2013).

1.6.2 The central nervous system

The larval ventral nerve cord, part of the larval central nervous system, is important in fly neurobiology due to being a central component of the nervous system, being the site of the axonal terminals of peripheral nervous system (PNS) neurons, interneurons, and the cell bodies and dendrites of motoneurons. The simple, repetitive, and genetically tractable nature of the VNC makes it an ideal location for visualising a range of neuronal types and for the study of circuitry (Landgraf et al., 2003).

In late larval third instar (L3) the central brain and the VNC are kept together in a compact structure. This is unlike the adult fly, where despite being connected, the VNC is located in the anteroventral thorax, separate from the central brain located in the head (Venkatasubramanian et al., 2019).

The larval VNC is segmented in a manner similar to the overall animal with 3 thoracic segments, and 8 abdominal segments (Gowda et al., 2021). The 8 abdominal segments are mostly stereotypical and structurally repetitive between each segment (Gowda et al., 2021).

At the centre of each segment are a left and a right neuropil connected by commissures (Kyriacou 2011). Due to the repetitive nature of the VNC, the left and right neuropil form as two cords running down the length of the VNC (Kyriacou 2011). The cell bodies of neurons that innervate the VNC neuropil exist in the cortex of the VNC that surrounds the neuropil (Hartenstein et al., 2008). Glial cells also make up the cells living in the VNC cortex (Hartenstein et al., 2008).

1.6.3 The neuromuscular junction

1.6.3.1 NMJ layout and imaging

The *Drosophila* larvae is a good model system for studying synaptogenesis (Prokop 2006). *Drosophila* larvae possess 8 abdominal sections (A1-8), with A2-7 being highly similar to each other (Prokop 2006). Each segment has 36 motoneurons innervating 30 muscles (Prokop 2006). The branched structure of the axonal terminals being stereotypical between segments (Prokop 2006). The larval NMJ is highly plastic and subject to activity-dependant plasticity (Prokop 2006).

At 25^{o}C it takes five days from egg-laying for larvae to reach L3 wandering, when they are preparing to pupate. At the NMJ neuronal growth is necessary because as the larval muscles grow, they become less conductive to synaptic transmission, therefore motoneuron neurites expand to facilitate a constant level of signal transmission. Due to the high amounts of synaptogenesis occurring in this model system, and the large size of the synapse, the larval NMJ has been used to study processes that regulate synaptogenesis, such as synaptic plasticity (Prokop 2006).

Much of the research into structural synaptic plasticity has been carried out in the fly's larval stage, specifically late in L3. At this stage of development larvae exhibit a

‘wandering’ behaviour, whereby they emerge from their food source and prepare to undergo pupation. The relatively large size of the larvae make them easier to dissect than earlier larval stages and the wandering behaviour makes them more accessible (Budnik et al., 2006).

The larval NMJ can be accessed by making an incision along the dorsal axis of the larvae and two incisions perpendicular to the dorsal axis on the anterior and posterior of the animal on the dorsal side. The body wall of the larvae can then be opened like a book and the organs can be removed. Access is then available to the NMJ which lies on the surface of the body wall musculature. The sample can then be fixed in Bouin’s solution or formaldehyde to preserve the tissue (Budnik et al., 2006).

The axonal terminal can be identified via immunofluorescent staining of horseradish peroxidase (HRP) of the larval fillet (Menon et al., 2013). The antigen of the anti-HRP antibody is, perhaps surprisingly, not horseradish peroxidase but a set of neuronal-specific glycoproteins (Snow et al., 1987). After staining with an appropriate fluorescent secondary antibody, the fillet can then be mounted and scanned using a confocal microscope to acquire microphotographs of the NMJ.

Motoneuron axons exit the VNC and fasciculate together into three nerves per hemisegment, before diverging to innervate their targets at the body wall. The three nerves are the segmental (SN), intersegmental (ISN) and transverse nerves (TN). The ISN and SN are subdivided into smaller nerves based on the spatial location and orientation of the muscle groups they innervate (Prokop 2006).

The axonal terminal of muscle 6/7 is often analysed as this axonal terminal innervates two muscles and hence has twice as many boutons as other axons (Atwood et al.,

1993). Muscle 6/7 is innervated by two motoneurons from the ISNb nerve: RP3, which produces Ib boutons and MN6/7 which produces the Is boutons (Chiba et al., 1993).

1.6.3.2 Different types of bouton at the Drosophila NMJ

Four types of chemical synapses form at the *Drosophila* NMJ, these are distinguishable from each other by the anatomy of the pre-synaptic boutons. When investigating synaptic morphology at the NMJ it is imperative to know what boutons one is working with as the different types are functionally distinct. Each motoneuron only forms one type of synapse at the NMJ (Atwood et al., 1993, Stocker et al., 2018, Gorczyca et al., 1993).

Type Ib and Is are glutamatergic, type II synapses are octopaminergic and type III synapses are insulinergic (Prokop 2006, Stocker et al., 2018, Gorczyca et al., 1993). Type I synapses, being glutamatergic are excitatory, while type II and III synapses thought to have a modulatory function (Aponte-Santiago et al., 2020).

Most synapses at the *Drosophila* NMJ are glutamatergic, with 24 motoneurons possessing type Ib boutons and ~2 motoneurons forming type Is boutons (Aponte-Santiago et al., 2020). Type II and III synapses are uncommon, with ~3 Type II bouton forming motoneurons and ~1 Type III motoneuron innervating muscle 12. Type Ib and Is boutons are present at NMJ 6/7 but not type II or III boutons (Atwood et al., 1993).

Type I boutons can be identified by staining the NMJ to visualise the distribution of PSD protein Dlg. Type I boutons can be located by densities of Dlg protein, which are absent for Type II boutons (Lahey et al., 1994). Type Ib boutons are bigger than Is boutons. Type II boutons are typically smaller than Is, while Type III boutons are a typically between the sizes of Type Ib and Is boutons (Stocker et al., 2018).

Synaptic transmission in glutamatergic synapses at the *Drosophila* NMJ can be either an evoked or spontaneous release (Melom et al., 2013). Evoked releases are the result of an action potential triggering the fusion of glutamate-containing vesicles to the pre-synaptic membrane, releasing a large amount of glutamate into the synaptic cleft (Melom et al., 2013). Spontaneous releases are action potential and calcium-independent and appear to occur stochastically (Melom et al., 2013). Spontaneous releases are significantly smaller than evoked releases and are single quanta (Melom et al., 2013).

Although both type Is and Ib boutons are glutamatergic they, have different evoked synaptic transmission properties (Aponte-Santiago and Littleton 2020). Motoneurons that produce Is boutons have phasic synaptic transmission, meaning they have brief but strong firing (Aponte-Santiago and Littleton 2020). In Drosophila type Is boutons release 2-3 times more glutamate than Ib boutons (Aponte-Santiago and Littleton 2020). Motoneurons that produce Ib boutons have tonic synaptic transmission at the NMJ, and produce weaker but sustained firing over time. Ib boutons contain more synaptic vesicles and mitochondria than Is boutons, allowing them to sustain synaptic transmission for longer (Aponte-Santiago and Littleton 2020). Phasic boutons are responsible for producing rapid and powerful muscle movements, such as those in escape behaviours, whereas tonic boutons are responsible for spontaneous or voluntary muscle movement e.g., during foraging behaviour (Aponte-Santiago and Littleton 2020).

Glutamatergic boutons first form as ‘ghost boutons’, which lack apposition by a PSD and often lack active zones (Menon et al., 2013). Ghost boutons can be identified in immunofluorescence staining by being HRP+ but Dlg- (Menon et al., 2013). Ghost

boutons are transitory structures as the bouton either stabilises or retracts (Menon et al., 2013). If the bouton stabilises and becomes a mature bouton it gains apposition by a PSD, which can be labelled with an anti-Dlg staining (Menon et al., 2013).

Ghost boutons are rare in wildtype larvae; however, the number of ghost boutons can increase when motoneurons undergo potentiating activity (Ataman et al., 2008). Ghost bouton number can also increase when genes involved in synaptogenesis are manipulated (Menon et al., 2013).

Ghost boutons have been used as markers of activity-dependent structural plasticity. The presence of ghost boutons at the NMJ can indicate a disturbance in structural plasticity (Menon et al., 2013). Ghost boutons can indicate alterations in synaptic stability, which is important for long-lasting structural plasticity (Menon et al., 2013).

1.6.3.3 Active zones

Active zones are the sites of neurotransmitter release in the presynaptic cell of the NMJ (Vactor and Sigrist 2017). Due to the importance of AZ function in synaptic transmission alterations to AZs are important indicators of synaptic plasticity. The abundance of active zones is a quantifiable metric for measuring structural plasticity (Ulian-Benitez et al., 2017).

At the *Drosophila* NMJ Brp is a marker for the active zone and is a key component of the AZ machinery (Vactor and Sigrist 2017). Brp recruits the voltage-gated Ca^{2+} channel Cac to the active zone and is important for evoked releases (Fouquet et al., 2009, Kawasaki et al., 2000).

Brp forms toroid-like structure at active zones called a T-bar (Vactor and Sigrist 2017). The N-terminal of Brp proteins in T-bars are associated with Cac, while the C-terminal end is important for the tethering and recruitment of synaptic vesicles.

In *Drosophila* RIM-binding protein (RBP) forms a ring around the core of the T-bar and encircles the Cac channels (Vactor and Sigrist 2017). RBP appears to be important for the formation and maintenance of active zone structure as RBP mutants possess structurally defective active zones (Sigrist and Schmitz 2010). Around the T-bar is the active zone cytomatrix, a network of proteins that are responsible for the assembly and regulation of the active zone (Sigrist and Schmitz 2010).

1.6.3.4 Post-synaptic densities

In apposition to the active zone in the post-synaptic muscle cell is the post-synaptic density (Budnik et al., 1996). The scaffold protein Dlg is enriched in the PSD (Budnik et al., 1996). Dlg is a membrane-associated guanylate kinase (MAGUK) family member (Budnik et al., 1996). Dlg is important for the development and structure of the PSD, and via its PDZ domain is responsible for the recruitment of K^+ channels, neurotransmitter receptors and cell adhesion molecules (Budnik et al., 1996).

An essential component of the PSD are ligand gated Na^+ channels, which are required for synaptic transmission. Implantation of iGluRs into the post-synaptic membrane can be activity-dependent and is important for potentiating the post-synapse during plasticity (Schmid et al., 2008).

1.6.3.5 Inducing synaptic plasticity at the Drosophila larval NMJ

To study activity-dependent structural plasticity one must be able to induce it. There are different methods of inducing activity-dependent structural plasticity at the larval NMJ with different advantages and disadvantages. Temperature sensitive alleles of ion channels and synaptic genes have been used to induce or inhibit neuronal activity (Guan et al., 2005). As previously mentioned, mutations in K+ channels, such as *slowpoke*, *eag*, and *Sh*, can possess hyperexcitability phenotypes (Guan et al., 2005). In these mutants the permeability of the hyperpolarising anion K+ is impaired resulting in enhanced neuronal activity. Furthermore, mutations in Na+ channels, such as *paralytic*, can reduce activity (Guan et al., 2005).

Some alleles of these genes are temperature-sensitive, meaning that the protein operates nominally below a certain threshold temperature. After reaching this threshold the mutant phenotype may be induced (Ganetzky et al., 1986). This is useful for ruling out phenotypes that may be caused by altering the development of the organism. For many temperature-sensitive channels this threshold is at 38^{o}C (Ganetzky et al., 1986).

Repeated washes of dissected larval NMJ preparations with a high K^+ concentration saline has been reported to induce the formation of ghost boutons (Maldonado-Díaz et al., 2021). This method of inducing structural plasticity is simple and effective at producing ghost boutons (Maldonado-Díaz et al., 2021). A drawback of this technique is that it can only be performed in dissected tissue and the preparation dies soon after, making this not ideal for studying long-term effects of activity. Additionally, this method is non-specific and may cause excitotoxicity (Maldonado-Díaz et al., 2021).

TrpA1 is a temperature sensitive member of the transient receptor potential (TRP) family of cation channels (Hamada et al., 2008). TrpA1 is expressed endogenously in *Drosophila* and mediates the detection of changes in temperature (Luo et al., 2017). TrpA1 expression can be manipulated using the UAS/GAL4 system to localise TrpA1 to desired neurons (Hamada et al., 2008). TrpA1 is activated at 25^{o}C and can cause a significant increase to axonal terminal length (Pulver et al., 2009, Oswald et al., 2018). This effect is enhanced at 27^{o}C, which reflects electrophysiological data indicating that TrpA1 is activated more strongly at 27^{o}C (Pulver et al., 2009, Oswald et al., 2018).

In addition to temperature, activity-dependent structural plasticity can be modulated using light. The green light sensitive cation channel Channelrhodopsin-2 (ChR-2) was initially discovered in the green alga *Chlamydomonas reinhardtii* (Nagel et al., 2003). ChR-2 and its engineered derivatives have been used to depolarise neurons via illumination. Red activated channelrhodopsin (ReaChR) was developed for use in adult *Drosophila* CNS, as red light penetrates through the cuticle significantly better than shorter wavelengths (Inagaki et al., 2014).

Using light to induce activity, rather than heat may avoid experimental interference from behavioural and/or physiological responses to the abrupt changes in temperature (Simpson et al., 2018). Furthermore, a beam of light may be used with greater physical precision than temperature changes, as temperature affects the whole body at once whereas a light beam could be directed to specific neurons (Simpson et al., 2018). Therefore, optogenetic stimulation is a promising method for the induction of activity-dependent plasticity in *Drosophila*.

1.7 Aims and Objectives

The aim of this thesis was to investigate the potential role that the Drosophila kinase-less Trk-like Kek receptors play in molecular mechanisms of activity-dependent structural synaptic plasticity. It was critical to know if the Keks were functionally similar to each other, thereby potentially redundantly sharing the same function(s). Conversely, if they were functionally diverse instead, this would add an additional layer of complexity to *Drosophila* neurotrophin signalling.

I sought to address the aims of this thesis via pursuing the following objectives:

- Objective 1 (Chapter 3): To investigate the spatial distribution of Keks in the *Drosophila* larval nervous system and within neurons. To this end, I used RT-PCR, generated a *kek5*-GAL4 knock-in with CRISPR-Cas9 gene editing, generated a Kek6-TSTEP endogenous protein fusion with CRISPR-Cas9 gene editing and GOLIC+-enhanced homologous recombination, and I used overexpression of *kek*-RFP protein fusions to visualise the subcellular distributions of Keks.

- Objective 2 (Chapter 4): To investigate whether all Keks can regulate Ca^{2+} dynamics, and if so, how they do this. To accomplish this objective, I used Western blot to investigate the influence of *kek* over-expression on CaMKII, used the Ca^{2+} reporter GCaMP with ReaChR optogenetics in *kek* overexpressing larvae to study how *kek*s influence post-stimulation Ca^{2+} dynamics, and an endogenously tagged allele of the voltage-gated plasma membrane calcium channel Cac to investigate how *kek4* and *-6* can influence channel distribution and clustering at the synapse.

- Objective 3 (Chapter 5): To investigate the function of Keks in activity-dependent structural synaptic plasticity. To tackle this objective, I used optogenetics to activate neurons and immunofluorescent staining of axonal marker HRP and synaptic markers Dlg and Brp to study the effect of *kek4* and -*6* overexpression and loss of function on activity-dependent structural plasticity in NMJ morphology and synaptogenesis.

The findings would contribute to understanding how the nervous system adapts to experience, not only in flies, but impacting also in humans, where the functions of numerous kinase-less Trk receptors remain scarcely investigated.

2 METHODS

2.1 Fly Husbandry

Drosophila melanogaster were cultured in vials with a standard cornmeal/agar media. Crosses and working stocks were incubated at 25^{o}C with a 12-hour light/dark cycle and were transferred to fresh vials every 2-5 days. Vials containing larvae were watered as needed to prevent dehydration. Fly stocks were incubated at 18^{o}C with a 12-hour light/dark cycle and were transferred to fresh vials every 4 weeks.

Virgin female flies were collected once in the morning, the virgin-producing vials were then incubated at 25^{o}C for 8 hours before another round of collection. After this second round of collection, the virgin-producing vials were incubated at 18^{o}C for 16 hours. At this stage, the morning collection occurs again.

To minimize the chance for release of genetically modified organisms into the environment, fly pushing was performed in a dedicated fly room and undesirable flies were destroyed. The selection and handling of flies was performed while the flies were anesthetised with CO_2. Table 2.1 and 2.2 lists the genetic elements and fly lines used in this project.

2.1.1 Preparation of fly food for Ca^{2+} imaging

Houston fly food was melted in the microwave until liquid. 6ml of molten food was dispensed into individual plastic vials. After the food had cooled to below 50^{o}C, 60µl of 50mM All-trans retinal (ATR), the channelrhodopsin co-factor, was added and mixed into the food until homogenous. The ATR-containing food vials were then plugged with cotton balls and wrapped in aluminium foil to protect them from light. ATR-containing

Table 2.1 – Genetic elements used

Genetic element	Source
C(I)DX	Muller, 1943
w	Safir, 1913
Fm7	Merriam, 1969
Sb	Beaton et al., 1988, Shearn et al., 1971
Tm3-Ser	Campos-Ortega and Haenlin, 1992
Irregular facets (IF)	Ives, 1967
CyO	Oster, 1956
MKRS	McCarron et al., 1973
SM6a-Tm6B	Basu et al., 1999
Fm7actGFP	Wasser and Chia, 2003
y	Sturtevant, 1915
Sna[Sco]	Krivshenko, 1959
CyO P[Cre Recombinase}	Siegal and Hartl, 2000
Kek5-GFP	Hidalgo Lab, Joan Roig
10xUAS-myr-Td-Tomato	Pfeiffer et al., 2010
TM2	Lewis, 1952
TM6B	Craymer, 1984
109(2)80-GAL4	Gao et al., 1999
UAS-mCD8::GFP	Lee and Luo, 1999
uas-brp-short-Cherry D3	Kremer et al., 2010
D42-GAL4	Yeh et al., 1995

bam898-CF	Chen et al., 2020
3xriTS Rac^{V12}	Chen et al., 2020
nsybLexA	Shearin et al., 2013
Tm3 Sb	Lindsley and Zimm, 1992
Kek6-TSTEP	This work, Koles et al., 2016
uasReaChR	Inagaki et al., 2014
GMR-GAL4	Freeman, 1996
uas-IVS-GCAMP6m	Chen et al., 2013
uas-Kek1-RFP	Bishop, 2014
uas-Kek2-RFP	Bishop, 2014
uas-Kek3-RFP	Bishop, 2014
uas-Kek4-RFP	Bishop, 2014
uas-Kek5-RFP	Bishop, 2014
uas-Kek6-RFP	Bishop, 2014
Cac-sfGFP	Gratz et al., 2019
kek4 ^{23}	Bishop, 2014
kek4 ^{20}	Bishop, 2014
kek6 ^{35}	Bishop, 2014
kek6 ^{34}	Bishop, 2014

Table 2.2 – Fly stocks used

Genotype	Source
OregonR	Bloomington #5, wildtype flies collected in or before 1925 in Roseburg, Oregon. (Lidsley and Grell, 1968)
C(I)DX / Fm7 ; + ; Sb / Tm3-Ser	Hidalgo Lab collection
w ; IF/CyO ; MKRS/Tm6B	Hidalgo Lab collection
w ; + ; MKRS/Tm6B	Hidalgo Lab collection
w ; IF/CyO ; +	Hidalgo Lab collection
w ; IF;MKRS / Sn6aTm6B	Hidalgo Lab, Zhu et al., 2008
w+ Kek5-T2A-GAL4 (3xp3-DsRed) / Fm7actGFP	This work
yw ; Sna[Sco]/CyO, P{Cre Recombinase}	Bloomington #1092
Kek5-GFP ; + ; +	Hidalgo Lab, Joan Roig
w ; + ; 10xUAS-myr-Td-Tomato^{VK0005}	Gift from B. Pfeiffer
Kek5-GFP/Fm7 ; + ; 10xUAS-myr-Td-Tomato^{VK0005}	This work
w ; + ; uasKek1-RFP / TM2	Bishop 2014
w ; uasKek2-RFP / CyO	Bishop 2014
w ; uasKek3-RFP / CyO	Bishop 2014
w ; + ; uasKek4-RFP / MKRS	Bishop 2014
w : + ; uasKek5-RFP / TM6B	Bishop 2014
w ; + ; uasKek6-RFP / MKRS	Bishop 2014
yw ; 109(2)80-GAL4, UAS-mCD8::GFP	Bloomington #8768
w ; uas-brp-short-Cherry D3	Gift from G. Tavosanis

w ; + ; D42-GAL4 / Tm6B	Bloomington #8816
bam898-CF ; 3xriTS Rac^{V12} / CyO	Gift from T. Lee
nsybLexA ; Tm3 Sb / Tm6B	Gift from T. Lee
w ; + ; Kek6-TSTEP / Tm6B	This work
GMR-GAL4 (MF815)	Gift from M. Freeman
w ; uas-IVS-GCAMP6m ; D42-GAL4 / Tm6B	Hidalgo Lab, Suzana Ulian-Benitez
w ; uasReaChR ^{attp40}	Bloomington #53741
w ; + ; uasReaChR	Inagaki et al., 2014
w ; uasReaChR ; uasKek1-RFP / Sn6aTm6B	This work
w ; uasKek2-RFP / CyO ; uasReaChR / Tm6B	This work
w ; uasKek3-RFP ; uasReaChR / Sm6aTm6B	This work
w ; uasReaChR / CyO ; uasKek4-RFP / Tm6B	This work
w ; uasReaChR ; uasKek5-RFP / Sn6aTm6B	This work
w ; uasReaChR ; uasKek6-RFP / Sn6aTm6B	Hidalgo Lab, Suzana Ulian-Benitez
Cac-sfGFP ; + ; +	Gift from K. O'Connor-Giles
Cac-sfGFP/Fm7 : + ; Kek6-TSTEP / Tm6B	This work
Cac-sfGFP/Fm7 ; + ; D42-GAL4 / Tm6B	This work
kek4 ^{23} ; + / Sn6aTm6B	Bishop 2014
kek4 ^{20} ; + / Sn6aTm6B	Bishop 2014
w ; kek4 ^{23} / CyO ; D42-GAL4 / Tm6B	This work
w ; kek4 ^{20} ; uas-ReaChR / Sn6aTm6B	This work
w ; uasReaChR ; kek6 ^{35} / Tm6B	Hidalgo Lab, Suzana Ulian-Benitez

w ; + ; D42-GAL4, kek6 ^{34} */ Tm6B*	Hidalgo Lab, Suzana Ulian-Benitez

food was allowed to set and was kept at 4^{o}C until used. ATR-containing food was used within 1 week of manufacture.

2.1.2 Preparation of fly food for optogenetic plasticity experiments

Fly food was made in weekly batches where the amount of food per batch was sufficient to meet the required amount for that week's experiments. The reagents used, and their quantities in producing an example 50ml batch of food are given in Table 2.3

To produce an example 50ml batch of food 3.57g of table sugar and 0.14g of table salt were added to a 200ml glass beaker. 7.1ml of ddH_2O was then added to the beaker, and the beaker was placed on a magnetic hot plate stirrer, an appropriately sized magnetic fly was added to the beaker and the hot plate stirrer was set to ~70^{o}C and 300 RPM. A sheet of aluminium foil was used to cover the beaker to prevent contamination, and to trap condensation and heat.

While the sugar and salt were dissolving, 3.57g of dried active yeast powder was dissolved in 7.1 ml of ddH_2O with the aid of a microwave in a separate beaker. The dissolved yeast was then added to the stirring beaker with the warm sugar and salt solution. In a separate beaker 0.43g of Agar was dissolved into 7.1 ml of ddH_2O by heating in the microwave. The agar was added to the warm stirring beaker while hot. Similarly, 1.79g of flour was dissolved into 14.2g of ddH_2O before being added to the mixture on the stirring hotplate. 1.07ml of concentrated grape juice was then added to the mixture in the hotplate beaker.

The mixture was brought up to a volume of 50ml with ddH_2O and was brought to a light boil, before being allowed to cool while spinning. When the mixture had fallen to ~60oC 210µl of propionic acid was added and was incorporated into the mixture.

Table 2.3 – Fly food for optogenetically induced plasticity experiments

Reagent	Amount for 50ml batch
ddH_2O	To 50ml
Table sugar	3.57g
Table salt	0.14g
Active dry yeast powder	3.57g
Agar (powder)	0.43g
Plain flour	1.79g
Concentrated grape juice	1.07ml
Propionic acid	210µl

The molten fly food was then decanted into empty fly food vials with 2ml of food per vial. Any leftover food was stored in a glass bottle in at 4^{o}C for up to 1 week. A portion of the vials were set aside for the no optogenetic stimulation controls. For the optogenetic stimulation condition food 20µl of ATR was added and mixed until homogenous into each 2ml food containing vials while the food was still molten.

All vials were wrapped in aluminium foil to prevent photodegradation of ATR, and for the sake of experimental fairness in the case of non-ATR food. Vials were labelled appropriately and were stored at 4^{o}C until use or until 1 week old whereupon they were discarded.

2.1.3 Preparation of grape juice plates

Grape juice plates were prepared at a scale proportionate to need, an example batch of 300ml is described here. 6.6g of agar was dissolved in 262ml of ddH_2O by bringing to a light boil in the microwave. The total volume of the molten agar solution was brought up to 300ml with concentrated grape juice. The molten agar/grape juice was then decanted into 90mm diameter plastic petri dishes with 15ml per dish. Plates were stored at 4^{o}C until use.

2.2 Genetics

Conventional Drosophila genetics protocols were followed for changing balancers, 2nd and 3rd combinations, X and 3rd combinations (Appendix I, Fig. A1.1 and A1.2 respectively). The protocol for the removal of the *3XP3-RFP* cassette used standard techniques to combine chromosomes from different fly lines (Fig. A1.3). CRE recombinase on the second chromosome was combined with the *kek5-GAL4*$^{3XP3\text{-}RFP}$

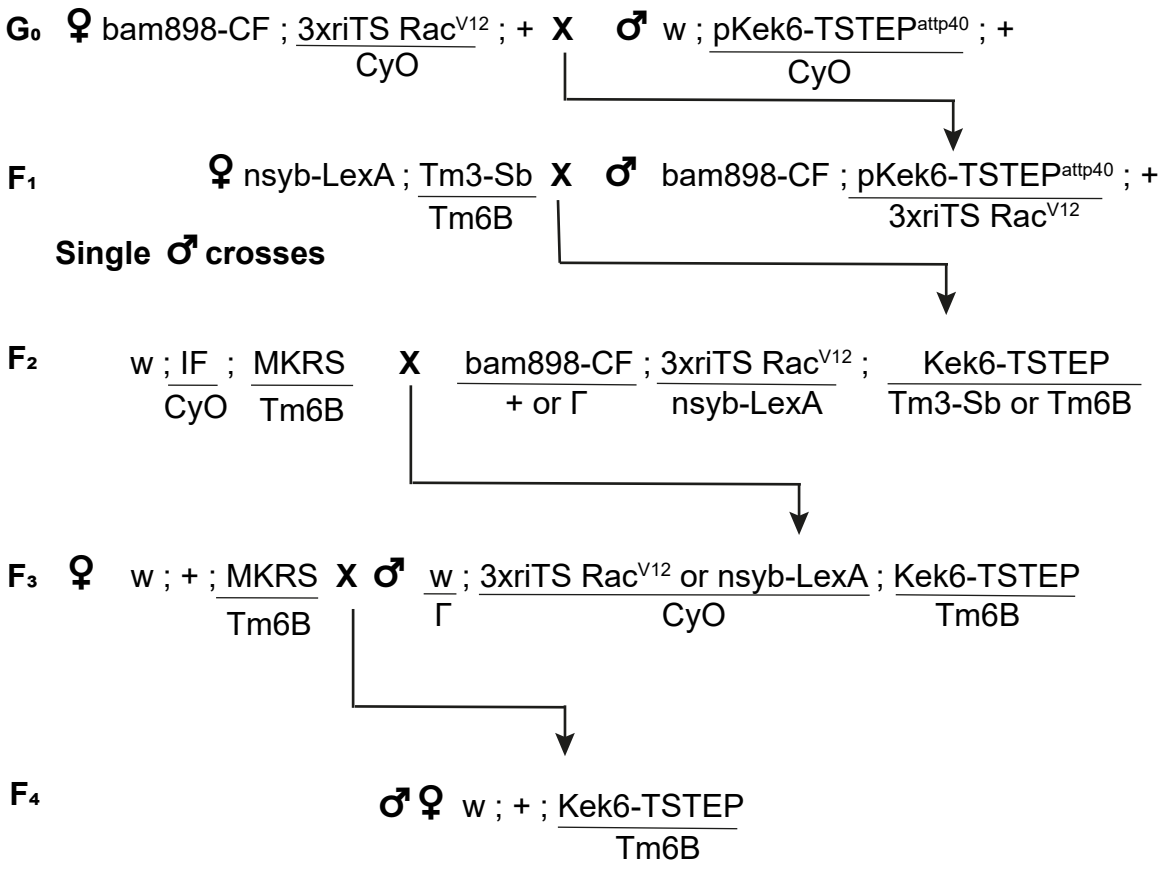
line on X to remove *3XP3-RFP*. Progeny without *3XP3-RFP* were isolated and balanced to create a stock.

For the generation of the *kek6-TSTEP* line, embryos were injected by BestGene Inc. with the donor plasmids to insert the construct into a *phiC31* site. Transgenic flies that had successfully had the construct inserted were screened for using a protocol described by Chen et al 2020.

The *kek6-TSTEP* fly line was generated following the enhanced GOLIC+ protocol described by Chen et al 2020 (Fig. 2.1). Briefly, to create a protein fusion of a gene on the 3rd chromosome, male flies carrying the donor construct in *attP40* were crossed to *bam898-CF ; 3xRiTS Rac^{V12} / CyO* females. The genetic element *bam898-CF* expresses Cas9 and Flippase under the control of the *bam898* promoter which is restricted to germline cells (Chen et al., 2020). The full name of genetic element *3xRiTS Rac^{V12} is 3XLexAopo2-riTS-RacV^{12} (3XP3-RFP)*. It is used in eGOLIC+ to ensure candidates undergo the lethality screen (Chen et al., 2020). In the presence of LexA, *3xRiTS Rac^{V12}* drives the expression of a repressible constitutively active GTPase Rac^{V12} which is toxic to cells when expressed. (Chen et al., 2020) Rac^{V12} can be repressed by the expression of an RNAi which is expressed when the construct has successfully been inserted into the genome (Chen et al., 2020). The *3XP3-RFP* marker allows flies that have passed through and survived the lethality screen to be selected for (Chen et al., 2020).

CRISPR knock-in events occurred in the germline cells of the progeny of this cross. These F1 flies were then crossed to *nsyb-LexA*, which in the F2 drives lethality by overexpressing a constitutively active GTPase in all neurons. Lethality occurs in the pupal stage.

Figure 2.1 - Generation of Kek6-TSTEP with GOLIC+



Flies with a successful CRISPR knock-in are spared from the lethality screen by expressing an RNAi targeting the constitutively active GTPase. Survivors of the lethality screen are crossed to a balancer line and the candidate protein fusion is balanced. Candidate knock-in lines were then screened by PCR.

2.3 CNS Dissections

Third instar wandering larvae were anesthetised in ice-cold water prior to dissection in cold phosphate buffer saline (PBS). During dissection, the CNS was extracted from the larvae. The larval brain is then immediately placed into 4% formaldehyde on ice and are fixed for up to 20 minutes. Additional brains are acquired during the 20 minutes following the dissection of the first larva.

After the 20 minutes since the first dissection has elapsed, the larval brains were incubated in 4% formaldehyde at room temperature. After 45 minutes had elapsed, the fixative was removed and the brains were washed with phosphate buffered saline, 0.3% Triton-X (0.3% PBT) for 15 minutes, 5 times. The dissected brains were then stained with antibodies or mounted onto microscope slides in Vectashield without staining.

2.4 Body Wall Dissections

Third instar wandering larvae were dissected using a standard protocol described by Budnik et al 2006. Larvae were placed in a 40µl drop of ice-cold Ca^{2+}-free HL3 saline on a dissection platform. Pins, magnetically attached to the platform, were used to

restrain the larvae, by pinning the anterior and posterior ends of the larvae to the platform. Larvae were positioned dorsal side up for all dissections.

Using a set of micro-scissors, lateral incisions were made on the dorsal side near the anterior and posterior ends of the larvae. Following this, an incision along the dorsal midline was made connecting the two lateral incisions. The sides of the larvae between the two lateral incisions could then be pulled back using the pins, opening the larvae like a book. The inner organs of the larvae were then removed with sharp forceps. At this stage the larva was then pulled taut with the pins, and the saline was replaced with Bouin's solution (HT10132 SIGMA) for 10s before the being transferred to a multi-well plate for further fixation.

Larvae were allowed to wait for up to 10 minutes while other larvae were being dissected before further fixation began. Dissected larvae were incubated Bouin's solution, following which they were washed for 15 minutes in 0.1% PBT 6 times. Dissected larvae were then stained with antibodies to improve signal strength.

2.5 Immunostaining

After larvae had been dissected, fixed, and washed, larval brains were incubated in 10% Normal Goat Serum (NGS) in 0.3% PBT overnight at 4^{o}C to reduce background noise. NMJ preps were incubated in 10% NGS in 0.1% PBT.

The NGS was then removed and 100µl of primary antibody (diluted in 10% NGS in 0.3% PBT) was added to the brains, and 65µl of primary antibody was added to the NMJ preps. The samples were incubated in primary antibody overnight at 4^{o}C, after

which the primary antibody was removed and the brains were washed with 0.3% PBT for 15 minutes 4 times; NMJ preps were washed in 0.1% PBT for 15 minutes 5 times.

Any remaining PBT was removed and 100µl of secondary antibody was added (diluted in 10% NGS in 0.3% PBT for the CNS, 0.1% PBT for NMJ. The samples were incubated in secondary antibody overnight at 4^{o}C and were then washed with 0.3% PBT (0.1% for NMJ preps) for 15 minutes 5 times, and were washed for a final time in PBS for 15 minutes. Brains and NMJ preps were then mounted onto microscope slides in Vectashield®. The list of primary and secondary antibodies used in this thesis, and their dilutions, are detailed in Table 2.4.

2.6 Microscopy

All confocal microscopy was provided by the Birmingham Advanced Light Microscopy (BALM) facility. Unless otherwise stated, all images were acquired using a Zeiss LSM 710 inverted confocal microscope, and were analysed and processed in ImageJ/Fiji, and were acquired at a size of 1024x1024 pixels. VNC images were acquired using a 20x objective, transverse projections were generated using the 'Reslice' tool in Fiji. Images of PNS hemisegments were acquired by using the 'Tile' tool in Zen Black set to 1x3 512x512 pixel images. Images of the NMJ were acquired using a Zeiss 40x oil objective.

Images of boutons were acquired on a LSM 900 using the quasi-super-resolution module AIRYSCAN2. These images were acquired using a 60x oil objective and a zoom level of x4. For the experiments in Chapter 4 where the signal volume from these images were quantified, analysis was performed in Imaris. Here, signal volume was segmented via thresholding.

Table 2.4 –Antibodies used

Name	*Dilution used*	*Source*
Rabbit anti-GFP	1:200	Thermofisher (A11122)
Chicken anti-GFP	1:500	Aves (GFP-1010)
Rabbit anti-DsRed	1:100	Clonteck (632496)
Mouse anti-mCherry	1:20	DSHB (3a11-s 1 ea)
Mouse anti-22C10	1:5	DSHB
Mouse anti-NC82	1:10	DSHB
Rabbit anti-HRP	1:200	Jackson Immunoresearch (323-005-021)
Mouse anti-CAMKII	1:1000	Cosmo Bio (TNL-001-CAM)
Mouse anti-ß-Tubulin	1:1000	Sigma (T9026)
Mouse anti-Dlg	1:10	DSHB (4F3)
Goat anti-Rabbit 488	1:250	Molecular Probes (A11034)
Goat anti-Chicken 488	1:250	Molecular Probes (A11039)
Donkey anti-Rabbit 546	1:250	Molecular Probes (A10040)
Goat anti-Mouse 546	1:250	Molecular Probes (A11030)
Goat anti-Mouse 647	1:250	Molecular Probes (A21236)
Horse anti-Mouse, cross-linked with Horseradish Peroxidase	1:1000	Vector Laboratories (PI-2000)

For the experiments in Chapter 5 investigating NMJ morphology images of the axonal terminal were acquired using a Zeiss LSM 900 and a set of settings were used for all acquisitions. There images were acquired on a Zeiss 40x oil lens with a zoom of 0.9. All images were acquired with dimensions of 1024x1024 pixels, with a pixel depth of 16-bit. Z-stacks were acquired at varying total ranges in order to fully capture the axonal terminal of NMJ 6/7 but had a consistent step size of 0.5µm. Across all images the digital gain was set to 1, and the channel gain was set to 518.96 V for the 488 channel and 483.90 V for the 647 channel. For images with anti-NC82 stained NMJs, the laser power for the 488 channel was 44.99% and for the 647 channel was 79.19%. For images with anti-Dlg stained NMJs, the laser power for the 488 channel was 42.71% and was 85.95% for the 647 channel.

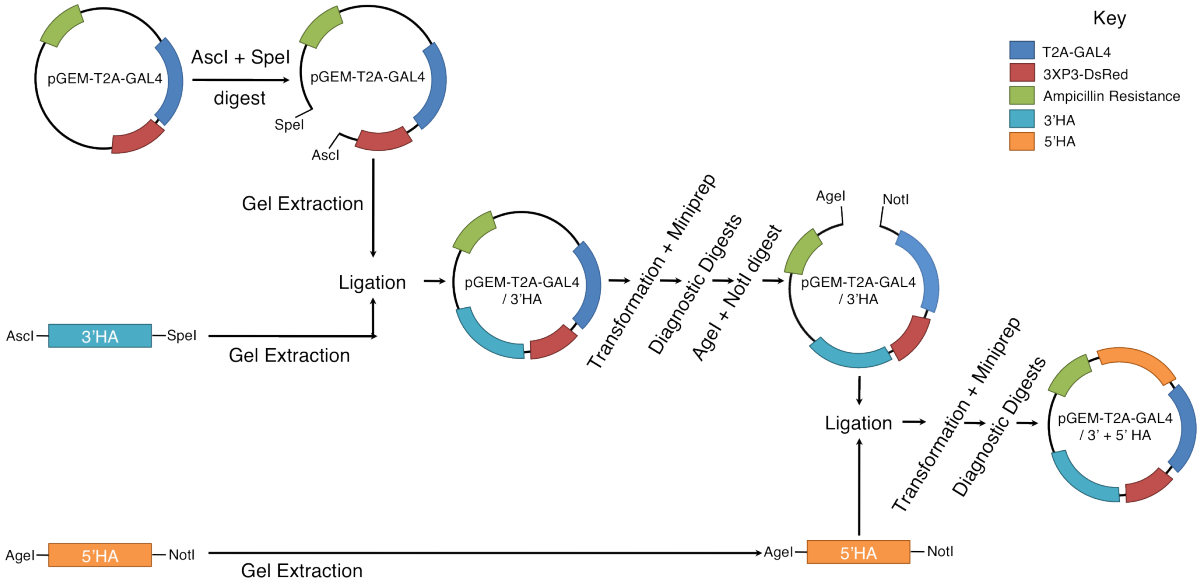
Images for these experiments were also acquired in order to quantify the muscle surface area of muscle 6 and 7. These images were acquired using a Zeiss 20x oil immersion lens at varying zoom level in order to fit the entirety of the muscles into the field of view. In addition to 488 and 647 channels, a transmitted light channel was used for these images in order to better visualise the muscles.

2.7 Molecular biology

2.7.1 Kek-5 GAL4 cloning strategy

To clone pT-GEM(2)-Kek-5 HRs the strategy was based on the protocol described by Gratz et al 2015, was followed (Fig. 2.2). The start codon of *kek5* was found using cDNA transcripts from Flybase. The homologous regions (HRs) for *kek5* were cloned into pT-GEM(2) (Diao et al 2016) via conventional cloning with restriction enzymes. The primers for the HRs were designed with restriction enzyme sites on their 5’ end,

Figure 2.2 - Cloning strategy for Kek5-T2A-GAL4



for the 5'HR these were AgeI on the forward primer and NotI on the reverse. For the 3'HR these sites were for AscI and SpeI respectively. The primers were also designed with an additional 5-7 bases on their 5' end to ensure efficient endonuclease activity. The two HRs were then obtained via PCR of OregonR genomic DNA.

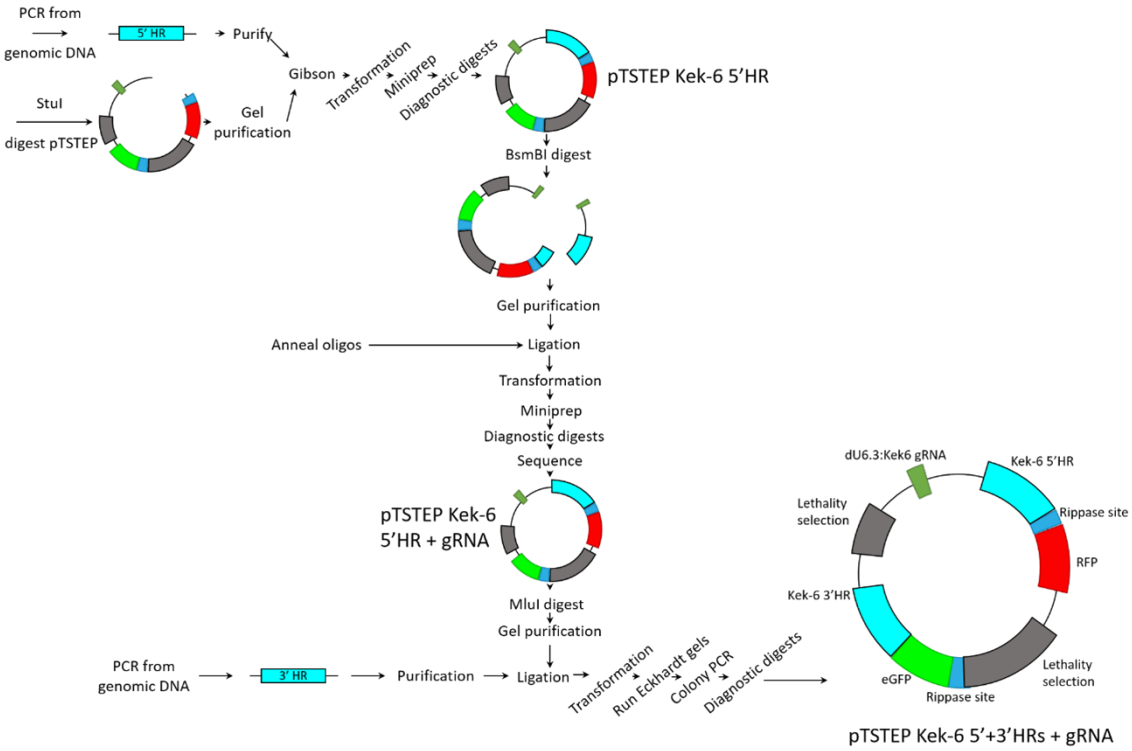
The 3'HR was arbitrarily selected to be cloned first. The pT-GEM(2) vector and the 3'HR were digested with AscI and SpeI, and were subsequently purified via gel extraction. The two were then ligated together with T4 DNA ligase and their ligation product was chemically transformed into NEB 5-alpha competent cells. The intermediate plasmid pT-GEM(2)-Kek-5 3'HR was isolated from single colonies via Miniprep and was validated via restriction digest. The 5'HR was then cloned into pT-GEM(2)-Kek-5 3'HR in a similar manner to the 3'HR. After the final construct had been characterised via restriction digest, both kek-5 HRs on the construct were then sequenced to check their integrity in order to ensure successful HDR.

2.7.2 Kek6 T-STEP cloning strategy

The strategy used to clone the Kek6 pT-STEP construct is outlined in Fig. 2.3. The T-STEP tag was designed to be fused to the C-terminal end of the Kek6 protein. Currently T-STEP has only been developed for C-terminal ends. Additionally, the signal peptide of Kek6 lies at the N-terminal end, the potential disruption of which would result in inaccurate localisation of Kek6. The end of the *kek6* coding sequence was found using cDNA transcripts submitted to Flybase.

The *kek6* 5'HR was cloned into pT-STEP via Gibson cloning (NEB HiFi DNA Assembly). Following validation that the 5'HR had been successfully ligated into pT-STEP, the *kek6* gRNA was ligated into pT-STEP-*kek6* 5'HR. The *kek6* 3'HR was

Figure 2.3 - Cloning strategy for *kek6-TSTEP*



cloned into pT-STEP *kek6* 5'HR + gRNA via conventional cloning with restriction enzyme MluI. Both *kek6* HRs were produced from PCR of OregonR genomic DNA.

As the *kek6* 3'HR was cloned into a single MluI site it could have been ligated in either orientation or the plasmid may have re-ligated with itself. To select for successful ligations 36 colonies were ran on an Eckhardt gel, with the promising 19 candidates being further screened by colony PCR, the remaining 4 candidates were then characterised by restriction digest, revealing 2 successful clones. Following further validation via Sanger sequencing, one of these successful clones was then selected for microinjection.

2.7.3 Genomic DNA extraction

Genomic DNA was purified from whole flies using an Invitrogen Purelink Genomic DNA kit following the protocol provided with the kit. In sacrifice, 15-20 flies were frozen in a microcentrifuge tube overnight at -80^{o}C. 180µl of Genomic digestion buffer was added to the frozen flies, which were then crushed with a P1000 pipette tip. 20µl of Proteinase K was added to crushed flies and buffer. The crushed flies, buffer and proteinase was incubated at 55^{o}C for 3-4 hours.

20µl of RNAse A was then added to the mix, which was then incubated for 2 minutes at room temperature. The crushed and digested flies were then centrifuged for 5 minutes at 13,000 RPM on a table-top centrifuge. The supernatant was transferred to a clean microcentrifuge tube and was mixed thoroughly with 200µl of Genomic Binding Buffer. 200µl of 100% ethanol was then added to the supernatant, and was mixed until homogenous.

The supernatant, ethanol and buffer was then placed into a spin column that was then centrifuged for 1 minute at 10,000 g. The flow-through was then discarded and column was then washed by running 500µl of Wash Buffer 1 through the tube at 10,000 g for 1 minute. The flow-through was discarded and the column was washed again with 500µl of Wash Buffer 2 for 3 minutes at 10,000 g. The flow-through was discarded and any remaining wash buffer was removed from the column by centrifuging for 1 minute at 13,000 RPM.

The spin column was then placed in a clean microcentrifuge tube. 75µl of Genomic elution buffer was then added to the tube, which was then incubated for 1 minute. The elution buffer was then passed through the column by centrifuging for 1 minute at 13,000 RPM. The elution buffer and the eluted DNA was then passed back through the column by centrifugation for 1 minute at 13,000 RPM to increase the yield of DNA. The concentration of the DNA was then measured using a Nanodrop spectrophotometer.

2.7.4 PCR

Two DNA polymerases have been used thus far in this project: Promega GoTaq Polymerase and Thermofisher Phusion Polymerase. PCR reactions have been set up following the protocol provided for each polymerase by their manufacturers.

Primer Tm has been estimated using the manufacturers' online Tm calculators (Promega Biomath calculator and Thermofisher Tm calculator respectively). Primer dimer formation has been estimated using Thermofisher's 'Multiple Primer Analyzer' online tool. Table 2.5 lists the primers used in this project.

Table 2.5 –Primers used

Name	Sequence
Kek1seqFwd1	GCAAGATCGGCGAAATCGAG
kek1seqrev3	ATCGATAATCCTTTCGGGGC
kek2seqFwd2	CAACGTTGGTGCCGAGGATA
kek2seqRev2	GACACTCTCCGCATCGTTGA
kek3seqFwd1	AGTGGAACTGGATCTAAGCC
kek3seqrev4	TTGGGGTACTCCTTCCACGT
Kek4seqFwd1	CTGTTGCAAGCACTTCGCCA
Kek4seqRev2	TATTGGGAGATCCGTGGACG
kek5seqRev3	GGTGGTGTCCTTTTGATAGG
kek5seqFwd1	GCGCAACGTGATCATCAACA
kek6seqFwd2	CATCGCCTCGGATAAGCTGT
kek6seqRev2	TGCAACCTGTTGCTGTTGCG
Kek-5 5'HR F	AATGCACCGGTcaacttacacttgcaacgcataatc
Kek-5 5'HR R	gcctgcgagcggccgcCGCTcGCTGTgGCTCTAAGTCT
Kek-5 3'HR F	tcataGgcgcgccATGATGGGCAACAGAACGGAACGAA
Kek-5 3'HR R	aattacagactagtCATCTGTTCCACGGAGGTGAGG
K5gRNA - S	gtcgGTTCTGTTGCCCATCATCGC
K5gRNA - NS	aaacGCGATGATGGGCAACAGAAC
M13 Reverse	caggaaacagctatgac
Kek-5 UP-5'F	ttttgccacccctcccaccgaaa
Kek-5 DOWN-3'R	CGTTGTGCGTCTTGTCCATC
Down-5'HA-rev	ttctcctccacatcgccgcaggtca
pGEM-GAL4-Fwd	Aatcaaccgatttatctctcttccg

pGEM-GAL4-REV	atggccaagattgaaacttagagga
GAL4/RFP fwd	gatcgatgatggcaacaacagca
GAL4/RFP rev	tttcaaactcgtgcccattgacc
UP-3'HA-fwd	gcgaaagctaagcaaataaacaagc
Kek-6 5'HR F	ccggcaccggtgatatcaggTGACAGCTATGGCATCGACAACCAG
Kek-6 5'HR R	ttctttcatcaatgcataggcGAGCGACACGAACTCGCCAGGAC
Kek-6 3'HR F	ATCCGacgcgtTAGTATTATGGTACCCAcGTGTAAA
Kek-6 3'HR R	GCAACacgcgtCGTCTAAACAATCGCATGAGGCTAA
Kek-6 CTRM gRNA S	gtcgGCTCTAGTATTATGGTACCC
Kek-6 CTRM gRNA NS	aaacGGGTACCATAATACTAGAGC
pTL2 5'HR SeqF	GAGAACTCTGAATGAAGTTCCTATTCC
pTSTEP 5'HR SeqR	Ttgttcacggtgccctccatg
pTSTEP 3'HR SeqF	catggtcctgctggagttcgtg
pTSTEP 3'HR SeqR	aagagcaagcgcaagtgc
Kek6 SeqF 2	CATCGCCTCGGATAAGCTGT
Kek6 TSTEP 3'SeqR	GCGTGGTCATGTAAGTGGAATTTAT
GOLIC gRNA SeqR	AATAGGCGTATCACGAGGC

2.7.5 Colony PCR

For Colony PCR, 1ml of a Miniprep culture or equivalent was centrifuged for 5 minutes at 13,000 RPM to produce a bacterial pellet. The supernatant was removed and discarded. Bacteria were transferred from the pellet to a pre-made GoTaq PCR mix by dipping a pipette tip into the pellet and then washing the tip in the PCR master mix. The bacteria was used in place of template DNA and was assumed to have a volume of 0µl. The initial denaturation step of the PCR was extended to 15 minutes to lyse the bacterial cells and release any plasmids they may have been carrying. All other conditions fit the polymerase's specifications for a standard PCR.

2.7.6 Gel electrophoresis

50 ml agarose gels were made to 0.8%. 0.5µl of SERVA DNA stain G was added to the molten agarose prior to placement in the gel tank. Gels were left to set for at least 30 minutes, and were run at 70V for 25-40 minutes as appropriate to visualise bands.

In the cases where the DNA would be extracted and purified following electrophoresis, 100ml gels were made to 0.8% agarose and 1µl of SERVA DNA stain G was added to the molten agarose. These larger gels were left for at least 45 minutes to set, and were run at 120V for 1 hour.

The following NEB DNA ladders were used to determine band size: 1kb Plus (N3200), 1kb (N3232) and 100bp (N3231). All gels were visualised and imaged in a Syngene G:BOX gel dock.

2.7.7 Eckhardt gels

Eckhardt gels were used to screen for ‘pT-STEP *kek6* HRs + gRNA’ clones with a successfully ligated Kek6 3’HR from a pool of 36 candidates. The principle behind an Eckhardt gel is to load lysed cells into a gel to determine the size of the carried plasmids. An unsuccessful ligation product would be ~1kb smaller than a successful one; this difference may be observable when run on an agarose gel.

Each candidate originated from a single colony on an LB/carb agar plate. Single colonies were used to establish 5ml LB/carb broth cultures by incubating overnight at 37^{o}C. 250µl of each culture was then centrifuged at 10,000 RPM for 5 minutes to produce a pellet of cells. The supernatant was discarded and the pellet was resuspended 45µl of a Lysozyme/RNAse solution (Table 2.6). 45µl of SDS/BB solution (Table 2.6) was then added to the mixture. The mixture was then loaded into a 0.75% agarose gel. The gels were then run at 70V for 30-50 minutes until the sizes of the plasmids could be resolvable.

2.7.8 Gel purification

DNA was purified using a Qiagen QIAquick Gel extraction kit following the kit protocol. DNA was run on a 100ml 0.75% agarose gel (Gel electrophoresis) for 1 hour at 120V. The desired bands were then excised from the gel with a razor. The gel chunk containing the desired band was placed in a 1.5mL microcentrifuge tube with 3 gel volumes of buffer QG. The gel and buffer was then incubated at 50^{o}C in a heat block for 10 minutes, while being agitated via vortex every 2 minutes.

After the gel had melted, 1 gel volume of 100% isopropanol was added to the tube. 750µl of the mixture was placed in the top of a QIAquick spin column, which was then

Table 2.6 - Eckhardt gel reagents

Solution	*Reagent*	*Amount*
Lysozyme/RNAse	ddH_2O	To 10ml
	Lysozyme (7500u/ml)	5mg
	RNAse (0.3u/ml)	120µl
	Sucrose	4g
SDS/BB	ddH_2O	To 10 ml
	10% SDS	500µl
	Bromophenol Blue	5mg
	Sucrose	4g

centrifuged for 1 minute at 13,000 RPM. The flow-through was discarded and the previous step was repeated until all of the mixture had passed through the column. The column was washed by passing 750µl of Buffer PE through the column by centrifugation for 1 minute at 13,000 RPM. The flow-through was discarded and the column was centrifuged again for 1 minute at 13,000 RPM to remove any Buffer PE remaining in the column.

The column was placed in a sterile 1.5mL microcentrifuge tube and 30µl of Buffer EB was added to the top of the column. DNA was eluted by incubating the buffer in the tube for up to 4 minutes and then passing Buffer EB through the column for 1 minute at 13,000 RPM. This step was repeated by placing the flow-through into the top of the column to increase yield. The concentration of the eluted DNA was then measured using a Nanodrop spectrophotometer.

2.7.9 Spin/PCR purification

DNA was purified using a Qiagen QIAquick PCR Purification kit following the kit protocol. 5 volumes of buffer PB was added to 1 volume of impure DNA. The buffer and DNA was mixed to homogeneity. The homogenous mixture was then added to a QIAquick spin column prior to being centrifuged for 1 minute at 13,000 RPM. The flow-through was replaced into the top of the column and the previous centrifugation step was repeated. The DNA was washed by passing 750µl of buffer PE through the column at 13,000 RPM for 1 minute. The flow-through was discarded and the previous centrifugation step was repeated to remove any leftover wash buffer.

The column was placed in a clean 1.5 mL microcentrifuge tube. DNA was eluted by passing 30µl of Buffer EB or ddH_2O through the column at 13,000 RPM for 1 minute.

The eluted DNA was placed back into the top of the column and the elution step was repeated to increase yield. The concentration of the eluted DNA was measured using a Nanodrop spectrophotometer.

2.7.10 Restriction digests

All restriction digests were performed for 2-4 hours. The digests were incubated at the temperature recommended by the manufacturer. For diagnostic digestions, the amount of DNA used was 400-500ng. The contents of an example restriction digest are given in Table 2.7. For reactions with digestion products that had further downstream uses (e.g. cloning) 1-1.5µg of DNA was used.

The online tool NEBcloner (https://nebcloner.neb.com/#!/redigest) was used to design two-enzyme digestions to ensure the appropriate buffers were used for maximum digestion efficacy. Enzymes were heat-inactivated following each enzymes specifications, as provided by the manufacturer. In the case of double digests, the higher temperature heat-inactivation step was used.

2.7.11 Transformation

All transformations were chemical transformations of NEB 5-alpha competent cells. 2-5µl (<100ng) of plasmid DNA was pipetted into 30µl of thawed competent cells on ice. The DNA and cells were allowed to incubate on ice for 30 minutes. The competent cells were then heat-shocked for exactly 30s in 42^{o}C water bath to allow the entry of plasmid DNA through the temporarily disrupted cell wall. The cells were then incubated on ice for a further 5 minutes before the addition of 470µl of SOC media to the cells. The cells were then allowed to recover for 1 hour at 37^{o}C in a shaking incubator set to

Table 2.7 –Restriction digest example reaction

Reagent	*Volume*
ddH_2O	Up to 25µl
10x Buffer	2.5µl
DNA	300-500ng
Enzyme	1.0µl

250 RPM. The transformed cells were then plated onto LB/carbenicillin (carb) agar plates, and were then allowed to form single colonies overnight in a 37^{o}C incubator.

2.7.12 Miniprep

5ml LB/carb broth cultures were established from single colonies from LB/carb agar plates. The 5ml cultures were incubated at 37^{o}C overnight. 3ml of the liquid culture was centrifuged for 1 minute at 10,000 RPM to produce a pellet of bacteria. The supernatant was discarded and the bacterial pellet was resuspended in 400µl of a resuspension buffer (10mM EDTA, 25mM Tris-HCl at pH 8.0 and 100µg/ml RNAse). 200µl of a lysis buffer (1% SDS, 0.2 M NaOH) was added to the mixture, which was then thoroughly mixed by inversion. 200µl of an ice-cold Precipitation buffer (3M potassium-acetate at pH 5.5) was added and solution was mixed thoroughly by inversion.

The solution was then centrifuged for 20 minutes at 13,000 RPM. The supernatant was transferred to a new microcentrifuge tube and the precipitants were discarded. 400µl of 100% isopropanol thoroughly mixed into the supernatant. The supernatant and isopropanol was then incubated on ice for 5 minutes prior to being centrifuged for 30 minutes at 13,000 RPM.

The supernatant was discarded and 400µl of 70% ethanol was added to the pellet, and was then centrifuged for 10 minutes at 13,000 RPM. The supernatant was removed and the DNA pellet was allowed to air dry for up to 1 hour. After this, the pellet was resuspended in ddH_2O or TE buffer. The concentration of the plasmid DNA was measured using a Nanodrop spectrophotometer.

2.7.13 Midiprep

Purification of plasmid DNA from 100ml LB broth cultures was performed using a Qiagen Plasmid Midi kit following the protocol provided with the kit. 100ml cultures were established using 100µl of a Miniprep culture or an equivalent 5ml starter culture.

To yield a bacterial pellet, 100ml of the culture was centrifuged, 50ml at a time, in a 50ml Falcon Tube for 15 minutes at 5000 g at 4^{o}C. The pellet was resuspended in buffer 4ml of P1. 4ml of buffer P2 was added and thoroughly mixed with the resuspended pellet to lyse cells. 4ml of ice-cold buffer P3 was then added and was thoroughly mixed in via inversion. The mixture was then incubated on ice for 15 minutes before being centrifuged for 30 minutes at >20,000 g at 4^{o}C. The supernatant was transferred to a sterile 50ml Falcon tube and the precipitants were discarded. To remove any remaining precipitants, the supernatant was centrifuged for a further 15 minutes at >20,000 g at 4^{o}C.

A Qiagen-tip was equilibrated by allowing 5mL of buffer QBT to pass through the column via gravity flow. After all of Buffer QBT had passed through the column, the supernatant from the previous centrifugation step was added to the column, carefully avoiding adding any leftover precipitant to the column. After the column had passed through all of the supernatant, 20mL of buffer QC was passed through the column. The column was then placed into a new sterile Falcon tube and 5mL of buffer QF was allowed to pass through. With the DNA eluted into the new Falcon tube, the Qiagen-tip was discarded.

3.5mL of 100% isopropanol was added to the eluted DNA and the tube was then centrifuged for 30 minutes at >20,000 g at 4^{o}C. The supernatant was then removed from the DNA pellet and replaced with 4mL of 70% ethanol. The DNA pellet and 70%

ethanol was then centrifuged for 10 minutes at >20,000 g at 4ºC. The supernatant was removed and the DNA pellet was allowed to air dry. The pellet was resuspended in 70µl of ddH_2O. The concentration of the plasmid DNA was measured using a Nanodrop spectrophotometer.

2.7.14 DNA ligation

All DNA ligations were performed using Promega T4 DNA Ligase following the manufacturer's protocol. DNA fragments were added to the reaction for a 3:1 insert:vector molar ratio. 100ng of vector was used in all cases. Ligation reactions were left to run overnight at 4ºC prior to use in transformation. The contents of an example DNA ligation reaction is given in Table 2.8.

2.7.15 Gibson cloning

A NEBuilder® HiFi DNA Assembly Cloning kit (E5520S) was used to perform the Gibson reactions needed for the molecular cloning of DNT2-YPET and Kek6 T-STEP. The NEBuilder online tool (https://nebuilder.neb.com/#!/) was used to design the overlap sequences (on the HR primers) required to enable the Gibson reaction to work.

Within the Gibson reactions, all DNA fragments were in an equimolar ratio. The reactions were incubated in a thermocycler at 50º C for 1 hour. Following this the reactions were put on ice and 2µl of the reactions were used to transform NEB 5-alpha competent cells.

Table 2.8 –Example ligation reaction

Reagent	*Volume*
ddH_2O	To 20µl
10x T4 DNA ligase buffer	2µl
Vector DNA	100ng
Insert DNA	3:1 insert to vector molar ratio
T4 DNA ligase	1µl

2.7.16 gRNA cloning

To clone the target-specific 20nt gRNA sequence into the gRNA-driving vectors a protocol based on Gratz et al 2015 was used. Each gRNA-driving vector carried a ubiquitous Drosophila promoter driving a chimeric scaffold gRNA that can bind Cas9. The 20nt-long target-specific oligos were conventionally cloned into the vector to fuse the target sequence to the chimeric gRNA scaffold.

The target-specific 20nt gRNA sequence required for CRISPR/Cas9-catalyzed HDR was found using the online tool CRISPR Optimal Target finder. For all clonings the gRNA was found in a within 120bp of the desired insertion site. gRNAs were selected to have no predicted off-targets and to have a G at the 5' end to increase expression under the dU6.3 promoter. In cases where the most specific gRNA did not have a G at the 5' end, the base at the 5' end was replaced with a G. Additional bases required to ligate the gRNA oligos into the gRNA-driving vectors were added to their 5' end. gRNA oligos were synthesized by Eurofins Genomics

gRNA-driving vectors were digested with the appropriate enzyme (Table 2.9). The gRNA oligos were annealed together in a thermocycler by raising the temperature of the oligos to 95^{o}C for 5 minutes and then lowering the temperature to 25^{o}C at a rate of -0.1^{o}C/s. The annealed oligos were then ligated with the digested vector. A 20:1 insert:vector ratio was used for these ligations due to the small size of the insert DNA.

To eliminate any remaining undigested vectors remaining in the ligation reaction, the ligation product was purified via Spin/PCR Purification and then digested again with the respective enzyme (Table 2.9). The digestion reaction was heat-inactivated and 2-5µl of the digestion product was used to transform NEB 5-alpha competent cells.

Table 2.9 – gRNA cloning

Cloning	*gRNA-driving vector*	*Enzyme*
Kek-5 GAL4	pCFD3-dU6.3:gRNA	BsbI
Kek-6 T-STEP	pT-STEP 5'HR	BsmBI

2.7.17 RNA extraction from larval tissues

RNA was extracted from two different larval tissues, the CNS, and the body wall (BW). In all cases L3 wandering OregonR larvae were used. Larvae were reared under three different temperature conditions: 18, 25 and 30^{o}C. For each temperature condition, adult flies were transferred into fresh 12ml vials of Houston fly food and were incubated at the respective temperature. Vials were flipped every 3-4 days and were incubated at the appropriate temperature until larvae had entered L3 wandering, after which larvae were dissected and the vial was discarded.

For the CNS, the standard CNS dissection protocol was followed, however, to prevent RNA degradation gloves were worn during the dissection. Additionally, to prevent contamination from other tissues, such as the imaginal discs, the samples were thoroughly cleaned before being deposited into 20µl of ice-cold TRI reagent. 10 CNSs were enough for each condition to extract a sufficient amount of RNA.

For the BW, the standard NMJ dissection protocol was followed. Similar to the CNS dissections, gloves were worn to prevent RNA degradation and the care was taken to clean the BW of extraneous tissues, including the CNS. BW samples were also deposited into 20µl of ice-cold TRI reagent immediately after dissection. 5 BWs per condition was enough to extract a sufficient amount of RNA. For both CNS and BW samples, the tissues were frozen at -80^{o}C until use.

While extracting RNA gloves were worn at all times to prevent RNA degradation. Additionally, fresh sterile pipette tips and microcentrifuge tubes were used, and all work surfaces were wiped down with 70% ethanol. Samples were defrosted gently on ice. Sterile plastic pestles were used to break down the tissues suspended in the 20µl

TRI reagent. To avoid contamination, samples did not share pestles, and each had their own. After this, 980µl of TRI reagent was added to the sample, by gently pipetting the additional TRI reagent over the pestle so as to remove any tissue fragments that had become adhered to the plastic pestle. Used pestles were cleaned in 100% ethanol before being washed with tap water and being autoclaved.

The freshly homogenised tissue suspended in 1ml of TRI reagent was then allowed to incubate at room temperature for 5 minutes to allow for the dissociation of RNA from nucleoprotein complexes. The homogenate was then centrifuged at 12,000g for 10 minutes at 4^{o}C. The supernatant was then transferred to a new sterile 1.5ml microcentrifuge tube. To this, 100µl of 1-Bromo-3-chloropropane (BCP) was added. The tube was shaken vigorously for ~15 seconds to homogenise the solution. The TRI-Reagent/BCP solution was then allowed to incubate for 10 minutes at room temperature. Following this, the TRI-Reagent/BCP solution was then centrifuged again at 12,000g for 13 minutes at 4^{o}C.

After centrifugation the solution separates into a colourless aqueous phase and a pink organic phase. The aqueous phase, containing the RNA, was then pipetted into a fresh 1.5ml microcentrifuge tube (typically 300-400µl). 500µl of 100% isopropanol was then added to the separated aqueous phase, which was then vortexed for ~5 seconds before an incubation for 10 minutes at room temperature. This solution was then centrifuged at 12,000g for 8 minutes at 4^{o}C. After this centrifugation step the RNA is condensed into a small white pellet. The supernatant was then removed gently, to prevent undesirable removal of the RNA pellet.

To wash the RNA 1ml of 75% ethanol was then added to the pellet, and the tube was then centrifuged at 10,000g for 5 minutes at 4^{o}C. The ethanol was then carefully

removed, and the pellet was allowed to air-dry for up to 5 minutes. 10µl of Nuclease-free water was then used to dissolve the RNA pellet.

The RNA was then treated to remove any potential DNA lingering in the sample. This was done by the addition 1µl of DNAse I and 1.2µl of 10x DNAse I buffer to the RNA from an Ambion DNA-free kit. This mixture was then incubated at 37^{o}C for 30 minutes in a heat block. 2µl of DNAse inactivation reagent was then added to stop the reaction. The inactivation reagent was allowed to incubate for 2 minutes at room temperature, before the sample was then centrifuged at 10,000g for 2 minutes to separate the inactivation reagent from the RNA. The RNA supernatant was then carefully pipetted away from the opaque DNA inactivation reagent pellet and transferred to a fresh microcentrifuge tube.

The RNA concentration was then measured using a Nanodrop spectrophotometer. The purity was assessed by checking that the 260/280 ratio was between 1.8 and 2.2, within this range the RNA was considered to have an acceptable level of purity.

2.7.18 cDNA synthesis

For each sample, cDNA was synthesized from 200ng of purified RNA. cDNA was synthesized using GoScript Reverse Transcriptase. Firstly, to anneal the random primers to the RNA, 200ng of the purified RNA was mixed with 1µl of a random primer mix, and enough purified nuclease-free water to make up the mixture to 5µl. The RNA/primer mixture was then incubated at 70^{o}C for 5 minutes in a thermocycler, after which it was immediately incubated on ice for at least 5 minutes.

While the RNA/primer mix was incubating on ice, the remaining reagents (Table 2.10) were combined in a separate tube on ice. This RT-PCR mixture was then added to the

Table 2.10 – Reverse transcriptase PCR reagents

Reagent	*Volume*
Nuclease-free Water	7µl
GoScript 5x reaction buffer	4µl
25mM $MgCl_2$	2µl
Nucleotide mix (0.5mM of each dNTP)	1µl
GoScript Reverse Transcriptase	1µl
Total volume	**15µl**

5µl of RNA/primer mix and the tube was placed in a thermocycler. The thermocycler program then ran as follows: 25ºC for 5 minutes, 42ºC for 60 minutes, 70ºC for 15 minutes, then finally, 4ºC indefinitely. The cDNA was then retrieved from the thermocycler during the final indefinite 4ºC step of the program.

For use in PCRs cDNA was diluted 1:3 with nuclease-free water to bring the total volume to 60µl. To control for the presence of DNA contamination, these PCRs were accompanied with a no-RT control. The no-RT control consisted of 200ng of the purified RNA sample, diluted with nuclease-free to make up 60µl total.

2.7.19 Analysis of RT-PCR data

PCRs were done to amplify DNA from each of the 7 genes being tested (GAPDH, *kek1-6*). cDNA for each tissue and condition were used as the template. PCR products were then ran on gels with each gel containing all the tissue/condition combinations for one gene, including no-RT controls.

Gels were processed in ImageJ. Signal intensity of a band was measured by creating an ROI around the band and measuring the IntDen within. To compensate for differences in background levels, a measurement was made of the IntDen of the background close to the band in question. A band here represents the amount of RNA for a given gene in a given tissue under a given temperature condition, e.g., the level of *kek1* in the CNS of a larvae reared at 30ºC. The background was then subtracted from the signal of a band. The background-adjusted signal intensity was then normalised to the signal intensity of housekeeping gene *GAPDH* from that cDNA sample. The normalised signal intensity was then plotted onto bar graphs.

2.7.20 Western Blot

2.7.20.1 Protein extraction

For each genotype 30 males and 30 female 3–5-day old adult flies were collected and frozen at -80ºC in a 1.5ml microcentrifuge tube. The fly-containing microcentrifuge tubes were then dipped in liquid nitrogen and were then violently vortexed to decapitate flies. The contents of the tube were tipped out onto a petri dish and the heads were collected into a fresh microcentrifuge tube. The contents of buffers and solutions used in this protocol is given in Table 2.11.

60µl of ice-cold lysis buffer was then added to the heads. Fly heads were then homogenised using a clean, sterile plastic pestle. After incubating in lysis buffer on ice for 30 minutes the homogenised fly heads were then spun in a table-top microcentrifuge at 600G for 6 minutes at 4ºC. The supernatant was collected into a fresh 1.5ml microcentrifuge tube and the pellet of debris was discarded. The supernatant was then centrifuged again at 14,000G for 15 minutes at 4ºC. The supernatant was then removed to a fresh microcentrifuge tube. The supernatant was then frozen at -80ºC until use

Immediately prior to use samples were defrosted on ice and 19.5µl of sample was placed in a fresh 1.5ml microcentrifuge tube with 7.5µl of 4x NuPAGE LDS buffer and 3µl of 10x NuPAGE Reducing buffer. NuPAGE LDS buffer is alternative to Laemmli buffer and was used due to lab preference. The sample was then heated to 90ºC for 5 minutes and was then centrifuged at 13,000 RPM for 1 minute.

Table 2.11 – Western blot buffers and solutions

Buffer	*Component*	*Quantity*
Lysis buffer (For 500µl)	RIPA buffer (25 mM Tris-HCl, pH 7.6, 150 mM NaCl, 1% NP-40, 1% sodium deoxycholate, 0.1% SDS)	495µl
	Complete Mini Protease inhibitor	5µl
Running buffer	Tris	25mM
	Glycine	190mM
	SDS	0.1%
Transfer buffer	Tris	25mM
	Glycine	190mM
	Methanol	20%
Tris-buffering saline with Tween-20 (TBST)	Tris, pH 7.5	20mM
	NaCl	150mM
	Tween20	0.1%
Blocking buffer	Non-fat dry milk powder	5% (diluted in TBST)

2.7.20.2 SDS PAGE

To separate proteins by size samples were run through a 12% SDS-PAGE gel via gel electrophoresis using a Bio-Rad Mini-PROTEAN Tetra Vertical Electrophoresis Cell tank (161-0182). Gels were prepared following manufacturer's guidance. Briefly, 15ml of a 12% Resolving gel was prepared by combining 6ml of 30% Acrylamide/bis, 3.75ml of pH 8.8 1.5M Tris-HCl and 150µl of 10% SDS, 5.03ml of ddH_2O. To initiate polymerisation, 7.5µl of TEMED and 75µl of 10% Ammonium persulfate (APS) were added to the mixture. ~8.4ml of the resolving gel mixture was then pipetted into a 1.5mm glass gel cassette. To ensure the resolving gel would set with a level top and not dry out, isopropanol was added to fill the gel cassette and cover the polymerising resolving gel.

After the resolving gel had fully set (~45 minutes) the isopropanol was removed, and a 4% stacking gel solution was added. The 4% stacking gel solution was prepared by mixing together 1.98ml 30% Acrylamide/bis, 3.78ml pH 6.8 0.5M Tris-HCl, 150µl SDS, 9ml of ddH_2O and lastly, 15µl of TEMED and 75µl of 10% APS. Enough stacking gel solution was added to fully fill the gel cassette. A 1.5mm comb was then added to the cassette to form wells in the stacking gel. After the stacking gel had set, gels were then either used immediately or were stored at 4^{o}C wrapped in wet paper towel for up to 1 week.

The gels were loaded into the gel electrophoresis tank, and the tank was filled with 1X running buffer. After samples and a protein ladder were loaded into their own wells in the gel, the gel was run at 100V for 15 minutes or until the samples had reached the threshold between the stacking and resolving gels. Following this the voltage was increased to 150V and was run for a further 45 minutes.

2.7.20.3 Membrane transfer

While the gel was running, the membrane transfer cassette was prepared. 8 sheets of filter paper and the PVDF transfer membrane were cut to the size of the gel and were left to incubate in transfer buffer with 2 sponge sheets at 4ºC. When the gel electrophoresis finished, the transfer cassette was assembled in the following order from the cassette's cathode side to the anode: 1 sponge sheet, 4 layers of filter paper, the excised SDS-PAGE gel, the transfer membrane, 4 layers of filter paper and 1 layer of sponge sheet. Care was taken to prevent and remove air bubbles remaining between layers the assembly.

Once assembled, the cassette was placed into the transfer cell in the transfer tank. An ice pack was added to the tank, and the tank was filled with cold transfer buffer. The tank was placed in a 4ºC cold room and was connected to a power pack. The transfer was run for 90 minutes at 90V. Following this the transfer membrane was removed from the cassette.

2.7.20.4 Immunostaining

To prepare the membrane for immunostaining, the membrane was first incubated in a blocking buffer for 1 hour while being gently agitated by a shaker. After this the blocker was removed and the primary antibody diluted in blocking buffer was added. Incubation of the primary antibody took place overnight in 4ºC with gentle agitation by a shaker. The list of primary and secondary antibodies used in this thesis, and their dilutions, are detailed in Table 2.4.

The next day the primary antibody was removed, and the membrane was washed three times with PBS-T for 15 minutes. Following this the secondary antibody conjugated with horseradish peroxidase was diluted in blocking buffer was added to the membrane and was allowed to incubate for 1 hour at room temperature with gentle agitation. The secondary antibody was then discarded, and the membrane was again washed thrice with PBS-T for 15 minutes each time.

2.7.20.5 Visualisation

To visualise the antibody staining, a 1:1 mixture of the substrates from a Thermo Scientific SuperSignal West Pico PLUS Chemiluminescent kit (Cat. 34580) was prepared. The membrane was placed on a sheet of plastic film wrap and was covered with a light-proof box. The chemiluminescent mixture was then poured over the membrane was allowed to incubate for 5 minutes under the light-proof box. After 5 minutes had elapsed the chemiluminescent mixture was removed by gently drying the membrane with paper towel. The membrane was then transported to a Syngene G:BOX gel dock where an image of the membrane was taken. Immunostaining of the membrane was revealed by the chemical reaction between the chemiluminescent mixture and the HRP conjugated to the secondary antibodies, which produces light.

2.8 Calcium imaging

2.8.1 Dissection of larvae

Larvae were reared on ATR-containing Houston fly food for ~5 days after egg laying, until larvae had reached the wandering phase of the third larval instar. Larvae were

briefly anesthetised in ice cold water. Larvae were then placed within a 40µl droplet of ice-cold HL3 saline on the dissection plate.

A larva was then oriented dorsal side up. Insect pins were then inserted into the larvae between the anterior spiracles, and then another pin between the posterior spiracles. Larvae were protected from the light as much as possible during dissection. Using micro-scissors, incisions perpendicular to the midline were made posterior to the anterior pin and anterior to the posterior pin. A third incision was made along the midline to connect the first two incisions. Viscera was then carefully removed using dissection forceps. Insect pins were then used to hold open the corners of the body wall. The HL3 saline was then replaced with fresh saline and the larva was taken to the microscope.

2.8.2 Live Ca^{2+} imaging microscopy

Data was acquired as a Time Series using a Zeiss Axioimager.M2 microscope using a 20x water immersion lens controlled using Zen Blue software. NMJ 6/7 was identified by eye, and then the sample was moved to be within a 672 x 400-pixel ROI. The ROI was used to ensure performance quality of the software and microscope during acquisition.

The Experiment Designer window was used to program the experiment. 5 acquisition blocks were used. Block 1 was to habituate the sample and capture GCaMP signal pre-activity. Block 1 was recording only the green (488nm) channel at 30% LED power, with an exposure time of 0.2s/frame for a duration of 60s. Block 2 was used to stimulate the motoneurons with a 590nm LED set to 100% power for 0.5s. Block 3 recorded the GCaMP signal in the green 488nm channel for 20s with an exposure time

of 0.2s. Block 4 was used a second stimulation and was identical to Block 2. Block 5 recorded the GCaMP response to the second stimulation of Block 4 and was identical to Block 3.

A single sample was not used for longer than 20 minutes since the start of dissection as after that point the larva would have perished. Typically, 2-3 NMJs could be scanned within this time.

2.8.3 Data analysis of bouton intensity

Stacks were analysed in ImageJ-FIJI and were imported using the Bio-Formats Importer plugin. For analysis, the all the frames in a stack from Frame 250 until the end of the stack were duplicated and saved as a separate file. These frames correspond to a time point from 10s before stimulation to the end of the recording of the second stimulation. A false-colour Thermal look-up table (LUT) was applied to better visualise changes in intensity.

Each stack was then manually assessed to determine the number of Ib boutons within the recording. Ib boutons were identified by their size and morphology. Boutons were discarded from consideration if they went out of focus or were ‘backlit’ (if a bouton was in front of a light source deeper in the prep) for greater than 10 frames. If a stack contained at least one in-focus, non-backlit Ib bouton a copy of the file was made, and the viable boutons were labelled.

To quantify the signal intensity of a given bouton in a single frame, a rectangular ROI was set tightly around the bouton and the Integrated Density (IntDen) was measured. Each stack was moved through manually frame by frame to measure the IntDen of the bouton through time. The labelled copy of the file was used as a reference for the

location of the bouton, as this changed with muscle contractions. The measurement of a given bouton's GCaMP signal profile began 21 frames before the stimulation and ran until the end of the recording of the first response (Block 3). The second response (Block 4-5) was measured separately. The size and shape of the region of interest (ROI) was not changed while measuring throughout the stack (Block 1-5).

The IntDen measurements of each bouton were then imported into a Microsoft Excel file for analysis. For each bouton the IntDen values for each frame were normalised to the mean of the IntDen values of the 21 frames prior to stimulation. For each genotype the mean for each frame was calculated and plotted onto a line graph. The standard error of the mean for each frame was calculated and was displayed as the error bars on the graph.

2.9 Optogenetics and Activity Experiments

2.9.1 Staging of larvae

Crosses were conducted in fly cages based with grape juice agar plates with a small amount of yeast paste placed on the centre of the plate. On the first day of the staging protocol 100-200 virgins and 50-100 males for each cross were placed into a fly cage in staging protocol and were allowed to acclimatise to the cage for that day. The overnight plate for each day was discarded and replaced with a fresh grape juice plate. On the second day the plate was replaced every two hours and the old plates were discarded. On the third day of the protocol the plate was removed every two hours and the old plates were kept at 25^{o}C until the following day.

On the fourth day, 24 hours after a given plate was placed in the cage, that plate was used to select for L1 larvae. L1 larvae were then transferred to foil-lined food vials

containing 2ml of fly food. For the ’No stimulation’ condition larvae were placed into food vials that lacked ATR, for the ‘Stimulation’ condition the food contained 50µM ATR. Both sets of food vials were enwrapped in aluminium foil to prevent light entering the vials and prematurely stimulating larvae. Regardless of condition, the larvae-containing vials were then incubated at 25^{o}C until the fifth day of the protocol.

On the fifth day, larvae were transferred from the food vial to an agar plate. 30µl of 40% sucrose solution was placed on the plate with the larvae. The larvae for the ‘Stimulation’ condition were then subjected to the stimulation regime. Larvae for the ‘No Stimulation’ condition did not receive optogenetic stimulation and skipped this to the next step. Following optogenetic stimulation a small amount of yeast paste was applied to the plate and the plate was incubated at 25^{o}C for 24 hours. On the sixth day of the protocol larvae were dissected and fixed.

2.9.2 Optogenetic stimulation

A custom lightbox was made to elicit optogenetic stimulation. The lightbox consisted of an opaque hollow plastic box containing four high power 590nm LEDs (ThorLabs PCB Mounted LEDs) connected to a ThorLabs T-Cube LED driver (LEDD1B). The lightbox was fitted with a translucent pane of white plastic on the top surface of the box to act as a stage allowing light from the LEDs to reach larvae placed on top of the box. The lightbox was fitted to a ThorLabs aluminium BreadBoard (MB3945/M) with four ThorLabs CF125 Clamping Forks to prevent the box moving. The lightbox was placed inside a large cardboard box to prevent light from the laboratory environment interfering with the stimulation regime.

The intensity of the light from the LEDs was controlled using a potentiometer built into the LED driver. To control the pattern of illumination of the LEDs during the stimulation regime the LED driver was connected to an Arduino Mega board (A000067). The Arduino Mega board was connected to a Windows PC via USB and was controlled by the Serial Monitor window in the Arduino IDE.

The program in Fig. 2.4 was used to control the LEDs. The program receives user input from the Serial Monitor window for the variables required for to execute the regime. It first asks which digital pin the Arduino board is connected to the LED driver. It then asks how long the LEDs are on and off for during a pulse in a stimulation period, then how long the resting period is within a block. Finally, it asks how many times the block should repeat. By receiving user input in this way, the program was able to provide flexibility for optimisation by allowing each aspect of the stimulation regime to modified at runtime.

The optogenetic stimulation regime used in the plasticity experiments was based on the regime described by Maldonado-Díaz et al 2021. The regime consisted of repeating blocks of stimulation and rest. Within a block the first 2.5 minutes were stimulating, and the remaining 7.5 minutes made up a rest period. Within the 2.5 minutes of stimulation LEDs flashed on for 1 second and off for 1.5 seconds. This block of stimulation and rest was repeated 10 times for a total run time of 100 minutes. The light intensity used was the lowest intensity that caused control (D42>ReaChR, reared on ATR-containing food) larvae to contract.

Figure 2.4 – Arduino code controlling optogenetics set-up

```
1
2
3     void setup() {
4       Serial.begin(9600);
5       Serial.println("#######################################");
6       Serial.println("#~~~###-- HELLO AND WELCOME! --###~~~#");
7       Serial.println("#######################################");
8     }
9
10      int Pin;
11      int LED_ON;
12      int LED_OFF;
13      long TargetTime;
14      long TimeRightNow;
15      long TimeActive;
16      long TimeResting;
17      int Blocks;
18      int SerMem;
19
20
21    void loop() {
22
23    Serial.println("====================================");
24    Serial.println(" ~~~###--    LET'S BEGIN     --###~~~ ");
25    Serial.println("====================================");
26    Serial.println("");
27
28    SerMem = Serial.available();
29    Serial.println("What pin are we using today?: ");
30    while (Serial.available() == SerMem){}
31      Pin = Serial.parseInt();
32      pinMode(Pin, OUTPUT);
33      Serial.print("Pin #");
34      Serial.print(Pin);
35      Serial.println(" is ready!");
36      Serial.println(" ");
37
38
39    SerMem = Serial.available();
40    Serial.println("Activity period duration in ms: ");
41    while (Serial.available() == SerMem){}
42      TimeActive = Serial.parseInt();
43      Serial.print("Activity period duration will be: ");
44      Serial.print(TimeActive);
45      Serial.println(" milliseconds!");
46      Serial.println(" ");
47
48    SerMem = Serial.available();
49    Serial.println("Resting period duration in ms: ");
50    while (Serial.available() == SerMem){}
51      TimeResting = Serial.parseInt();
52      Serial.print("Resting period duration will be: ");
53      Serial.print(TimeResting);
54      Serial.println(" milliseconds!");
55      Serial.println(" ");
56
57
58    SerMem = Serial.available();
```

```
59    Serial.println("In a pulse, how long will the LEDs be ON for in ms?:
");
60    while (Serial.available() == SerMem){}
61      LED_ON = Serial.parseInt();
62      Serial.print("LED will be ON for: ");
63      Serial.print(LED_ON);
64      Serial.println(" milliseconds!");
65      Serial.println(" ");
66
67
68    SerMem = Serial.available();
69    Serial.println("In a pulse, How long will the LEDs be OFF for in ms?:
");
70    while (Serial.available() == SerMem){}
71      LED_OFF = Serial.parseInt();
72      Serial.print("LED will be OFF for: ");
73      Serial.print(LED_OFF);
74      Serial.println(" milliseconds!");
75      Serial.println(" ");
76
77
78    SerMem = Serial.available();
79    Serial.println("How many blocks?: ");
80    while (Serial.available() == SerMem) {}
81      Blocks = Serial.parseInt();
82      Serial.print("There will be: ");
83      Serial.print(Blocks);
84      Serial.println(" block(s)!");
85      Serial.println(" ");
86
87
88    SerMem = Serial.available();
89    Serial.println("~~~###-- ENTER ANY KEY TO BEGIN --###~~~");
90    while (Serial.available() == SerMem) {}
91
92
93
94
95    for (int i = 0; i < Blocks; i++){
96
97    TimeRightNow = millis();
98    TargetTime = TimeRightNow + TimeActive;
99
100   Serial.println(millis());
101
102   while(TimeRightNow < TargetTime){
103
104    digitalWrite(Pin, HIGH); // sets the digital pin on
105    delay(LED_ON);            // waits
106    digitalWrite(Pin, LOW);  // sets the digital pin off
107    delay(LED_OFF);            // waits
108
109    TimeRightNow = millis();
110    Serial.println(millis());
111   }
112   delay(TimeResting);
113   Serial.println(millis());
114   Serial.println(" ");
115   Serial.print("End of Block #");
116   Serial.println(i+1);
117   Serial.println("");
```

```
118   }
119
120   Serial.println("============================");
121   Serial.println("~~~###-- END OF TASK --###~~~");
122   Serial.println("============================");
123   Serial.println(" ");
124   Serial.println(" ");
125   Serial.println(" ");
126   }
127
```

2.9.3 Data analysis of NMJ morphology

Muscle surface area (MSA) was quantified by measuring the area of muscle 6 and 7 in FIJI using the polygon tool to outline each muscle and the Measure tool was used to access the value for the area. The areas of muscle 6 and 7 for each NMJ was then exported as a .csv file. The sum of the areas of muscle 6 and 7 was used to normalise mature and ghost bouton number, HRP volume and Brp volume.

Bouton counting was only carried out on samples stained with both HRP and Dlg. Mature boutons were identified by being both HRP+ and Dlg+. Ghost boutons were identified by being HRP+ but Dlg-. Mature and Ghost bouton counting was carried out using the Cell counter function of Fiji. Boutons were counted as separate cell types. The results of the counts were exported as .csv files. Ib boutons were identified by their size and morphology. If it was unclear if a bouton was Ib or Is, it was not counted.

HRP and Brp volumes quantified in Imaris. Images were imported into Imaris and were converted into .ims files. For a given NMJ, an ROI was drawn around the axonal terminal to remove unwanted signal and noise from other NMJs, debris and background. The HRP and Brp volumes were then segmented by thresholding. Volumes were then exported as .csv.

In all cases exported data in .csv file format was first imported into a master spreadsheet in Microsoft Excel, containing all the processed data from each sample from each genotype. Data was then imported into GraphPad Prism for statistical analysis and visualisation.

3 RESULTS - SPATIAL DISTRIBUTION OF THE KEKS

3.1 Introduction

To understand the role the *keks* may play in the nervous system, it is critical to determine what their differences are, particularly their spatial expression. *kek1*, *-2*, *-5* and *-6* are expressed in the embryonic central nervous system (Musacchio and Perrimon 1996, Evans et al., 2009, Bishop 2014). There is evidence that *kek6* is expressed in motoneurons in third instar, although the subcellular localisation is unknown (Ulian-Benitez et al., 2017). In this chapter I investigated the spatial distribution of the Kek family.

3.2 Results

3.2.1 All *keks* are expressed in the larval nervous system

Within the context of activity-dependent structural plasticity, it would be important to know if *kek* expression is regulated by neuronal activity. In *Drosophila* larvae, temperature can be used as a proxy for activity, as higher temperatures (>27^{o}C) can be sufficient to evoke activity-dependent structural plasticity (Sigrist et al., 2003). This provides a simple method for testing if *kek*s can be regulated by activity.

To address the question of which *kek*s are expressed in the nervous system in L3 larvae and if their expression can be modulated by activity, semi-quantitative RT-PCRs were carried out to investigate the expression of each of the *kek*s.

RNA was extracted from the CNS and body wall (BW) of wildtype OregonR L3 wandering larvae. The BW includes the cuticle, PNS and muscles of the larvae that

have been cleaned of gut and other organs. It was important to include the BW in this experiment in the event that *keks* were expressed in the PNS or muscle. To test the effect of activity, larvae were reared at three different temperatures 18, 25 and 30^{o}C.

Bright bands in the CNS lanes in for each *kek* indicated that all *kek*s were expressed in the CNS (Fig. 3.1). Temperature had no significant effect on the expression of the *kek*s. For *kek2, -3, -4* and *-6*, expression in the BW was little to none, however for *kek1* and *-5* there was some expression in the BW (Fig. 3.2). This could be expression within the PNS, the muscles, glia, or the epidermis.

3.2.2 Generation of *kek5-GAL4* constructs

Genetic tools such as GAL4 lines and endogenously tagged proteins are valuable for delineating the expression pattern of *kek*s. Unfortunately, GAL4 and protein fusion lines are not available for all the *kek*s. *kek5* was chosen for the generation of a GAL4 line as the RT-PCR data indicated *kek5*, along with *kek1*, was expressed differently to the other *kek*s, and this warranted further exploration. *kek5* was selected over *kek1* as a protein fusion to *kek5* had been made previously, and the use of both a GAL4 and a protein fusion was thought to provide a greater depth of knowledge than just the GAL4 alone.

To study the expression pattern of *kek5* I aimed to generate a *kek5* GAL4 knock-in line. The *kek5*-T2A-*GAL4* line could be used to couple the expression of a reporter such as membrane-tethered GFP to the *kek5* promotor, and additionally opens the opportunity to specifically target *kek5*-expressing cells in genetic experiments.

To generate a *kek5-GAL4* line I used CRISPR-Cas9 mediated homology directed repair. This required injecting embryos with a donor construct bearing the *GAL4* coding

Figure 3.1 - *keks* are expressed in the CNS

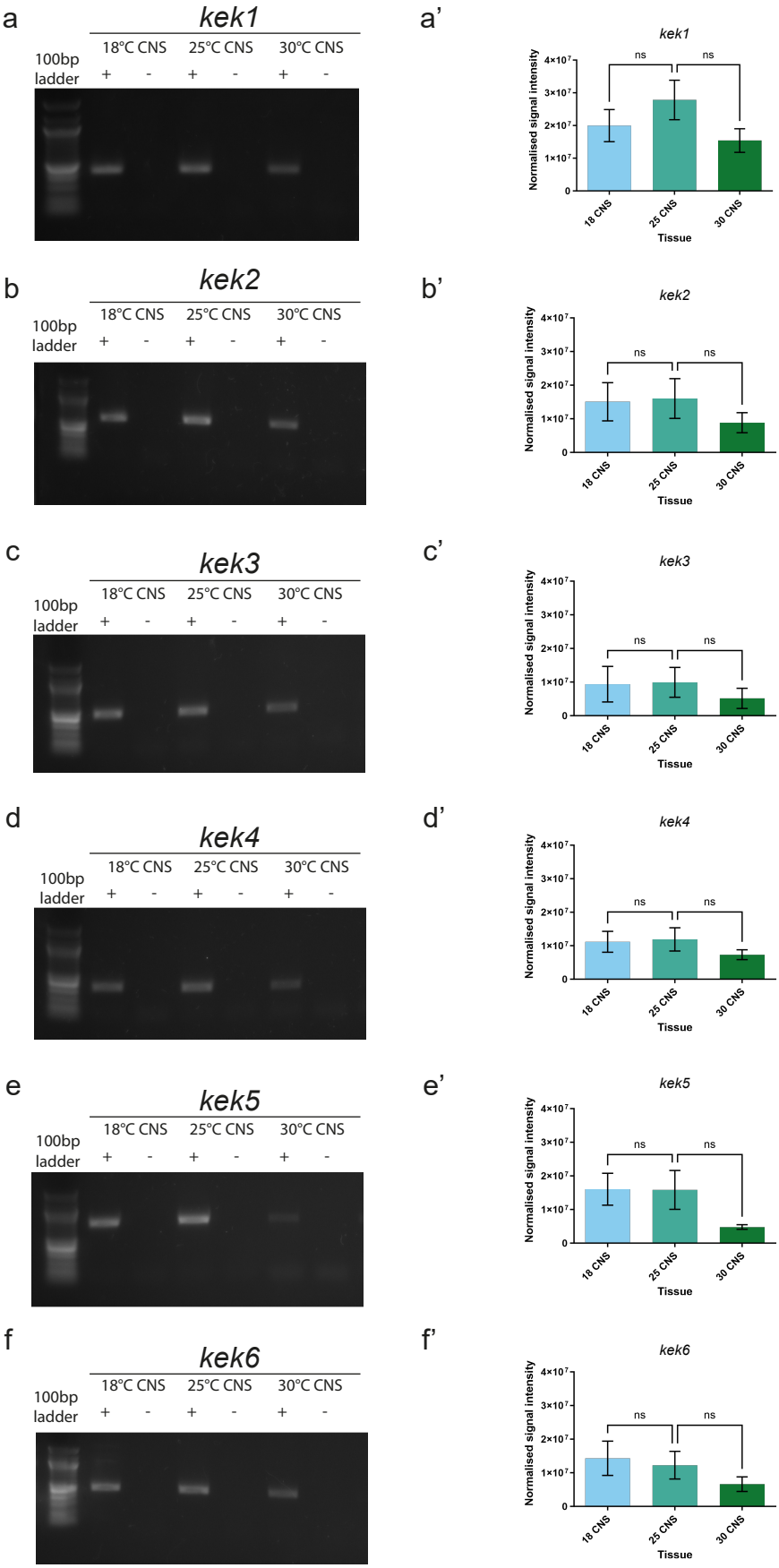


Figure 3.1 – *keks* are expressed in the CNS

Detection of *kek* transcripts via PCR of cDNA extracted from dissected larval CNSs reared at 18ºC, 25ºC, and 30ºC. **A-F:** Representative gels for each gene of interest. **A'-F':** Transcript abundance was quantified via measuring signal intensity of each band in ImageJ/Fiji. For each gene and condition RNA was extracted from 10 larvae, with 4-5 technical replicates. **A':** *kek1* in the CNS. For 18ºC, 25ºC, and 30ºC, Shapiro-Wilk p = 0.851, 0.7867, and 0.2576, respectively. Ordinary One-way ANOVA p =0.2543, not significant (ns). **B':** *kek2* in the CNS. Shapiro-Wilk p = 0.8476, 0.1793, and 0.9334, respectively. Ordinary One-way ANOVA p =0.5635, not significant (ns). **C':** *kek3* in the CNS. Shapiro-Wilk p = 0.1056, 0.462, and 0.0425, respectively. Ordinary One-way ANOVA p =0.7043, not significant (ns). **D':** *kek4* in the CNS. Shapiro-Wilk p = 0.9727, 0.8564, and 0.1787, respectively. Ordinary One-way ANOVA p =0.4904, not significant (ns). **E':** *kek5* in the CNS. Shapiro-Wilk p = 0.4223, 0.5506, and 0.8235, respectively. Ordinary One-way ANOVA p =0.1543, not significant (ns). **F':** *kek6* in the CNS. Shapiro-Wilk p = 0.5188, 0.9628, and 0.0361, respectively. Ordinary One-way ANOVA p =0.3959, not significant (ns).

Figure 3.2 - Keks are expressed in the BW

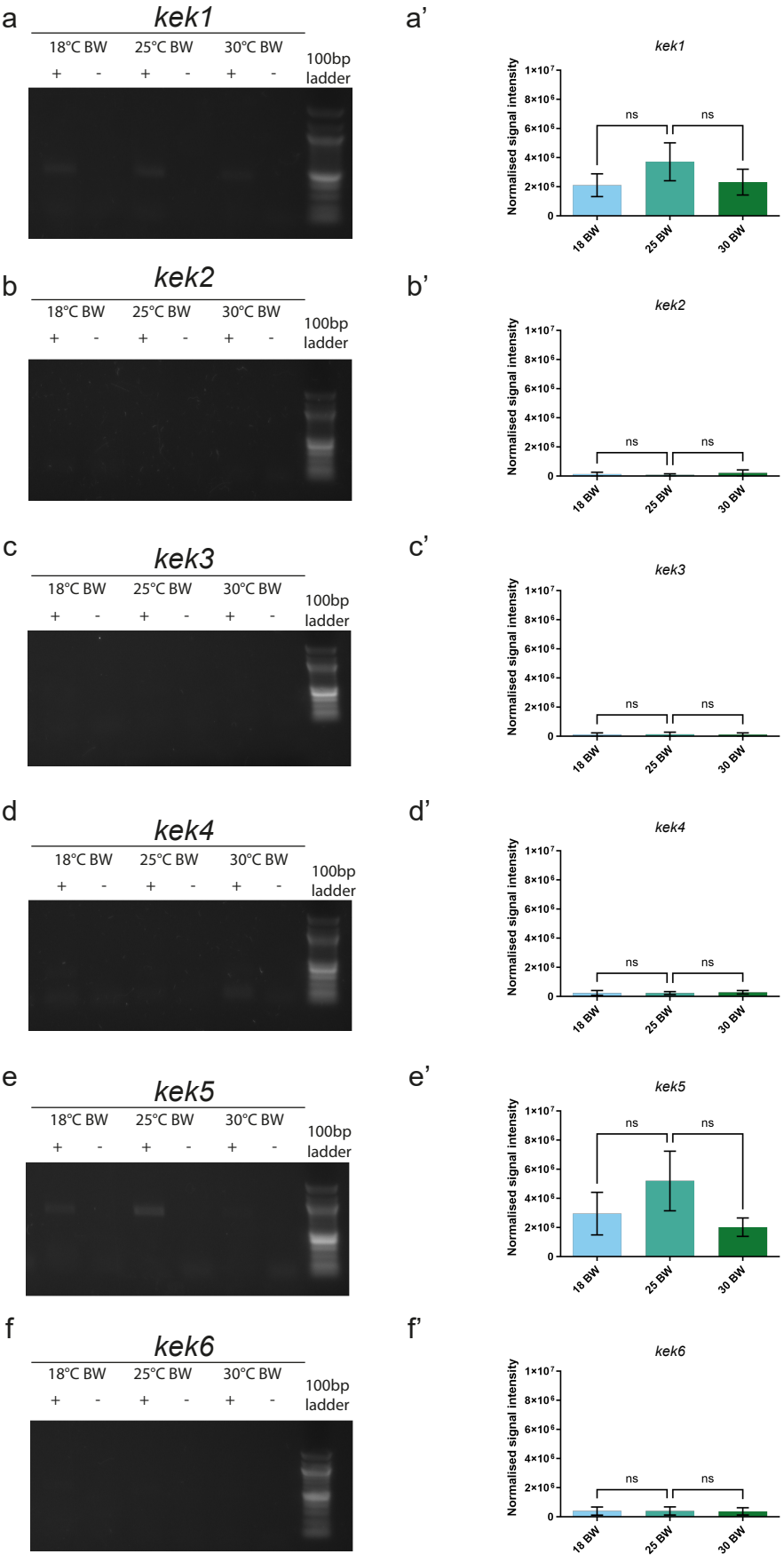


Figure 3.2 – *kek*s are expressed in the BW

Detection of *kek* transcripts via PCR of cDNA extracted from dissected larval BWs reared at 18ºC, 25ºC, and 30ºC. **A-F:** Representative gels for each gene of interest. **A'-F':** Transcript abundance was quantified via measuring signal intensity of each band in ImageJ/Fiji. For each gene and condition RNA was extracted from 10 larvae, with 4-5 technical replicates. **A':** *kek1* in the BW. For 18ºC, 25ºC, and 30ºC, Shapiro-Wilk p = 0.696, 0.4871, and 0.3723, respectively. Ordinary One-way ANOVA p = 0.5033, not significant (ns). **B':** *kek2* in the BW. Shapiro-Wilk p = 0.0001, 0.0001, and 0.0001, respectively. Kruskal-Wallis p >0.9999, not significant (ns). **C':** *kek3* in the BW. Shapiro-Wilk p = 0.0001, 0.0001, and 0.0001, respectively. Kruskal-Wallis p >0.9999, not significant (ns). **D':** *kek4* in the BW. Shapiro-Wilk p = 0.032, 0.4345, and 0.0854, respectively. Ordinary One-way ANOVA p =0.9501, not significant (ns). **E':** *kek5* in the BW. Shapiro-Wilk p = 0.1747, 0.5429, and 0.2222, respectively. Ordinary One-way ANOVA p =0.3386, not significant (ns). **F':** *kek6* in the BW. Shapiro-Wilk p = 0.0273, 0.0302, and 0.045, respectively. Kruskal-Wallis p =0.9956, not significant (ns).

sequence in addition to a plasmid driving the expression of *kek5*-targeting gRNA in the germline of embryos. A detailed description of the protocol can be found in the Methods section (Section 2.7.1, Fig. 2.5).

CRISPR-Cas9 can be used to generate knock-in insertions by firstly specifically creating a double strand break near the desired insertion site, as determined by a 20nt gRNA target sequence, which binds to the Cas9 protein (Gratz et al., 2015). This presence of this double strand break then recruits the cell's DNA repair pathways, including homology-directed repair (HDR). Under normal circumstances HDR uses the intact homologous chromosome as a template to for the broken strand, replacing it. HDR can be hijacked to create a knock-in allele by providing the repair mechanisms with an alternative template for repair, in this case, a plasmid carrying the desired insertion (Fig. 3.3). To ensure HDR occurs, and occurs specifically, two ~1 kb homologous regions (HRs) matching the regions immediately flanking the desired insertion site are inserted into the plasmid flanking the insert sequence (Gratz et al., 2015).

For *kek5-GAL4*, the desired insertion site was immediately upstream of the first coding exon, so as to have *GAL4* be under the influence of the same promoters and regulatory regions as *kek5*. Consequently, the gRNA and HRs were designed around this point.

For the plasmid carrying the insert sequence, the two ~1kb HRs were amplified via PCR that flanked the desired insertion site. These 1kb HRs were then conventionally cloned into the *GAL4* construct *pT-GEM(2)* (Diao et al., 2015).

To screen for constructs that had had both HRs inserted correctly, candidates were digested with restriction enzymes NcoI, and AgeI and EcoRI (Fig. 3.3c). Clone #1 was selected arbitrarily from the candidates that had the expected digestion profile and

Figure 3.3 - Cloning of *kek5-T2A-GAL4* donor plasmid

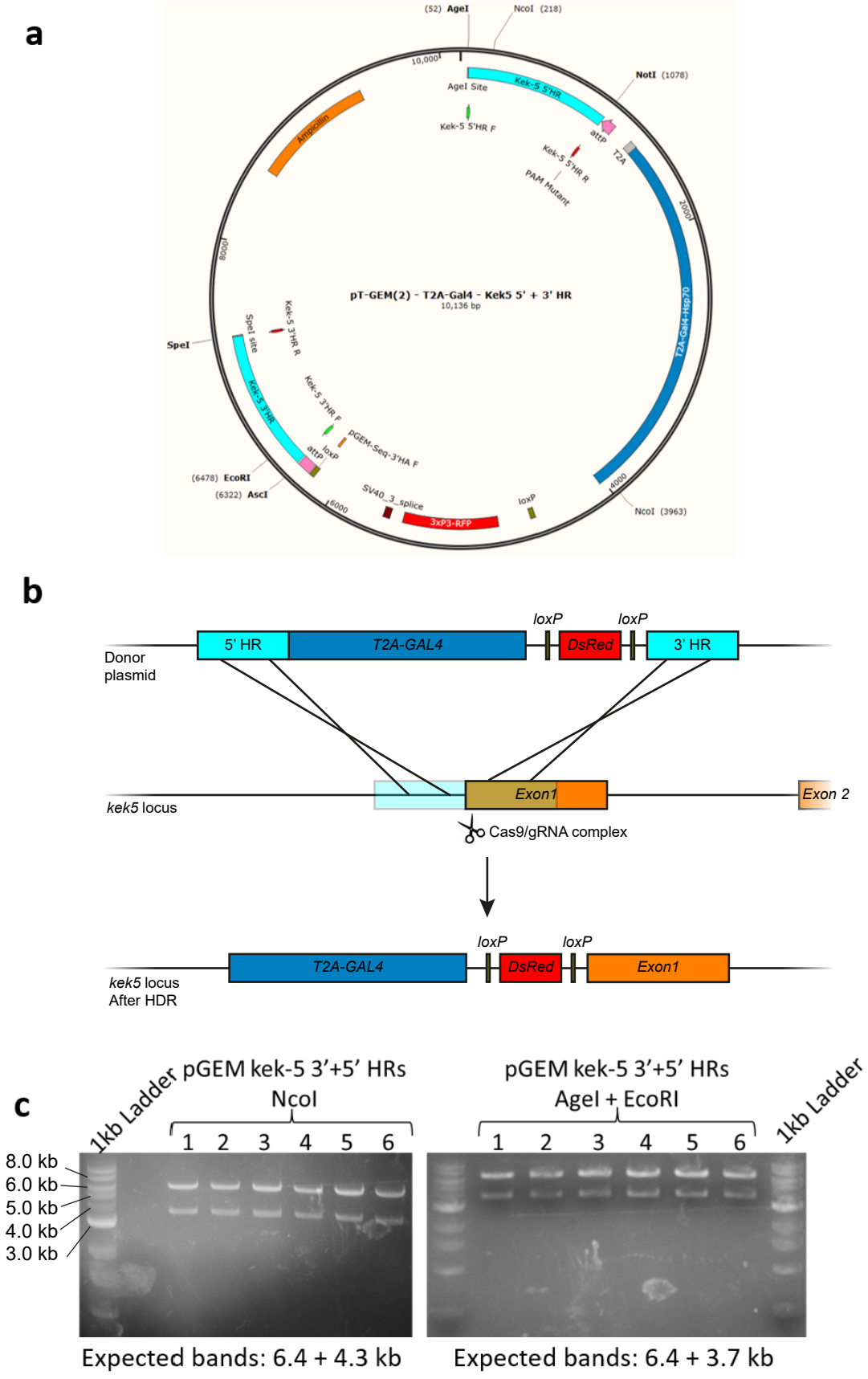


Figure 3.3 - Cloning of *kek5-T2A-GAL4* donor plasmid

A: Map of complete *pT-GEM(2)-kek5-T2A-GAL4* plasmid showing diagnostic restriction enzyme sites. **B:** Diagram showing HDR of *kek5-GAL4* construct being inserted into the endogenous kek5 locus. Following CRISPR/Cas9-mediated cleavage of the *kek5* locus, the HDR pathway replaces the broken sequence with the *kek5-GAL4* donor construct using the homologous regions flanking the insert. **C:** Restriction digests used to characterise candidate clones. (Left) NcoI, predicted bands = 6.4kb and 4.3kb, clones #1-3 appear to be the correct size. (Right) AgeI+EcoRI, predicted bands = 6.4kb and 3.7kb. All clones appear to be the correct size for this digest.

was then sequenced for the 5' and 3'HR (Fig. 3.4, Fig. 3.5). This was done to confirm that the HRs were not mutated in such a way that may render HDR unlikely or impossible, such as a large deletion or insertion.

For the 5'HR, the largest discrepancy detected was a 6bp insertion (Fig. 3.4 B). This was thought to be unlikely to disrupt HDR. Two single base pair changes were also detected within the *kek5* 5'HR.

For the 3'HR, two single base pair changes were detected (Fig. 3.5 B) . It was thought this would not have an impact on HDR. These base pair changes occur in an intron furthermore making them unlikely to impact protein folding.

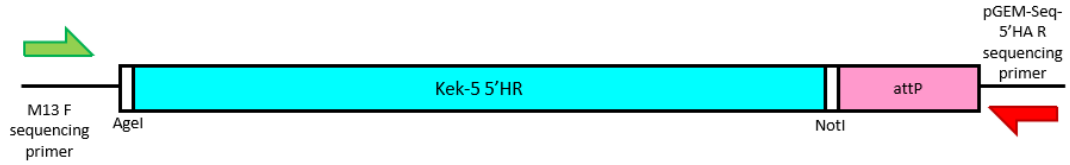
Candidate clones for the *kek5* gRNA construct (Fig. 3.6 A) were first digested with BbsI to determine if the ligation of the *kek5* gRNA had been successful. In the event of a successful ligation the BbsI sites would have been destroyed, meaning successful clones would not be digested by BbsI. From this, clones #1, 2, 3, 4 and 6 appeared to be successful (Fig. 3.6 B). Clone #1 of the gRNA construct was sequenced to ensure that the gRNA had been inserted correctly (Fig. 3.6 C and D). There were no mismatches detecting indicating that the gRNA cloning was a success.

3.2.3 Localisation of *kek5-GAL4* driven membrane-tethered fluorescent proteins

To assess the expression pattern driven by *kek5-T2A-GAL4*, it was crossed to a reporter line bearing *10x-UASmyrGFP*. Larvae with *kek5-T2A-GAL4* driving the expression of the effector *10x-UASmyrGFP* (*kek5>10xUASmyrGFP*) were dissected in L3 for the CNS as described previously. Z-stacks of representative VNCs were then

Figure 3.4 - *kek5* 5'HR sequencing

a



b



Figure 3.4 - *kek5* 5'HR sequencing

A: Diagram of the sequencing strategy for the *kek5-GAL4* 5'HR (light blue box). The forward (M13 F, green arrow) and reverse (*pGEM-Seq-5'HA R*, red arrow) are outside the sequence of the 5'HR. **B:** Alignment of sequencing data vs reference sequence. Red boxes indicate mismatches to the reference. Coloured boxes are overlaid on the alignment to highlight sequence elements per the diagram of the sequencing strategy.

Figure 3.5 - *kek5* 3'HR sequencing

a



b

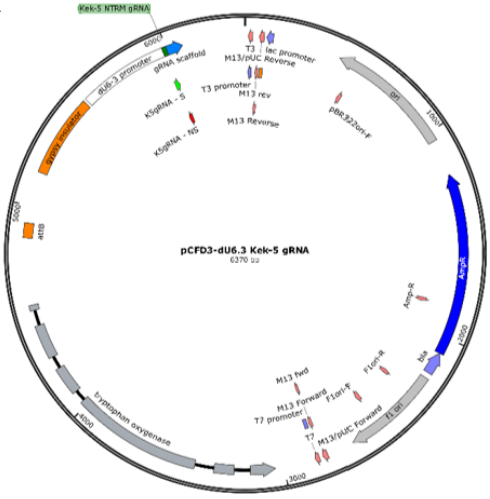


Figure 3.5 - *kek5* 3'HR sequencing

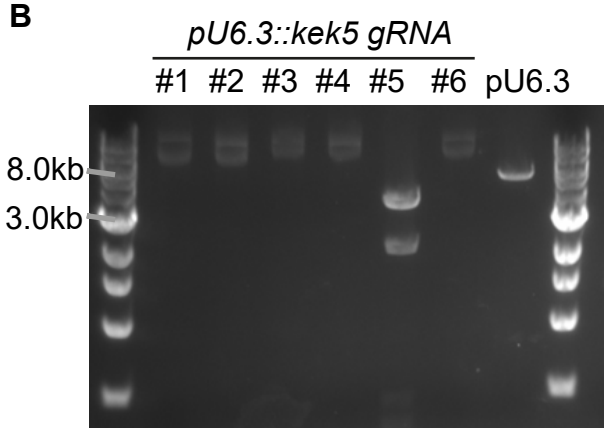
A: Diagram of the sequencing strategy for the *kek5-GAL4* 3'HR (light blue box). The forward (*pGEM-Seq-4'HA F*, green arrow) and reverse (*M13 R*, red arrow) are outside the sequence of the 3'HR. **B:** Alignment of sequencing data vs reference sequence. Red boxes indicate mismatches to the reference. Coloured boxes are overlaid on the alignment to highlight sequence elements per the diagram of the sequencing strategy.

Figure 3.6 - Cloning of *pU6.3 kek5 gRNA* plasmid

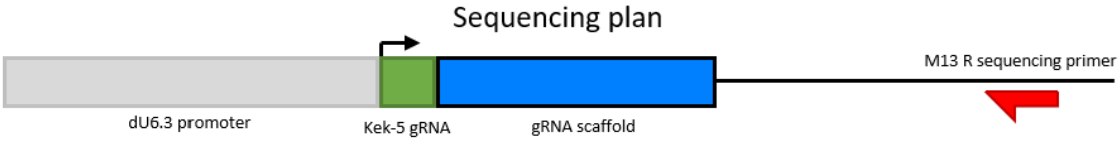
A



B



C



D

```
Reference                                                
```

Figure 3.6 – Cloning of *pU6.3 kek5 gRNA* plasmid

A: Map of complete *pU6.3-kek5-gRNA* plasmid. **B:** Restriction digest of candidate clones with BbsI. Undigested plasmids indicates a potentially successful ligation as the BbsI sites would be destroyed in a correct clone, a negative control (pU6.3 – the empty plasmid) was included for comparison. All clones except #5 appear to have had successful ligations. **C:** Diagram of sequencing strategy. *M13 R* sequencing primer is downstream of the gRNA insertion site. **D:** Alignment of Sequencing data from final construct to reference showing correct insertion of gRNA.

acquired (Fig. 3.7 A). *kek5-GAL4* drives expression in lateral and ventral neurons in the VNC, and their projections can be seen flanking the midline.

An endogenously tagged Kek5 protein fusion to GFP line, Kek5-GFP, had previously been generated by former lab member Joan Roig. As such this only shows the localisation of Kek5 protein but is not directly descriptive of the cells that express *kek5*. To compare the *kek5-GAL4* expression pattern against the previously generated Kek5-GFP line, Kek5-GFP was combined with *UAS-tdTomato*. The line *kek5-GFP ; + ; UAS-tdTomato* was then crossed to *kek5-GAL4* so that *kek5-GAL4* expression could be visualised in the 546nm channel, with Kek5-GFP in the 488nm channel.

Interestingly, the Kek5-GFP and *kek5-GAL4* line appear to have different expression patterns (Fig. 3.7 B). Kek5-GFP in cell bodies and neurites are not as obviously visible as the GAL4 line. Furthermore, the Kek5-GFP pattern is present along the midline of the VNC, where there is no GAL4-driven expression of *tomato*. Nonetheless there is some overlap between the two expression patterns. Both lines co-express in neurites that flank the midline of the VNC and Kek5-GFP can be seen in the soma of some cells that have *kek5*>Tomato signal (Fig. 3.7 B, arrows).

It appears that *kek5-T2A-GAL4* drove expression in a subset of *kek5-GFP* expressing cells. It could be that this an effect of using GAL4, wherein perdurance of GAL4, and the delay caused by requiring its synthesis, leads to *kek5-GAL4* revealing the cells in which *kek5* had been expressed in, whereas Kek5-GFP reveals the current position of Kek5 protein

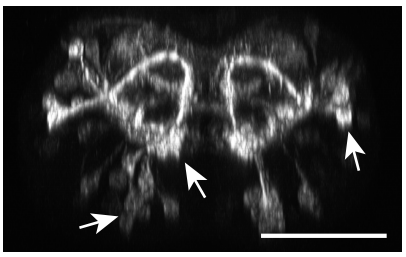
To determine if *kek5* is expressed in motoneurons, *kek5*>Tomato larvae were dissected to visualise NMJ 6/7. *kek5-GAL4* was found to drive expression in the

Figure 3.7 - *kek5-T2A-GAL4* drives expression in CNS neurons

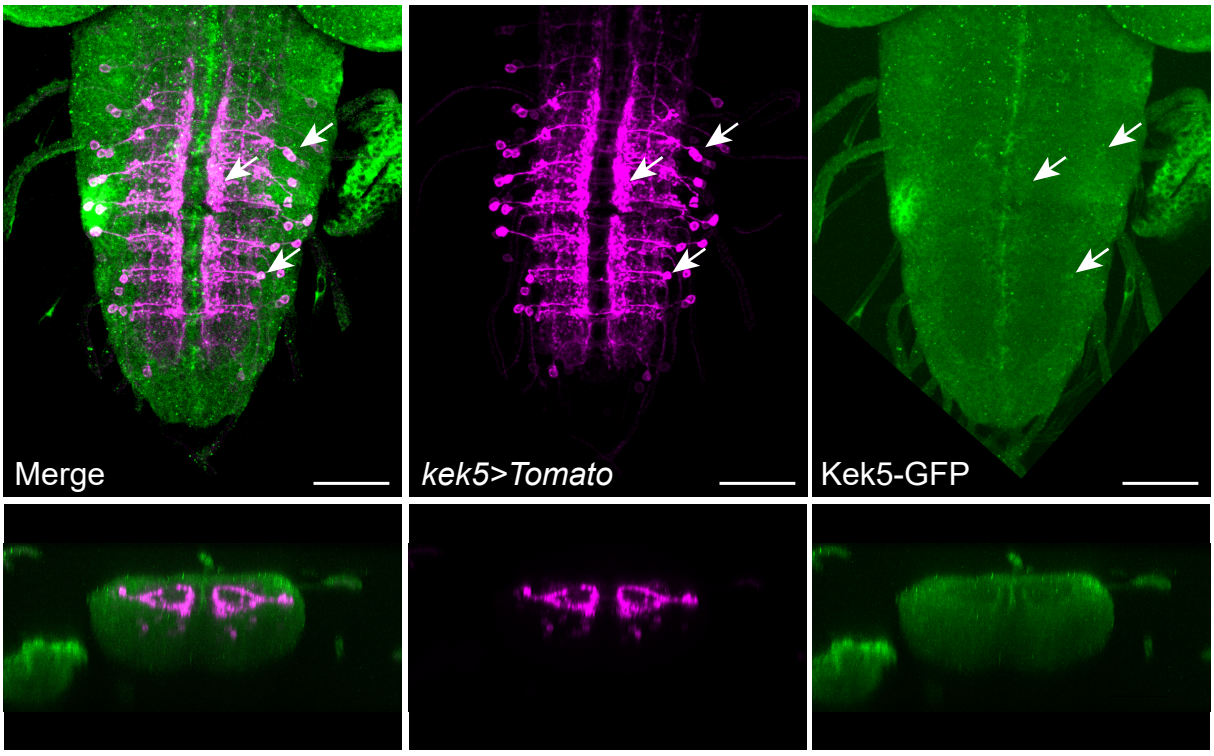
A - *kek5 GAL4* drives expression in the larval ventral nerve cord (VNC)



Transverse view



B - *kek5-GAL4* drives expression in a subset of Kek5-GFP cells



C - *kek5-GAL4* drives expression at NMJ 6/7 in L3 wandering larvae

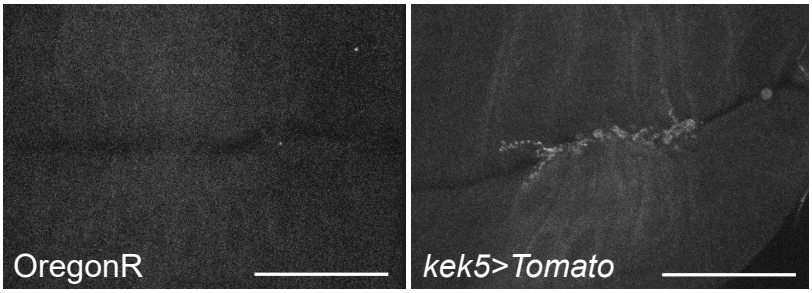


Figure 3.7 - *kek5-T2A-GAL4* drives expression in CNS neurons.

A: *kek5>myrGFP* L3 larval VNC stained imaged on a Zeiss 710 confocal microscope, n = 3 larvae. All scale bars = 50µm. (Left) Representative maximum projection of a VNC from a dorsal perspective. (Right) Transverse view of a single abdominal segment of the same VNC. **B:** VNC of *kek5-GFP, kek5>Tomato* larva, transverse view below, n = 5 larvae. There is some faint overlap between the *kek5>Tomato* and Kek5-GFP signals (Arrows). **C:** (Left) NMJ 6/7 in a L3 wandering OregonR larva, without staining (546nm). (Right) NMJ 6/7 in a L3 wandering *kek5>Tomato* larva without staining (546nm), showing *kek5>Tomato* expression at the NMJ, n = 3 NMJs from 3 larvae.

motoneurons that innervate muscle 6/7 (Fig. 3.7 C), indicating that *kek5* is indeed expressed naturally in motoneurons.

Following from the RT-PCR data that indicated the *kek5* was expressed in the body wall, *kek5-GAL4* larvae were dissected to image the PNS (Fig. 3.8). The antibody 22C10 (anti-Futsch) was used here to visualise peripheral neuron dendrites as it has been used previously by others in the field for this task (Hummel et al., 2000). *kek5-GAL4* drove expression in at least four PNS neurons. Three of these neurons were multiple dendritic arbour (mda) neurons, and the fourth was a bipolar neuron.

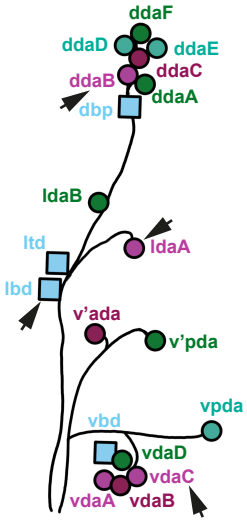
Based on the morphology of their dendritic arbours, the three *kek5-GAL4* mda neurons were Class II mda neurons, as they are more complex than typical Class I dendrites, but are not as complex as Class III and IV. Furthermore, the *kek5-GAL4* neurons lack the dendritic spines that are characteristic of the Class III and IV mda neurons (Grueber et al., 2002). In addition to morphology, *kek5-GAL4* neurons seem to share the positions of Class II mda neurons within the larval hemisegment. Based on position and morphology, *kek5* appears to be expressed in the Class II mda neurons: ddaB, ldaA and vdaC, and in the bipolar neuron lbd.

3.2.4 Subcellular distribution of Keks in the larval VNC

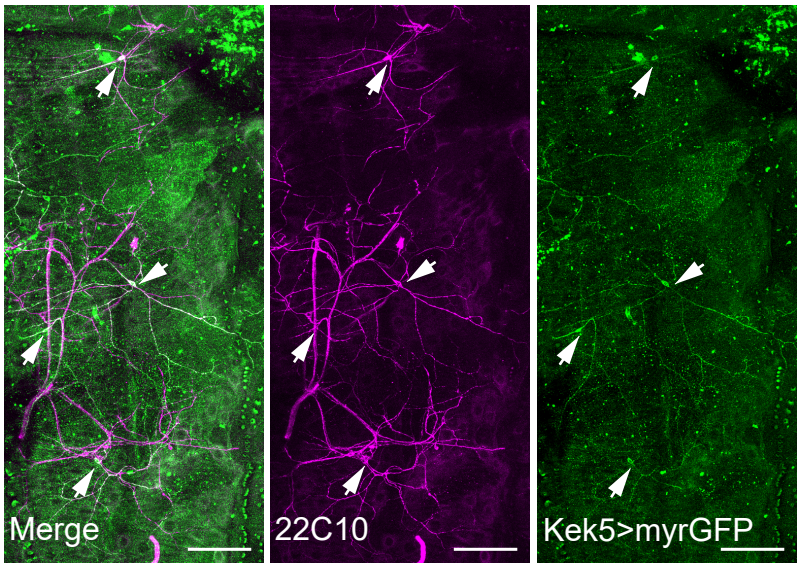
The localisation of proteins within a cell is a key piece of information that can be informative about the genes function and its interactions with other proteins and cellular pathways. This is especially true for neurons which are highly polar, with axons and dendrites being highly specialised for their respective function. Discovering the

Figure 3.8 - *kek5-T2A-GAL4* drives expression in the PNS

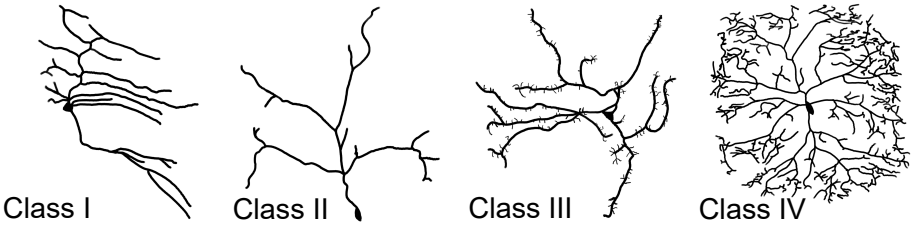
A - Map of the PNS



B - *kek5>myrGFP* in the PNS (hemisegment)



C - Classes of mda neurons



D - *kek5-GAL4* PNS neurons

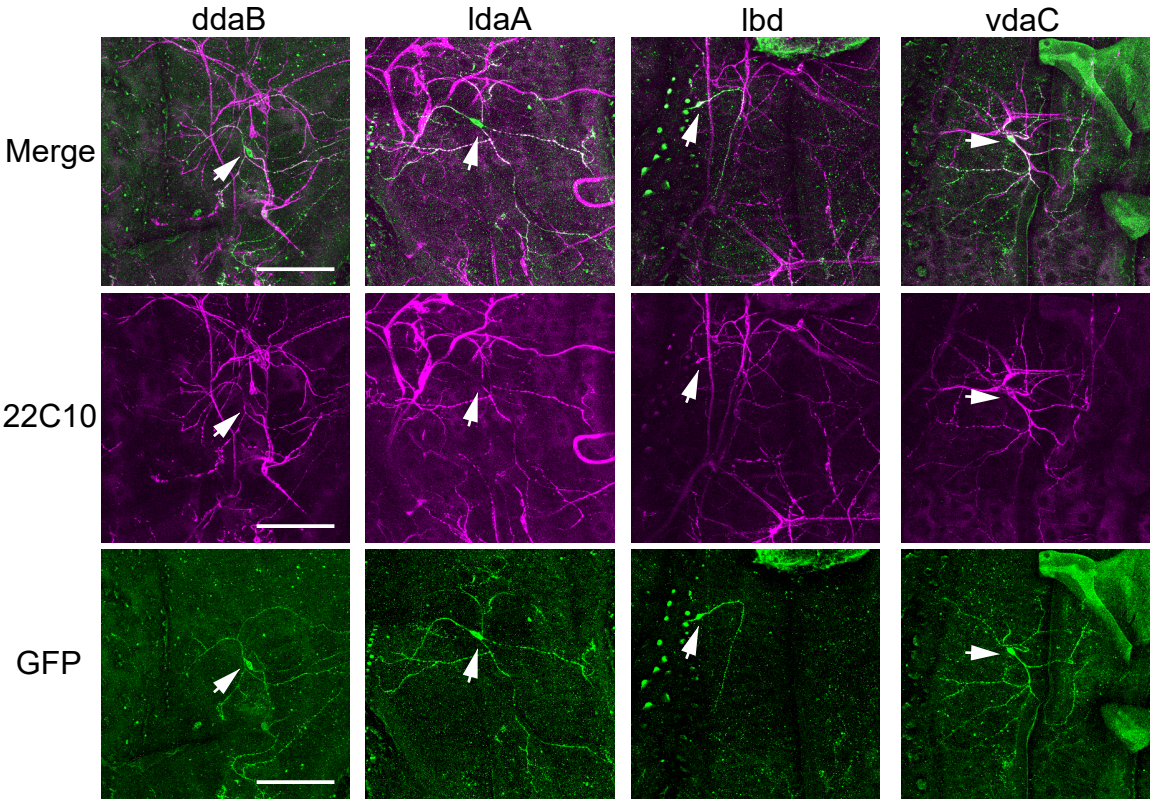


Figure 3.8 - *kek5-T2A-GAL4* drives expression in the PNS

kek5-GAL4 drives expression in a subset of PNS neurons. All scale bars = 100µm. **A:** Map of mda neurons in the larval PNS. Adapted from Grueber et al 2002, and Orgogozo and Grueber 2005. Shows Class I (turquoise circles), Class II (Magenta circles), Class III (dark green circles) Class IV (purple circles) and other (light blue squares) mda neurons. *kek5-GAL4* neurons are pointed out by arrows. **B:** Abdominal hemisegment of L3 wandering *kek5>myrGFP* larvae imaged on a Zeiss 710 confocal microscope, stained with anti-22C10 (Futsch) to visualise neurites, and anti-GFP, n = 11 hemisegements from 6 larvae. *kek5-GAL4* neurons are pointed to with arrows. **C:** Classes of mda neurons. Adapted from Grueber et al 2003. **D:** Representative images of identified *kek5-GAL4* PNS neurons cropped from hemisegment images. Left-to-Right: ddaB, ldaA, lbd, vdaC.

subcellular localisation of Keks within neurons will be vital for understanding the roles they play.

To further understand the function of Keks it was imperative to know their subcellular localisations. This is especially critical in neurons as they are highly polar cells, and the localisation of Keks could drive distinct functions. *D42-GAL4* was used to drive the expression of Kek-RFP protein fusions in motoneurons (Bishop, 2014). Firstly, larvae were dissected and stained to visualise the VNC (Fig. 3.9).

RFP signal appears to be absent in *D42>kek1-RFP* larvae making definitive statements about Kek1 localisation in the VNC impossible. For *D42>kek2-RFP* larvae however, Kek2-RFP localised strongly to the dorsal neuropil, which is composed of motoneuron dendrites (Landgraf et al., 2003). For *D42>kek3-RFP* signal can be seen in the dorsal neuropil, but also in cell bodies and in the segmental nerves, suggesting that Kek3 localises throughout the neuron. *D42>kek4-RFP* localises also to the dorsal neuropil, cell bodies and segmental nerves, indicating localisation throughout the neuron. Kek5 and 6 localise to the cell bodies and are faintly visible in the dorsal neuropil but appear to be absent in the interior of the neuropil. This indicates that Kek5 and Kek6 specifically localise to cell bodies and potentially the axonal terminals at the NMJ.

3.2.5 Peripheral nervous system expression of Kek proteins

To more closely examine the localisation of Keks to axonal terminals in the CNS, *109(2)80-GAL4*, a driver for PNS neurons was used (Gao et al., 1999). *109(2)80-GAL4* has been reported to drive expression in strongly in multidendritic neurons in the PNS (Gao et al., 1999). This allowed greater clarity, as PNS cell bodies and

Figure 3.9 - Keks have different sub-cellular localisations in *D42-GAL4* neurons

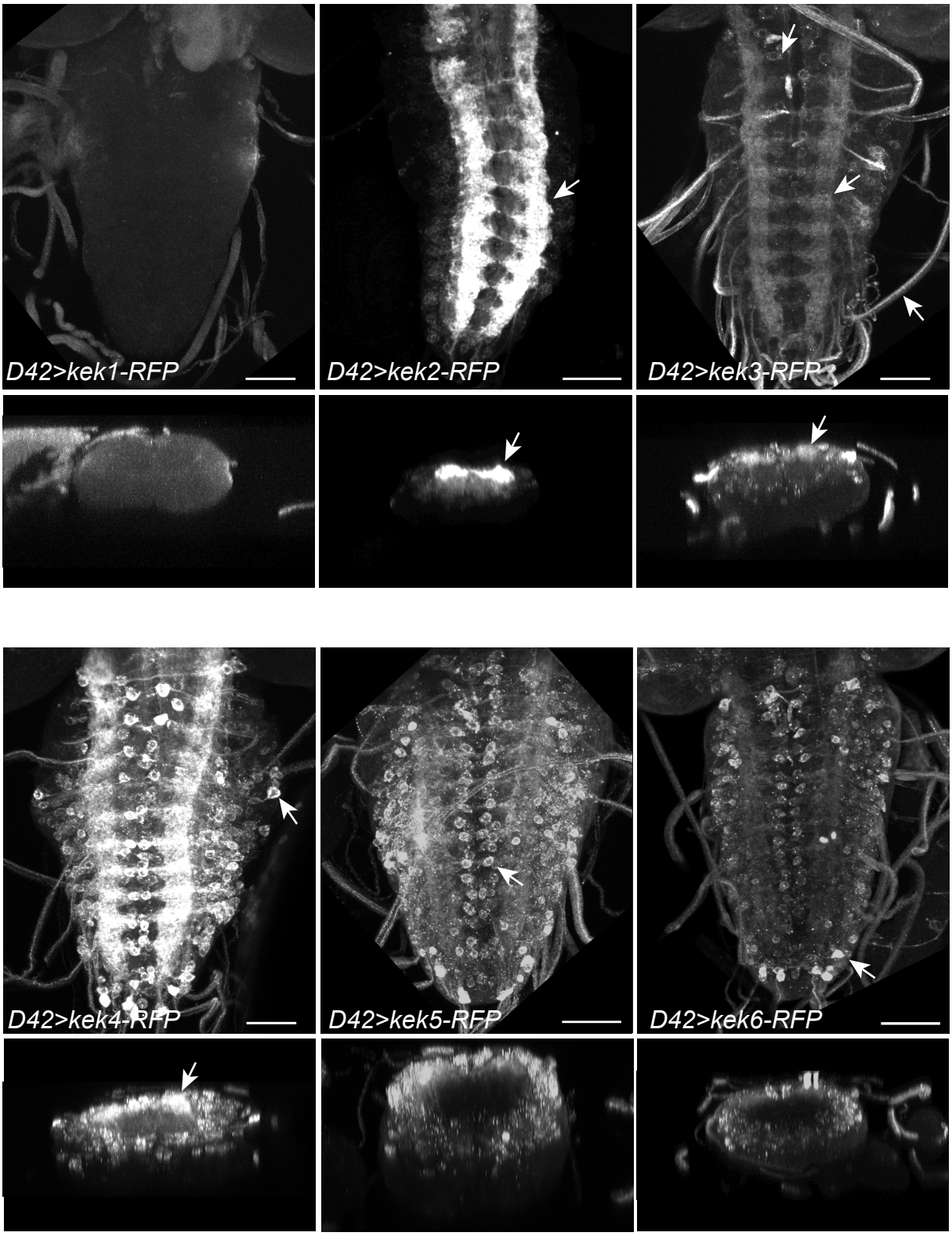


Figure 3.9 – Keks have different sub-cellular localisations in *D42-GAL4* neurons

Representative VNCs of *D42>kek-RFP* larvae, stained with anti-DsRed, acquired on a Zeiss 710 confocal microscope. All scale bars = 50µm. Top row, left-to-right: Kek1 (n = 4), Kek2 (n = 4), Kek3 (n = 4). Bottom row, left-to-right: Kek4 (n = 5), Kek5 (n = 3), Kek6 (n = 4). Transverse projections of a single abdominal section of the VNC is provided beneath each image. The staining in *D42>kek1-RFP* larvae has produced no signal. Kek2-RFP appears to strongly localise to motoneuron dendrites (arrow). Kek3-RFP localises throughout the neuron, in cell bodies (upper arrow), dendrites (middle arrow), and in axons (segmental nerves, lower arrow). Kek4 also appears to localise throughout the neuron (arrows). Kek5 and 6 appear to localise to cell bodies (arrows) and segmental nerves (axons).

dendrites are located in the body wall. The *GAL4* line used here had been previously recombined with *UAS-myrGFP*, this recombinant line was used to label the axons of PNS neurons in the VNC (*109(2)80>GFP*). The *109(2)80-GAL4* expression pattern features nerves entering the CNS and terminating adjacent to the midline in a pattern that allows the commissures of each segment in the VNC to be visible (Fig. 3.10). Additionally, lines of neural projections are visible laterally flanking these commissures (Fig. 3.10). These neural projections are also more dorsal than the commissures. Interestingly, cell bodies of interneurons are visible within the *109(2)80-GAL4* pattern.

To visualise the pre-synaptic sites of PNS neurons, *109(2)80>GFP* flies were crossed to *UAS-brp-mCherry* flies (Fig. 3.10). Brp signal colocalizes with the more medial bands of GFP signal, indicating that these indeed correspond to the pre-synaptic sites of PNS neurons, consistent with the afferent nerves that are visible around the VNC.

Brp signal was also visible as dots inside the cell bodies of neurons in the VNC, which could represent nascent Brp being generated prior to trafficking to active zones. Strikingly, Brp signal is absent from the more lateral projections along the VNC, indicating that these are not axonal in nature (Fig. 3.10, left-hand arrow). They could be the dendrites of interneurons whose cell bodies are visible in the *109(2)80-GAL4* expression pattern in the VNC.

109(2)80>GFP flies were crossed to *uas-kek-RFP*s to visualise their subcellular distributions in this expression pattern in the VNC (Fig. 3.10-13). Attempts were made to visualise the distribution of the Kek-RFPs in the dendrites of peripheral neurons with these genotypes, however the staining could not be optimised to a satisfactory level to be able to visualise dendrites in control larvae. In *109(2)80>GFP>kek1-RFP larvae*,

Figure 3.10 - Distribution of Brp in *109(2)80-GAL4* neurons

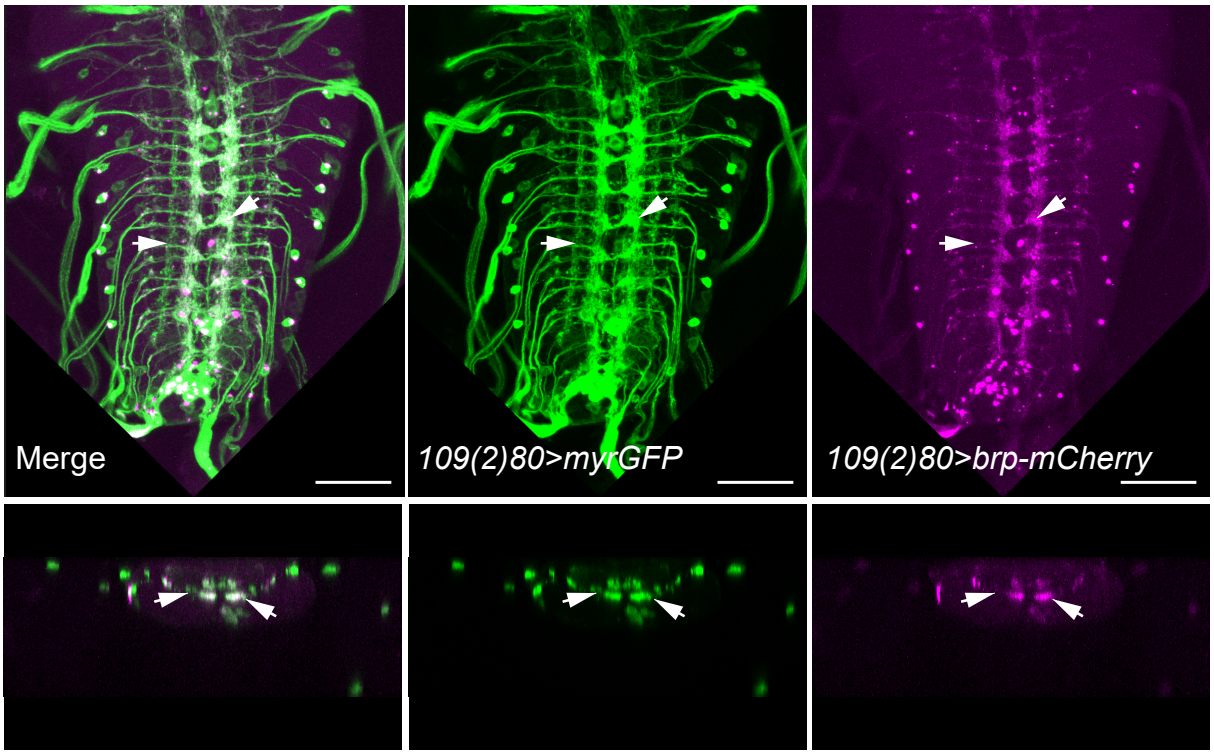
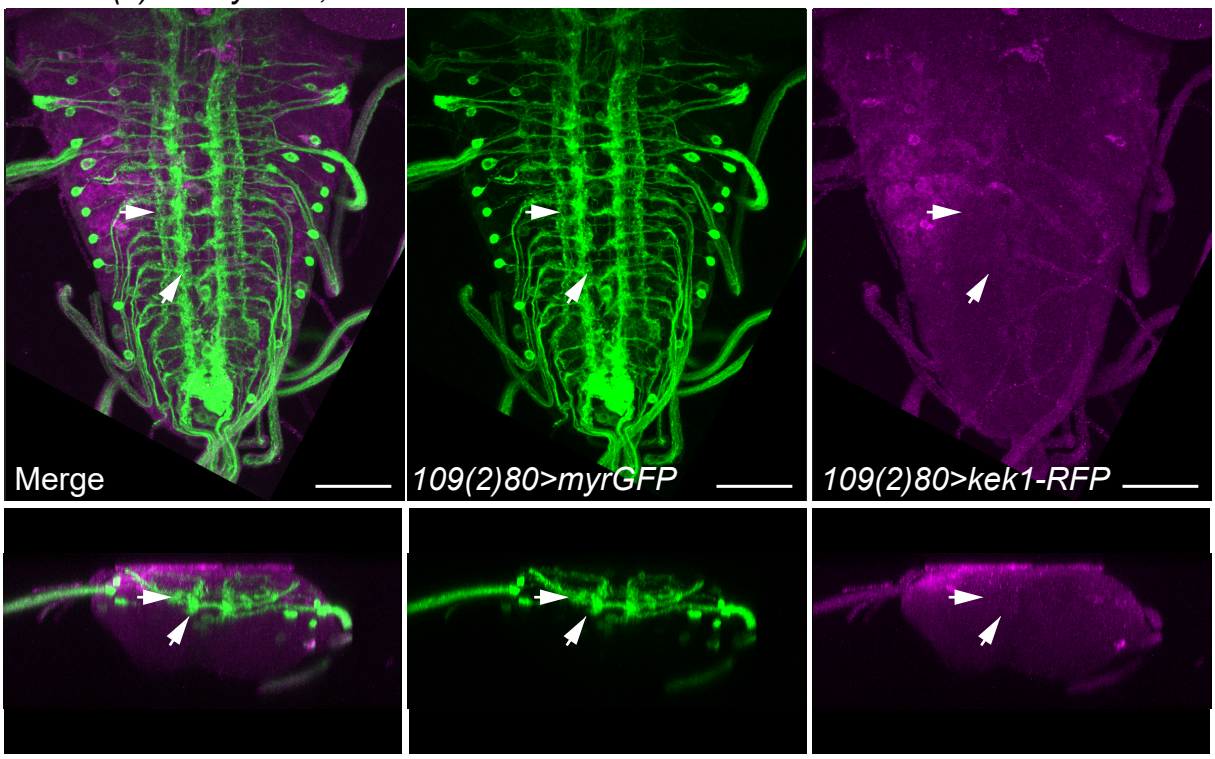


Figure 3.10 – Distribution of Brp in *109(2)80-GAL4* neurons

Expression pattern of *109(2)80>myrGFP* reveals axonal terminals and non-axonal neurites in the VNC. Representative VNC of *109(2)80>myrGFP*, *brp-mCherry* larvae, acquired on a Zeiss 710 confocal microscope, n = 4. All scale bars = 50µm. Brp-mCherry labels presynaptic sites. Left arrows point to putative dendrites, right arrows point to PNS neuron axonal terminals.

Figure 3.11 - Localisation of Kek1-RFP and Kek2-RFP with *109(2)80-GAL4*

A - 109(2)80>myrGFP, kek1-RFP



B - 109(2)80>myrGFP, kek2-RFP

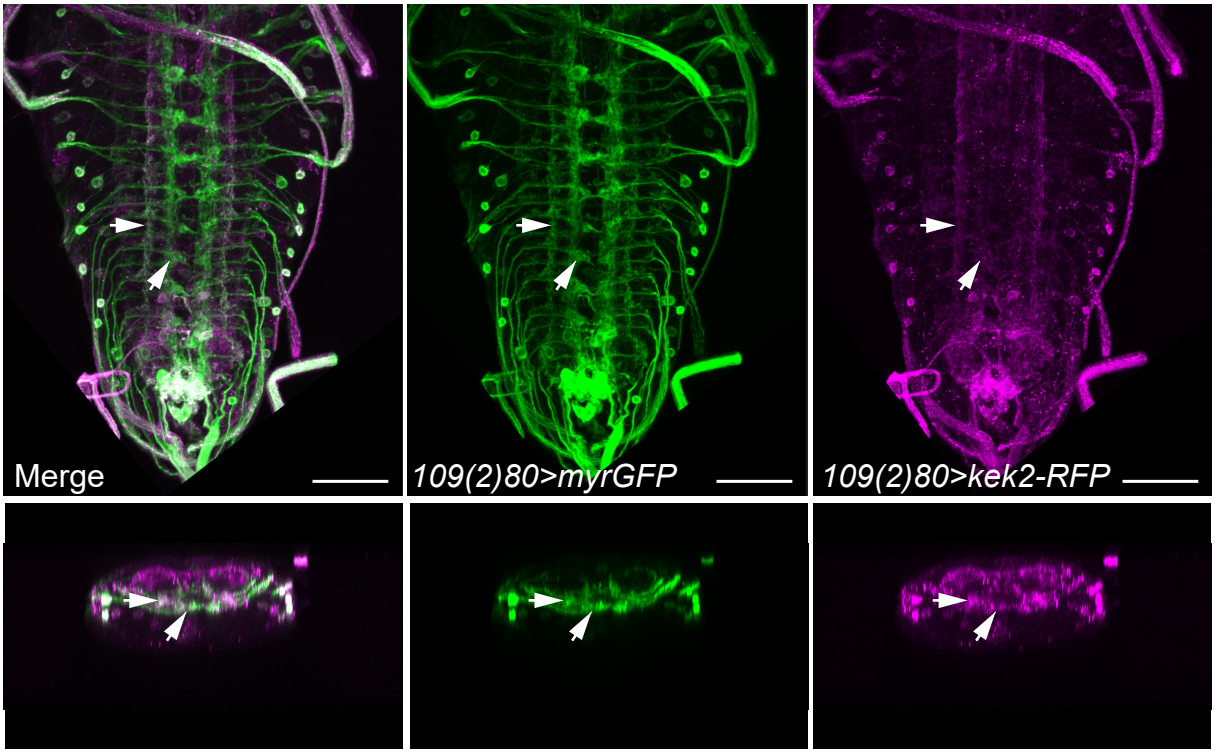
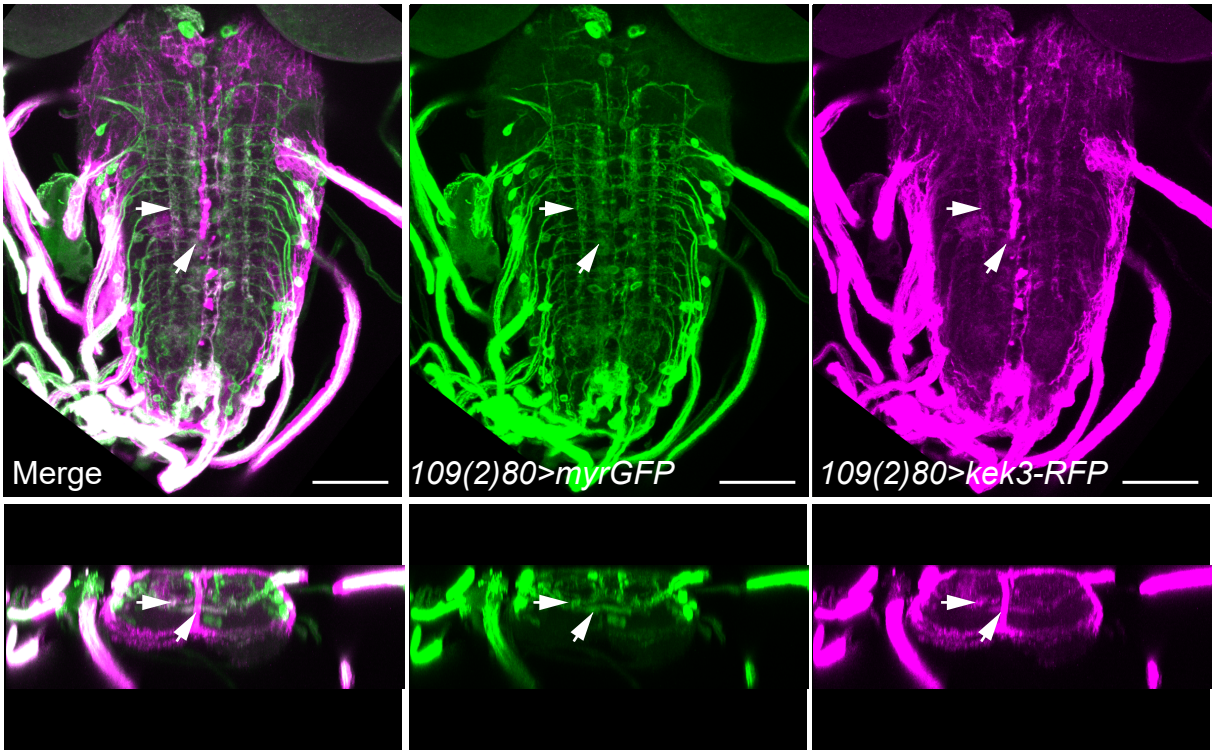


Figure 3.11 – Localisation of Kek1-RFP and Kek*2-RFP* with *109(2)80-GAL4*

Subcellular localisation of Kek1-RFP and Kek2-RFP overexpressed with *109(2)80-GAL4*. All images acquired with a Zeiss 710 confocal microscope. All scale bars = 50µm. In both genotypes and views, the upper arrows point to the dendritic projections and the lower arrows point to axonal terminals. The staining of *109(2)80>myrGFP*, *kek1-RFP* appears to have no signal. Kek2 localised in the non-axonal neurites suspected to be dendrites, but not in the axonal terminals of PNS neurons. **A:** Representative VNC of a *109(2)80>myrGFP*, *kek1-RFP* larva, n = 3. **B:** Representative VNC of a *109(2)80>myrGFP*, *kek2-RFP* larva, n = 5.

Figure 3.12 - Localisation of Kek3-RFP and Kek4-RFP in *109(2)80-GAL4* neurons

A - 109(2)80>myrGFP, kek3-RFP



B - 109(2)80>myrGFP, kek4-RFP

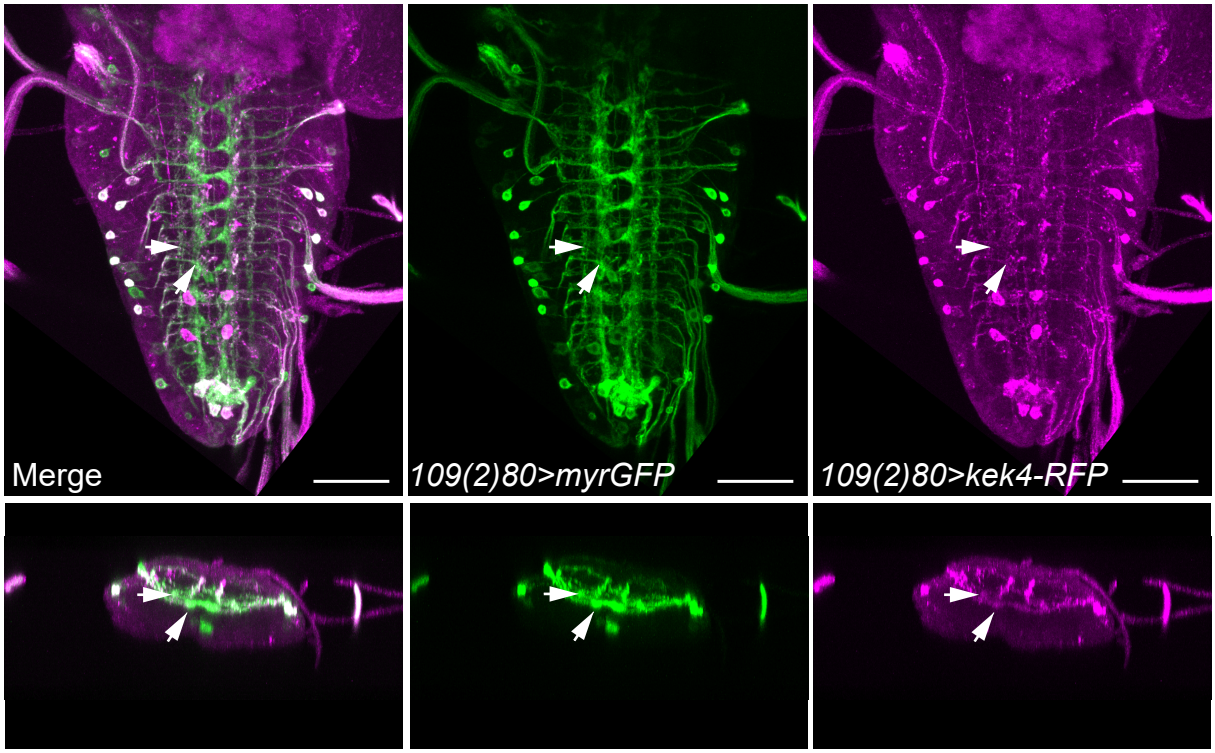
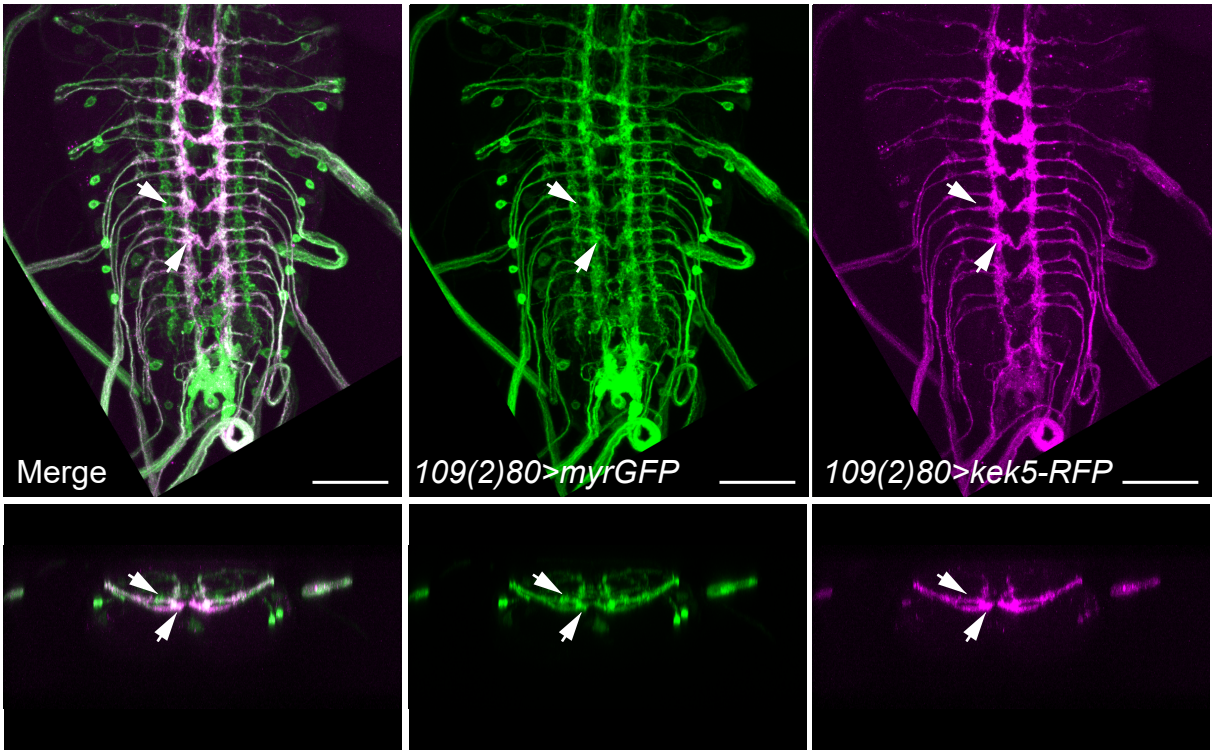


Figure 3.12 – Localisation of Kek3-RFP and Kek4-RFP in *109(2)80-GAL4* neurons

Subcellular localisation of Kek3-RFP and Kek4-RFP overexpressed with *109(2)80-GAL4*. All images acquired with a Zeiss 710 confocal microscope. All scale bars = 50µm. In both genotypes and views, the upper arrows point to the dendritic projections and the lower arrows point to axonal terminals. Kek3 and -4-RFP appeared to localise throughout the neurons, colocalising with PNS axonal terminals and non-axonal neurites (arrows). **A:** Representative VNC of a *109(2)80>myrGFP*, *kek3-RFP* larva, n = 5. **B:** VNC of a *109(2)80>myrGFP*, *kek4-RFP* larva, n = 3.

Figure 3.13 - Localisation of Kek5-RFP and Kek6-RFP with *109(2)80-GAL4*

A - 109(2)80>myrGFP, kek5-RFP



B - 109(2)80>myrGFP, kek6-RFP

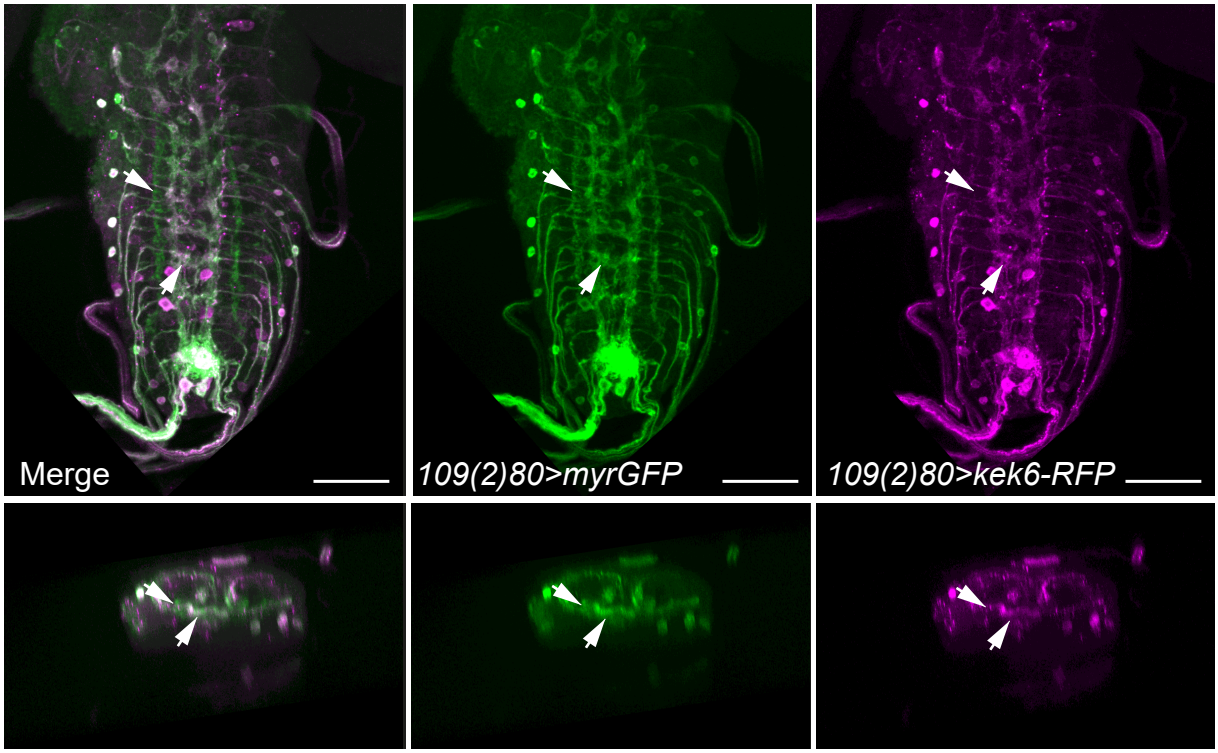


Figure 3.13 – Localisation of Kek5-RFP and Kek6-RFP with *109(2)80-GAL4*

Subcellular localisation of Kek5-RFP and Kek6-RFP overexpressed with *109(2)80-GAL4*. All images acquired with a Zeiss 710 confocal microscope. All scale bars = 50µm. In both genotypes and views, the upper arrows point to the dendritic projections and the lower arrows point to axonal terminals. Kek5- and Kek6-RFP appear to localise to axonal terminals but not non-axonal neurites. **A:** Representative VNC of a *109(2)80>myrGFP*, *kek5-RFP* larva, n = 4. **B:** Representative VNC of a *109(2)80>myrGFP*, *kek6-RFP* larva, n = 3.

Kek1-RFP signal appears to be absent, as was the case for the *D42>kek1-RFP* larvae (Fig 3.11 A).

For *109(2)80>GFP>kek2-RFP* larvae, Kek2-RFP localised strongly to cell bodies, and to the projections that potentially mainly receive synaptic input (Fig, 3.11 B). Notably, Kek2-RFP signal was weak in the PNS axonal terminals, indicating that Kek2 localises preferentially to dendrites instead of axons.

In the case of Kek3, Kek3-RFP signal could be seen strongly in the afferent nerves from the PNS and along the midline of the VNC (Fig. 3.12 A). Kek3-RFP signal is also in the axonal terminals of PNS neurons, and in the dendrites of CNS neurons. This further supports the notion that Kek3 localised throughout the neuron.

In *109(2)80>GFP, kek4-RFP* larvae, Kek4-RFP localised strongly to the cell bodies of CNS neurons and afferent axons (Fig. 3.12 B). Kek4-RFP localised to the PNS axonal terminals and CNS dendrites.

For *109(2)80>GFP, kek5-RFP*, Kek5-RFP localised strictly to axonal terminals (Fig. 3.13 A). Signal was absent from CNS dendrites and was weak in the cell bodies of 109(2)80 CNS neurons. Kek5-RFP signal was also present in afferent nerves.

Finally, *109(2)80>GFP, kek6-RFP* larvae had Kek6-RFP signal in the cell bodies of 109(2)80 CNS neurons and in the axonal terminals of PNS neurons (Fig. 3.13 B). Kek6-RFP was absent from the dendrites of CNS neurons.

3.2.6 Keks localised to axonal terminals of motoneurons

To further understand the role Keks may play at the synapse, *D42>kek-RFP* larvae were dissected to visualise NMJ 6/7 (Fig. 3.14). Again, Kek1-RFP signal was absent,

Figure 3.14 - Keks have varied subcellular localisation in motoneurons

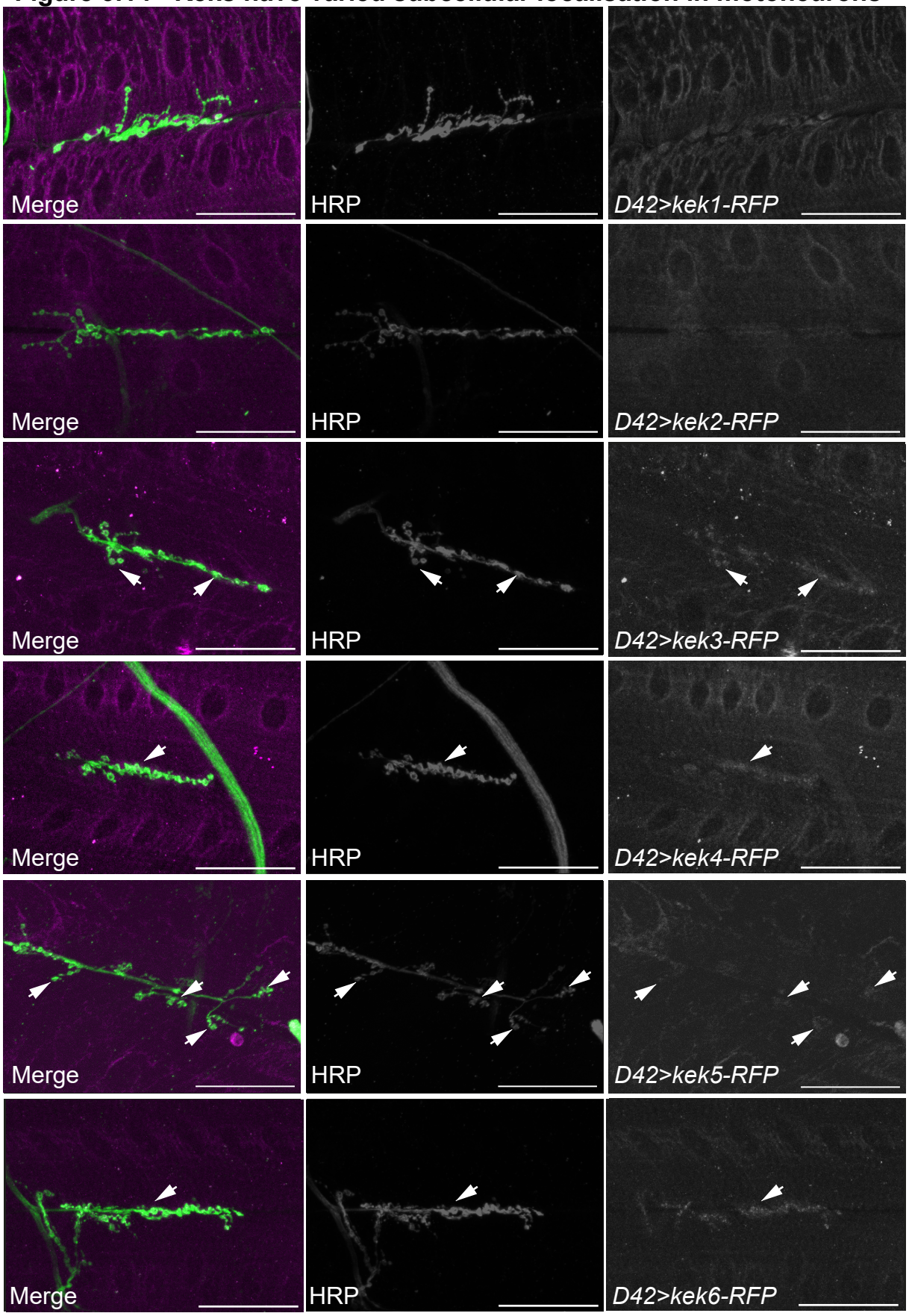


Figure 3.14 – Keks have varied subcellular localisation in motoneurons

Overexpression of the *kek-RFPs* at NMJ6/7 A3-4 in L3 wandering larvae. Stained with anti-HRP and anti-mCherry. Arrows point to examples of Kek-RFP signal. All scale bars = 50µm. Top-to-Bottom: *D42>kek1-RFP* (n = 4 NMJs from 4 larvae), *D42>kek2-RFP* (n = 3 NMJs from 2 larvae), *D42>kek3-RFP* (n = 4 NMJs from 3 larvae), *D42>kek4-RFP* (n = 4 NMJs from 3 larvae), *D42>kek5-RFP* (n = 3 NMJs from 2 larvae), *D42>kek6-RFP* (n = 3 NMJs from 3 larvae).

which was further indication that the RFP protein fusion may not be folding correctly. Kek2-RFP did not appear to be localised to the axonal terminal. Kek3-RFP to localised throughout the axonal terminal. Keks 4, 5 and 6 localised to boutons but not the axon itself.

To get a clearer picture of the localisation of Kek3-6 within boutons, images of Ib boutons at NMJ 6/7 in *D42>kek-RFP* larvae were acquired using Airyscan quasi-super-resolution (Fig. 3.15). Keks 3-6 all localised to puncta within Ib boutons at NMJ 6/7. Furthermore, Kek3 and 4 puncta appear to be larger and fewer than for other Keks.

3.2.7 Generation of *kek6-TSTEP*

To study the expression and subcellular localisation of Kek6 in greater detail I aimed to produce a protein fusion to Kek6. The *TSTEP* (Tissue-specific tagging of endogenous proteins) construct was selected due to its potential utility as a protein fusion that could be conditionally swapped from RFP to GFP under the influence of GAL4 (Koles et al., 2016, Fig. 3.16).

Previous reports of the *kek6-GAL4* expression pattern suggested that *kek6* would be widely expressed in the larval VNC, making the observation and characterisation of individual *kek6* neurons difficult (Ulian-Benitez, 2018). TSTEP, in its default state, is a C-terminal protein fusion to RFP, fused to the protein of interest via a linker peptide encoded by a recombinase recognition site (Koles et al., 2016). When the recombinase is expressed the RFP tag is flipped out and replaced by an eGFP tag (Fig. 3.16 A, Koles et al., 2016). The intention here was to be able to visualise single *kek6* neurons amongst a potentially dense field of other *kek6* neurons by swapping

Figure 3.15 - Overexpressed Kek3-6 localise to puncta in Ib boutons

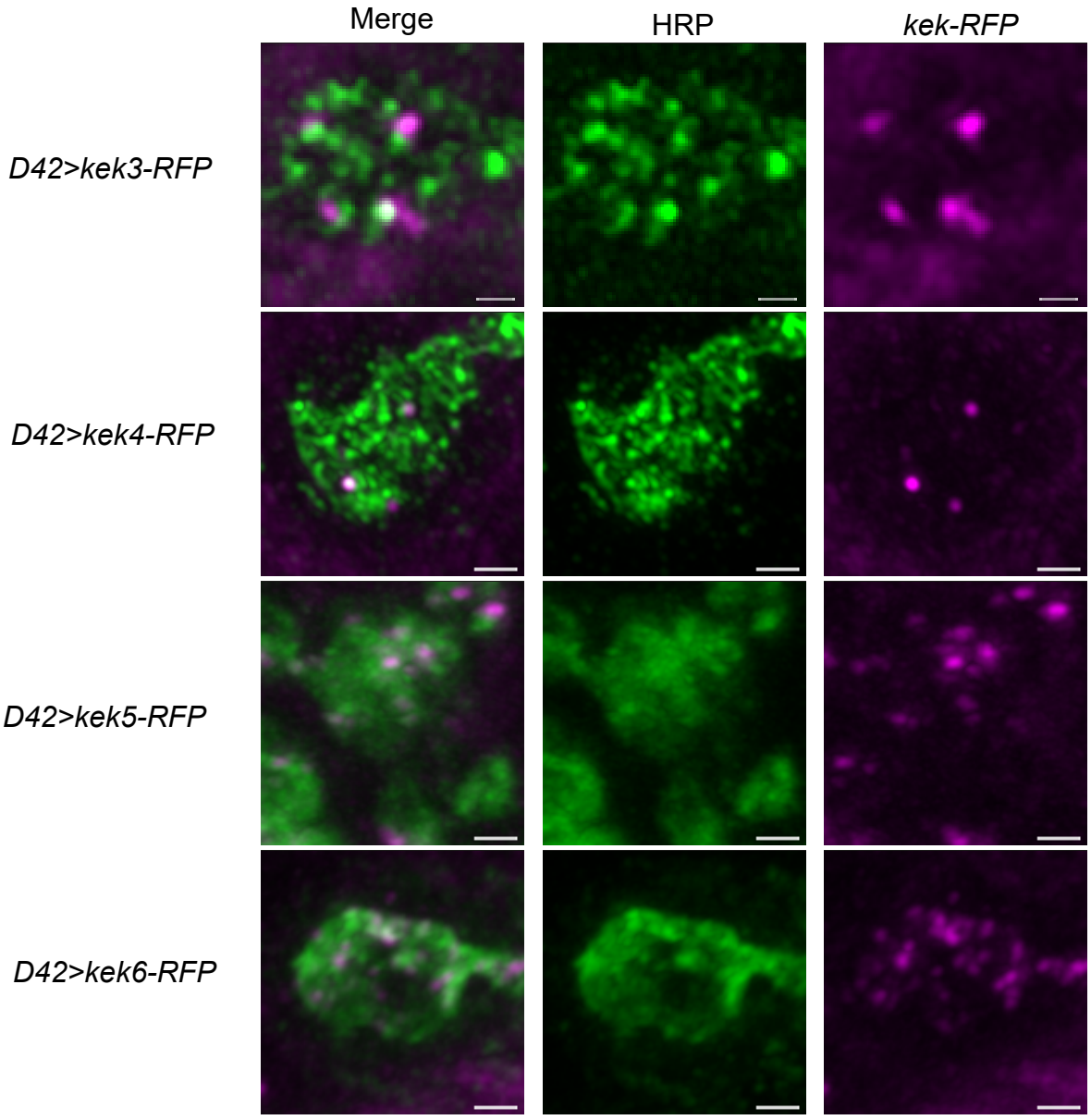
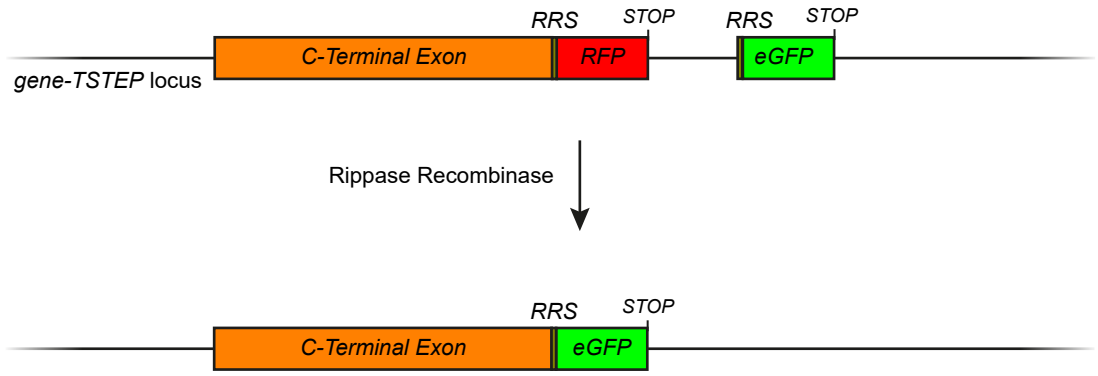


Figure 3.15 – Overexpressed *kek3-6* localise to puncta in Ib boutons

Overexpression of the *kek-RFPs* in Ib boutons at NMJ6/7 A3-4 in L3 wandering larvae. Kek-RFPs appear to localise to puncta in Ib boutons. Acquired using Zeiss LSM900 with Airyscan 2. Stained with anti-HRP and anti-mCherry. Arrows point to examples of Kek-RFP signal. All scale bars = 1µm. Top-to-Bottom: *D42>kek3-RFP* (n = 6 boutons from 4 larvae), *D42>kek4-RFP* (n = 6 boutons from 3 larvae), *D42>kek5-RFP* (n = 3 boutons from 3 larvae), *D42>kek6-RFP* (n = 3 boutons from 3 larvae).

Figure 3.16 - Tissue-specific tagging of endogenous proteins (TSTEP)

A



B

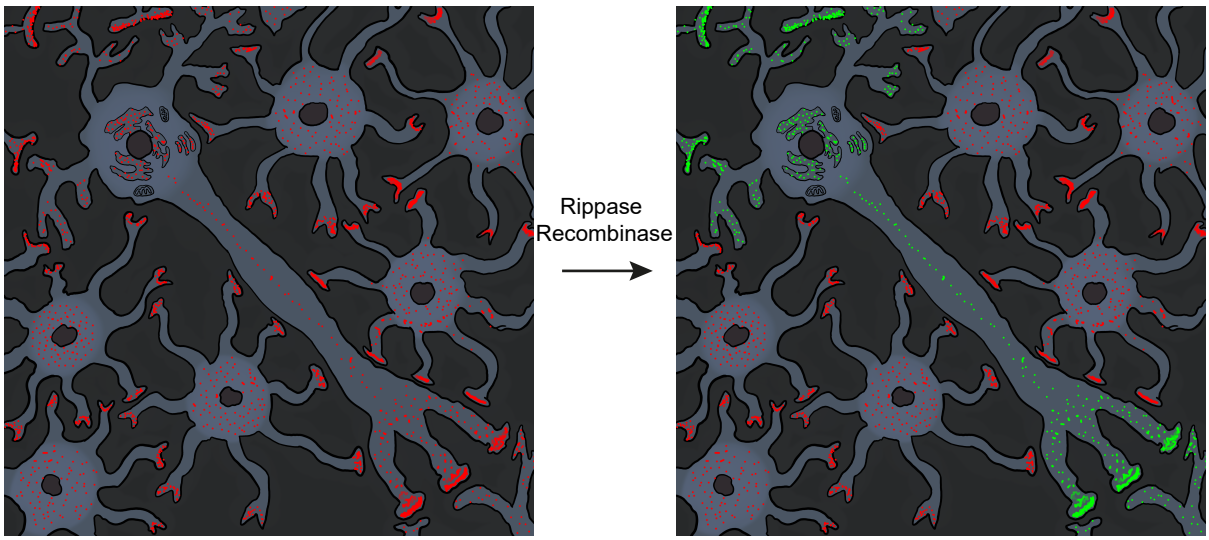


Figure 3.16 – Tissue-specific tagging of endogenous proteins (TSTEP)

Diagram illustrating mechanism of TSTEP tag. Adapted from (Koles et al., 2016). **A:** At an example gene locus, a TSTEP protein fusion has been made to the exon encoding the C-terminal end of the gene product. The linker between the C-terminal and RFP is a Rippase recombinase site (RRS). When Rippase recombinase is present, it flips out the sequence located between two RRSs and leaves a single RRS in its place, thereby leaving the gene product to be tagged with GFP. **B:** An example application of TSTEP tagging. In this example, Protein-TSTEP is widely expressed in neurons and glia. In its default state, all of the example Protein is tagged with RFP (Left). Rippase recombinase is expressed under the effect of a neuronal driver, causing the TSTEP tag to flip from RFP to GFP, leading to all neuronal Protein-TSTEP fusions to be visible in the green channel (Right).

the fluorescent protein tag by driving the expression of the recombinase with a restricted *GAL4* (Fig. 3.16 B).

Similar to the *kek5-GAL4* cloning CRISPR Cas9-acclerated HDR would be exploited to generate the knock-in. However, for the *kek6-TSTEP* knock-in the GOLIC+ method was used. In theory the GOLIC+ method is more time-efficient and should produce more knock-in candidates, which was the rationale behind its adoption here.

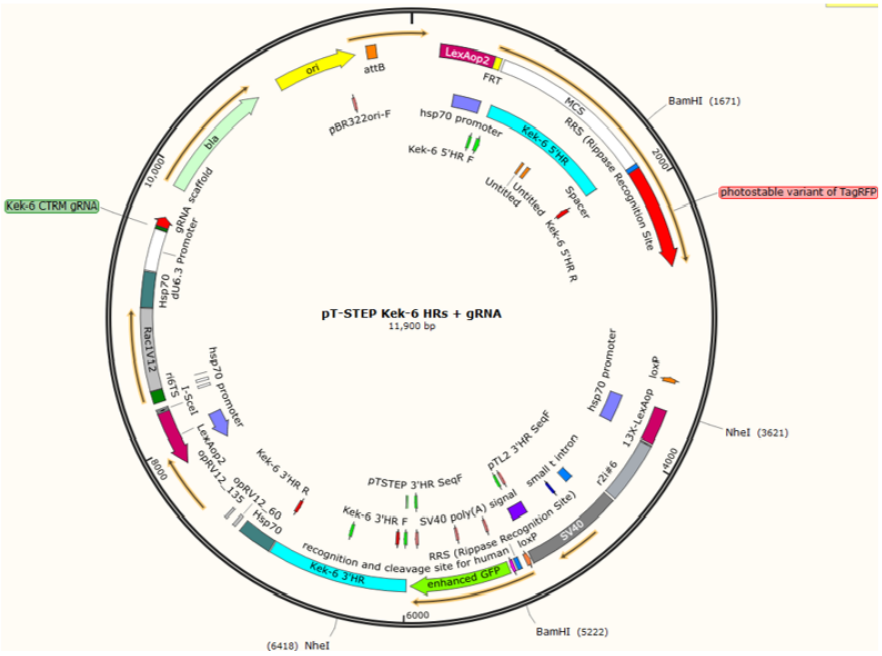
Unlike the *kek5-GAL4* cloning the *pTSTEP* construct holds both the *gRNA* and the HRs for the insertion (Fig. 3.17 A). Additionally, here the aim was to produce a C-terminal tag, therefore the point of insertion needed to be after the final coding codon, but before the final stop codon of *kek6* (Fig. 3.17 B). Two ~1kb fragments, upstream and downstream of this point were then amplified by PCR to be used as the HRs for HDR.

Generation of the final construct was verified by screening candidate clones via diagnostic digest with BamHI and NheI (Fig. 3.17 C). Clone #24 did not match the expected digest profile and appeared to have a double insertion of the 3'HR. Clones #33 and #35, having the expected digest profile, were then sequenced along the 5' and 3'HR to check the HRs had not been damaged and that HDR would not be disrupted. The sequencing data for clone #35 is presented here.

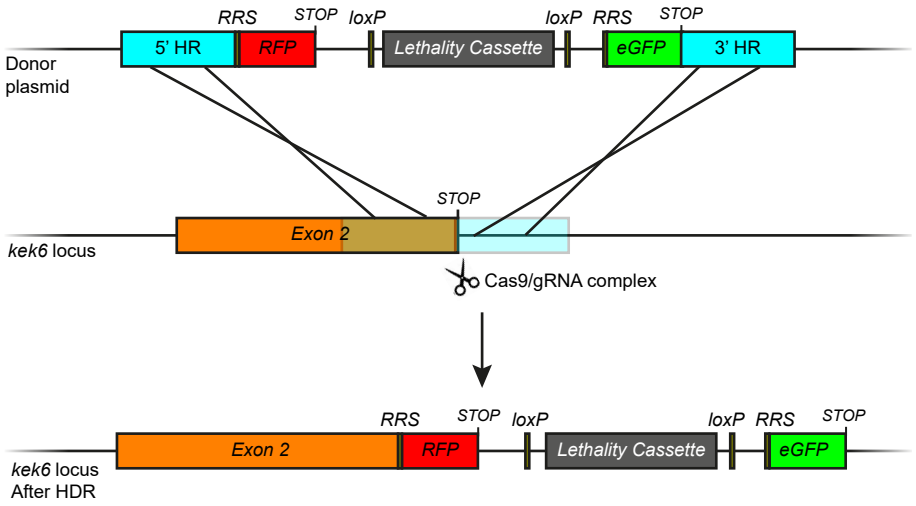
For the *5'HR* of the 11 mismatches detected, 9 are for ambiguity, where the sequencing quality was not high enough to distinguish which base was present (Fig. 3.18). In each of the 9 cases, the expected base is one of the candidates, indicating that these mismatches could be artefacts of the sequencing process. The other 2 mismatches are single base pair changes, that represent silent mutations, and were therefore deemed unlikely to cause problems for HDR or protein function.

Figure 3.17 - Cloning of *kek6-TSTEP* donor template plasmid

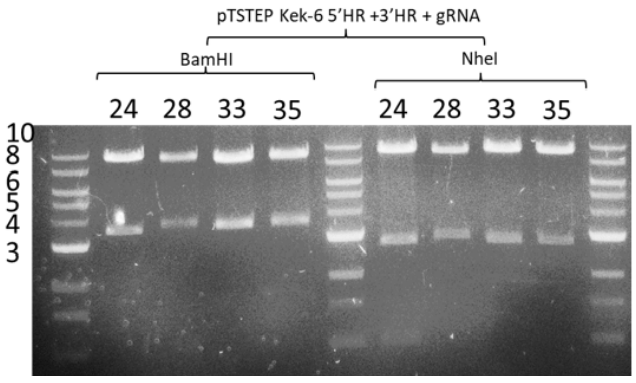
a



b



c



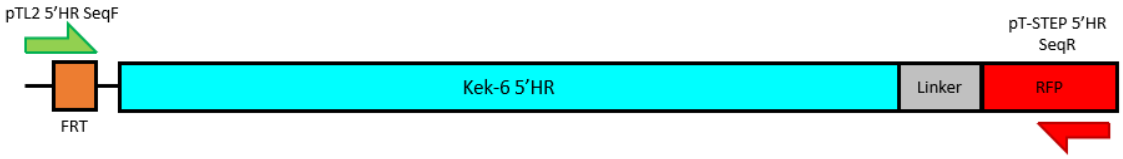
BamHI Expected bands: 8.3 + 3.6 kb NheI Expected bands: 9.1 + 2.8 kb

Figure 3.17 – Cloning of *kek6-TSTEP* donor template plasmid

A: Map of complete *pT-STEP-kek6 HRs+gRNA* plasmid showing diagnostic restriction enzyme sites. **B:** Diagram showing HDR of *kek6-TSTEP* construct being inserted into the endogenous *kek6* locus. Following CRISPR/Cas9-mediated cleavage of the *kek6* locus, the HDR pathway replaces the broken sequence with the *kek6-TSTEP* donor construct using the homologous regions flanking the insert. **C:** Restriction digests used to characterise candidate clones. (Left) BamHI, predicted bands = 8.3kb and 3.6kb. (Right) NheI, predicted bands = 9.1kb and 2.8kb.

Figure 3.18 - Sequencing *kek6* 5'HR

a



b

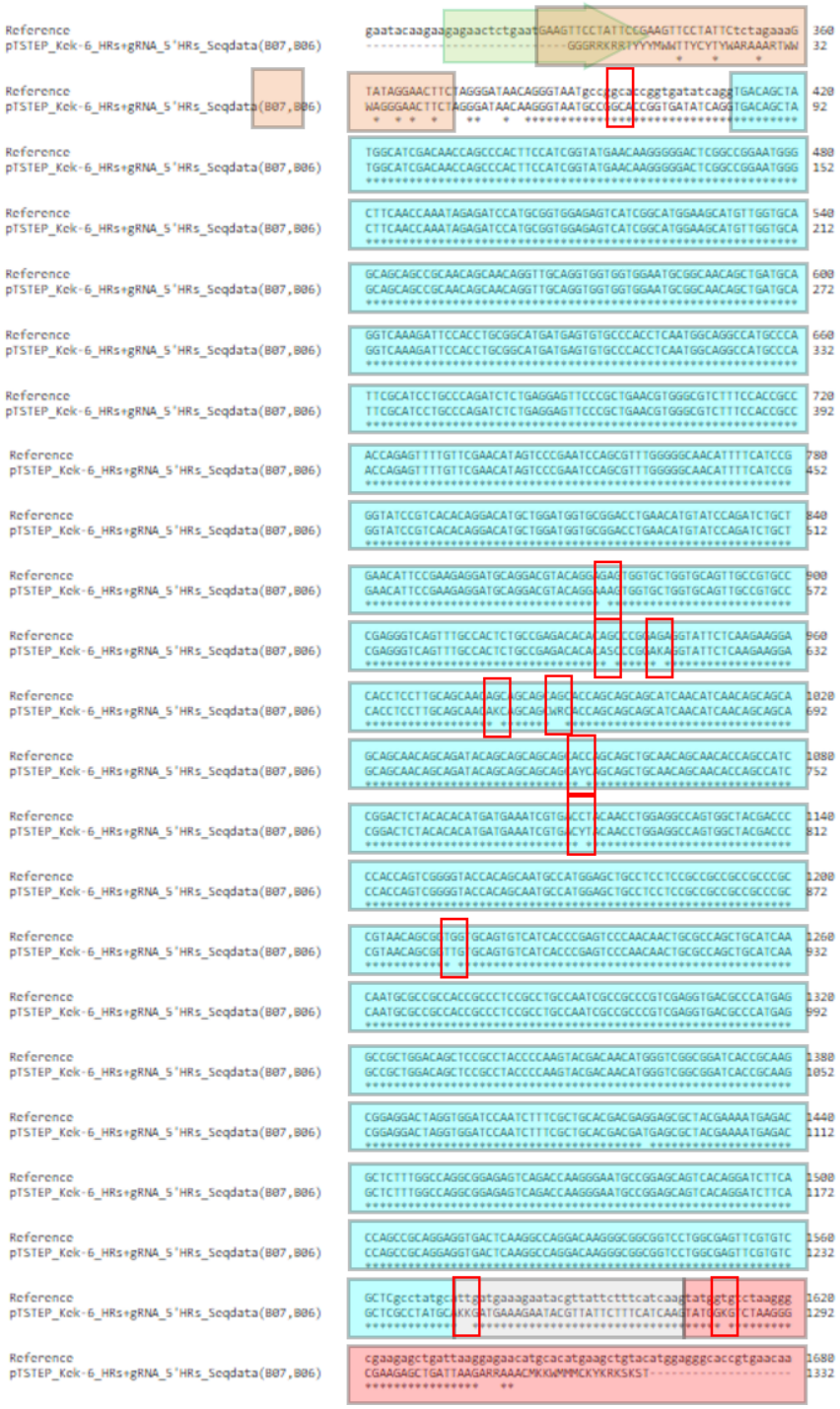


Figure 3.18 – Sequencing *kek6* 5'HR

A: Diagram of the sequencing strategy for the *kek6-TSTEP 5'HR* (light blue box). The forward (*pTL2 5'HR SeqF*, green arrow) and reverse (*pT-STEP 5'HR SeqR*, red arrow) are outside the sequence of the 5'HR. **B:** Alignment of sequencing data vs reference sequence. Red boxes indicate mismatches to the reference. Coloured boxes are overlaid on the alignment to highlight sequence elements per the diagram of the sequencing strategy.

The *3'HR* contained >15 mismatches to the reference sequence (Fig. 3.19). It was thought that this could pose a problem for HDR, however it was a necessary risk to take as all other candidates sequenced had the same deviations from expectations. Additionally, it is possible these mismatches represent natural polymorphisms between the genomes of the flies used to produce the reference data and the flies in the lab from which the DNA had been extracted. This seemed plausible as the *3'UTR* may be less well conserved than the actual coding sequence of the protein.

For clone #35 the sequencing of the *kek6 gRNA* did not reveal any mismatches, indicating that the insertion of the gRNA oligonucleotides into the construct had been successful (Fig. 3.20). Clone #35 was then used for microinjection.

3.2.8 Localisation of Kek6-TSTEP

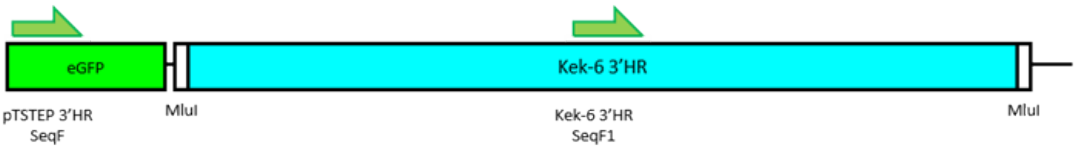
To determine the expression pattern of *kek6-TSTEP* larvae were dissected to visualise the VNC. Following staining, Kek6-TSTEP was found to have localised to cells lateral to the neuropil in the VNC (Fig. 3.21 A (Centre)). In contrast, *kek6-GAL4* drove expression in several more cells around the nerve cord, and the reporter myrGFP can be observed within and in projections segmentally separated along the neuropil (Fig. 3.21 A (Right)).

The expression patterns of Kek6-TSTEP and the existing *kek6-GAL4* line (Ulian-Benitez et al., 2017) are different in the VNC: Kek6-TSTEP is far more restricted (Fig. 3.21 A). *kek6-GAL4* appears to be expressed in more cells in the VNC than *kek6-TSTEP*.

To determine if *kek6* is expressed in motoneurons (Ulian-Benitez et al., 2018), *kek6-TSTEP* larvae were dissected and stained for visualisation of NMJ 6/7 (Fig. 3.21 B).

Figure 3.19 - *kek6* 3'HR sequencing

a



b

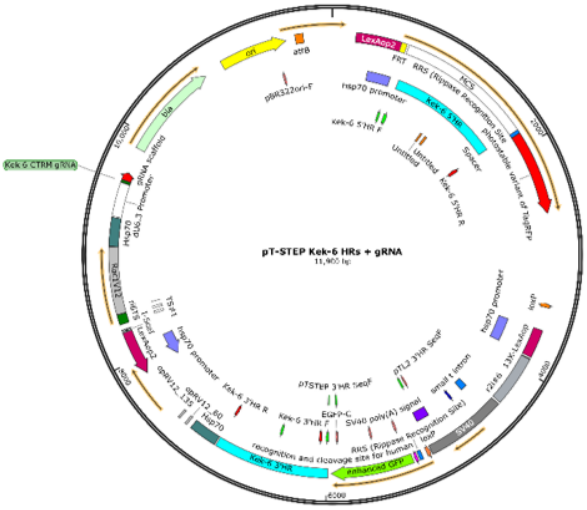


Figure 3.19 – Sequencing *kek6* 3'HR

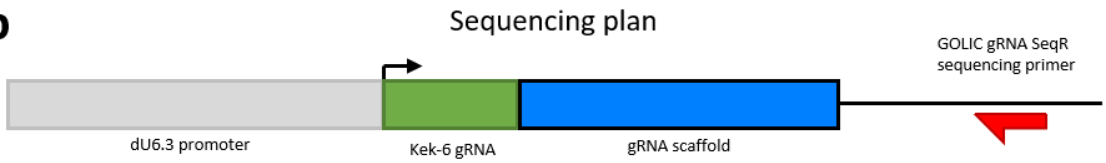
A: Diagram of the sequencing strategy for the *kek6-TSTEP 3'HR* (light blue box). The forward (*pTSTEP 3'HR SeqF*, green arrow) is located upstream of the 3'HR, a second forward primer (*kek-6 3'HR SeqF1*, green arrow) was also used. **B:** Alignment of sequencing data vs reference sequence. Red boxes indicate mismatches to the reference. Coloured boxes are overlaid on the alignment to highlight sequence elements per the diagram of the sequencing strategy.

Figure 3.20 - Sequencing of *kek6 TSTEP gRNA*

a



b



c

```
Reference                                          ----------------------------------------------tgtttcaattcta  13
pT-STEP+Kek6-HRs+gRNA#4-Seqdata(D04)                TTTCATACGTTTTATAACTTATGCCCCTAAGTATTTTTTGACCATAGTGTTTCAATTCTA  600
                                                                                                 *************

Reference                                          cattaattttacagagtagaatgaaacgccacctactcagccaagaggcgaaaaggttag  73
pT-STEP+Kek6-HRs+gRNA#4-Seqdata(D04)                CATTAATTTTACAGAGTAGAATGAAACGCCACCTACTCAGCCAAGAGGCGAAAAGGTTAG  660
                                                    ************************************************************

Reference                                          ctcgccaagcagagagggcgccagtgctcactacttttttataattctcaacttctttttc  133
pT-STEP+Kek6-HRs+gRNA#4-Seqdata(D04)                CTCGCCAAGCAGAGAGGGCGCCAGTGCTCACTACTTTTTTATAATTCTCAACTTCTTTTTC  720
                                                    ************************************************************

Reference                                          cagactcagttcgtatatatagacctattttcaatttaacgtcgGCTCTAGTATTATGGT  193
pT-STEP+Kek6-HRs+gRNA#4-Seqdata(D04)                CAGACTCAGTTCGTATATATAGACCTATTTTCAATTTAACGTCGGCTCTAGTATTATGGT  780
                                                    ************************************************************

Reference                                          ACCCgttttagagctagaaatagcaagttaaaataaggctagtccgttatcaacttgaaa  253
pT-STEP+Kek6-HRs+gRNA#4-Seqdata(D04)                ACCCGTTTTAGAGCTAGAAATAGCAAGTTAAAATAAGGCTAGTCCGTTATCAAMAMWGAA  840
                                                    ************************************************      **

Reference                                          aagt-ggcaccgagtcggtgctttttttaaagaattaattcttgaagacgaaaggg      308
pT-STEP+Kek6-HRs+gRNA#4-Seqdata(D04)                AAAGTGGCACCGAGTCGGTGCTTTTTTAA-AGAWTWATTSSKTRMGGC--------      887
                                                    **   ********************* * *** * * *   *   *
```

Figure 3.20 - Sequencing of *kek6 TSTEP gRNA*

A: Map of complete *pTSTEP-kek6 HRs+gRNA* plasmid. **B:** Diagram of sequencing strategy. Candidate clones were Sanger sequenced with *GOLIC gRNA SeqR* sequencing primer, located downstream of the gRNA insertion site. **C:** Alignment of Sequencing data from final construct to reference showing correct insertion of gRNA (Green box).

Figure 3.21 - Kek6-TSTEP is expressed in the larval VNC and NMJ

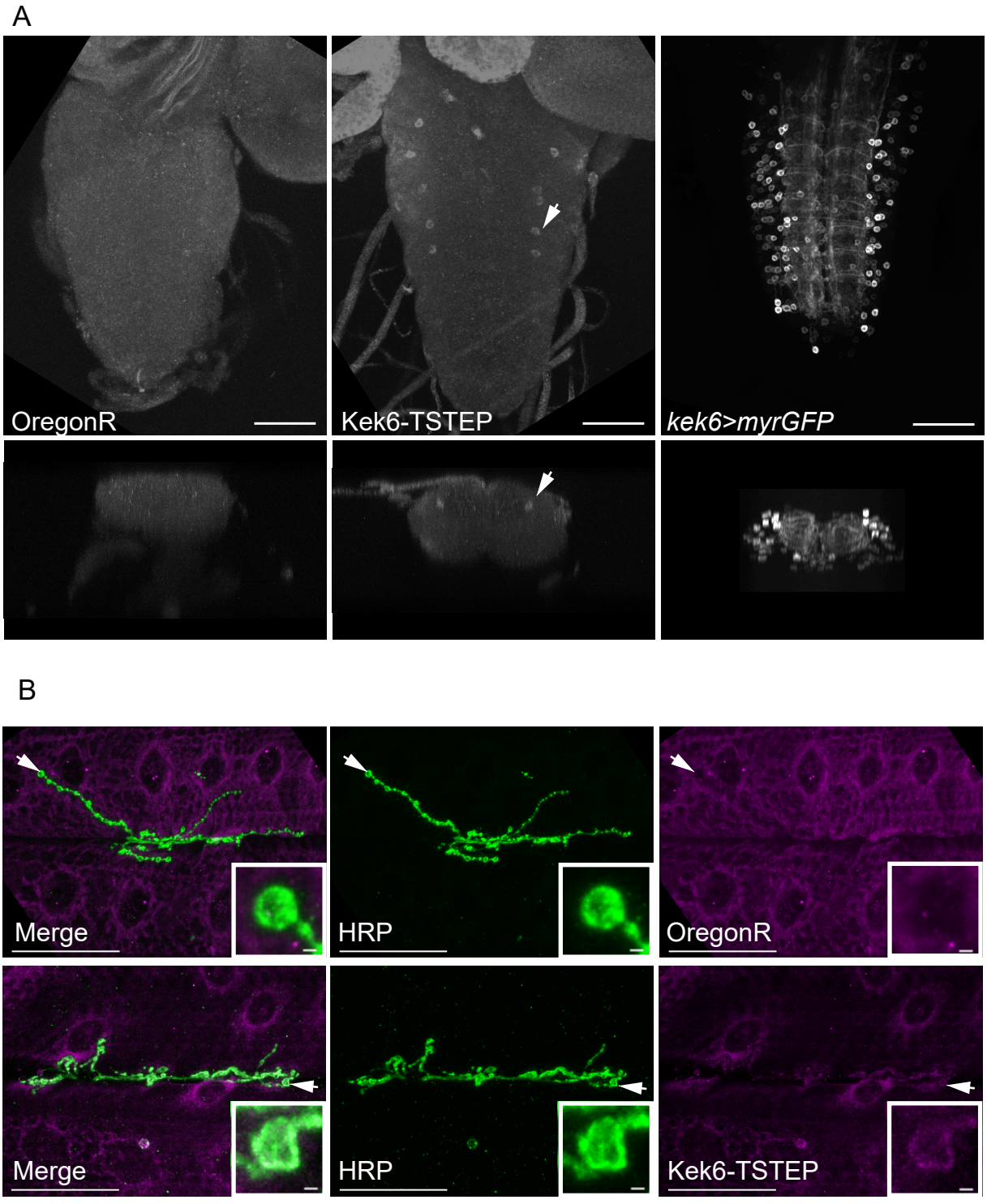


Figure 3.21 – Kek6-TSTEP is expressed in the larval VNC and NMJ

Expression and localisation of Kek6-TSTEP in the larval CNS and motoneurons. **A:** Expression of Kek6 in the larval VNC, scale bars = 50µm. **Left:** Control staining of OregonR VNC with anti-DsRed, n = 2. **Middle:** *kek6-TSTEP* VNC stained with anti-DsRed, n = 3. **Right:** *kek6>myrGFP* VNC stained with anti-GFP, n =2, *kek6-GAL4* generated by Ulian-Benitez et al., 2017. **B:** Expression and subcellular localisation of Kek6-TSTEP at NMJ 6/7 stained with anti-HRP and anti-mCherry, scale bars = 50µm. Arrow pointing to the representative bouton shown in the expanded view (bottom right of each image, scale bars = 1µm. Top: Control staining of OregonR NMJ with anti-HRP and anti-mCherry, n = 3 NMJs (A2-A3) from 3 larvae. Bottom: Kek6-TSTEP localises to boutons at NMJ 6/7, n = 5 NMJs (A3) from 5 larvae.

Here, Kek6-TSTEP can be seen colocalizing with axonal terminal marker HRP in boutons, but not in the axon. This data, and data from the VNC, indicated that *kek6* was distributed in motoneurons and localised exclusively to the soma and the presynapse, consistent with data from the overexpression of *kek6-RFP*.

3.3 Discussion

In this chapter I have shown that all that *kek*s are nervous system genes that have differing spatial expression. *kek*s are expressed in the CNS at what appears to be qualitatively comparable levels, with only *kek1* and *-5* being expressed in the periphery. Keks have varying but overlapping subcellular localisations, with Kek2 localising preferentially to dendrites, Kek3 and 4 localising throughout the neuron, and Kek5 and 6 localising presynaptically. Additionally, in this chapter I have generated *kek5-T2A-GAL4* and *kek6-TSTEP*, and used these tools to demonstrate that *kek5* is expressed in motoneurons and in the PNS, and that *kek6-TSTEP* is expressed in motoneurons. Furthermore Kek6-TSTEP confirmed that Kek6 localises to the presynapse when expressed at endogenous levels.

The findings from this chapter indicate that Keks have different but overlapping subcellular distributions. The diversity of *kek*s is further explored in the next chapter, with a focus on the functional diversity of *kek*s with respect to Ca^{2+} signalling.

4 RESULTS - DIFFERENTIAL REGULATION OF CALCIUM SIGNALLING BY KEKS

4.1 Introduction

In this chapter I investigated if all *keks* could signal via Ca^{2+}, and if so, how are they similar/different? As only *kek6* had previously been reported to signal via CaMKII (Ulian-Benitez et al., 2017) I first looked at the abundance of CaMKII in *kek* overexpression genotypes via Western blot to probe if and how *kek*s regulate levels of this important signalling protein. I then asked if all *kek*s could modulate Ca^{2+} dynamics at the NMJ like *kek6* has been shown to with GCaMP and optogenetic stimulation.

From here I decided to focus on *kek4* and *-6*, and used Kek6-TSTEP, generated in the previous chapter, to determine if Kek6 can physically interact with Cac channels when expressed at endogenous levels. Keks have been shown before to contain a PDZ domain that is involved in protein-protein interaction (Evans et al., 2005). Thus, they could function to recruit Cac channels at the synapse membrane. An interaction of Kek6 with Cac could affect the opening probability of the Cac channels (Gratz et al., 2019). Finally, I investigated potential phenotypes in Cac distribution in *kek4* and *-6* overexpression conditions.

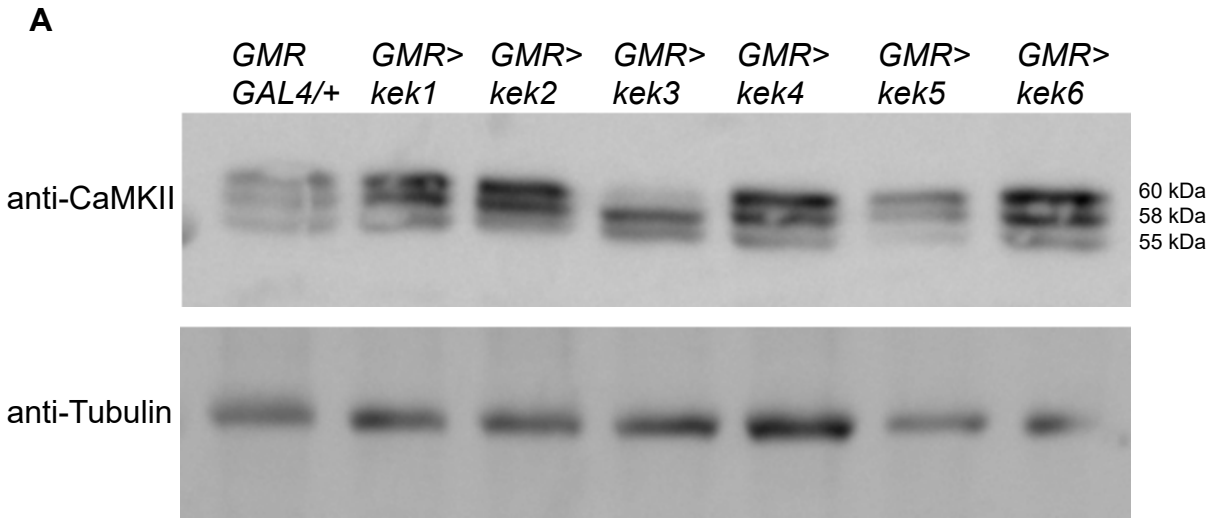
4.2 *kek*s differentially regulate CaMKII isoform abundance

Western blot was used to explore the effect of *kek*s on *CaMKII* expression (Fig. 4.1). In order to enrich the samples for neuronal tissue *GMR-GAL4* was used to overexpress the *kek*s, as it strongly drives expression specifically in the retina of the adult fly (Escobedo et al., 2021). Adult heads were used to ensure a useable yield of protein. *GMR/+* was used as the negative control genotype. Protein was extracted from 60 3–5-day old fly heads per genotype per replicate. To control for sexual dimorphism half of the heads were from males, and half from females.

The effect of *kek1* overexpression on CaMKII abundance was assessed here despite the lack of Kek1-RFP visualisation in the previous chapter. This was due to the presence of a rough-eye phenotype that was noticeable in *GMR>kek1-RFP* adult flies collected for the Western blot. This phenotype was previously reported by Bishop, 2014, and was consistent with previous reports of Kek1 behaving as an EGFR inhibitor. This indicated that the overexpression construct was indeed functional even if the RFP tag was not.

With the anti-CaMKII antibody, which specifically binds to the unphosphorylated form of CaMKII, three bands are present and represent different splice isoforms of CaMKII that have different molecular weights: 60, 58 and 55 kDa respectively (Takamatsu et al., 2003) (Fig. 1a). Signal intensity for each band was quantified using ImageJ-FIJI. Signal intensity was measured in an area of the membrane near each band and was taken as ‘background’ local to that band. Background was subtracted to control for local variation in intensity on the membrane. The background-subtracted signal intensity was divided by the respective loading control band, which was anti-beta-tubulin, to make the samples comparable. Lastly, to produce fold change figures, the

Figure 4.1 - *keks* modulate CaMKII abundance



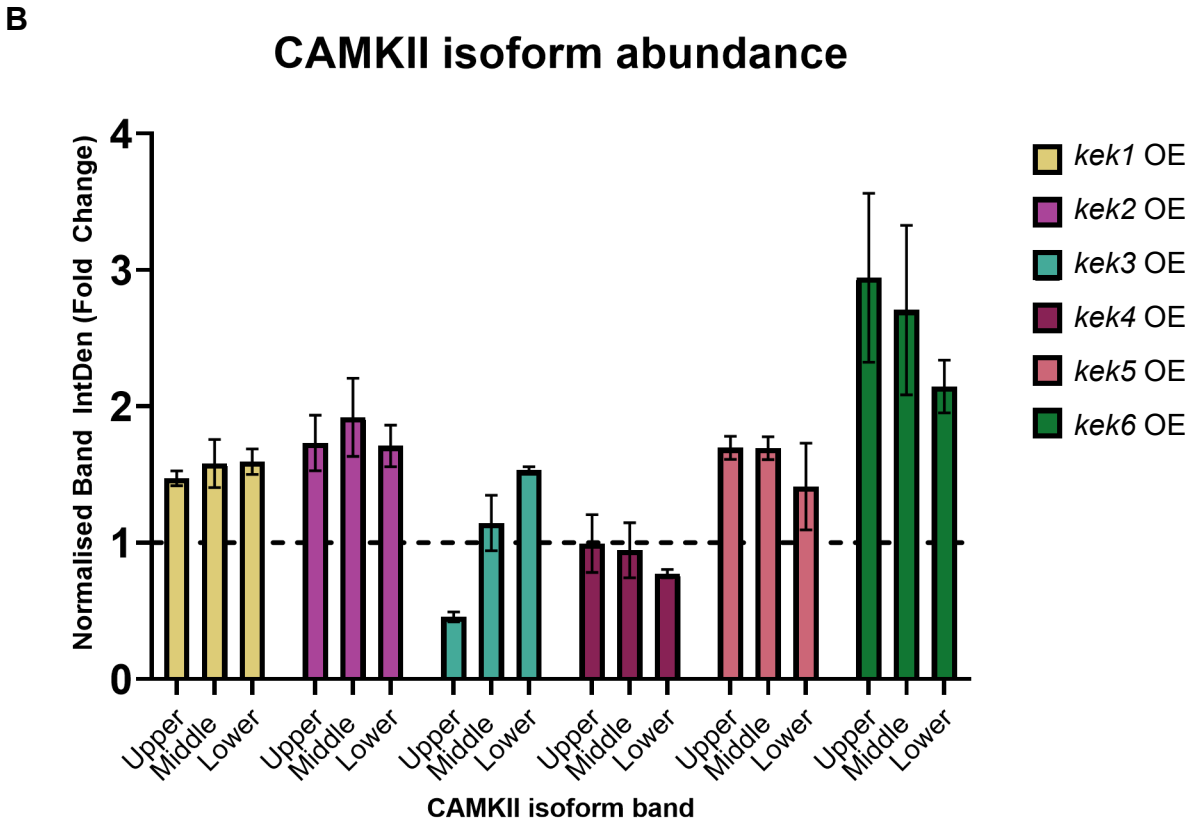


Figure 4.1 – *keks* modulate CaMKII abundance

kek overexpression under the retinal driver *GMR-GAL4* alters CaMKII abundance. **A** – Western blot stained with anti-CaMKII. Each lane's protein sample derives from 60 2-5 day old adult flies. 30 females and 30 males were selected to control for sex. The three bands visible on the blot are from different CaMKII isoforms (Takamatsu et al 2003). Blots were counterstained for beta-tubulin for a loading control. **B** – Quantification of band intensity. Data collected from 2 biological replicates. Background levels were subtracted from band IntDen and then divided by the loading control for each lane. Broadly *kek1*, *-2*, *-5* and *-6* upregulate CaMKII levels. OE of *kek3* differently modulates CaMKII abundance, with the higher molecular weight isoforms being downregulated and the lower molecular weight isoforms being upregulated. OE of *kek4* downregulates the lower molecular weight isoforms, but the higher and middle weight isoforms are unaffected.

adjusted signal intensity was normalised to the corresponding control band's adjusted signal intensity (Fig. 4.1b).

Interestingly, it appears that overexpression of *kek1*, *-2*, *-5* and *-6* increase the expression levels of CaMKII protein. This effect is most prominent with *kek6*, which has been previously reported to signal via CaMKII (Ulian-Benitez et al., 2017). *kek3* and *-4* are different from the other *kek*s and indeed each other.

*kek*s appear to be differentially regulating different CaMKII isoforms, as the proportions of CaMKII isoforms are altered differently in different *kek* overexpression genotypes. This is most dramatic for *kek3*, where the 60 kDa isoforms are apparently downregulated to about half their normal levels, whereas the 58 kDa and 55 kDa isoforms are increased. In *kek1*, *-2*, *-5* and *-6* overexpression, CaMKII level increases, although the amount they increase appears to vary with isoform. In *kek4* overexpression, CaMKII levels do not appear to be affected but are slightly lower. The expression levels of the 55 kDa isoforms appear to be reduced by 23%.

4.3 *kek*s modulate pre-synaptic Ca^{2+} dynamics at the NMJ

Work by a previous PhD student in the Hidalgo lab (Ulian-Benitez 2018) demonstrated that *kek6* can influence Ca^{2+} dynamics at the NMJ pre-synapse in boutons following optogenetic stimulation, as measured using GCaMP, a fluorescent Ca^{2+} reporter (Ulian-Bentiez 2018). Boutons are round bleb-like protrusions from the axonal terminal that house neurotransmitter release sites. Overexpression of *kek6* enhanced the GCaMP signal and resulted in a slower decay of Ca^{2+} over time. In *kek6* KO mutants the GCaMP response following stimulation was reduced (Ulian-Bentiez 2018).

GCaMP is a genetically encoded fluorescent Ca^{2+} reporter can be used to assess cytosolic calcium levels (Nakai et al., 2001). GCaMP is a modified form of GFP that requires the binding of Ca^{2+} to become fluorescent (Nakai et al., 2001). Combined with optogenetics to stimulate neurons into firing when exposed to light (Nagel et al., 2003, Lin et al., 2013), GCaMP can be used to monitor Ca^{2+} levels before during and after stimulation.

Optogenetics uses the GAL4/UAS system to express light-sensitive cation channels called Channelrhodopsins (ChRs) in desired neurons (Zhang et al., 2007). Different ChRs have been engineered for optogenetics since their discovery including the red-light activated ChR (ReaChR) (Lin 2011, Lin et al., 2013). Red-light is preferable for use in live animals as the longer wavelength penetrates deeper into tissue than blue light (Lin et al., 2013, Inagaki et al., 2013). Additionally, red light does not activate the *Drosophila* visual system, therefore using ReaChR reduces non-specific stimulation (Inagaki et al., 2013).

To investigate the functional diversity of *kek*s, I examined the effect of *kek* overexpression on post-stimulation Ca^{2+} dynamics in Ib boutons of the presynaptic terminal of NMJ6/7 (Fig. 4.2). Larvae expressing *uasGCaMP6m*, *uasReaChR* and a given *uas-kek-RFP* (or none, for the control) under a motoneuron *GAL4* (*D42-GAL4*) were dissected to access NMJ 6/7 in living larvae. A 200ms pulse of 590nm amber light was used to depolarise motoneurons via ReaChR in living preps. The green GCaMP signal was recorded in the 488nm channel for 1 minute prior to stimulation, and then for 20s following stimulation, whereby another stimulation would occur, followed by another 20s of recording the GCaMP response (Fig. 4.2 A).

Figure 4.2 - Presynaptic NMJ Ca2+ dynamics in *kek* OE larvae

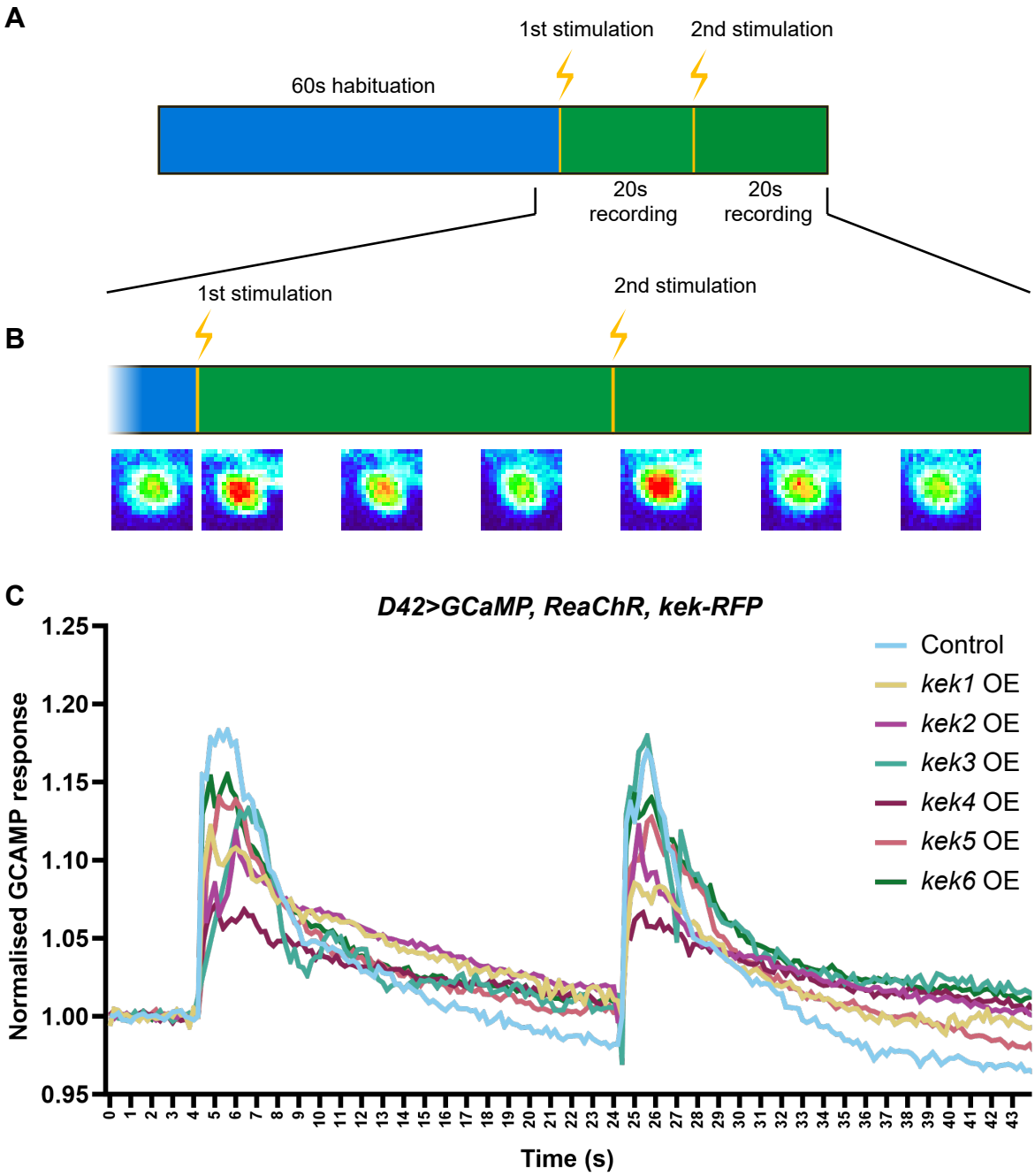


Figure 4.2 - Presynaptic NMJ Ca2+ dynamics in Kek OE larvae

GCaMP recordings of Ca^{2+} dynamics in Ib boutons at NMJ 6/7 following optogenetic stimulation. **A+B:** Diagram of protocol program. **A:** After loading the dissected larvae into the microscope larvae are recorded for 60s in the 488nm channel for habituation. The synapse is then illuminated with high-intensity 590nm light for 0.2s and is recorded for a further 20s in the 488nm channel to observe the change in GCaMP intensity. After this the stimulation and recording is repeated. **B:** Focussing on the time around the stimulations with reference to an example bouton from control (*D42>GCaMP, ReaChR*) larvae, the change in intensity can be observed over time. A false-colour image has been used with a Thermal LUT to facilitate the observation of changes in intensity, with dark blue representing areas of low intensity, and red representing areas of high intensity. **C:** Plot of mean signal intensity of firing Ib boutons at NMJ 6/7 at each time point for the control genotype and each *kek* OE genotype (*D42>GCaMP, ReaChR*, *kek-RFP*).

Ca^{2+} dynamics were recorded as changes to GCaMP signal intensity over time inside Ib Boutons (Fig. 4.2 B). Signal intensity was defined as the integrated density (the product of the mean gray value for all the pixels in the ROI and the area of the ROI) of a bouton in a given frame normalised to the mean integrated density of that bouton from the 20 frames preceding the first stimulation. Signal intensity for each time point was subsequently calculated from all boutons analysed, and this was then plotted over time (Fig. 4.2 C).

In all cases the first stimulation occurs at 4.2s and the second stimulation occurs at 24.4s (Fig. 4.2). For both stimulations the control curve follows a similar trajectory, with an initial peak in intensity that decayed sharply until becoming more gradual when the normalised GCaMP intensity drops below 1.05. The first peak reaches this point at 9s, and the second at 27.8s (4.8 and 3.4s following stimulation, respectively). When the GCaMP signal drops below 1.0, this indicates that Ca^{2+} levels have fallen relative to their initial level. (Fig. 4.2 C).

To assess variation within the change in GCaMP signal following stimulation, there were two characteristics of the GCaMP signal profile that were of interest, the initial peak of GCaMP signal intensity and the lowest point of the GCaMP signal in the curve. The initial peak in the first phase of the curve, the amplitude, was quantified as the highest signal intensity value for a given curve. The lowest point in GCaMP signal in the curve was used to assess the decay in intracellular Ca^{2+} levels, as a greater minimum value would indicate sustained Ca^{2+} levels.

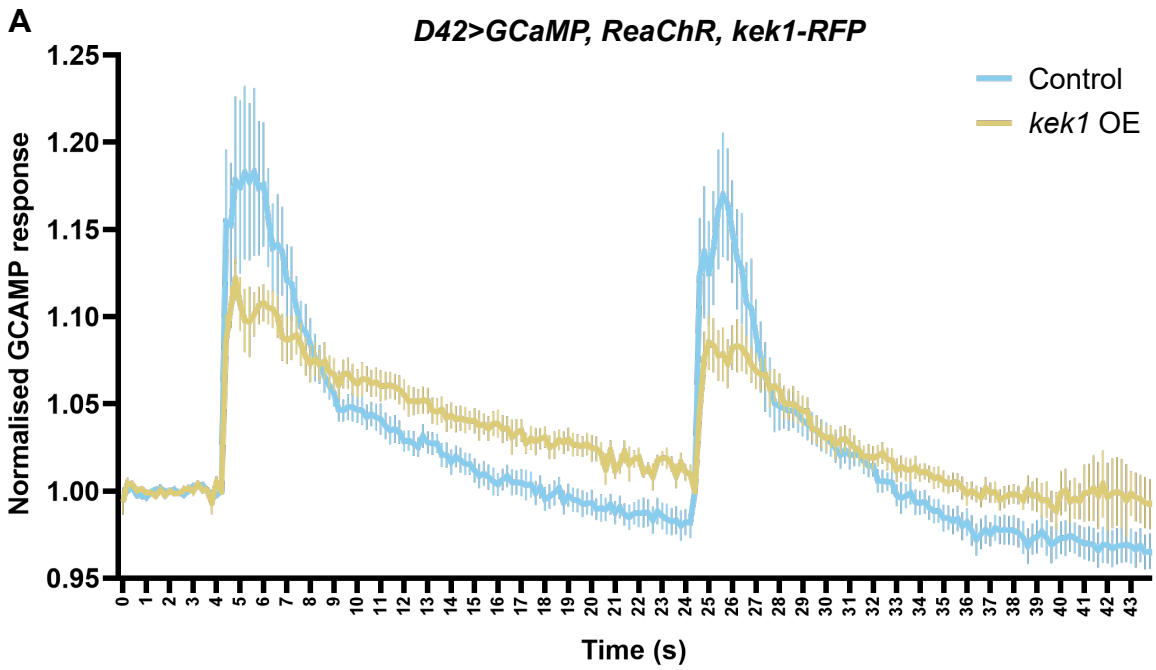
4.3.1 Ca^{2+} dynamics *kek* overexpression larvae

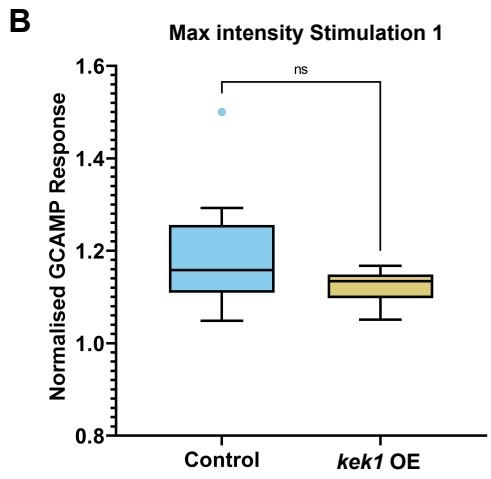
Across the *kek*s there are similarities between the effect of each *kek*'s overexpression on post-stimulation Ca^{2+} dynamics in boutons, although each *kek* appears to be functionally distinct (Fig. 4.2). There were two effects on Ca^{2+} dynamics that *kek1, -2, -3, -4* and *-6* shared to different degrees: 1) a decrease the initial influx of Ca^{2+} following stimulation and 2) a delayed decay in Ca^{2+} following stimulation.

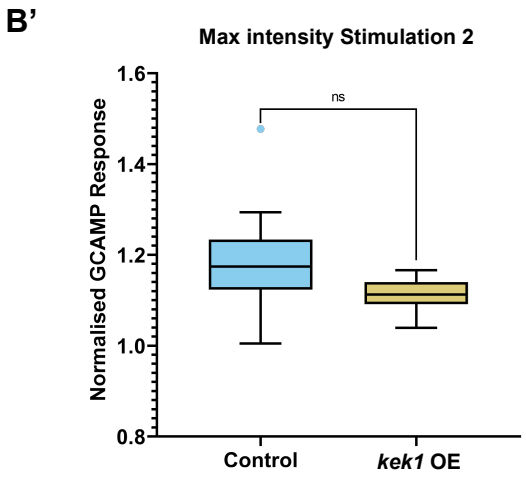
kek1 overexpression did not significantly impact the initial influx of Ca^{2+}, however the minimum intensity was significantly greater than the control in the first stimulation but not the second (Fig. 4.3). *kek2* overexpression lowered the initial influx in the second stimulation, but not the first, and significantly raised the minimum intensity in either case (Fig. 4.4). Overexpression of *kek3* did not appear to significantly alter the amplitude of Ca^{2+} influx but did sustain GCaMP signal level following the second stimulation (Fig. 4.5). *kek4* overexpression larvae had significantly lower amplitudes than the control, and had a significantly greater minimum intensity following the second stimulation (Fig. 4.6). *kek5* overexpression notably did not significantly impact Ca^{2+} dynamics (Fig. 4.7). In contrast, while *kek6* overexpression did not significantly alter the amplitude of GCaMP signal, it did sustain signal levels significantly following both stimulations as evidenced by the heightened minimum intensities (Fig. 4.8).

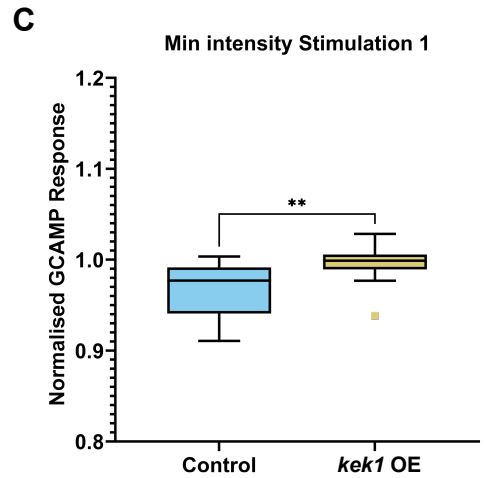
Most *keks*, except for *kek5*, could raise the minimum intensity in GCaMP signal, indicating a sustained level of Ca^{2+} in the bouton following stimulation. Only *kek2* and *kek4* had a significant impact on the amplitude of GCaMP signal, both lowering it. *kek6* and *kek4* were selected for further study due to their differing effects on amplitude.

Figure 4.3 - Presynaptic NMJ Ca2+ dynamics in *kek1* OE larvae









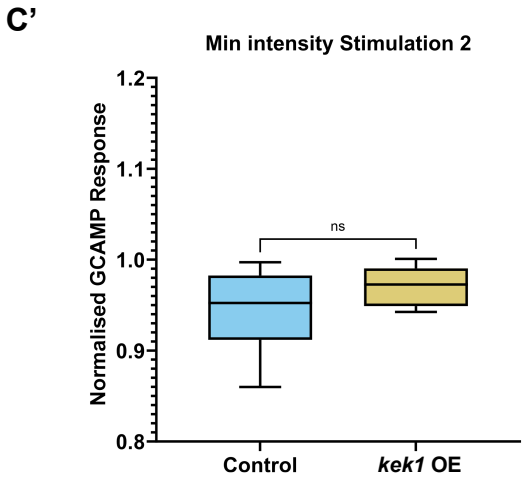


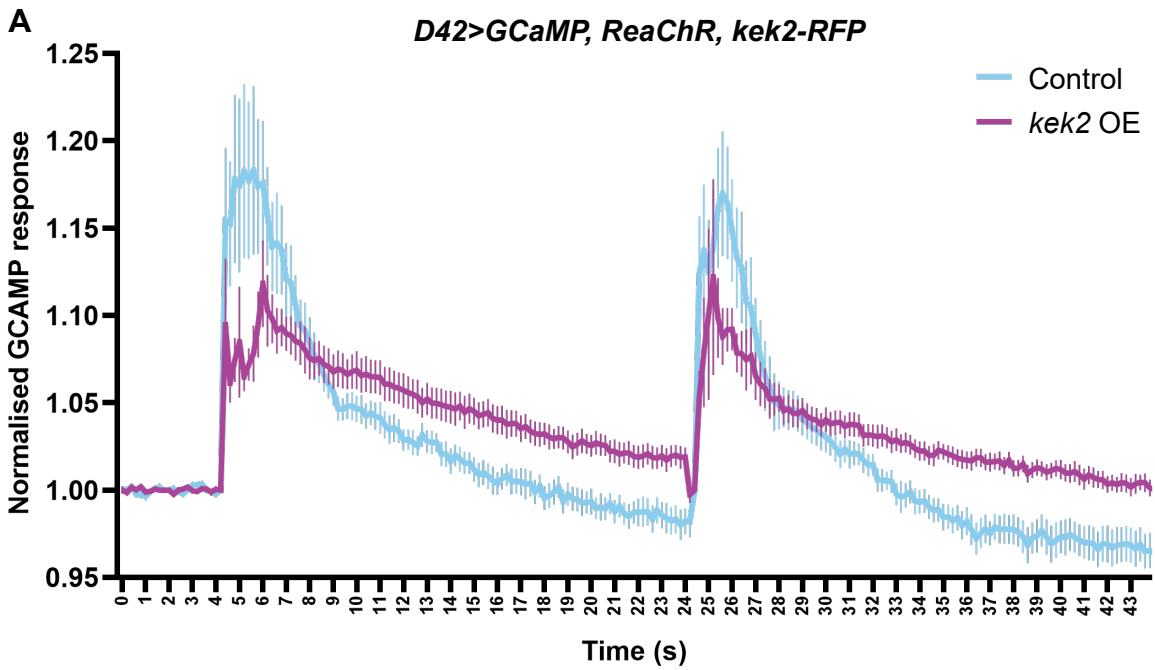
Figure 4.3 - Presynaptic NMJ Ca2+ dynamics in *kek1* OE larvae

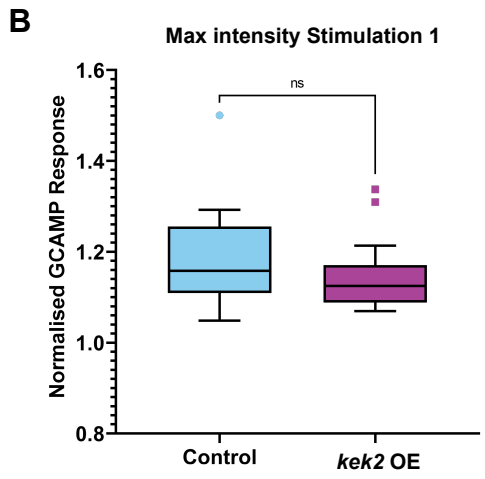
kek1 OE alters fluorescent Ca^{2+} reporter GCaMP signal levels following optogenetic stimulation. **A** – Plot of mean signal intensity of firing Ib boutons at NMJ 6/7 at each time point. Following both stimulations, the initial peak of GCaMP response in *kek1* overexpression is lower than the control but remains higher than control over time.

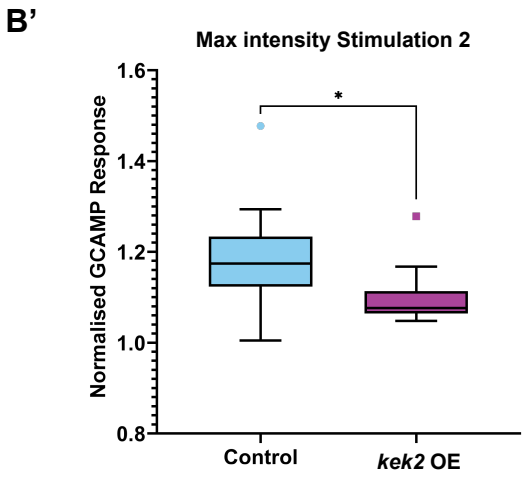
B and **B'** – Box-and-whisker plots of highest GCaMP response value regardless of time following stimulation 1 and 2 respectively. The Max intensity in *kek1* OE is not significantly different to the control following either stimulation. Stimulation 1: Control (*D42>GCaMP, ReaChR*), n = 14 boutons from 6 larvae, Shapiro-Wilk p = 0.0475. *kek1* OE (*D42>GCaMP, ReaChR*, *kek1-RFP*), n = 12 boutons from 6 larvae, Shapiro-Wilk p=0.3042. Unpaired Student's t-test, p = 0.097, not significant (ns). Stimulation 2: Control, n = 14 boutons from 6 larvae, Shapiro-Wilk p = 0.2936. *kek1* OE, n = 10 boutons from 5 larvae, Shapiro-Wilk p = 0.8458. Unpaired Student's t-test, p = 0.0733, not significant (ns).

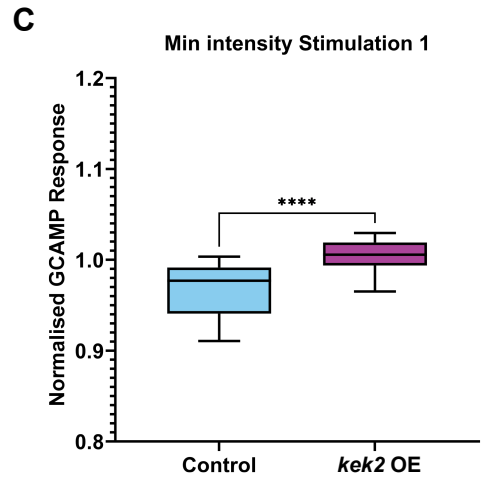
C and **C'** – Box-and-whisker plots of lowest GCaMP response value regardless of time following stimulation 1 and 2 respectively. The Min intensity is significantly higher than the control following the first stimulation but not the second. Stimulation 1: Control, n = 14 boutons from 6 larvae, Shapiro-Wilk p = 0.1603. *kek1* OE, n = 12 boutons from 6 larvae, Shapiro-Wilk p=0.978. Unpaired Student's t-test, p = 0.0093, significant (**). Stimulation 2: Control n = 14 boutons from 6 larvae, Shapiro-Wilk p = 0.2412, *kek1* OE n = 10 boutons from 5 larvae, Shapiro-Wilk p = 0.3579. Unpaired Student's t-test, p = 0.1403, not significant (ns).

Figure 4.4 - Presynaptic NMJ Ca2+ dynamics in *kek2* OE larvae









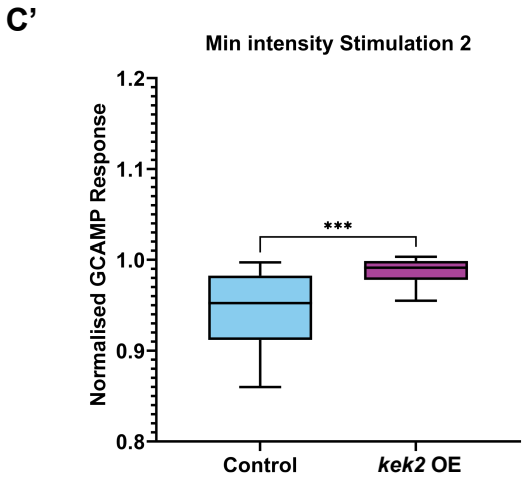


Figure 4.4 - Presynaptic NMJ Ca^{2+} dynamics in *kek2* OE larvae

kek2 alters fluorescent Ca^{2+} reporter GCaMP signal levels following optogenetic stimulation. **A** – Plot of mean signal intensity of firing Ib boutons at NMJ 6/7 at each time point. Following both stimulations, the initial peak of GCaMP response in *kek2* overexpression is lower than the control but remains higher than control over time.

B and **B'** – Box-and-whisker plots of highest GCaMP response value regardless of time following stimulation 1 and 2 respectively. The Max intensity in *kek2* OE is not significantly different to the control following the first stimulation but is significantly lower after the second stimulation. Stimulation 1: Control (*D42>GCaMP, ReaChR*), n = 14 boutons from 6 larvae, Shapiro-Wilk p = 0.0475. *kek2* OE (*D42>GCaMP, ReaChR*, *kek2-RFP*), n = 17 boutons from 6 larvae, Shapiro-Wilk p=0.0023. Unpaired Student's t-test, p = 0.097, not significant (ns). Stimulation 2: Control, n = 17 boutons from 6 larvae, Shapiro-Wilk p = 0.2936. *kek2* OE, n = 17 boutons from 6 larvae, Shapiro-Wilk p = 0.0005. Unpaired Student's t-test, p = 0.0129, significant (*).

C and **C'** – Box-and-whisker plots of lowest GCaMP response value regardless of time following stimulation 1 and 2 respectively. The Min intensity is significantly higher than the control following both stimulations. Stimulation 1: Control, n = 14 boutons from 6 larvae, Shapiro-Wilk p = 0.1603. *kek2* OE, n = 17 boutons from 6 larvae, Shapiro-Wilk p=0.3188. Unpaired Student's t-test, p <0.0001, significant (****). Stimulation 2: Control n = 14 boutons from 6 larvae, Shapiro-Wilk p = 0.2412, *kek2* OE n = 17 boutons from 6 larvae, Shapiro-Wilk p = 0.0775. Unpaired Student's t-test, p = 0.0007, significant (***).

Figure 4.5 - Presynaptic NMJ Ca2+ dynamics in *kek3* OE larvae

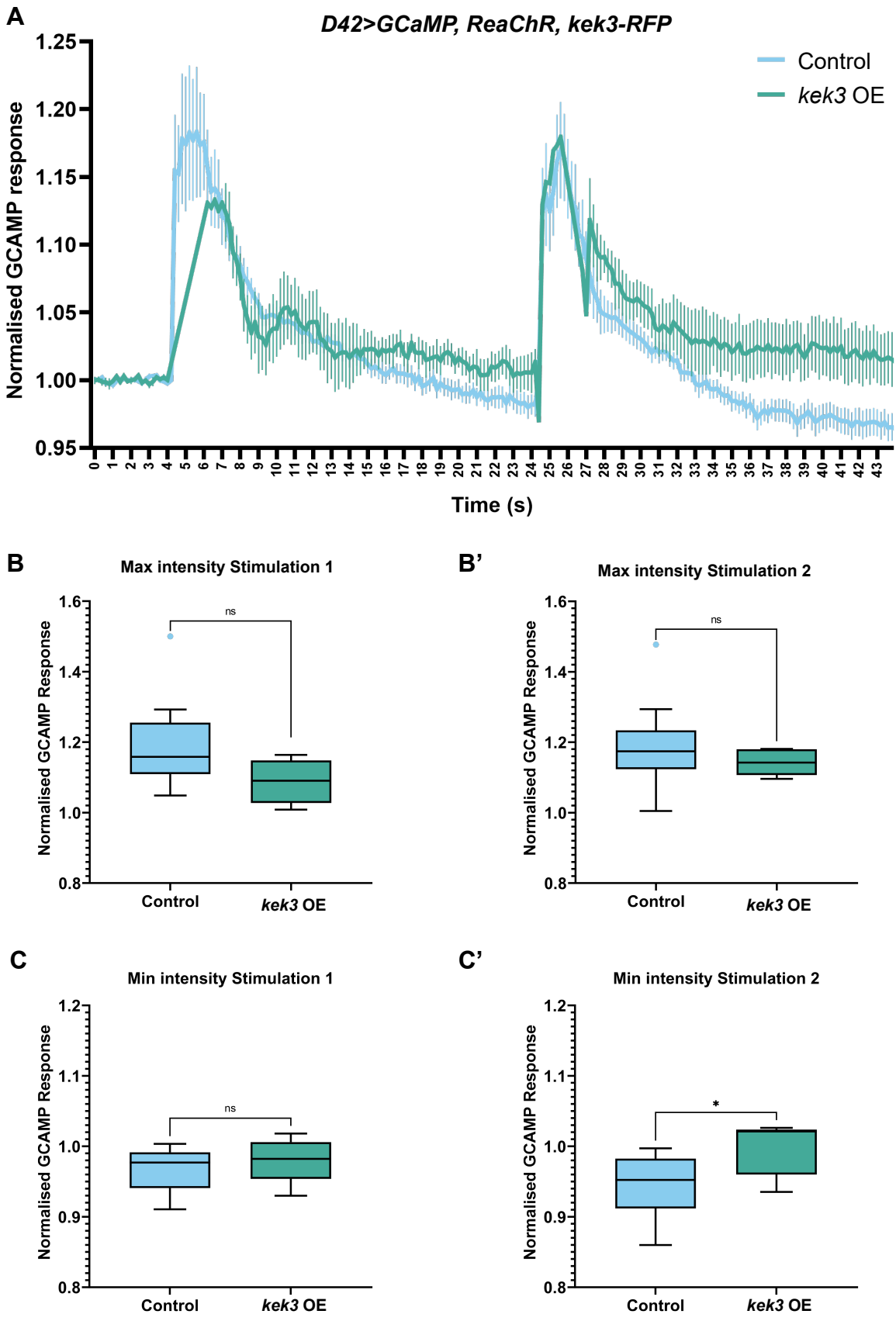


Figure 4.5 - Presynaptic NMJ Ca^{2+} dynamics in *kek3* OE larvae

kek3 alters fluorescent Ca^{2+} reporter GCaMP signal levels following optogenetic stimulation. **A** – Plot of mean signal intensity of firing Ib boutons at NMJ 6/7 at each time point. Following the second stimulation, the GCaMP response in *kek3* overexpression remains higher than control over time.

B and **B'** – Box-and-whisker plots of highest GCaMP response value regardless of time following stimulation 1 and 2 respectively. The Max intensity in *kek3* OE is not significantly different to the control following either stimulation. Stimulation 1: Control (*D42>GCaMP, ReaChR*), n = 14 boutons from 6 larvae, Shapiro-Wilk p = 0.0475. *kek3* OE (*D42>GCaMP, ReaChR*, *kek3-RFP*), n = 5 boutons from 3 larvae, Shapiro-Wilk p = 0.9002. Unpaired Student's t-test, p = 0.102, not significant (ns). Stimulation 2: Control, n = 17 boutons from 6 larvae, Shapiro-Wilk p = 0.2936. *kek3* OE, n = 5 boutons from 3 larvae, Shapiro-Wilk p = 0.4481. Unpaired Student's t-test, p = 4663, not significant (ns).

C and **C'** – Box-and-whisker plots of lowest GCaMP response value regardless of time following stimulation 1 and 2 respectively. The Min intensity is significantly higher than the control following the second but not the first stimulation. Stimulation 1: Control, n = 14 boutons from 6 larvae, Shapiro-Wilk p = 0.1603. *kek3* OE, n = 5 boutons from 3 larvae, Shapiro-Wilk p = 0.6434. Unpaired Student's t-test, p = 0.3976, not significant (ns). Stimulation 2: Control n = 14 boutons from 6 larvae, Shapiro-Wilk p = 0.2412, *kek3* OE n = 5 boutons from 3 larvae, Shapiro-Wilk p = 0.0845. Unpaired Student's t-test, p = 0.0296, significant (*).

Figure 4.6 - Presynaptic NMJ Ca2+ dynamics in *kek4* OE larvae

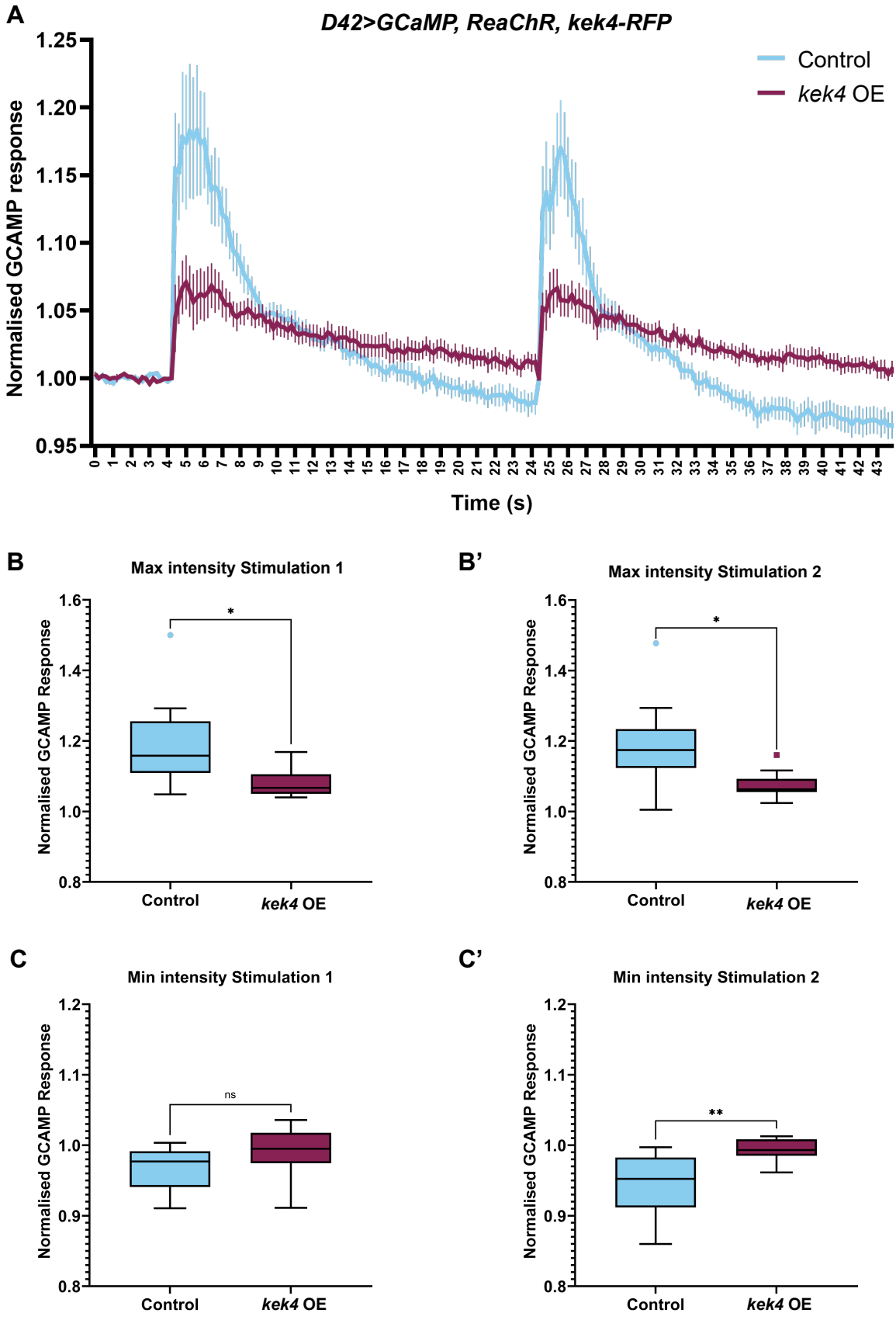


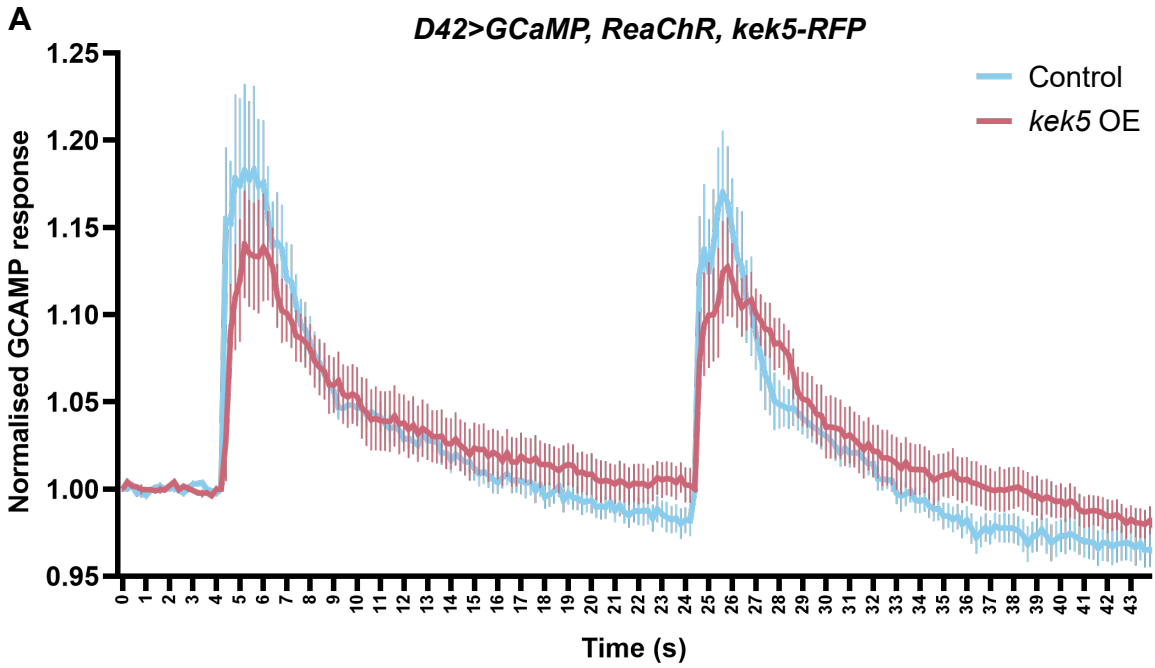
Figure 4.6 - Presynaptic NMJ Ca^{2+} dynamics in *kek4* OE larvae

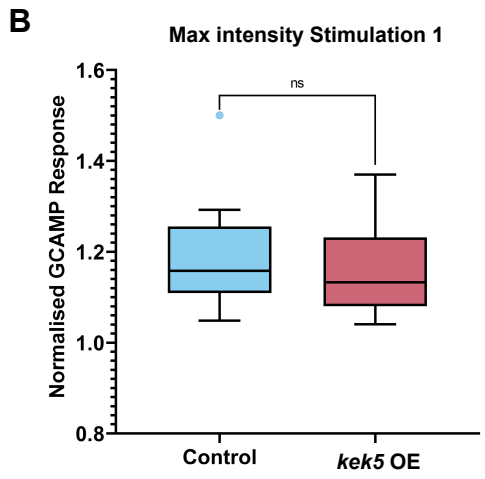
kek4 alters fluorescent Ca^{2+} reporter GCaMP signal levels following optogenetic stimulation. **A** – Plot of mean signal intensity of firing Ib boutons at NMJ 6/7 at each time point. Following both stimulations, the initial GCaMP response in *kek4* overexpression is much lower than the control but remains higher than control over time.

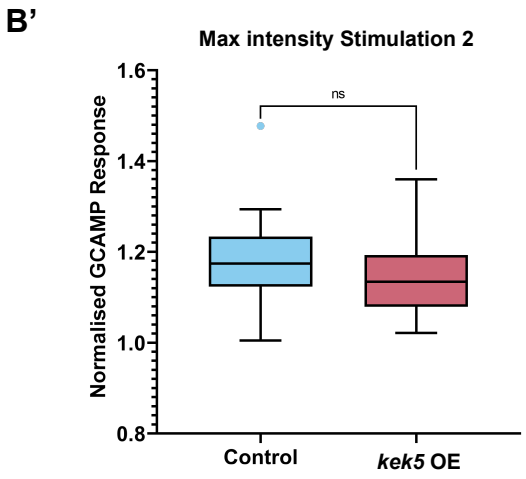
B and **B'** – Box-and-whisker plots of highest GCaMP response value regardless of time following stimulation 1 and 2 respectively. The Max intensity in *kek4* OE is significantly lower than the control following both stimulations. Stimulation 1: Control (*D42>GCaMP, ReaChR*), n = 14 boutons from 6 larvae, Shapiro-Wilk p = 0.0475. *kek4* OE (*D42>GCaMP, ReaChR*, *kek4-RFP*), n = 10 boutons from 7 larvae, Shapiro-Wilk p = 0.1163. Unpaired Student's t-test, p = 0.0134, significant (*). Stimulation 2: Control, n = 10 boutons from 7 larvae, Shapiro-Wilk p = 0.2936. *kek4* OE, n = 10 boutons from 7 larvae, Shapiro-Wilk p = 0.2013. Unpaired Student's t-test, p = 0.0105, significant (*).

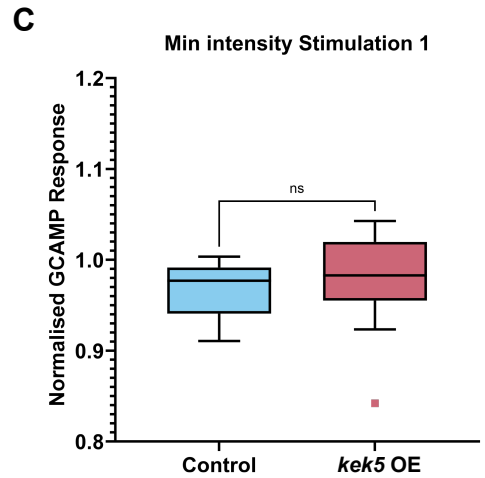
C and **C'** – Box-and-whisker plots of lowest GCaMP response value regardless of time following stimulation 1 and 2 respectively. The Min intensity is significantly higher than the control following the second but not the first stimulation. Stimulation 1: Control, n = 14 boutons from 6 larvae, Shapiro-Wilk p = 0.1603. *kek4* OE, n = 10 boutons from 7 larvae, Shapiro-Wilk p = 0.2743. Unpaired Student's t-test, p = 0.0739, not significant (ns). Stimulation 2: Control n = 14 boutons from 6 larvae, Shapiro-Wilk p = 0.2412, *kek4* OE n = 10 boutons from 7 larvae, Shapiro-Wilk p = 0.5419. Unpaired Student's t-test, p = 0.0029, significant (**).

Figure 4.7 - Presynaptic NMJ Ca2+ dynamics in *kek5* OE larvae









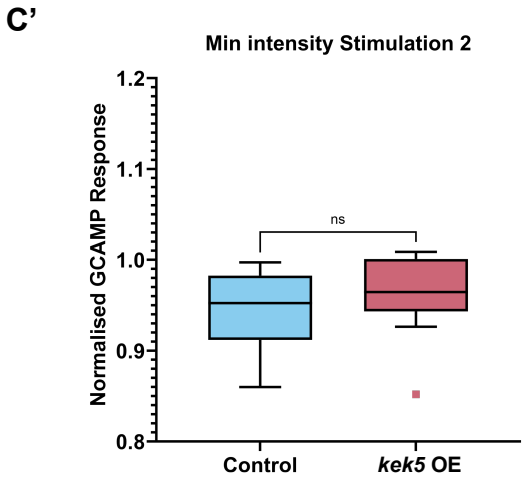


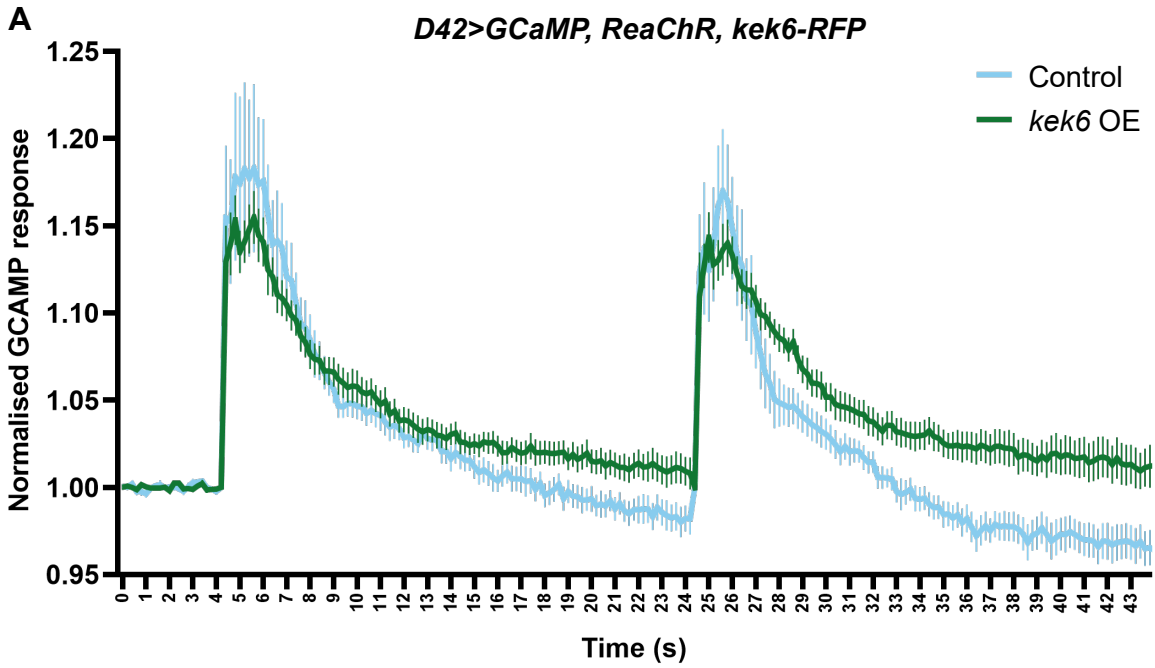
Figure 4.7 - Presynaptic NMJ Ca^{2+} dynamics in *kek5* OE larvae

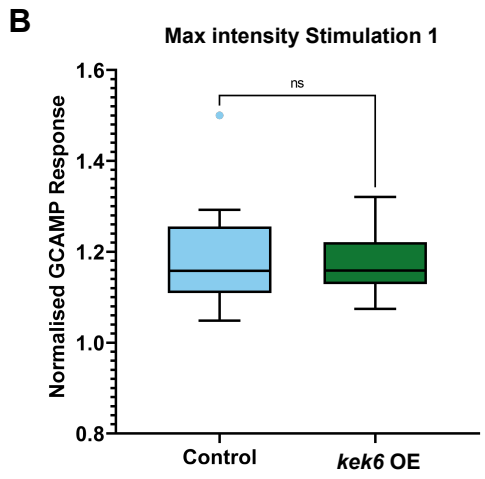
kek5 does not alter fluorescent Ca^{2+} reporter GCaMP signal levels following optogenetic stimulation. **A** – Plot of mean signal intensity of firing Ib boutons at NMJ 6/7 at each time point. Following both stimulations, the initial peak of GCaMP response in *kek5* is slightly lower than the control and GCaMP levels decay slightly slower than control over time.

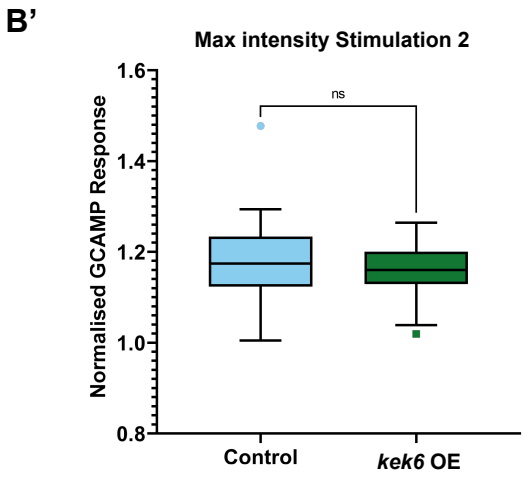
B and **B'** – Box-and-whisker plots of highest GCaMP response value regardless of time following stimulation 1 and 2 respectively. The Max intensity in *kek5* OE is not significantly different to the control following either stimulation. Stimulation 1: Control (*D42>GCaMP, ReaChR*), n = 14 boutons from 6 larvae, Shapiro-Wilk p = 0.0475. *kek5* OE (*D42>GCaMP, ReaChR*, *kek5-RFP*), n = 14 boutons from 7 larvae, Shapiro-Wilk p = 0.3574. Unpaired Student's t-test, p = 0.5044, not significant (ns). Stimulation 2: Control, n = 10 boutons from 7 larvae, Shapiro-Wilk p = 0.2936. *kek5* OE, n = 14 boutons from 7 larvae, Shapiro-Wilk p = 0.4497. Unpaired Student's t-test, p = 0.3494, not significant (ns).

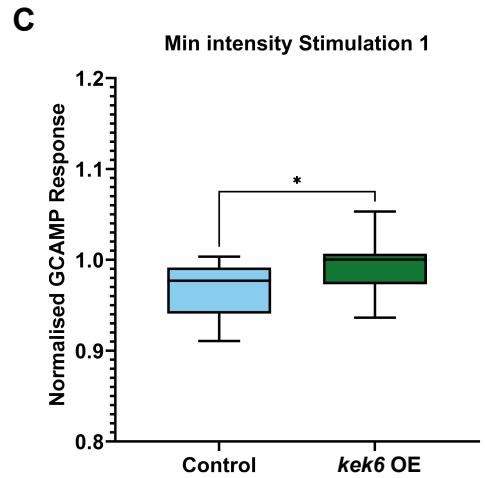
C and **C'** – Box-and-whisker plots of lowest GCaMP response value regardless of time following stimulation 1 and 2 respectively. The Min intensity is not significantly different to the control following the second but not the first stimulation. Stimulation 1: Control, n = 14 boutons from 6 larvae, Shapiro-Wilk p = 0.1603. *kek5* OE, n = 14 boutons from 7 larvae, Shapiro-Wilk p = 0.093. Unpaired Student's t-test, p = 0.5635, not significant (ns). Stimulation 2: Control n = 14 boutons from 6 larvae, Shapiro-Wilk p = 0.2412, *kek5* OE n = 14 boutons from 7 larvae, Shapiro-Wilk p = 0.0534. Unpaired Student's t-test, p = 0.3286, not significant (ns).

Figure 4.8 - Presynaptic NMJ Ca2+ dynamics in *kek6* OE larvae









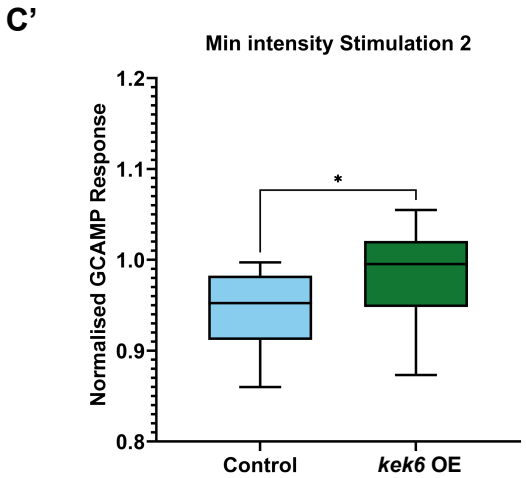


Figure 4.8 - Presynaptic NMJ Ca^{2+} dynamics in *kek6* OE larvae

kek6 alters fluorescent Ca^{2+} reporter GCaMP signal levels following optogenetic stimulation. **A** – Plot of mean signal intensity of firing Ib boutons at NMJ 6/7 at each time point. Following both stimulations, the initial peak of GCaMP response in *kek6* is close to the control value but GCaMP levels decay slower than control over time.

B and **B'** – Box-and-whisker plots of highest GCaMP response value regardless of time following stimulation 1 and 2 respectively. The Max intensity in *kek6* OE is not significantly different to the control following either stimulation. Stimulation 1: Control (*D42>GCaMP, ReaChR*), n = 14 boutons from 6 larvae, Shapiro-Wilk p = 0.0475. *kek6* OE (*D42>GCaMP, ReaChR*, *kek6-RFP*), n = 23 boutons from 8 larvae, Shapiro-Wilk p = 0.5949. Unpaired Student's t-test, p = 0.6524, not significant (ns). Stimulation 2: Control, n = 10 boutons from 7 larvae, Shapiro-Wilk p = 0.2936. *kek6* OE, n = 23 boutons from 8 larvae, Shapiro-Wilk p = 0.5398. Unpaired Student's t-test, p = 0.4427, not significant (ns).

C and **C'** – Box-and-whisker plots of lowest GCaMP response value regardless of time following stimulation 1 and 2 respectively. The Min intensity was significantly higher than the control following both stimulations. Stimulation 1: Control, n = 14 boutons from 6 larvae, Shapiro-Wilk p = 0.1603. *kek6* OE, n = 23 boutons from 8 larvae, Shapiro-Wilk p = 0.3576. Unpaired Student's t-test, p = 0.0163, significant (*). Stimulation 2: Control n = 14 boutons from 6 larvae, Shapiro-Wilk p = 0.2412, *kek6* OE n = 23 boutons from 8 larvae, Shapiro-Wilk p = 0.9528. Unpaired Student's t-test, p = 0.013, significant (*).

4.4 Kek6-TSTEP colocalises with Cacophony

As the initial influx of Ca^{2+} into the bouton is mediated by the voltage-gated Ca^{2+} channel Cacophony, the increase in GCaMP signal in *kek6* OE (*D42>GCaMP6m, uas-kek6-RFP*) larvae could indicate an interaction between Kek6 and Cac. Cac forms the core of the active zone, ergo, Cac puncta within boutons are likely to be active zones (Kawasaki et al., 2004).

To determine if Kek6 and Cac could interact, *kek6-TSTEP* was crossed with *cac-sfGFP* (Cac endogenously tagged with Superfolder GFP) so that both proteins express simultaneously (*cac-sfGFP; +, kek6-TSTEP*) (Fig. 4.9). Pearson's correlation coefficient was used quantify the degree of correlation due to is robustness and ease of interpretation (Adler and Parmryd, 2010). Intriguingly, Kek6-TSTEP colocalised with Cac-sfGFP with a fair to moderate correlation (r = ~0.4) that was significantly greater than the correlation of the two channels outside of the axonal terminal (Fig. 4.9) (Akoglu, 2018). This would suggest that Kek6-TSTEP not only localises to presynaptic boutons, but also to the active zone itself (Kawasaki et al., 2004).

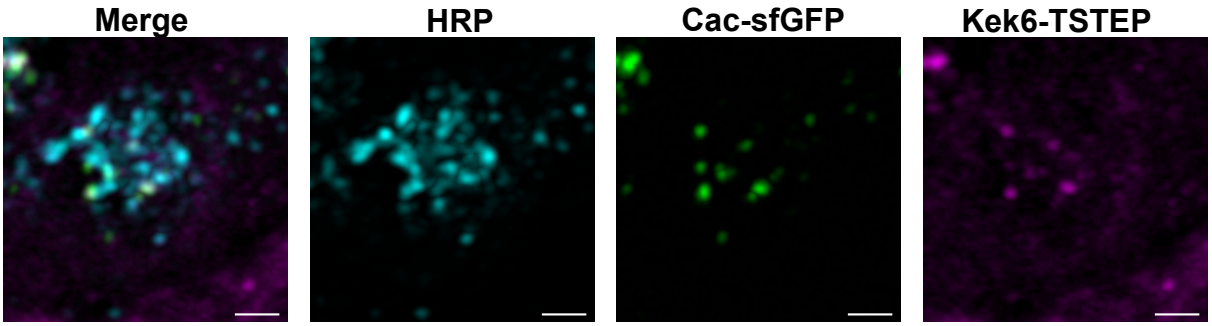
4.5 *kek4* and *kek6* enhance Cacophony channel clustering

As demonstrated in the experiment described in section 4.3, *kek4* and *-6* were demonstrably functionally distinct from each other in their influence on post-stimulation Ca^{2+} dynamics. I therefore aimed to test whether these *keks* were interacting with *cacophony*. As Cac function is directly correlated to its clustering, I asked if *keks* could modulate Cac clustering (Gratz et al., 2019).

Figure 4.9 - Kek6-TSTEP colocalises with endogenously tagged Cac

A

Genotype: *cac-sfGFP ; + ; kek6-TSTEP*



B

Pearson's Correlation Coefficient for Kek6-TSTEP and Cac-sfGFP

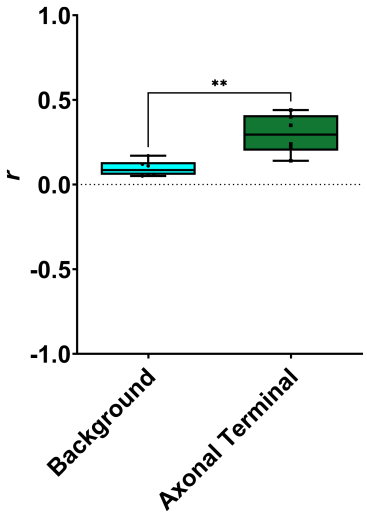


Figure 4.9 – Kek6-TSTEP colocalises with Cac in NMJ 6/7 boutons

Kek6-TSTEP colocalises with Cac puncta at NMJ 6/7 in boutons. **A:** Anti-HRP, anti-GFP and anti-mCherry staining of *cac-sfGFP ; + ; kek6-TSTEP* larval NMJ 6/7. Scale bar = 1µm. **B:** Co-localisation analysis using Pearson's correlation coefficient (PCC). PCC was quantified using ImageJ/Fiji plugin Coloc2. HRP stainings were used to define ROIs for the axonal terminal. PCC was quantified inside ("Axonal Terminal") and outside ("Background") the terminal to assess the apparent colocalization inside the terminal. For Background and Axonal Terminal, n = 6 NMJs from 3 larvae. Background, Shapiro-Wilk p = 0.2902. Axonal Terminal, Shapiro-Wilk p = 0.7132. Unpaired student's t-test, p = 0.0026, significant (**).

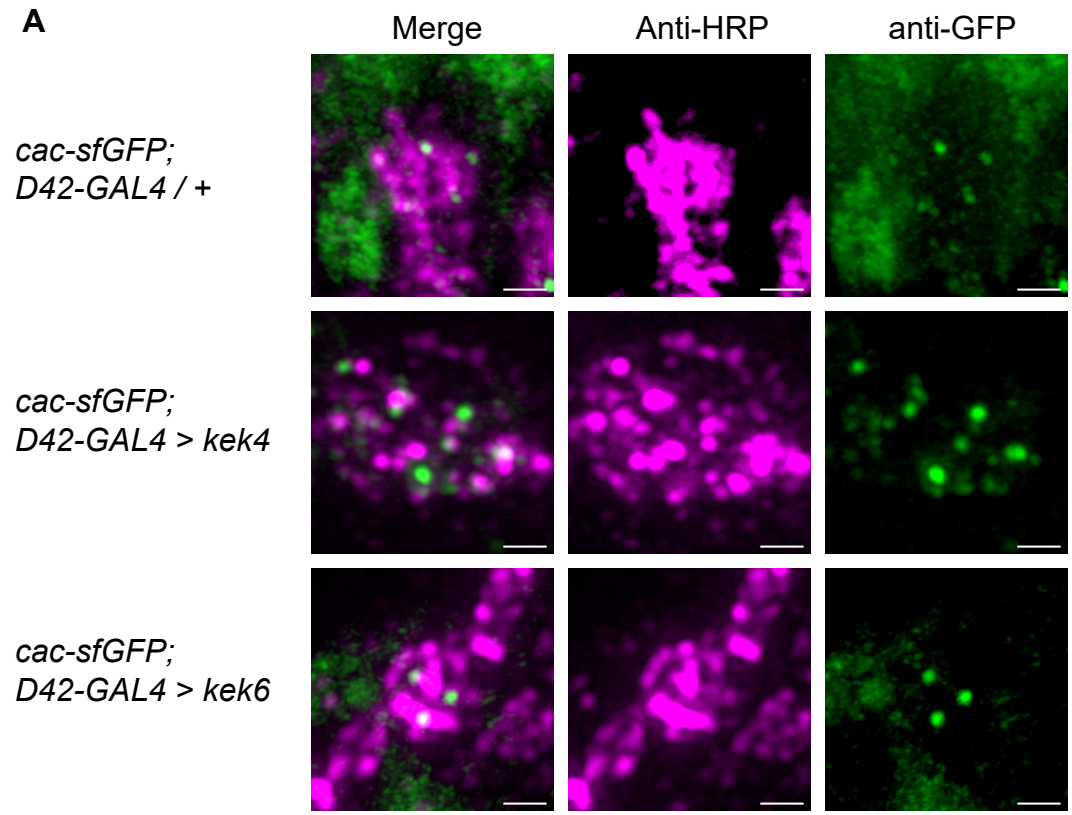
To be able to visualise Cac at physiological levels, I combined Cac-sfGFP, an endogenously tagged form of Cac (a gift from the O'Connor-Giles lab), with *D42-GAL4*. For the control this line was crossed to OregonR, and for the tests to *uas-kek4-RFP* and *uas-kek6-RFP* (Fig. 4.10). L3 wandering larvae were then dissected for the NMJ and were stained with anti-HRP to label axons and with anti-GFP to visualise Cac-sfGFP. Samples were acquired using a Zeiss LSM900 with a 63x Oil objective and the AIRYSCAN near-super-resolution module (Fig. 4.10a).

Images were analysed in Imaris to quantify bouton and Cac volume, the number of Cac dots, and the intensity and volume of individual Cac dots. These values were used to quantify different aspects of Cac-sfGFP distribution.

The number of Cac-sfGFP dots divided by Bouton volume to control for the different bouton sizes, as all else being equal larger boutons would have more Cac dots (Fig. 4.10 B). The mean volume of individual Cac dots was also measured (Fig. 4.10 C). Intensity of individual Cac dots was important to measure and is an indicator of that active zone's release probability (P_r) for synaptic vesicles (Gratz et al., 2019) (Fig. 4.10 D).

Total Cac-sfGFP volume divided by bouton volume gives the total amount of Cac-sfGFP signal within a bouton, this was important to quantify to determine if the overall amount of Cac-sfGFP in the bouton had changed (Fig. 4.10 E). Mean Cac-sfGFP dot volume normalised to bouton volume is the ratio between the mean volume of individual Cac-sfGFP dots and the volume of the bouton, this was quantified to determine if there was a relationship between the two (Fig. 4.10 G).

Figure 4.10 - *kek4* and *kek6* OE increases clustering of Cac



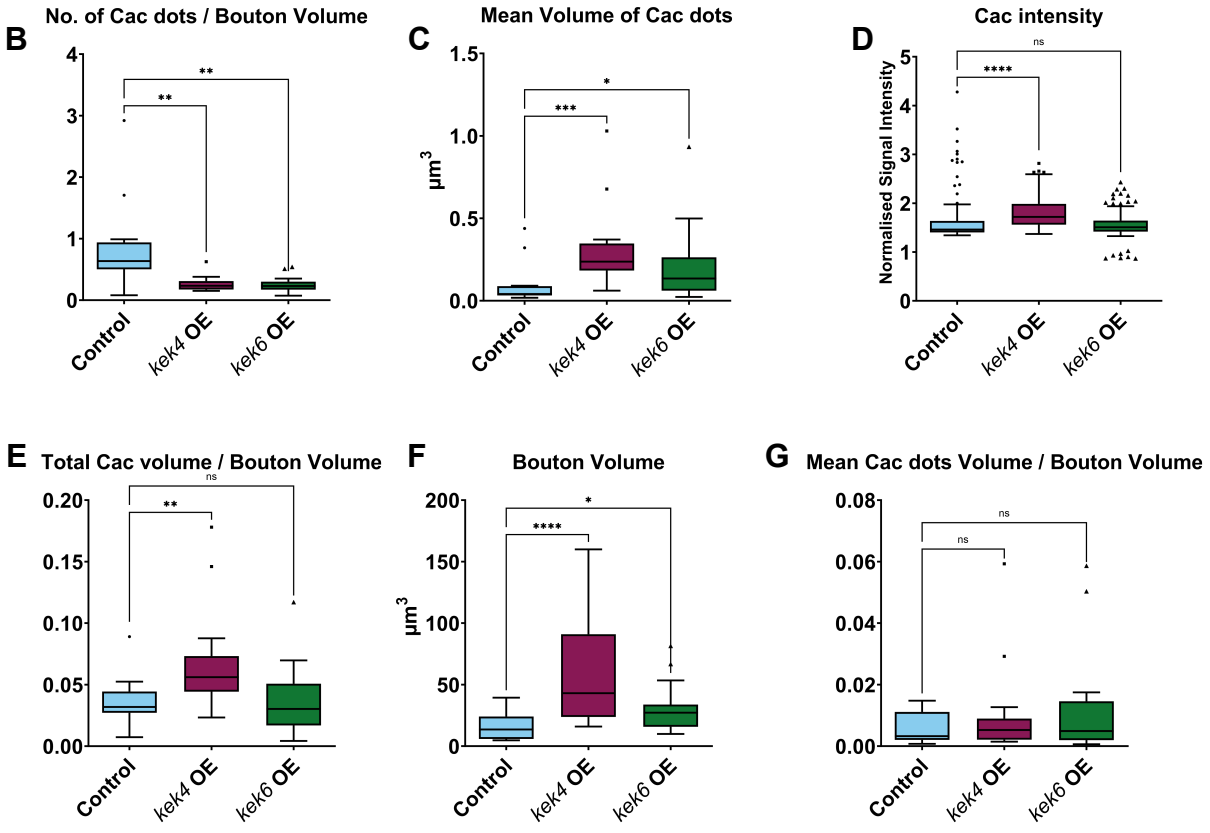


Figure 4.10 – *kek4* and *kek6* OE increases clustering of Cac

Overexpression of *kek4-RFP* and *kek6-RFP* alters Cac channel abundance and distribution in Ib boutons at NMJ 6/7. Bouton images were acquired with AIRYSCAN microscopy and analysed with Imaris for quantification of the Bouton and Cac volumes, number of Cac dots, and their intensities. **A:** Anti-HRP and anti-GFP staining of NMJ 6/7 Ib boutons in control genotype (top row, *cac-sfGFP; + ; D42-GAL4 /* +), *kek4* OE genotype (middle row, *cac-sfGFP; D42>kek4-RFP*), and *kek6* OE genotype (bottom row, *cac-sfGFP; D42>kek6-RFP*). Scale bars = 1µm. **B–G** – Quantification of Cac distribution and abundance.

B: Number of Cac puncta in a bouton normalised to the bouton volume. In *kek4* OE and *kek6* OE the number of Cac puncta per bouton is significantly lower than in the control. Control, n = 15 boutons from 4 larvae, Shapiro-Wilk p = 0.0019. *kek4* OE, n = 16 boutons from 7 larvae, Shapiro-Wilk p = 0.0039. *kek6* OE, n = 20 boutons from 6 larvae, Shapiro-Wilk p = 0.1075. Kruskal-Wallis p = 0.0015, significant (**), with Dunn's post-hoc multiple comparisons test (p = 0.0065 (**) for Control vs *kek4* OE, p = 0.0016 (**) for Control vs *kek6* OE).

C: Mean volume of individual Cac puncta within a bouton. The mean volume of Cac puncta in *kek4* OE and *kek6* OE larvae was significantly higher than in the control. Control, n = 15 boutons from 4 larvae, Shapiro-Wilk p <0.0001. *kek4* OE, n = 16 boutons from 7 larvae, Shapiro-Wilk p = 0.0005. *kek6* OE, n = 20 boutons from 6 larvae, Shapiro-Wilk p = 0.0001. Kruskal-Wallis p = 0.0006, significant (***), with Dunn's post-hoc multiple comparisons test (p = 0.0002 (***) for Control vs *kek4* OE, p = 0.0487 (**) for Control vs *kek6* OE).

D: Intensity of individual Cac dots, signal intensity normalised to mean grey value of the volume inside the bouton that did not belong to Cac dots to control for variation in staining. Cac dots in *kek4* OE larvae had significantly greater intensity than those in Control larvae. *kek6* OE larvae showed no significant difference to the control. Control, n = 146 Cac dots from 15 boutons from 4 larvae, Shapiro-Wilk p <0.0001. *kek4* OE, n = 213 Cac dots from 16 boutons from 7 larvae, Shapiro-Wilk p <0.0001. *kek6* OE, n = 141 Cac dots from 20 boutons from 6 larvae, Shapiro-Wilk p <0.0001. Kruskal-Wallis p <0.0001, significant (****), with Dunn's post-hoc multiple comparisons test (p <0.0001 (****) for Control vs *kek4* OE, p = 0.6785 (ns) for Control vs *kek6* OE).

E: Total volume of Cac in a bouton divided by the bouton's volume. *kek4* OE larvae there is more Cac in the bouton regardless of size or distribution of puncta. In *kek6* OE larvae the amount of Cac in the bouton is not significantly different to the control. Control, n = 15 boutons from 4 larvae, Shapiro-Wilk p = 0.0544. *kek4* OE, n = 16 boutons from 7 larvae, Shapiro-Wilk p = 0.0016. *kek6* OE, n = 20 boutons from 6 larvae, Shapiro-Wilk p = 0.013. Kruskal-Wallis p = 0.0038, significant (**), with Dunn's post-hoc multiple comparisons test (p = 0.0099 (**) for Control vs *kek4* OE, p >0.9999 (ns) for Control vs *kek6* OE).

F: The mean volume of boutons in *kek4* OE and *kek6* OE larvae is significantly higher than in control larvae. Control, n = 15 boutons from 4 larvae, Shapiro-Wilk p = 0.0897. *kek4* OE, n = 16 boutons from 7 larvae, Shapiro-Wilk p = 0.0128. *kek6* OE, n = 20 boutons from 6 larvae, Shapiro-Wilk p = 0.0041. Kruskal-Wallis p = 0.0001, significant (***), with Dunn's post-hoc multiple comparisons test (p <0.0001 (****) for Control vs *kek4* OE, p = 0.0375 (*) for Control vs *kek6* OE).

G: Mean volume of individual Cac puncta divided by the volume of the bouton. In *kek4* OE and *kek6* OE larvae this quantity is not significantly different to the control, suggesting that Cac puncta are scaling proportionately with bouton size**.** Control, n = 15 boutons from 4 larvae, Shapiro-Wilk p = 0.0056. *kek4* OE, n = 16 boutons from 7 larvae, Shapiro-Wilk p <0.0001. *kek6* OE, n = 20 boutons from 6 larvae, Shapiro-Wilk p <0.0001. Kruskal-Wallis p = 0.909, not significant (ns).

4.5.1 *kek4* can modulate Cac distribution

In *kek4* overexpression larvae (*Cac-sfGFP;+;D42>kek4-RFP*), there is a significant decrease in the number of Cac-sfGFP dots per bouton volume, from a mean of 0.81 dots/µm^3 in control larvae to 0.26 dots/µm^3 in *kek4* overexpression (Fig. 4.10 B). This decrease in the number of Cac-sfGFP dots was accompanied with a significant increase in the volume of individual Cac-sfGFP dots, from an average of 0.09 µm^3 in the control to 0.3 µm^3 in *kek4* overexpression (Fig. 4.10 C). This decrease in the number of Cac-sfGFP dots per bouton paired with the significant increase in Cac-sfGFP dot volume strongly indicated that increased Cac clustering is a phenotype of *kek4* overexpression. Interestingly, mean intensity of individual Cac dots is significantly greater than in the control, indicating that *kek4* overexpression leads to an increase in Cac density and P_r in those active zones (Fig. 4.10 D).

Furthermore, the ratio of the total volume of Cac-sfGFP signal to the total bouton volume significantly increases from a mean of 0.035 in the control to a mean of 0.067 in *kek4* OE, nearly doubling (Fig. 4.10 E). This indicates that *kek4* overexpression could be increasing the amount of Cac protein being produced, or that localisation of already synthesized Cac is enhanced to Ib boutons.

In *kek4* overexpression larvae, the volume of HRP+ Ib boutons increased, from a mean of 15.92µm^3 in control larvae to a mean of 55.78µm^3 in larvae with *kek4* overexpression (Fig. 4.10 F). Interestingly, the relative size of Cac-sfGFP dots to the size of the bouton they were in was not significantly different between the control and *kek4* overexpression, indicating that in this context, Cac dot volume scales with the overall volume of the bouton, or vice versa (Fig. 4.10 G).

4.5.2 *kek6* can modulate Cac distribution

When *kek6* is overexpressed (*Cac-sfGFP;+;D42>kek6-RFP*), there was a significant decrease in the number of Cac-sfGFP dots per bouton volume, from a mean of 0.81 dots/µm^3 in control larvae to 0.25 dots/µm^3 in *kek6* overexpression (Fig. 4.10 B). This decrease in the number of Cac-sfGFP dots was observed alongside a significant increase in the volume of individual Cac-sfGFP dots, thus indicating that *kek6* overexpression enhances Cac-sfGFP clustering at the NMJ (Fig. 4.10 C).

Unlike *kek4* overexpression, *kek6* overexpression did not produce a significant difference to the control level of individual Cac dot intensity (Fig. 4.10 D). Furthermore, when kek6 is overexpressed the ratio of the total volume of Cac-sfGFP to the overall bouton volume was not significantly different between the control and *kek6* overexpression (Fig. 4.10 E). This suggested that in *kek6* overexpression larvae, *kek6* did not increase the overall levels of Cac-sfGFP at the synapse but redistributed already present Cac-sfGFP channels.

kek6 overexpression boutons were significantly larger than the in control with the mean volume of HRP+ Ib boutons increasing from 15.92µm^3 in the control to 29.67µm^3 (Fig. 4.10 F). The volume of individual Cac-sfGFP dots was proportional to the overall volume of the bouton (Fig. 4.10 G).

4.6 Discussion

The key findings of this chapter were: 1) Overexpression of *keks* can alter the abundance of different CaMKII isoforms. 2) *keks* modulate Ca^{2+} dynamics in motoneurons following stimulation, and that the characteristics of this modulation are similar but different for each Kek. 3) Kek6-TSTEP co-localises with Cac-sfGFP puncta,

indicating it localises to active zones and suggests that other *keks* may as well. 4) *kek4* and *-6* can enhance Cac clustering in motoneurons.

The data from this chapter indicate that *keks* can influence Ca^{2+} signalling. This is interesting as this would indicate that *keks* could be modulating Ca^{2+} dependent processes including synaptic transmission and plasticity. As *kek4* and *-6* were found to be functionally distinct to each other, they were selected to be the focus of further study. The role that *kek4* and *kek6* play in activity-dependent structural plasticity is explored in the next chapter.

.

5 RESULTS - KEKS MODULATE NMJ MORPHOLOGY AND ACTIVITY-DEPENDENT STRUCTURAL PLASTICITY

5.1 Introduction

In this chapter, I aimed to investigate the role of *keks*, specifically *kek4* and *kek6*, in activity-dependent structural synaptic plasticity. To do this I used optogenetic stimulation with *kek4* and *-6* overexpression and loss of function (LoF) genotypes by over-expressing either *kek* with *D42-GAL4* or heteroallelic null mutants in the case of loss of function. I first investigated the effect of these manipulations on NMJ morphology in the absence of optogenetic stimulation. I then established an optogenetic stimulation regime using ReaChR to induce activity-dependent structural synaptic plasticity. Finally, I used optogenetic stimulation with *kek4* or *-6* gain or loss of function to investigate the role of these genes on synaptic plasticity.

NMJ 6/7 has been reported to be highly plastic and is commonly used by researchers to study plasticity (Griffith and Budnik 2006). Important markers of structural plasticity in the presynaptic cell at the *Drosophila* larval NMJ are axonal terminal size, active zones, and boutons.

In order to assess aspects of overall NMJ structure larval NMJs were stained with anti-HRP to visualise the axonal terminal. I used two metrics for assessing terminal size: axonal terminal length and axonal terminal volume. Terminal length quantifies the extent of the axonal terminal and has been used previously as a feature of NMJ morphology (Ulian-Benitez et al., 2017). Axonal volume quantifies the bulk of the HRP signal and may be indicative of the elaboration of the terminal with varicosities and branching. Both terminal length and volume were normalised to muscle surface area

(MSA) of the NMJ to control for differences in the size of larvae. MSA was multiplied by 1000 to ease handling of the numbers for interpretation (Ulian-Benitez et al., 2017).

I quantified the abundance of active zones by measuring the volume of nc82 staining, which is specific for the AZ component bruchpilot (Brp). This was assessed by two metrics, depicted in parts D and E of all figures for this chapter. This was done to observe the difference, if any, between the amount of Brp per terminal size and the amount of Brp per muscle surface area, i.e. the relative amount of Brp per presynaptic size vs per post-synaptic size.

I assessed the amount of mature and ghost Ib boutons by counting their number per NMJ, these numbers were then normalised to the MSA of the NMJ to control for differences in the size of larvae. Mature boutons are apposed by the post-synaptic density, a clustering of proteins including neurotransmitter receptors. Apposition by the PSD is required for the synapse to be functional and is labelled by the scaffolding protein discs-large (Dlg). The term ‘Ghost boutons’ refers to immature and unstable boutons that lack PSD apposition. Bouton area was also quantified to detect phenotypes on this feature of NMJ morphology.

Previous work has established that *kek6* plays a role in developmental and homeostatic plasticity (Ulian-Benitez et al., 2017, Ulian-Benitez 2018). However, the role of other *kek*s if any was unknown. As established in the previous chapter, *kek4* and *-6* are functionally distinct members of the Kek family. Here their role in plasticity and particularly activity-dependent structural synaptic plasticity is investigated.

5.2 The effect of *kek4* misexpression on synaptic morphology

To investigate whether *kek4* affects the structure of the synapse, NMJ morphology was examined in *kek4* misexpression larvae (Fig. 5.1, 5.2). *D42-GAL4* was used to drive expression of uas-*kek4*-RFP (*D42>kek4-RFP; ReaChR*). For Loss-of-function larvae heteroallelic for *kek4* were used with the mutant alleles $kek4^{20}$ and $kek4^{23}$ ($kek4^{20}/kek4^{23}$ *; D42>ReaChR*) (Bishop, 2014). The mutants used here were generated via FRT mediated mutagenesis, both are null mutants due to the deletion of the start codon (Bishop, 2014). *ReaChR* was expressed in these genotypes to make these data comparable to data from the same genotypes but with optogenetic stimulation.

The length of the axonal terminal was not significantly different to the control in either the *kek4* overexpression or loss-of-function genotypes (Fig. 5.1 B). Furthermore, NMJ size as quantified by the volume of the HRP staining was not significantly different to the control for either misexpression genotype (Fig. 5.1 C).

To determine the impact of *kek4* misexpression on the structure of the synapse the abundance of active zones was quantified by the volume of Brp signal (Fig. 5.1 D+E). In either case, *kek4* misexpression had no impact on the abundance of Brp at the NMJ.

The number of mature Ib boutons, characterised by being HRP+ and Dlg+, was not significantly different to the control genotype for either *D42>kek4-RFP; ReaChR or* $kek4^{20}/kek4^{23}$ *; D42>ReaChR* (Fig. 5.2 B). Additionally, the number of ghost boutons (boutons that are HRP+ but Dlg-) and bouton area was also not significantly different for either *D42>kek4-RFP; ReaChR* or $kek4^{20}/kek4^{23}$ *; D42>ReaChR* (Fig. 5.2 C+D).

Figure 5.1 - NMJ morphology in *kek4* misexpression larvae

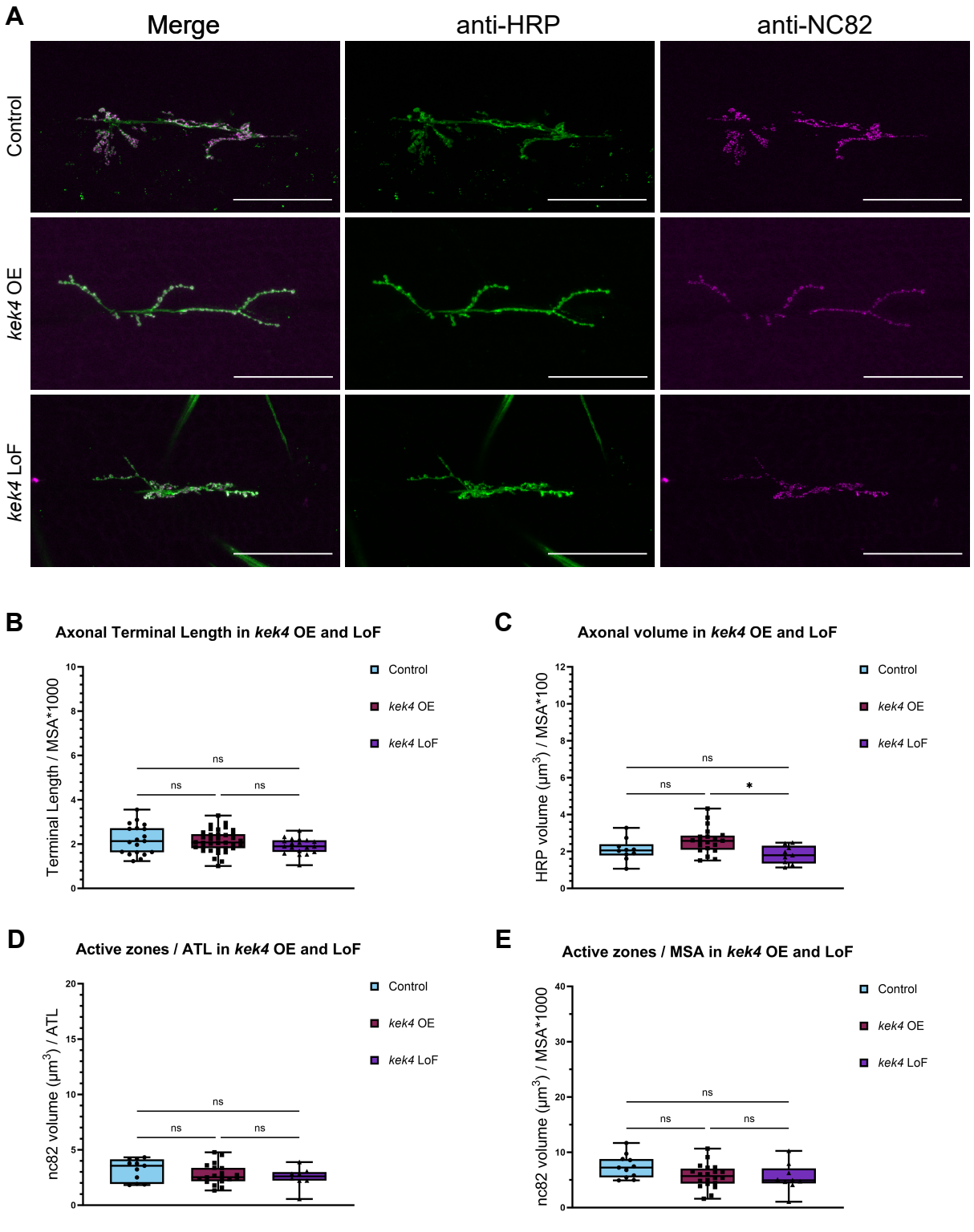


Figure 5.1 – NMJ morphology in *kek4* misexpression larvae

Under control conditions *kek4* misexpression had no apparent impact on NMJ morphology or AZ abundance in L3 larvae. **A:** Anti-HRP and anti-NC82 stainings of NMJ 6/7 in abdominal segment A3 from L3 larvae. *kek4* overexpression (*D42>ReaChR, kek4-RFP*) and loss-of-function (*kek4*^{20}/*kek4*^{23}; *D42>ReaChR*) had no observable impact on NMJ morphology compared to control larvae (*D42>ReaChR*). To avoid stimulation via ReaChR animals were reared in the dark without ChR co-factor ATR. All Scale bars = 50µm.

B: Box-and-whisker plot of axonal terminal length (ATL) normalised to MSA*1000. Neither *kek4* OE nor LoF significantly alters ATL. Control, n = 19 NMJs from 11 larvae, Shapiro-Wilk p = 0.4319. *kek4* OE, n = 36 NMJs from 22 larvae, Shapiro-Wilk p = 0.9989. *kek4* LoF, n = 19 NMJs from 11 larvae, Shapiro-Wilk p = 0.8593. Ordinary one-way ANOVA p = 0.1966, not significant (ns).

C: Box-and-whisker plot of axonal terminal volume normalised to MSA*1000. Neither *kek4* OE nor LoF significantly alters axonal terminal volume. Control, n = 11 NMJs from 7 larvae, Shapiro-Wilk p = 0.724. *kek4* OE, n = 20 NMJs from 12 larvae, Shapiro-Wilk p = 0.3744. *kek4* LoF, n = 9 NMJs from 5 larvae, Shapiro-Wilk p = 0.6471. Ordinary one-way ANOVA p = 0.0104, significant (*), with Tukey's post-hoc multiple comparisons test (see Appendix II for details). The value for *kek4* LoF was significantly lower than that for *kek4* OE larvae (p = 0.0125, *), however this is unlikely to be biologically relevant as neither were significantly different to the control.

D: Ratio of Brp (anti-NC82) volume to ATL per NMJ. Neither *kek4* OE nor LoF significantly alters Brp volume/ATL. Control, n = 11 NMJs from 7 larvae, Shapiro-Wilk p = 0.0575. *kek4* OE, n = 20 NMJs from 12 larvae, Shapiro-Wilk p = 0.7794. *kek4* LoF, n = 9 NMJs from 5 larvae, Shapiro-Wilk p = 0.3793. Ordinary one-way ANOVA p = 0.2811, not significant (ns).

E: Brp volume relative to post-synaptic target area (MSA * 1000). Neither *kek4* OE nor LoF significantly alters Brp volume/MSA. Control, n = 11 NMJs from 7 larvae, Shapiro-Wilk p = 0.5108. *kek4* OE, n = 20 NMJs from 12 larvae, Shapiro-Wilk p = 0.9454. *kek4* LoF, n = 9 NMJs from 5 larvae, Shapiro-Wilk p = 0.5226. Ordinary one-way ANOVA p = 0.0913, not significant (ns).

Figure 5.2 - Bouton morphology in *kek4* misexpression larvae

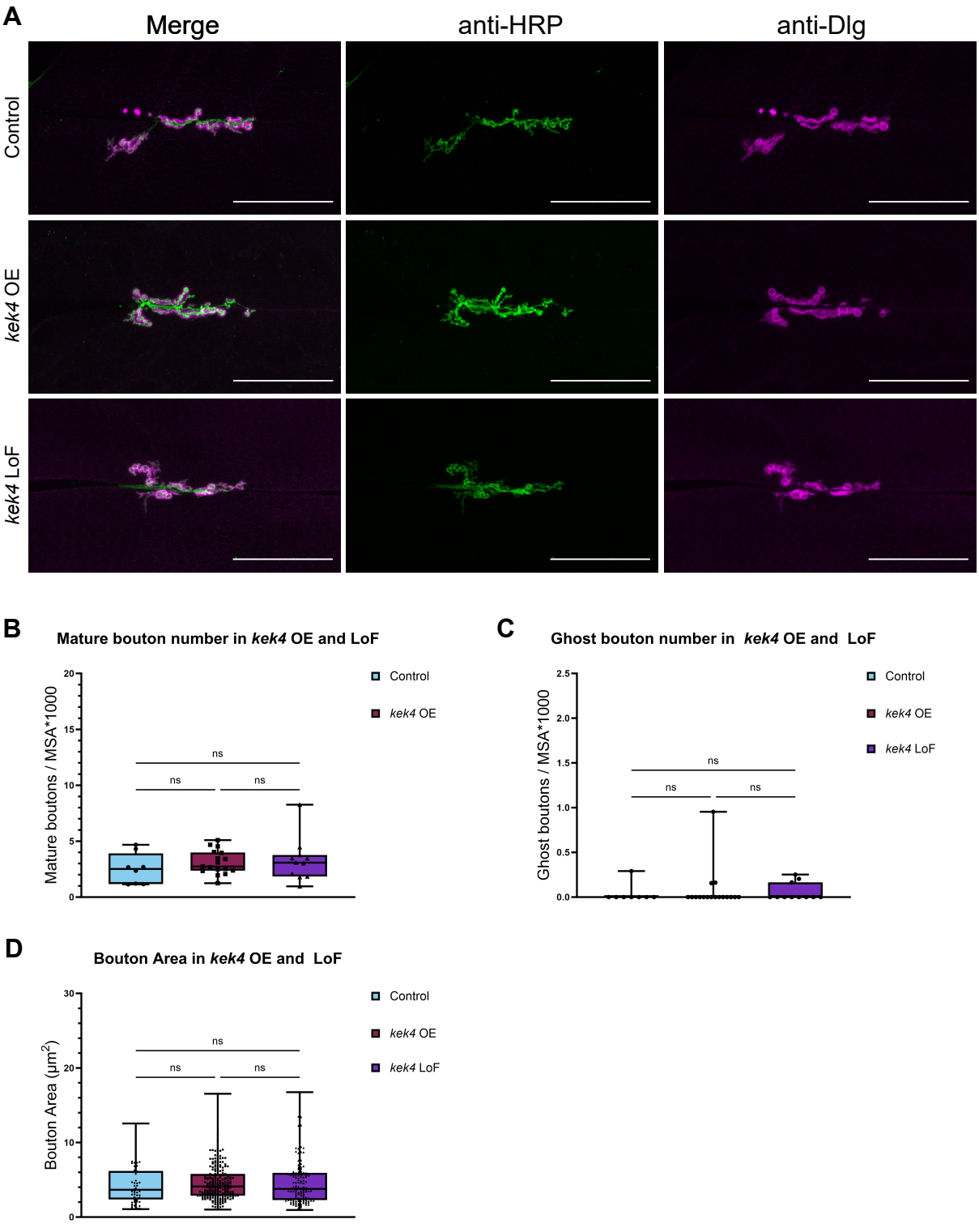


Figure 5.2 - Bouton morphology in *kek4* misexpression larvae

Under control conditions *kek4* misexpression had no apparent impact on bouton morphology in L3 larvae. **A:** Anti-HRP and anti-Dlg stainings of NMJ 6/7 in abdominal segment A3 from L3 larvae. *kek4* overexpression (*D42>ReaChR, kek4-RFP*) and loss-of-function (*kek4*^{20}/*kek4*^{23}; *D42>ReaChR*) had no observable impact on bouton morphology compared to control larvae (*D42>ReaChR*). To avoid stimulation via ReaChR animals were reared in the dark without ChR co-factor ATR. All Scale bars = 50µm.

B: Box-and-whisker plot of the number of mature boutons per NMJ normalised to postsynaptic target size (MSA*1000). Neither *kek4* OE nor LoF significantly alters mature bouton number. Control, n = 8 NMJs from 4 larvae, Shapiro-Wilk p = 0.1417. *kek4* OE, n = 16 NMJs from 10 larvae, Shapiro-Wilk p = 0.6503. *kek4* LoF, n = 10 NMJs from 6 larvae, Shapiro-Wilk p = 0.0342. Ordinary one-way ANOVA p = 0.5166, not significant (ns).

C: Box-and-whisker plot of the number of ghost boutons per NMJ normalised to postsynaptic target size (MSA*1000). N.B., Plot resembles a bar chart due to the high number of NMJs with 0 ghost boutons. Neither *kek4* OE nor LoF significantly alters ghost bouton number. Control, n = 8 NMJs from 4 larvae, Shapiro-Wilk p <0.0001. *kek4* OE, n = 16 NMJs from 10 larvae, Shapiro-Wilk p <0.0001. *kek4* LoF, n = 10 NMJs from 6 larvae, Shapiro-Wilk p <0.0001. Kruskal-Wallis p = 0.7314, not significant (ns).

D: Box-and-whisker plot of the number of HRP+ Ib bouton area (µm^2). Neither *kek4* OE nor LoF significantly alters bouton area. Control, n = 57 boutons from 4 larvae, Shapiro-Wilk p = 0.0003. *kek4* OE, n = 220 boutons from 10 larvae, Shapiro-Wilk p <0.0001. *kek4* LoF, n = 137 boutons from 6 larvae, Shapiro-Wilk p <0.0001. Kruskal-Wallis p = 0.3345, not significant (ns).

These data indicate that *kek4* misexpression did not impact the overall structure of the NMJ under normal conditions.

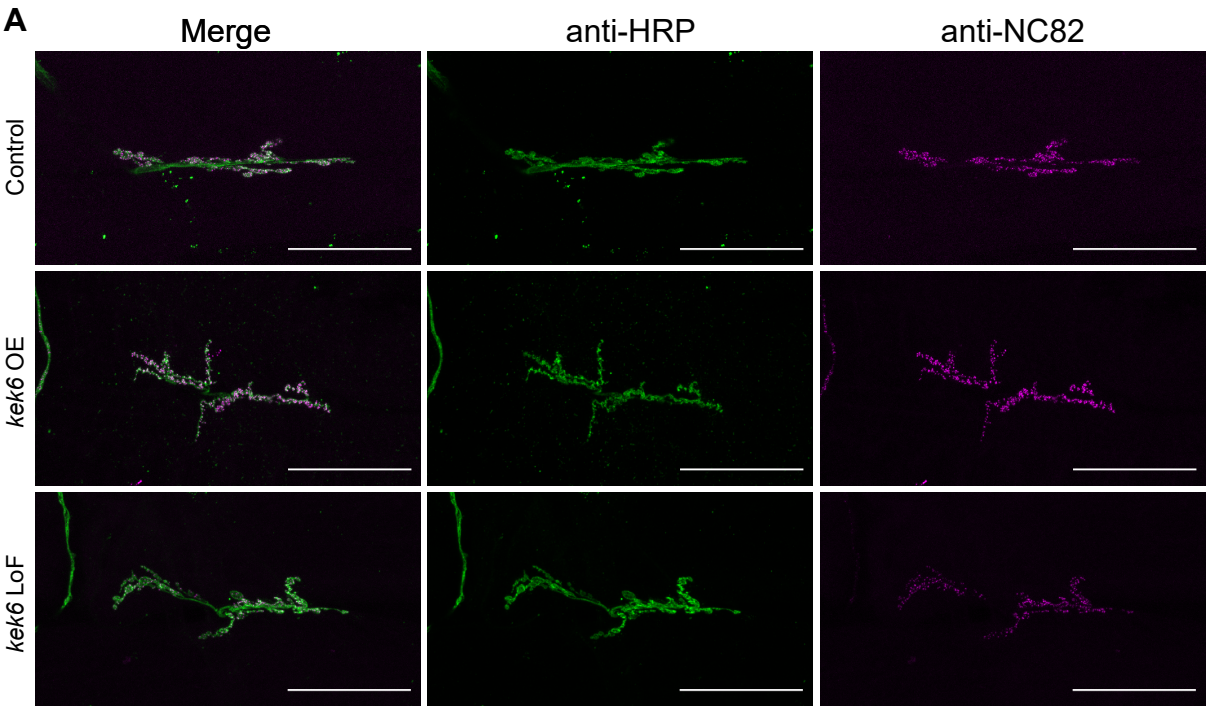
5.3 *kek6* regulates mature bouton number

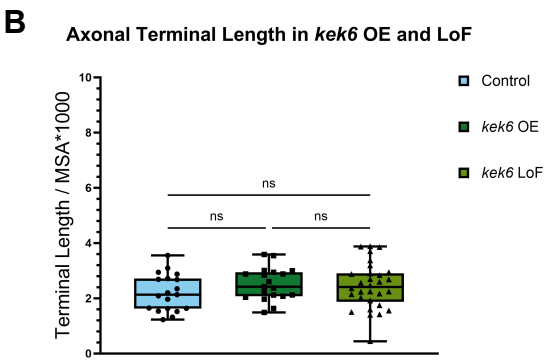
To explore the role of *kek6* on synapse structure, aspects of NMJ morphology were quantified using *kek6* misexpression larvae (Fig. 5.3 and 5.4). *D42-GAL4* was used to drive *uas-kek6-RFP* expression for the OE larvae (*D42>kek6-RFP, ReaChR*). Larvae with heteroallelic *kek6* mutant alleles $kek6^{35}$ and $kek6^{34}$ were used for the LoF genotype ($kek6^{35}/kek6^{34}$*, D42>ReaChR*). These *kek6* mutants were generated via FRT-mediated mutagenesis and are null mutants due to the deletion of the start codon (Bishop, 2014). Transvection is unlikely to have an impact due to the deletion of the start codon in both alleles. *ReaChR* was expressed in these genotypes to make these data comparable to data from the same genotypes but with optogenetic stimulation.

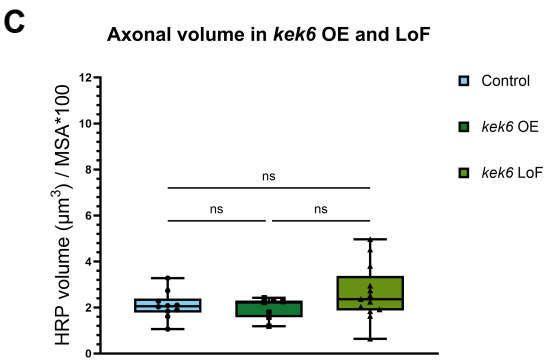
Larval NMJs were stained with anti-HRP and, anti-NC82 or anti-Dlg to assess NMJ structure as described previously. *kek6* misexpression had no impact on NMJ size in either of the metrics assessed here (Fig. 5.3 B+C). Brp abundance, relative to both terminal length and MSA, were not significantly different to the control in either of the *kek6* misexpression genotypes (Fig. 5.3 D+E).

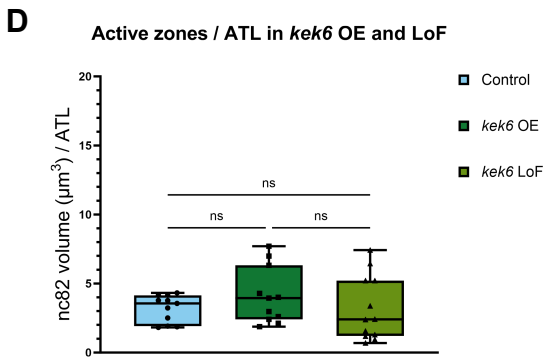
Interestingly, in both *D42>kek6-RFP, ReaChR* and $kek6^{35}/kek6^{34}$, *D42>ReaChR* larvae mature bouton number had significantly increased compared to the control (Fig. 5.4 B). The number of ghost boutons and bouton area were not significantly different to the control for either genotype. These data indicate that *kek6* is a regulator of bouton formation, and the specific abundance of *kek6* is required for a normal number of mature boutons.

Figure 5.3 - NMJ morphology in *kek6* misexpression larvae









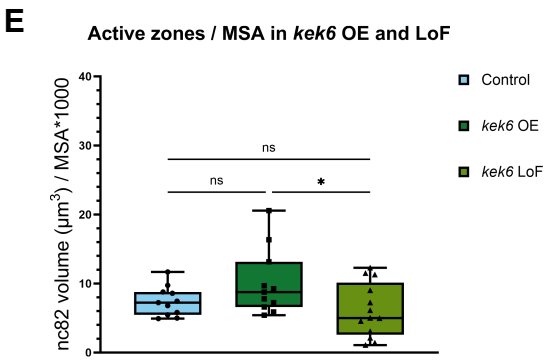


Figure 5.3 - NMJ morphology in *kek6* misexpression larvae

Under control conditions *kek6* misexpression had no apparent impact on NMJ morphology or AZ abundance in L3 larvae. **A:** Anti-HRP and anti-NC82 stainings of NMJ 6/7 in abdominal segment A3 from L3 larvae. *kek6* overexpression (*D42>ReaChR*, *kek6-RFP*) and loss-of-function ($kek6^{34}/kek6^{35}$; *D42>ReaChR*) had no observable impact on NMJ morphology compared to control larvae (*D42>ReaChR*). To avoid stimulation via ReaChR animals were reared in the dark without ChR co-factor ATR. All Scale bars = 50µm.

B: Box-and-whisker plot of axonal terminal length (ATL) normalised to MSA*1000. Neither *kek6* OE nor LoF significantly alters ATL. Control, n = 19 NMJs from 11 larvae, Shapiro-Wilk p = 0.4319. *kek6* OE, n = 19 NMJs from 14 larvae, Shapiro-Wilk p = 0.592. *kek6* LoF, n = 30 NMJs from 21 larvae, Shapiro-Wilk p = 0.5978. Ordinary one-way ANOVA p = 0.3698, not significant (ns).

C: Box-and-whisker plot of axonal terminal volume normalised to MSA*1000. Neither *kek6* OE nor LoF significantly alters axonal terminal volume. Control, n = 11 NMJs from 7 larvae, Shapiro-Wilk p = 0.724. *kek6* OE, n = 11 NMJs from 7 larvae, Shapiro-Wilk p = 0.2492. *kek6* LoF, n = 12 NMJs from 9 larvae, Shapiro-Wilk p = 0.4552. Ordinary one-way ANOVA p = 0.2188, not significant (ns).

D: Ratio of Brp (anti-NC82) volume to ATL per NMJ. Neither *kek6* OE nor LoF significantly alters Brp volume/ATL. Control, n = 11 NMJs from 7 larvae, Shapiro-Wilk p = 0.0575. *kek6* OE, n = 11 NMJs from 7 larvae, Shapiro-Wilk p = 0.131. *kek6* LoF, n = 12 NMJs from 9 larvae, Shapiro-Wilk p = 0.0958. Ordinary one-way ANOVA p = 0.4174, not significant (ns).

E: Brp volume relative to post-synaptic target area (MSA * 1000). Neither *kek6* OE nor LoF significantly alters Brp volume/MSA. Control, n = 11 NMJs from 7 larvae, Shapiro-Wilk p = 0.5108. *kek6* OE, n = 11 NMJs from 7 larvae, Shapiro-Wilk p = 0.0477. *kek6* LoF, n = 12 NMJs from 9 larvae, Shapiro-Wilk p = 0.2844. Ordinary one-way ANOVA p = 0.0482, significant (*), with Tukey's post-hoc multiple comparisons test (see Appendix II for details). The value for *kek6* LoF was significantly lower than that for *kek6* OE larvae (p = 0.0401, *), however this is unlikely to be biologically relevant as neither were significantly different to the control.

Figure 5.4 - Bouton morphology in *kek6* misexpression larvae

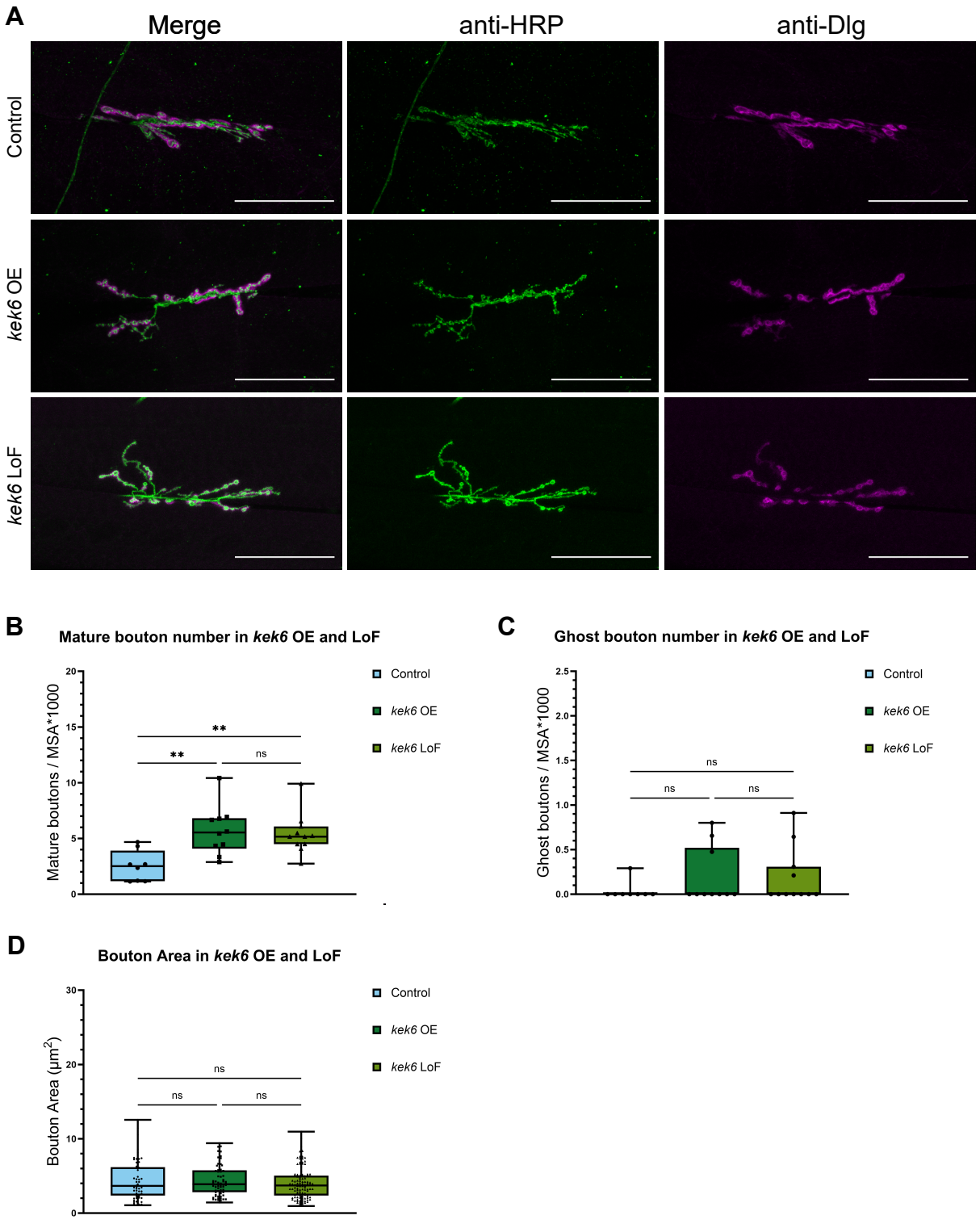


Figure 5.4 - Bouton morphology in *kek6* misexpression larvae .

Under control conditions *kek6* misexpression had no increased mature bouton number, but had no impact on ghost boutons or bouton size in L3 larvae. **A:** Anti-HRP and anti-Dlg stainings of NMJ 6/7 in abdominal segment A3 from L3 larvae. *kek6* overexpression (*D42>ReaChR*, *kek6-RFP*) and loss-of-function ($kek6^{34}$/$kek6^{35}$; *D42>ReaChR*) increased mature bouton number but had no observable impact on ghost bouton number or bouton size compared to control larvae (*D42>ReaChR*). To avoid stimulation via ReaChR animals were reared in the dark without ChR co-factor ATR. All Scale bars = 50µm.

B: Box-and-whisker plot of the number of mature boutons per NMJ normalised to postsynaptic target size (MSA*1000). Both *kek6* OE and LoF significantly increased mature bouton number. Control, n = 8 NMJs from 4 larvae, Shapiro-Wilk p = 0.1417. *kek6* OE, n = 8 NMJs from 7 larvae, Shapiro-Wilk p = 0.4319. *kek6* LoF, n = 18 NMJs from 12 larvae, Shapiro-Wilk p = 0.078. Ordinary one-way ANOVA p = 0.023, significant (**), with Tukey's post-hoc multiple comparisons test (*kek6* OE vs Control p = 0.0036 (**), *kek6* OE vs LoF p = 0.9313 (ns), Control vs *kek6* LoF p = 0.0069 (**)).

C: Box-and-whisker plot of the number of ghost boutons per NMJ normalised to postsynaptic target size (MSA*1000). N.B., Plot resembles a bar chart due to the high number of NMJs with 0 ghost boutons. Neither *kek6* OE nor LoF significantly alters ghost bouton number. Control, n = 8 NMJs from 4 larvae, Shapiro-Wilk p <0.0001. *kek6* OE, n = 8 NMJs from 7 larvae, Shapiro-Wilk p = 0.0002. *kek6* LoF, n = 18 NMJs from 12 larvae, Shapiro-Wilk p = 0.0003. Kruskal-Wallis p = 0.4581.

D: Box-and-whisker plot of the number of HRP+ Ib bouton area (μm^2). Neither *kek6* OE nor LoF significantly alters bouton area. Control, n = 57 boutons from 4 larvae, Shapiro-Wilk p = 0.0003. *kek6* OE, n = 68 boutons from 7 larvae, Shapiro-Wilk p = 0.0015. *kek6* LoF, n = 88 boutons from 5 larvae, Shapiro-Wilk p <0.0001. Kruskal-Wallis p = 0.5346, not significant (ns).

5.4 Optogenetically induced activity modifies NMJ morphology

Different methods have been used to induce activity-dependent structural plasticity, optogenetics was selected to be used here due to its specificity, precision, and ability to be used in live larvae (Maldonado-Díaz et al., 2021). Here I asked whether or not optogenetic stimulation could induce stable structural plasticity. Previous studies investigating activity-dependent structural plasticity with optogenetics assess NMJ morphology on short time scales, e.g. up to 130 minutes, following stimulation (Maldonado-Díaz et al., 2021). Additionally, this was focused on ghost boutons, which are known to be transient structures. In mammals, BDNF/TrkB signalling is thought to mediate long-lasting structural changes associated with long-term memory (Kowiański et al., 2018). Therefore, I sought to establish an optogenetic stimulation regime that could induce stable, long-lasting (up to 24 hours) plasticity.

Briefly, *D42-GAL4* was used to drive expression of the red-light sensitive cation channel *ReaChR*. Larvae were reared in the dark and were exposed to repeated bursts of high intensity 560nm light 96 hours after egg laying (AEL). Larvae were allowed to recover in the dark for 24 hours before dissection at third instar.

After optogenetic stimulation, the volume of the presynaptic terminal had also significantly increased following optogenetic stimulation, but interestingly not the length (Fig. 5.5 A-C). Furthermore, there was a significant increase in Brp relative to both terminal length and MSA (Fig. 5.5 D+E).

Additionally, the number of mature boutons had significantly increased from the no activity control indicating that activity induced formation of new functional synapses had occurred (Fig. 5.6 B). This, and the increased amount of Brp, indicated that the activity protocol used here increased the number of functional boutons at the NMJ.

Figure 5.5 - NMJ morphology following Optogenetic stimulation

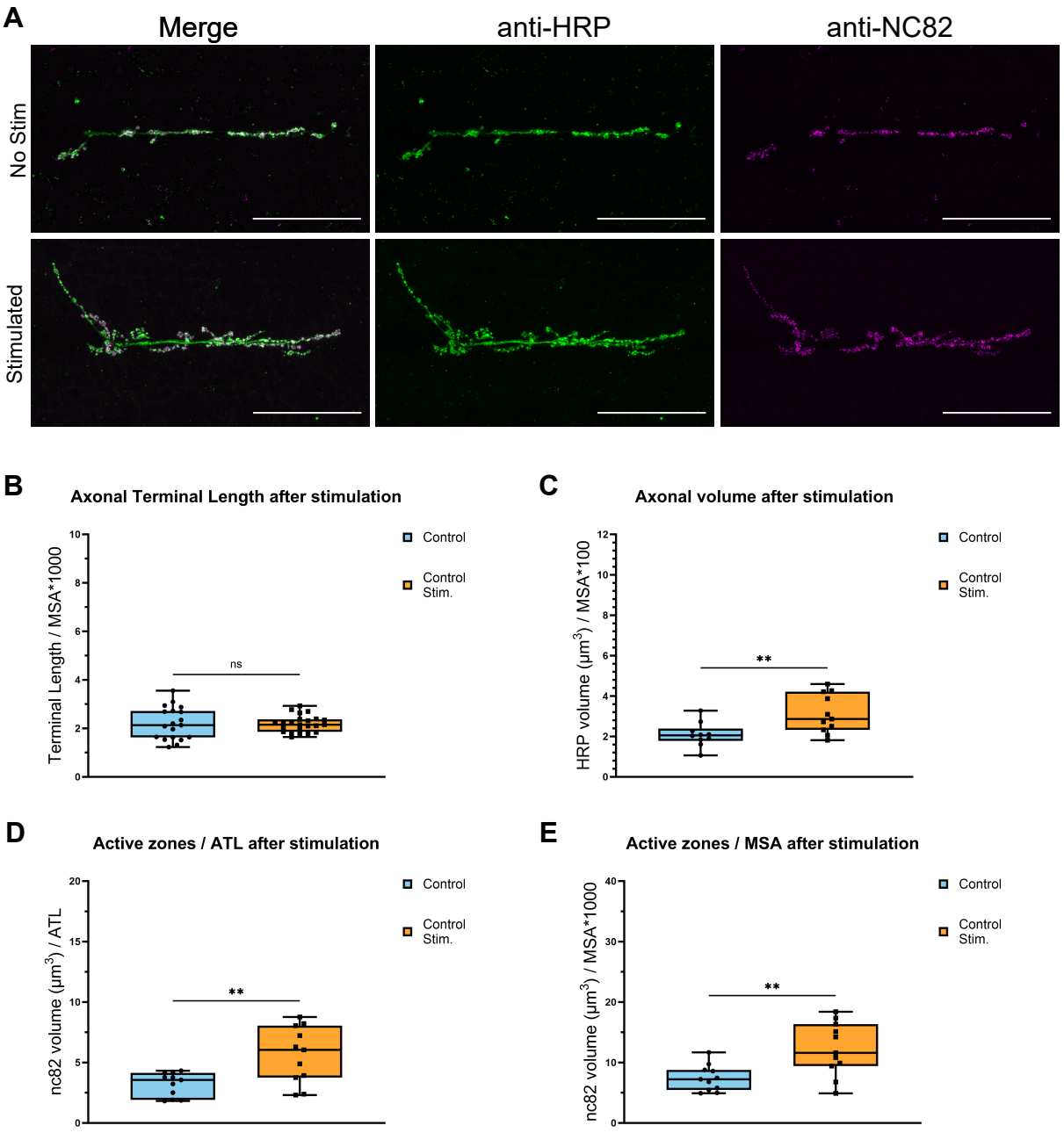


Figure 5.5 - NMJ morphology following Optogenetic stimulation

Optogenetic stimulation alters NMJ morphology in L3 larvae. **A:** Anti-HRP and anti-NC82 stainings of NMJ 6/7 in abdominal segment A3 from L3 larvae. Simulated control larvae (*D42>ReaChR*) were stimulated via optogenetics and were allowed to recover for 24 hours before dissection. To avoid unwanted stimulation animals were reared in the dark. Unstimulated larvae did not undergo the optogenetics protocol and were reared without ChR co-factor ATR. All Scale bars = 50µm.

B: Box-and-whisker plot of axonal terminal length (ATL) normalised to MSA*1000. Optogenetic stimulation did not significantly alter ATL. Unstimulated control, n = 19 NMJs from 11 larvae, Shapiro-Wilk p = 0.4319. Stimulated control, n = 23 NMJs from 16 larvae, Shapiro-Wilk p = 0.5142. Unpaired student's t-test p = 0.9769, not significant (ns).

C: Box-and-whisker plot of axonal terminal volume normalised to MSA*1000. Optogenetic stimulation significantly increased terminal volume. Unstimulated control, n = 11 NMJs from 7 larvae, Shapiro-Wilk p = 0.724. Stimulated control, n = 12 NMJs from 7 larvae, Shapiro-Wilk p = 0.374. Unpaired student's t-test p = 0.009, significant (**).

D: Ratio of Brp (anti-NC82) volume to ATL per NMJ. Optogenetic stimulation significantly increased Brp volume/ATL. Unstimulated control, n = 11 NMJs from 7 larvae, Shapiro-Wilk p = 0.0575. Stimulated control, n = 12 NMJs from 7 larvae, Shapiro-Wilk p = 0.4084. Unpaired student's t-test p = 0.0079, significant (**).

E: Brp volume relative to post-synaptic target area (MSA * 1000). Optogenetic stimulation significantly increased Brp volume/MSA. Unstimulated control, n = 11 NMJs from 7 larvae, Shapiro-Wilk p = 0.5108. Stimulated control, n = 12 NMJs from 7 larvae, Shapiro-Wilk p = 0.798. Unpaired student's t-test p = 0.0036, significant (**).

Figure 5.6 - Bouton morphology following Optogenetic stimulation

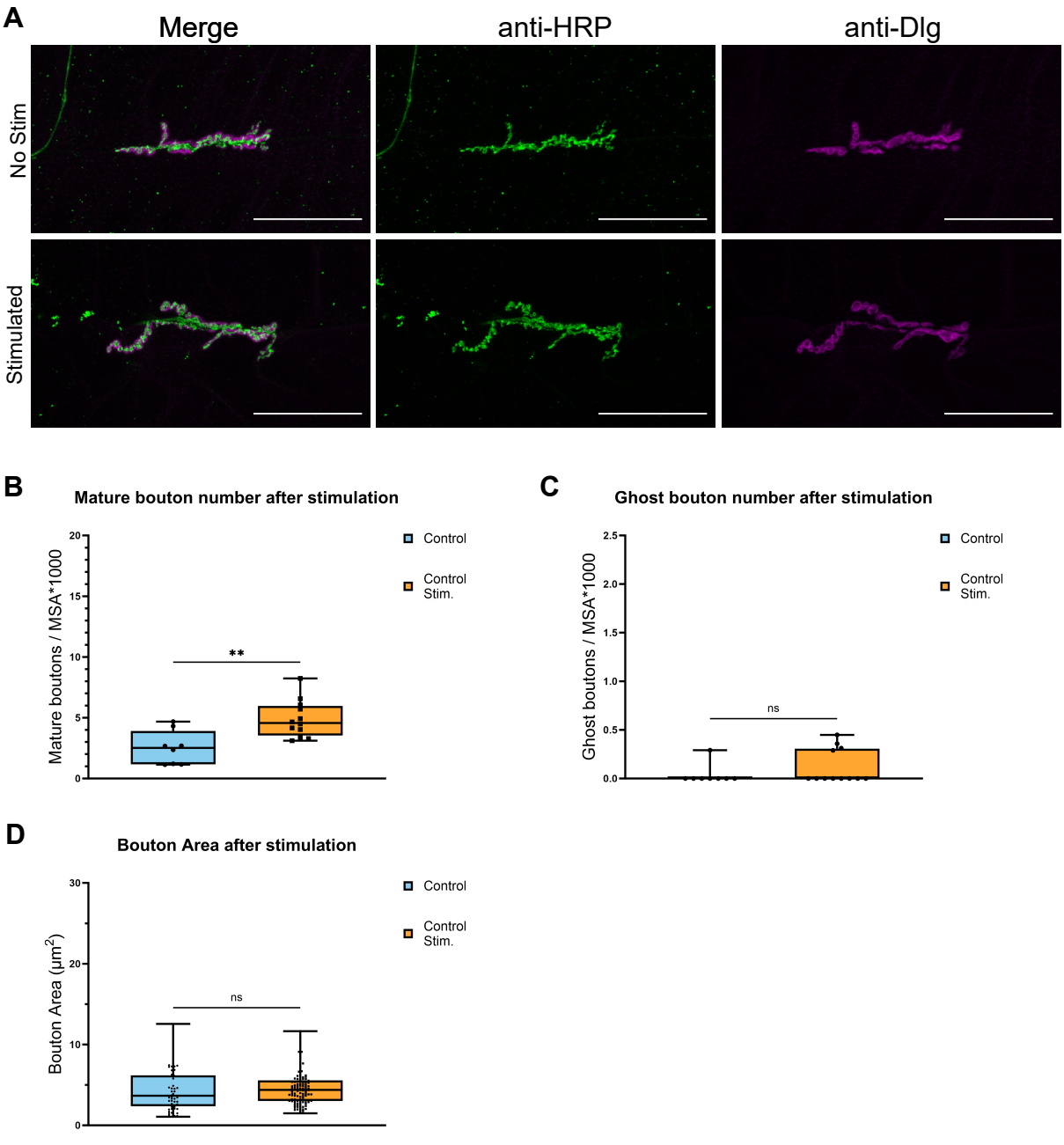


Figure 5.6 - Bouton morphology following Optogenetic stimulation

Optogenetic stimulation increases mature bouton number in L3 larval NMJs. **A:** Anti-HRP and anti-Dlg stainings of NMJ 6/7 in abdominal segment A3 from L3 larvae. Simulated control larvae (*D42>ReaChR*) were stimulated via optogenetics and were allowed to recover for 24 hours before dissection. To avoid unwanted stimulation animals were reared in the dark. Unstimulated larvae did not undergo the optogenetics protocol and were reared without ChR co-factor ATR. All Scale bars = 50µm.

B: Box-and-whisker plot of the number of mature boutons per NMJ normalised to postsynaptic target size (MSA*1000). Optogenetic stimulation significantly increased mature bouton number. Unstimulated control, n = 8 NMJs from 4 larvae, Shapiro-Wilk p = 0.1471. Stimulated control, n = 11 NMJs from 9 larvae, Shapiro-Wilk p = 0.3543. Unpaired student's t-test p = 0.0025, significant (**).

C: Box-and-whisker plot of the number of ghost boutons per NMJ normalised to postsynaptic target size (MSA*1000). N.B., Plot resembles a bar chart due to the high number of NMJs with 0 ghost boutons. Optogenetic stimulation had no impact on ghost bouton number. Unstimulated control, n = 8 NMJs from 4 larvae, Shapiro-Wilk p <0.0001. Stimulated control, n = 11 NMJs from 9 larvae, Shapiro-Wilk p = 0.0005. Mann-Whitney p = 0.3064, not significant (ns).

D: Box-and-whisker plot of the number of HRP+ Ib bouton area (μm^2). Optogenetic stimulation had no impact on bouton area. Unstimulated control, n = 57 boutons s from 4 larvae, Shapiro-Wilk p = 0.0003. Stimulated control, n = 114 boutons from 9 larvae, Shapiro-Wilk p <0.0001. Mann-Whitney p = 0.1914, not significant (ns).

There was no significant increase in the number of ghost boutons nor in bouton area, however (Fig. 5.6 C+D).

These data indicate that the optogenetic activity protocol used here could induce activity-dependent structural plasticity at larval NMJ 6/7. This allows for the exploration of the role of *kek4* and 6 in stable activity-dependent structural plasticity in this model.

5.5 *kek4* is required for activity-dependent structural plasticity

To investigate if *kek4* plays a role in activity-dependent structural plasticity at the NMJ, *kek4* misexpression larvae were stimulated with optogenetics using the previously described paradigm. *kek4* OE larvae (*D42>kek4-RFP; ReaChR*) were stimulated with optogenetics and were stained with anti-HRP and, anti-NC82 or anti-Dlg to assess NMJ structure (Fig. 5.7 and 5.8).

Interestingly *kek4* overexpression appears to have an activity-dependent phenotype in regard to axonal terminal length, with terminal length being significantly higher in stimulated *kek4* overexpression larvae than in either of the control conditions or unstimulated *kek4* overexpression larvae (Fig. 5.7 B). In contrast, in stimulated *D42>kek4-RFP; ReaChR* larvae NMJ volume did not increase compared to unstimulated *D42>kek4-RFP; ReaChR* (Fig. 5.7 C). This indicated that outgrowth of the NMJ following stimulation was impaired when *kek4* was overexpressed.

In stimulated *D42>kek4-RFP; ReaChR* larvae Brp volume did not change compared to unstimulated larvae of the same genotype (Fig. 5.7 D+E). This indicated that *kek4* overexpression was able to prevent the activity-dependent increase in AZs seen in the control.

Figure 5.7 - *kek4* OE inhibits active zone plasticity

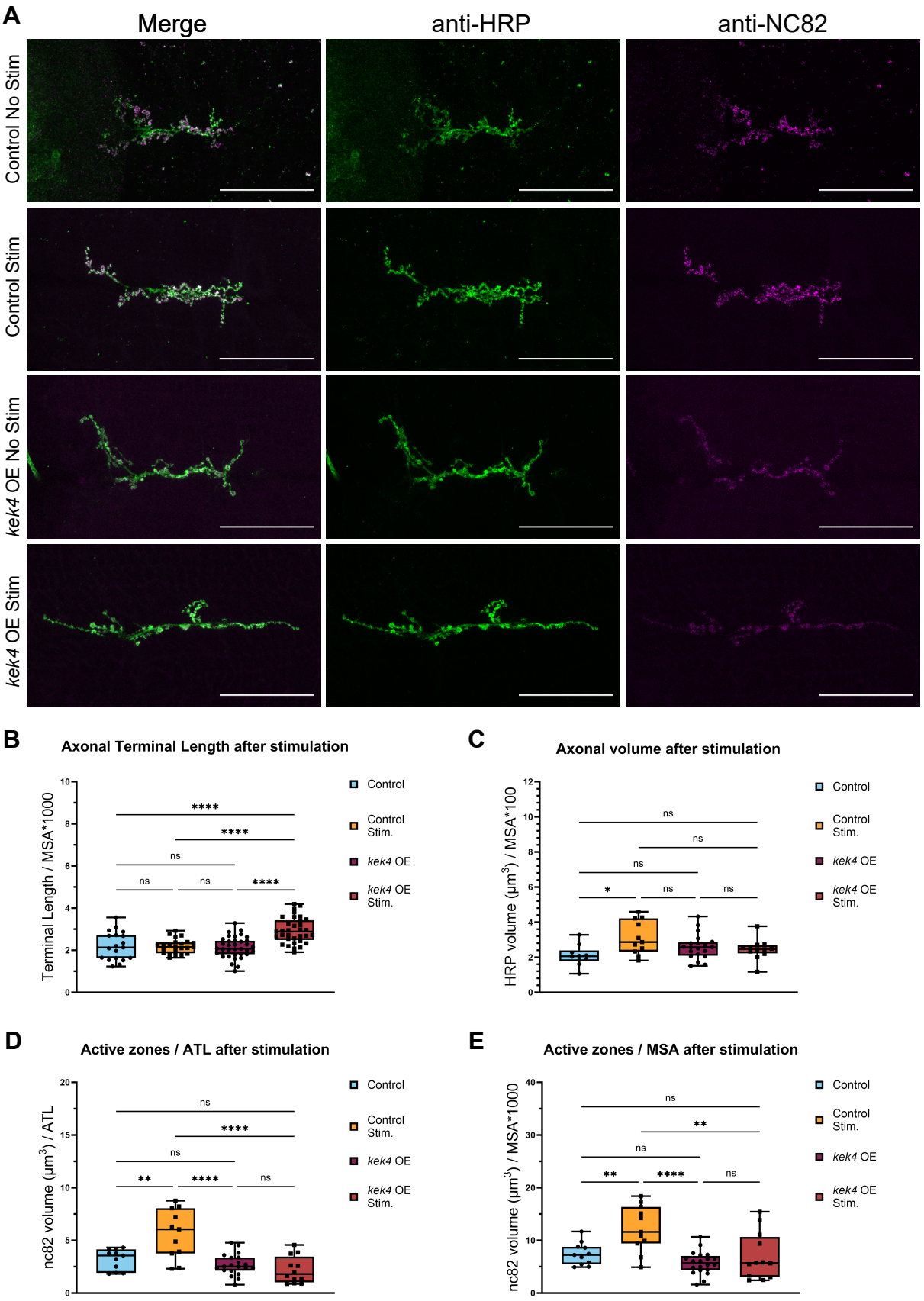


Figure 5.7 - *kek4* OE inhibits active zone plasticity

kek4 OE inhibits NMJ plasticity following optogenetic stimulation. **A:** Anti-HRP and anti-NC82 stainings of NMJ 6/7 in abdominal segment A3 from L3 larvae. Simulated control (*D42>ReaChR*) and *kek4* OE (*D42>ReaChR, kek4-RFP*) larvae were stimulated via optogenetics and were allowed to recover for 24 hours before dissection. To avoid unwanted stimulation animals were reared in the dark. Unstimulated larvae did not undergo the optogenetics protocol and were reared without ChR co-factor ATR. All Scale bars = 50µm.

B: Box-and-whisker plot of axonal terminal length (ATL) normalised to MSA*1000. Axonal terminal length in stimulated *kek4* OE larvae was significantly greater than that in the control genotype under both conditions and unstimulated *kek4* OE. Unstimulated control, n = 19 NMJs from 11 larvae, Shapiro-Wilk p = 0.4319. Stimulated control, n = 23 NMJs from 16 larvae, Shapiro-Wilk p = 0.5142. Unstimulated *kek4* OE, n = 36 NMJs from 22 larvae, Shapiro-Wilk p = 0.9989. Stimulated *kek4* OE, n = 33 NMJs from 20 larvae, Shapiro-Wilk p = 0.3839. Ordinary one-way ANOVA p <0.0001, significant (****), with Tukey's post-hoc multiple comparisons test: Unstimulated control vs Stimulated control p >0.9999 (ns), Unstimulated control vs Unstimulated *kek4* OE p = 0.9719 (ns), Unstimulated control vs Stimulated *kek4* OE p <0.0001 (****), Stimulated control vs Unstimulated *kek4* OE p = 0.9729 (ns), Stimulated control vs Stimulated *kek4* OE p <0.0001 (****), Unstimulated *kek4* OE vs Stimulated *kek4* OE p <0.0001 (****).

C: Box-and-whisker plot of axonal terminal volume normalised to MSA*1000. Axonal terminal volume in Stimulated *kek4* OE was not different to unstimulated *kek4* OE larvae. Unstimulated control, n = 11 NMJs from 7 larvae, Shapiro-Wilk p = 0.724. Stimulated control, n = 12 NMJs from 7 larvae, Shapiro-Wilk p = 0.374. Unstimulated *kek4* OE, n = 20 NMJs from 12 larvae, Shapiro-Wilk p = 0.3744. Stimulated *kek4* OE, n = 12 NMJs from 8 larvae, Shapiro-Wilk p = 0.0931. Ordinary one-way ANOVA p = 0.0184, significant (*), with Tukey's post-hoc multiple comparisons test: Unstimulated control vs Stimulated control p = 0.0128 (*), Unstimulated control vs Unstimulated *kek4* OE p = 0.2212 (ns), Unstimulated control vs Stimulated *kek4* OE p =0.4408 (ns), Stimulated control vs Unstimulated *kek4* OE p = 0.2212 (ns), Stimulated control vs

Stimulated *kek4* OE p = 0.151 (ns), Unstimulated *kek4* OE vs Stimulated *kek4* OE p = 0.5879 (ns).

D: Ratio of Brp (anti-NC82) volume to ATL per NMJ. Brp Volume/ATL did not increase after optogenetic stimulation in *kek4* OE larvae. Unstimulated control, n = 11 NMJs from 7 larvae, Shapiro-Wilk p = 0.0575. Stimulated control, n = 12 NMJs from 7 larvae, Shapiro-Wilk p = 0.4084. Unstimulated *kek4* OE, n = 20 NMJs from 12 larvae, Shapiro-Wilk p = 0.7794. Stimulated *kek4* OE, n = 12 NMJs from 8 larvae, Shapiro-Wilk p = 0.1122. Ordinary one-way ANOVA p <0.0001, with Tukey's post-hoc multiple comparisons test: Unstimulated control vs Stimulated control p = 0.0025 (**), Unstimulated control vs Unstimulated *kek4* OE p = 0.6612 (ns), Unstimulated control vs Stimulated *kek4* OE p =0.2678 (ns), Stimulated control vs Unstimulated *kek4* OE p <0.0001 (****), Stimulated control vs Stimulated *kek4* OE p <0.0001 (****), Unstimulated *kek4* OE vs Stimulated *kek4* OE p = 0.7941 (ns).

E: Brp volume relative to post-synaptic target area (MSA * 1000). Optogenetic stimulation significantly increased Brp volume/MSA. Unstimulated control, n = 11 NMJs from 7 larvae, Shapiro-Wilk p = 0.5108. Stimulated control, n = 12 NMJs from 7 larvae, Shapiro-Wilk p = 0.798. Unstimulated *kek4* OE, n = 20 NMJs from 12 larvae, Shapiro-Wilk p = 0.9454. Stimulated *kek4* OE, n = 12 NMJs from 8 larvae, Shapiro-Wilk p = 0.0689. Ordinary one-way ANOVA p <0.0001, significant (****), with Tukey's post-hoc multiple comparisons test: Unstimulated control vs Stimulated control p = 0.0061 (**), Unstimulated control vs Unstimulated *kek4* OE p = 0.5232 (ns), Unstimulated control vs Stimulated *kek4* OE p =0.9891 (ns), Stimulated control vs Unstimulated *kek4* OE p <0.0001 (****), Stimulated control vs Stimulated *kek4* OE p = 0.0019 (****), Unstimulated *kek4* OE vs Stimulated *kek4* OE p = 0.721 (ns).

Figure 5.8 - *kek4* OE alters Activity-dependent structural plasticity

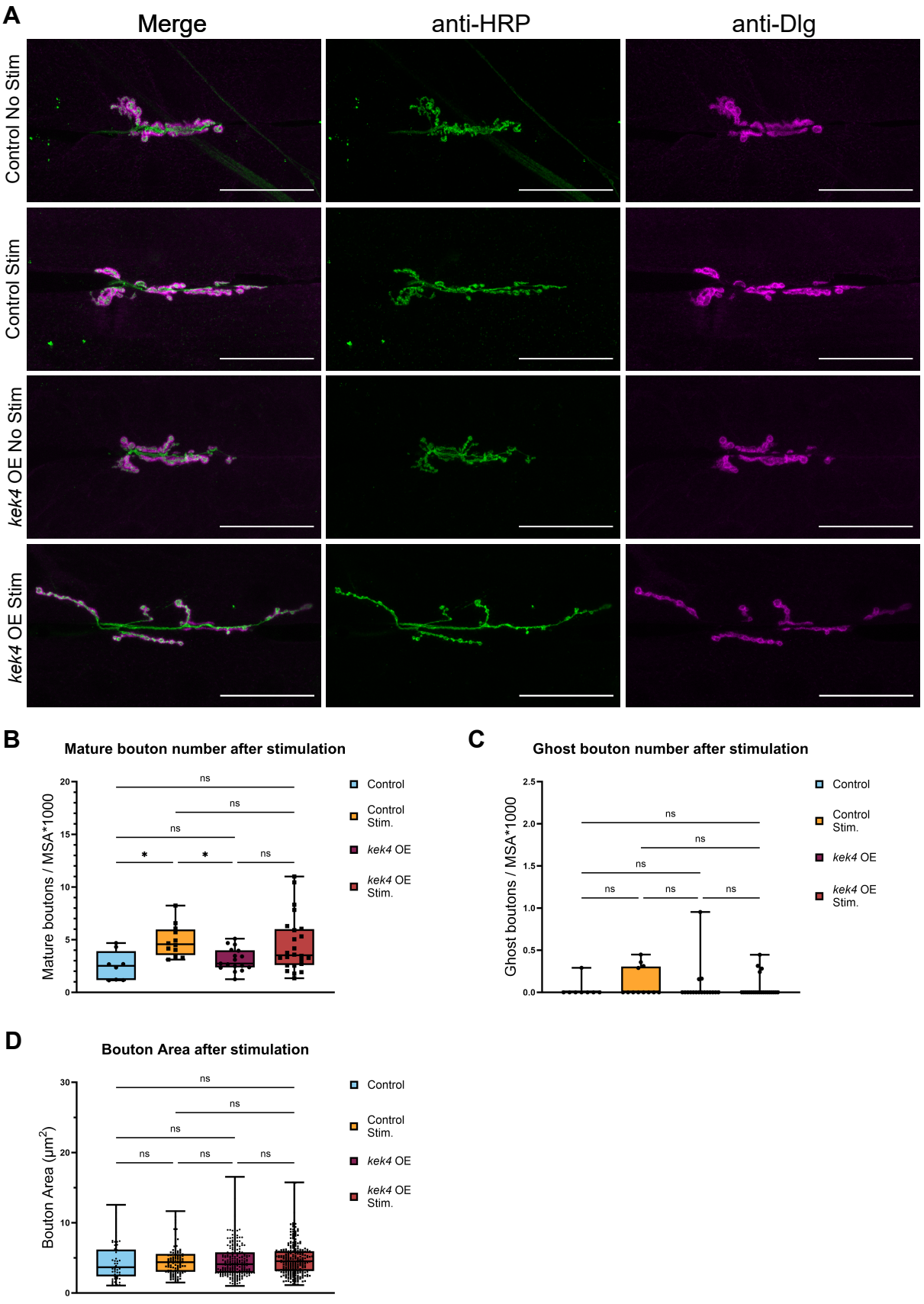


Figure 5.8 – *kek4* OE alters Activity-dependent structural plasticity

kek4 OE altered mature bouton number following optogenetic stimulation in L3 larvae. **A:** Anti-HRP and anti-Dlg stainings of NMJ 6/7 in abdominal segment A3 from L3 larvae. Simulated control (*D42>ReaChR*) and *kek4* OE (*D42>ReaChR, kek4-RFP*) larvae were stimulated via optogenetics and were allowed to recover for 24 hours before dissection. To avoid unwanted stimulation animals were reared in the dark. Unstimulated larvae did not undergo the optogenetics protocol and were reared without ChR co-factor ATR. All Scale bars = 50µm.

B: Box-and-whisker plot of mature bouton number normalised to MSA*1000. Mature bouton number in *kek4* OE larvae did not increase following optogenetic stimulation. Unstimulated control, n = 8 NMJs from 4 larvae, Shapiro-Wilk p = 0.1471. Stimulated control, n = 11 NMJs from 9 larvae, Shapiro-Wilk p = 0.3543. Unstimulated *kek4* OE, n = 16 NMJs from 10 larvae, Shapiro-Wilk p = 0.6503. Stimulated *kek4* OE, n = 24 NMJs from 13 larvae, Shapiro-Wilk p = 0.0088. Kruskal-Wallis p = 0.0056, significant (**), with Dunn's post-hoc multiple comparisons test: Unstimulated control vs Stimulated control p = 0.0145 (*), Unstimulated control vs Unstimulated *kek4* OE p >0.9999 (ns), Unstimulated control vs Stimulated *kek4* OE p =0.1497 (ns), Stimulated control vs Unstimulated *kek4* OE p = 0.0387 (*), Stimulated control vs Stimulated *kek4* OE p >0.9999 (ns), Unstimulated *kek4* OE vs Stimulated *kek4* OE p = 0.4718 (ns).

C: Box-and-whisker plot of the number of ghost boutons per NMJ normalised to postsynaptic target size (MSA*1000). N.B., Plot resembles a bar chart due to the high number of NMJs with 0 ghost boutons. *kek4* OE and optogenetic stimulation had no impact on ghost bouton number. Unstimulated control, n = 8 NMJs from 4 larvae, Shapiro-Wilk p <0.0001. Stimulated control, n = 11 NMJs from 9 larvae, Shapiro-Wilk p = 0.0005. Unstimulated *kek4* OE, n = 16 NMJs from 10 larvae, Shapiro-Wilk p <0.0001. Stimulated *kek4* OE, n = 24 NMJs from 13 larvae, Shapiro-Wilk p <0.0001. Kruskal-Wallis p = 0.5453, not significant (ns).

D: Box-and-whisker plot of the number of HRP+ Ib bouton area (μm^2). *kek4* OE and optogenetic stimulation had no impact on bouton area. Unstimulated control, n = 57 boutons s from 4 larvae, Shapiro-Wilk p = 0.0003. Stimulated control, n = 114 boutons

from 9 larvae, Shapiro-Wilk p <0.0001. Unstimulated *kek4* OE, n = 220 boutons from 10 larvae, Shapiro-Wilk p <0.0001. Stimulated *kek4* OE, n = 253 boutons from 9 larvae, Shaprio-Wilk p <0.0001. Kruskal-Wallis p = 0.2648, not significant (ns).

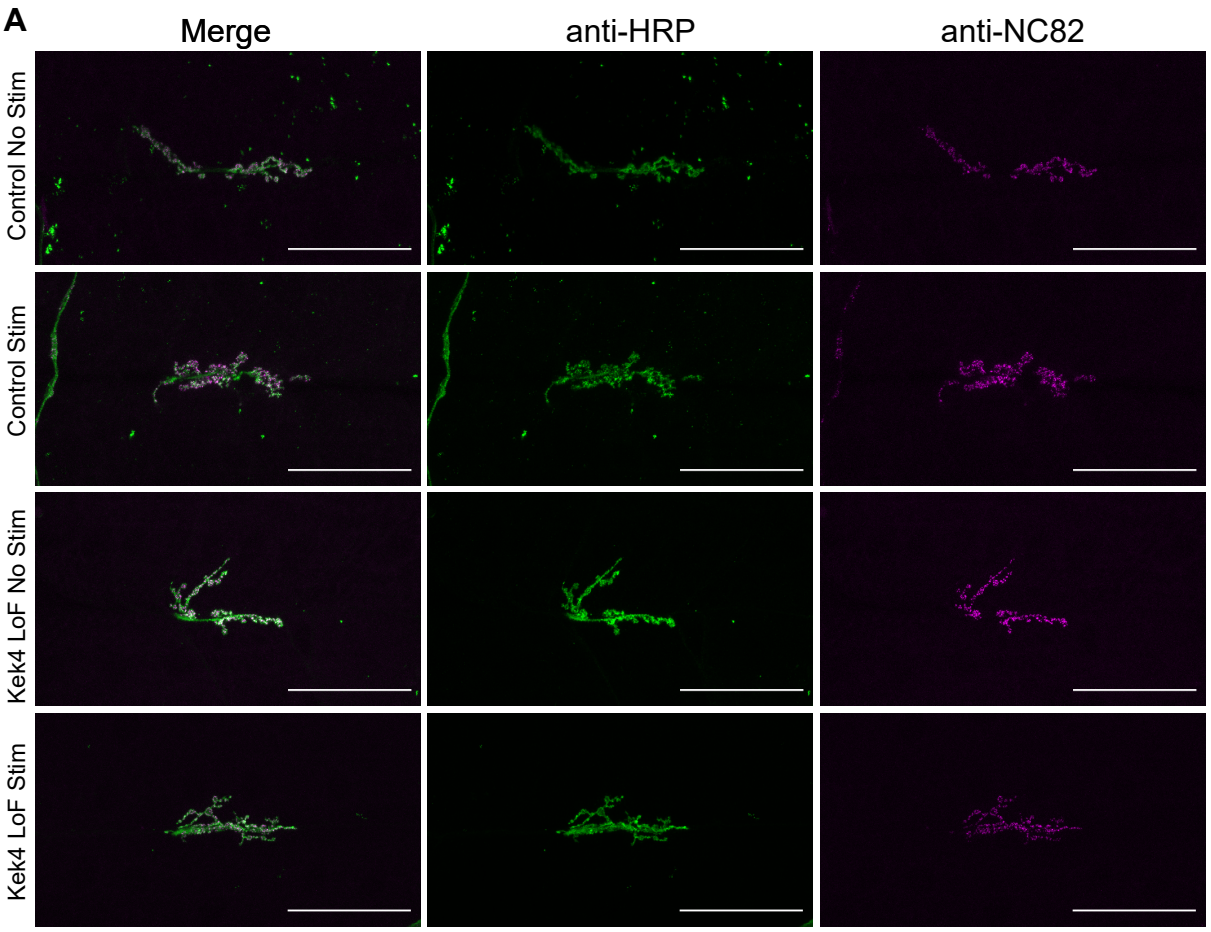
Mature bouton number did not increase in the stimulated *kek4* overexpression larvae compared to equivalent unstimulated condition (Fig. 5.8 B). Additionally, comparing mature bouton number to the control genotype, stimulated *kek4* overexpression larvae was not significantly different to the control without stimulation, suggesting that plasticity was impaired in this genotype. In stimulated *kek4* overexpression larvae there was no effect on the number of ghost boutons or bouton area over the control genotypes (Fig. 5.8 C+D).

NMJ morphology was assessed in unstimulated and stimulated *kek4* LoF (*kek4*^{20}/*kek4*^{23} *; D42>ReaChR*) larvae. Terminal length was unaffected in stimulated *kek4* LoF larvae compared to the control genotypes in either condition or the unstimulated *kek4* LoF larvae (Fig. 5.9 B). In stimulated *kek4* LoF larvae the volume of the presynaptic terminal is not significantly different to the unstimulated *kek4* LoF larvae or the unstimulated control larvae (Fig. 5.9 C). Additionally, terminal volume in stimulated *kek4* LoF is significantly lower than in the stimulated control (Fig. 5.9 C). Taken together this indicates that *kek4* is required for the activity-dependent increase in terminal volume.

In *kek4*^{20}/*kek4*^{23} *; D42>ReaChR* larvae there was no increase in Brp signal following optogenetic stimulation (Fig. 5.9 D+E). These data indicate that *kek4* is required for the activity-dependent increase in AZs.

In stimulated *kek4* LoF larvae the number of mature boutons was not significantly different to unstimulated larvae of the same genotype, nor to stimulated and unstimulated control larvae (Fig. 5.10 B). This indicates that activity-dependent mature bouton formation had been impaired in *kek4* LoF larvae. Ghost bouton formation and

Figure 5.9 - Kek4 is required for NMJ structural plasticity



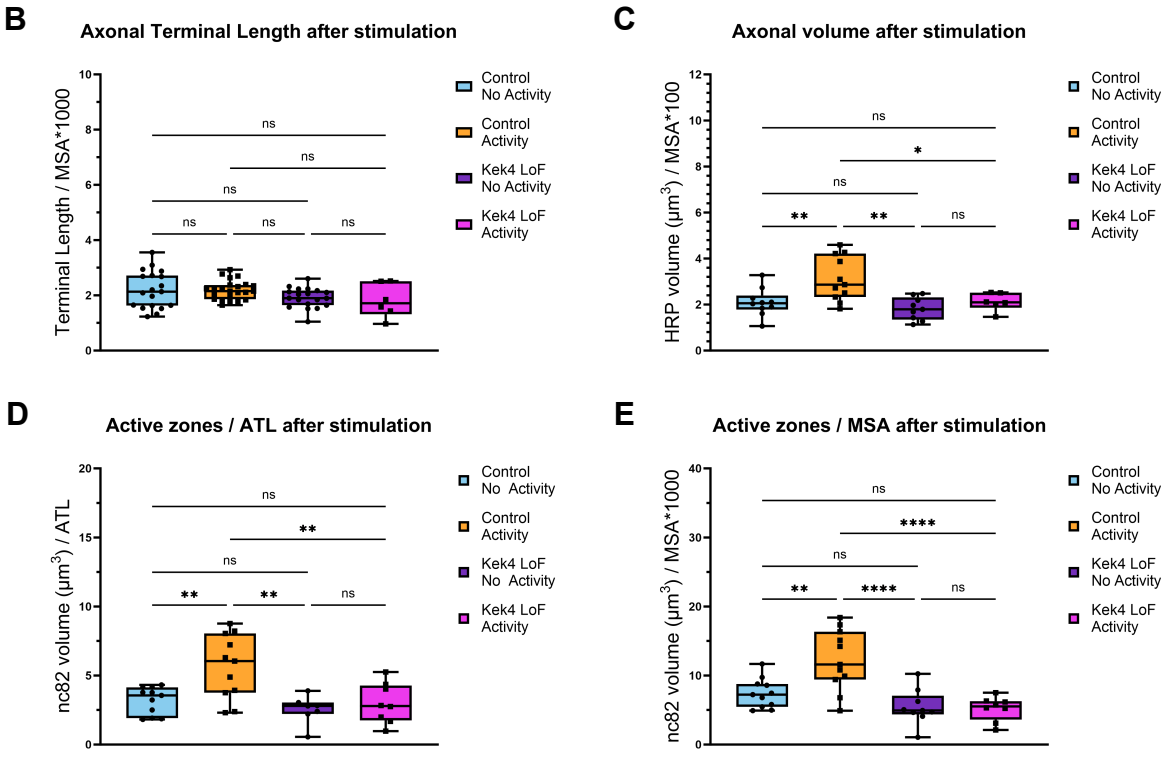


Figure 5.9 – *kek4* is required for NMJ structural plasticity

kek4 LoF is required for NMJ plasticity following optogenetic stimulation. **A:** Anti-HRP and anti-NC82 stainings of NMJ 6/7 in abdominal segment A3 from L3 larvae. Simulated control (*D42>ReaChR*) and *kek4* LoF ($kek4^{20}/kek4^{23}$; *D42>ReaChR*) larvae were stimulated via optogenetics and were allowed to recover for 24 hours before dissection. To avoid unwanted stimulation animals were reared in the dark. Unstimulated larvae did not undergo the optogenetics protocol and were reared without ChR co-factor ATR. All Scale bars = 50µm.

B: Box-and-whisker plot of axonal terminal length (ATL) normalised to MSA*1000. *kek4* LoF and optogenetic stimulation did not impact ATL. Unstimulated control, n = 19 NMJs from 11 larvae, Shapiro-Wilk p = 0.4319. Stimulated control, n = 23 NMJs from 16 larvae, Shapiro-Wilk p = 0.5142. Unstimulated *kek4* LoF, n = 19 NMJs from 11 larvae, Shapiro-Wilk p = 0.8593. Stimulated *kek4* LoF, n = 14 NMJs from 8 larvae, Shapiro-Wilk p = 0.5232. Ordinary one-way ANOVA p = 0.0977, not significant (ns).

C: Box-and-whisker plot of axonal terminal volume normalised to MSA*1000. Axonal terminal volume in Stimulated *kek4* LoF was not different to unstimulated *kek4* LoF larvae. Unstimulated control, n = 11 NMJs from 7 larvae, Shapiro-Wilk p = 0.724. Stimulated control, n = 12 NMJs from 7 larvae, Shapiro-Wilk p = 0.374. Unstimulated *kek4* LoF, n = 9 NMJs from 5 larvae, Shapiro-Wilk p = 0.6471. Stimulated *kek4* LoF, n = 8 NMJs from 4 larvae, Shapiro-Wilk p = 0.3823. Ordinary one-way ANOVA p = 0.0009, significant (*), with Tukey's post-hoc multiple comparisons test: Unstimulated control vs Stimulated control p = 0.0088 (**), Unstimulated control vs Unstimulated *kek4* LoF p = 0.8265 (ns), Unstimulated control vs Stimulated *kek4* LoF p =0.9999 (ns), Stimulated control vs Unstimulated *kek4* LoF p = 0.0011 (**), Stimulated control vs Stimulated *kek4* LoF p = 0.0336 (*), Unstimulated *kek4* LoF vs Stimulated *kek4* LoF p = 0.8488 (ns).

D: Ratio of Brp (anti-NC82) volume to ATL per NMJ. Brp Volume/ATL did not increase after optogenetic stimulation in *kek4* LoF larvae. Unstimulated control, n = 11 NMJs from 7 larvae, Shapiro-Wilk p = 0.0575. Stimulated control, n = 12 NMJs from 7 larvae, Shapiro-Wilk p = 0.4084. Unstimulated *kek4* LoF, n = 9 NMJs from 5 larvae, Shapiro-Wilk p = 0.3793. Stimulated *kek4* LoF, n = 8 NMJs from 4 larvae, Shapiro-Wilk p = 0.8612. Ordinary one-way ANOVA p = 0.0006, significant (***), with Tukey's post-hoc

multiple comparisons test: Unstimulated control vs Stimulated control p = 0.006 (**), Unstimulated control vs Unstimulated *kek4* LoF p = 0.8333 (ns), Unstimulated control vs Stimulated *kek4* LoF p =0.9925 (ns), Stimulated control vs Unstimulated *kek4* LoF p = 0.0019 (**), Stimulated control vs Stimulated *kek4* LoF p = 0.0063 (**), Unstimulated *kek4* LoF vs Stimulated *kek4* LoF p = 0.9486 (ns).

E: Brp volume relative to post-synaptic target area (MSA * 1000). Brp Volume/MSA did not increase after optogenetic stimulation in *kek4* LoF larvae. Unstimulated control, n = 11 NMJs from 7 larvae, Shapiro-Wilk p = 0.5108. Stimulated control, n = 12 NMJs from 7 larvae, Shapiro-Wilk p = 0.798. Unstimulated *kek4* LoF, n = 9 NMJs from 5 larvae, Shapiro-Wilk p = 0.5226. Stimulated *kek4* LoF, n = 8 NMJs from 4 larvae, Shapiro-Wilk p = 0.4137. Ordinary one-way ANOVA p <0.0001, significant (****), with Tukey's post-hoc multiple comparisons test: Unstimulated control vs Stimulated control p = 0.0029 (**), Unstimulated control vs Unstimulated *kek4* LoF p = 0.4713 (ns), Unstimulated control vs Stimulated *kek4* LoF p = 0.3946 (ns), Stimulated control vs Unstimulated *kek4* LoF p <0.0001 (****), Stimulated control vs Stimulated *kek4* LoF p <0.0001 (****), Unstimulated *kek4* LoF vs Stimulated *kek4* LoF p = 0.9981 (ns).

Figure 5.10 - Loss of Kek4 alters bouton plasticity

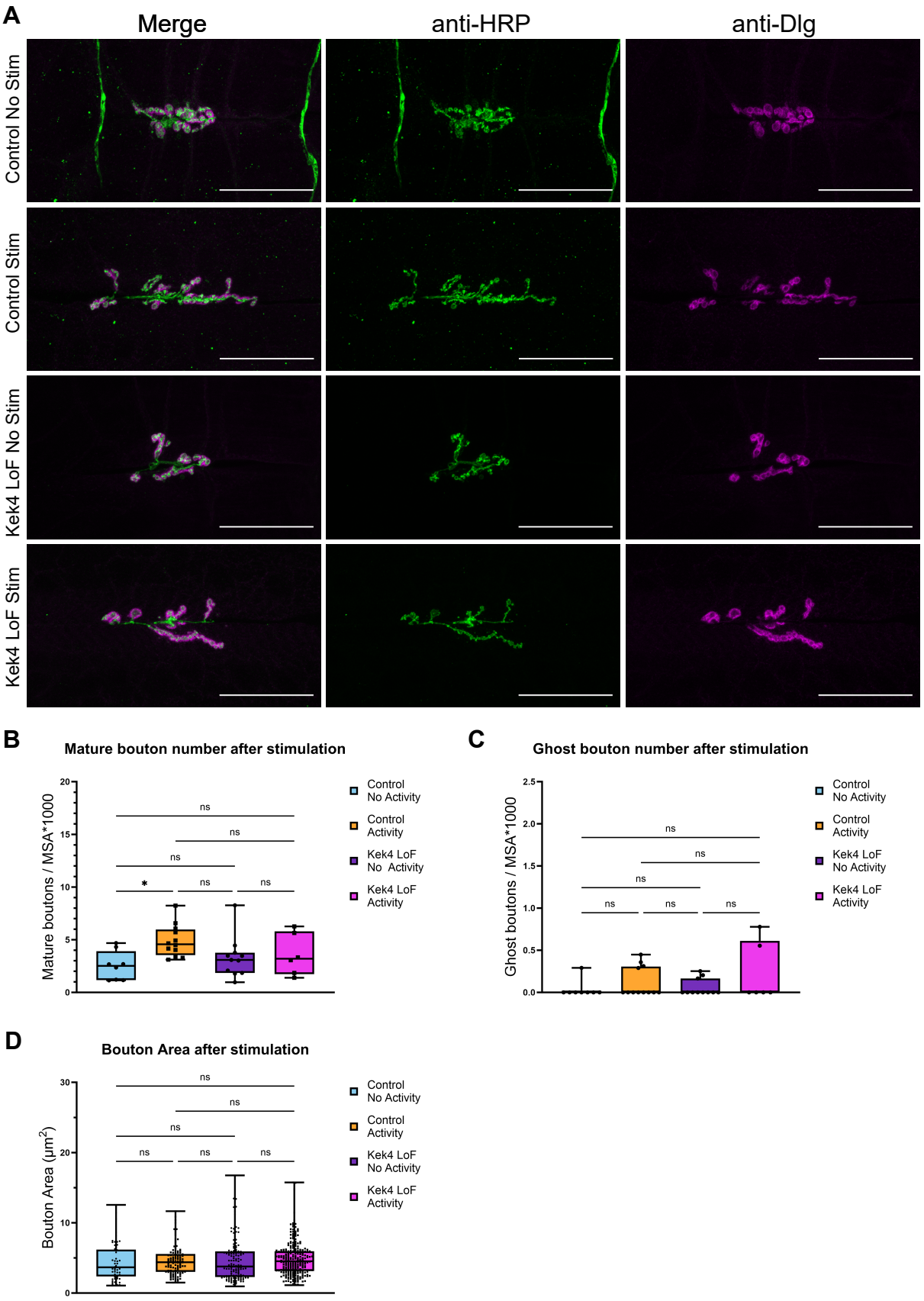


Figure 5.10 – Loss of *kek4* alters bouton plasticity

kek4 LoF is required for the increase in mature bouton number following optogenetic stimulation. **A:** Anti-HRP and anti-Dlg stainings of NMJ 6/7 in abdominal segment A3 from L3 larvae. Simulated control (*D42>ReaChR*) and *kek4* LoF (*kek4*^{20}/*kek4*^{23}; *D42>ReaChR*) larvae were stimulated via optogenetics and were allowed to recover for 24 hours before dissection. To avoid unwanted stimulation animals were reared in the dark. Unstimulated larvae did not undergo the optogenetics protocol and were reared without ChR co-factor ATR. All Scale bars = 50µm.

B: Box-and-whisker plot of mature bouton number normalised to MSA*1000. Mature bouton number in *kek4* LoF larvae did not increase following optogenetic stimulation. Unstimulated control, n = 8 NMJs from 4 larvae, Shapiro-Wilk p = 0.1471. Stimulated control, n = 11 NMJs from 9 larvae, Shapiro-Wilk p = 0.3543. Unstimulated *kek4* LoF, n = 10 NMJs from 6 larvae, Shapiro-Wilk p = 0.0342. Stimulated *kek4* LoF, n = 6 NMJs from 4 larvae, Shapiro-Wilk p = 0.4397. Ordinary one-way ANOVA p = 0.0293, significant (*), with Tukey's post-hoc multiple comparisons test: Unstimulated control vs Stimulated control p = 0.0239 (*), Unstimulated control vs Unstimulated *kek4* LoF p >0.7718 (ns), Unstimulated control vs Stimulated *kek4* LoF p =0.6638 (ns), Stimulated control vs Unstimulated *kek4* LoF p = 0.1357 (ns), Stimulated control vs Stimulated *kek4* LoF p = 0.4384 (ns), Unstimulated *kek4* LoF vs Stimulated *kek4* LoF p = 0.9863 (ns).

C: Box-and-whisker plot of the number of ghost boutons per NMJ normalised to postsynaptic target size (MSA*1000). N.B., Plot resembles a bar chart due to the high number of NMJs with 0 ghost boutons. *kek4* LoF and optogenetic stimulation had no impact on ghost bouton number. Unstimulated control, n = 8 NMJs from 4 larvae, Shapiro-Wilk p <0.0001. Stimulated control, n = 11 NMJs from 9 larvae, Shapiro-Wilk p = 0.0005. Unstimulated *kek4* LoF, n = 10 NMJs from 6 larvae, Shapiro-Wilk p <0.0001. Stimulated *kek4* LoF, n = 6 NMJs from 4 larvae, Shapiro-Wilk p = 0.0058. Kruskal-Wallis p = 0.6084, not significant (ns).

D: Box-and-whisker plot of the number of HRP+ Ib bouton area (µm^2). *kek4* LoF and optogenetic stimulation had no impact on bouton area. Unstimulated control, n = 57 boutons s from 4 larvae, Shapiro-Wilk p = 0.0003. Stimulated control, n = 114 boutons from 9 larvae, Shapiro-Wilk p <0.0001. Unstimulated *kek4* LoF, n = 137 boutons from

6 larvae, Shapiro-Wilk p <0.0001. Stimulated *kek4* LoF, n = 68 boutons from 4 larvae, Shaprio-Wilk p <0.0001. Kruskal-Wallis p = 0.1286, not significant (ns).

bouton size in *kek4*^{20}/*kek4*^{23} *; D42>ReaChR* larvae were not affected by optogenetic stimulation (Fig. 5.10 C+D).

5.6 *kek6* is required for activity-dependent structural plasticity

To investigate the role of *kek6* in activity-dependent structural plasticity the effects of *kek6* misexpression on NMJ morphology was studied in optogenetically unstimulated and stimulated larvae.

Stimulated *kek6* overexpression larvae had significantly greater terminal length than either of the control genotype conditions, however terminal length in stimulated *kek6* overexpression larvae was not significantly different to unstimulated larvae of the same genotype (Fig. 5.11 B). Terminal volume in stimulated *kek6* overexpression larvae was significantly greater than in unstimulated control larvae and is not significantly different to the HRP volume of stimulated control larvae (Fig. 5.11 C). These data indicate that *kek6* overexpression did not impact the activity-dependent increase in terminal volume.

Brp volume in stimulated *kek6* overexpression larvae was not significantly different compared to unstimulated synapses from the same genotype, indicating plasticity had been impaired (Fig. 5.11 D+E). Additionally, the amount of Brp in stimulated *kek6* overexpression larvae was not significantly different to either control condition (Fig. 5.11 D+E).

In optogenetically stimulated *kek6* overexpression larvae the number of mature boutons was not significantly different to those of unstimulated larvae of the same genotype (Fig. 5.12 B). This indicates that the ability of the NMJ to form mature

Figure 5.11 - *kek6* OE alters Activity-dependent structural plasticity

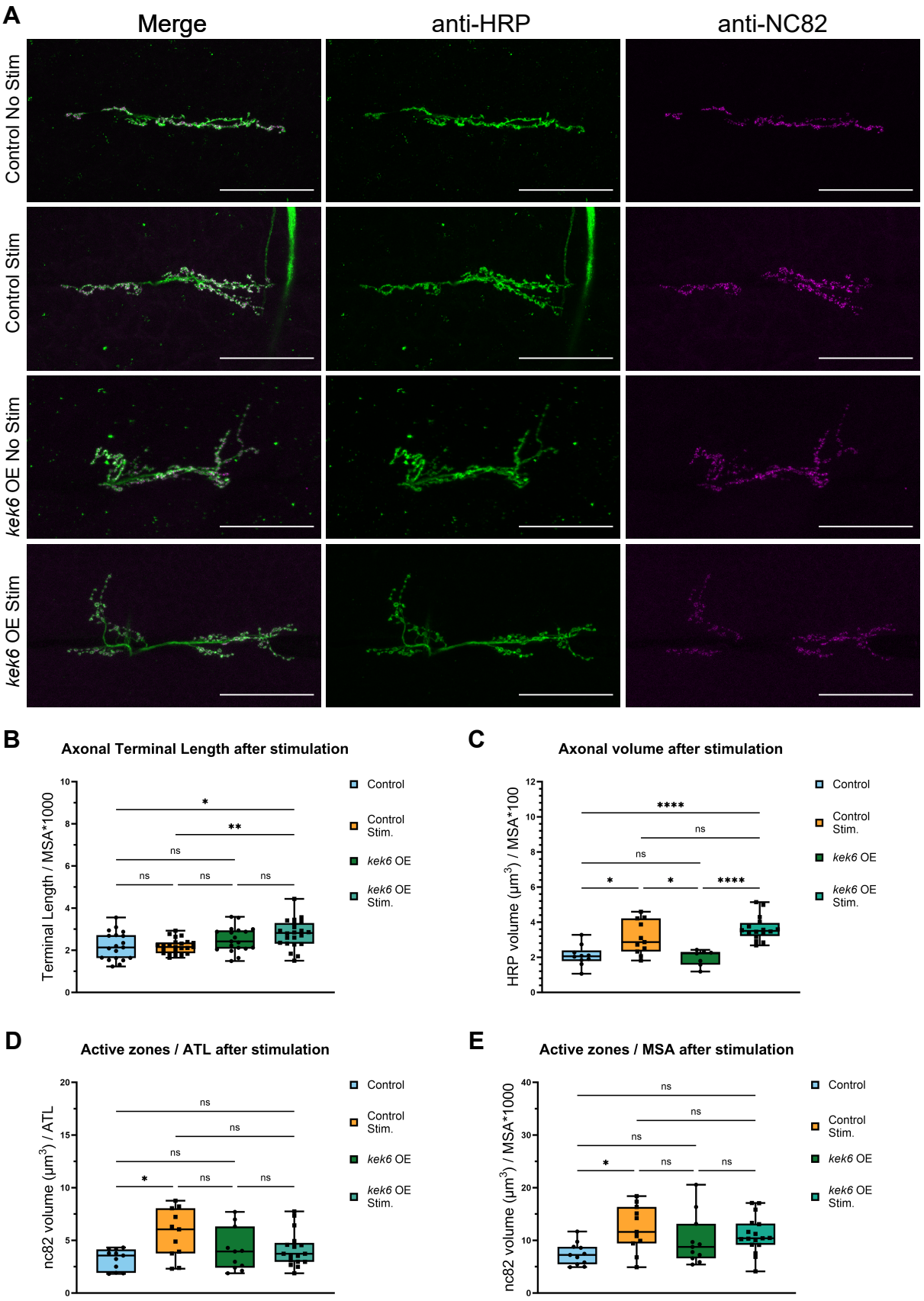


Figure 5.11 – *kek6* OE alters Activity-dependent structural plasticity

kek6 OE alters NMJ plasticity following optogenetic stimulation. **A:** Anti-HRP and anti-NC82 stainings of NMJ 6/7 in abdominal segment A3 from L3 larvae. Simulated control (*D42>ReaChR*) and *kek6* OE (*D42>ReaChR*, *kek6-RFP*) larvae were stimulated via optogenetics and were allowed to recover for 24 hours before dissection. To avoid unwanted stimulation animals were reared in the dark. Unstimulated larvae did not undergo the optogenetics protocol and were reared without ChR co-factor ATR. All Scale bars = 50μm.

B: Box-and-whisker plot of axonal terminal length (ATL) normalised to MSA*1000. Axonal terminal length in stimulated *kek6* OE larvae was significantly greater than that in the control genotype under both conditions and unstimulated *kek6* OE. Unstimulated control, n = 19 NMJs from 11 larvae, Shapiro-Wilk p = 0.4319. Stimulated control, n = 23 NMJs from 16 larvae, Shapiro-Wilk p = 0.5142. Unstimulated *kek6* OE, n = 19 NMJs from 14 larvae, Shapiro-Wilk p = 0.592. Stimulated *kek6* OE, n = 39 NMJs from 23 larvae, Shapiro-Wilk p = 0.8428. Ordinary one-way ANOVA p = 0.0029, significant (**), with Tukey's post-hoc multiple comparisons test: Unstimulated control vs Stimulated control p >0.9999 (ns), Unstimulated control vs Unstimulated *kek6* OE p = 0.3462 (ns), Unstimulated control vs Stimulated *kek6* OE p = 0.01 05 (*), Stimulated control vs Unstimulated *kek6* OE p = 0.2935 (ns), Stimulated control vs Stimulated *kek6* OE p = 0.006 (**), Unstimulated *kek6* OE vs Stimulated *kek6* OE p = 0.4611 (ns).

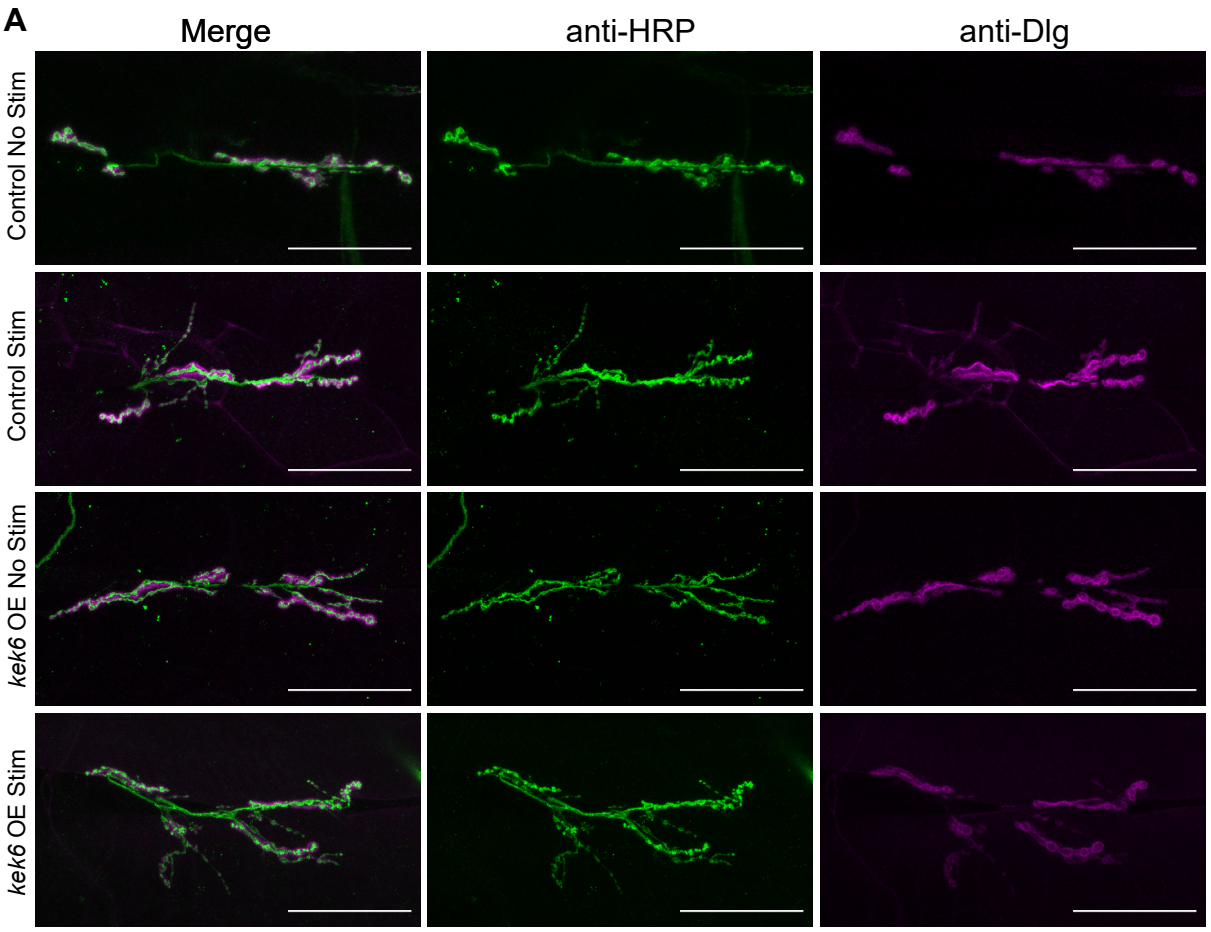
C: Box-and-whisker plot of axonal terminal volume normalised to MSA*1000. Axonal terminal volume in Stimulated *kek6* OE was greater than in unstimulated *kek6* OE larvae. Unstimulated control, n = 11 NMJs from 7 larvae, Shapiro-Wilk p = 0.724. Stimulated control, n = 12 NMJs from 7 larvae, Shapiro-Wilk p = 0.374. Unstimulated *kek6* OE, n = 11 NMJs from 7 larvae, Shapiro-Wilk p = 0.2492. Stimulated *kek6* OE, n = 17 NMJs from 9 larvae, Shapiro-Wilk p = 0.0927. Ordinary one-way ANOVA p <0.0001, significant (****), with Tukey's post-hoc multiple comparisons test: Unstimulated control vs Stimulated control p = 0.0118 (*), Unstimulated control vs Unstimulated *kek6* OE p = 0.9854 (ns), Unstimulated control vs Stimulated *kek6* OE p <0.0001 (****), Stimulated control vs Unstimulated *kek6* OE p = 0.0106 (*), Stimulated

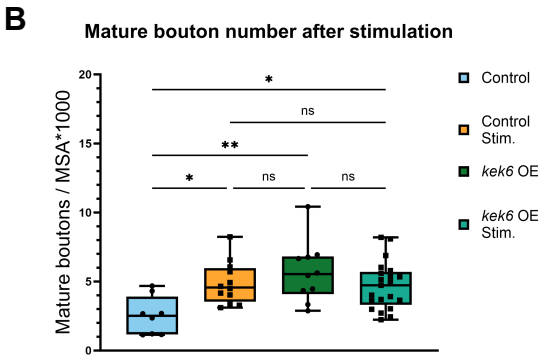
control vs Stimulated *kek6* OE p = 0.2857 (ns), Unstimulated *kek6* OE vs Stimulated *kek6* OE p <0.0001 (****).

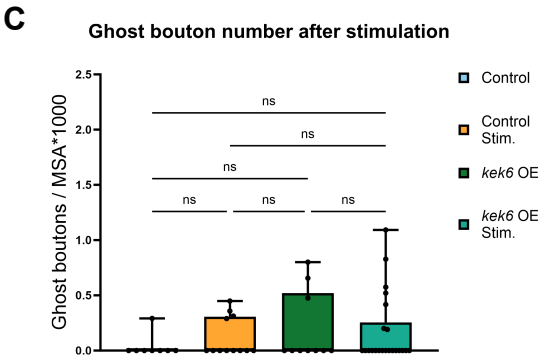
D: Ratio of Brp (anti-NC82) volume to ATL per NMJ. Brp Volume/ATL did not increase after optogenetic stimulation in *kek6* OE larvae. Unstimulated control, n = 11 NMJs from 7 larvae, Shapiro-Wilk p = 0.0575. Stimulated control, n = 12 NMJs from 7 larvae, Shapiro-Wilk p = 0.4084. Unstimulated *kek6* OE, n = 11 NMJs from 7 larvae, Shapiro-Wilk p = 0.131. Stimulated *kek6* OE, n = 17 NMJs from 9 larvae, Shapiro-Wilk p = 0.0673. Ordinary one-way ANOVA p 0.0366, with Tukey's post-hoc multiple comparisons test: Unstimulated control vs Stimulated control p = 0.0235 (*), Unstimulated control vs Unstimulated *kek6* OE p = 0.7307 (ns), Unstimulated control vs Stimulated *kek6* OE p = 0.6357 (ns), Stimulated control vs Unstimulated *kek6* OE p = 0.6357 (ns), Stimulated control vs Stimulated *kek6* OE p = 0.1735 (ns), Unstimulated *kek6* OE vs Stimulated *kek6* OE p >0.9999 (ns).

E: Brp volume relative to post-synaptic target area (MSA * 1000). Brp Volume/MSA did not increase after optogenetic stimulation in *kek6* OE larvae. Unstimulated control, n = 11 NMJs from 7 larvae, Shapiro-Wilk p = 0.5108. Stimulated control, n = 12 NMJs from 7 larvae, Shapiro-Wilk p = 0.798. Unstimulated *kek6* OE, n = 11 NMJs from 7 larvae, Shapiro-Wilk p = 0.9454. Stimulated *kek6* OE, n = 17 NMJs from 9 larvae, Shapiro-Wilk p = 0.4984. Ordinary one-way ANOVA p = 0.0266, significant (*), with Tukey's post-hoc multiple comparisons test: Unstimulated control vs Stimulated control p = 0.0212 (*), Unstimulated control vs Unstimulated *kek6* OE p = 0.3635 (ns), Unstimulated control vs Stimulated *kek6* OE p =0.0767 (ns), Stimulated control vs Unstimulated *kek6* OE p = 0.5277 (ns), Stimulated control vs Stimulated *kek6* OE p = 0.836 (ns), Unstimulated *kek6* OE vs Stimulated *kek6* OE p = 0.9096 (ns).

Figure 5.12 - *kek6* OE alters Activity-dependent bouton plasticity







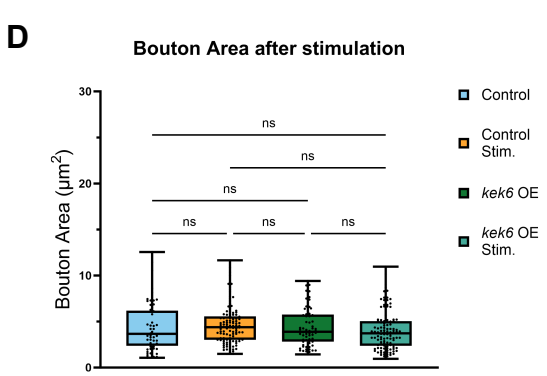


Figure 5.12 – *kek6* OE alters Activity-dependent bouton plasticity

kek6 OE altered mature bouton number following optogenetic stimulation in L3 larvae. **A:** Anti-HRP and anti-Dlg stainings of NMJ 6/7 in abdominal segment A3 from L3 larvae. Simulated control (*D42>ReaChR*) and *kek6* OE (*D42>ReaChR*, *kek6-RFP*) larvae were stimulated via optogenetics and were allowed to recover for 24 hours before dissection. To avoid unwanted stimulation animals were reared in the dark. Unstimulated larvae did not undergo the optogenetics protocol and were reared without ChR co-factor ATR. All Scale bars = 50µm.

B: Box-and-whisker plot of mature bouton number normalised to MSA*1000. Mature bouton number in *kek6* OE larvae did not increase following optogenetic stimulation, but was greater than the unstimulated control. Unstimulated control, n = 8 NMJs from 4 larvae, Shapiro-Wilk p = 0.1471. Stimulated control, n = 11 NMJs from 9 larvae, Shapiro-Wilk p = 0.3543. Unstimulated *kek6* OE, n = 8 NMJs from 7 larvae, Shapiro-Wilk p = 0.4319. Stimulated *kek6* OE, n = 22 NMJs from 14 larvae, Shapiro-Wilk p = 0.3088. Kruskal-Wallis p = 0.0055, significant (**), with Dunn's post-hoc multiple comparisons test: Unstimulated control vs Stimulated control p = 0.0289 (*), Unstimulated control vs Unstimulated *kek6* OE p 0.0044 (**), Unstimulated control vs Stimulated *kek6* OE p =0.0375 (*), Stimulated control vs Unstimulated *kek6* OE p >0.9999 (ns), Stimulated control vs Stimulated *kek6* OE p >0.9999 (ns), Unstimulated *kek6* OE vs Stimulated *kek6* OE p >0.9999 (ns).

C: Box-and-whisker plot of the number of ghost boutons per NMJ normalised to postsynaptic target size (MSA*1000). N.B., Plot resembles a bar chart due to the high number of NMJs with 0 ghost boutons. *kek6* OE and optogenetic stimulation had no impact on ghost bouton number. Unstimulated control, n = 8 NMJs from 4 larvae, Shapiro-Wilk p <0.0001. Stimulated control, n = 11 NMJs from 9 larvae, Shapiro-Wilk p = 0.0005. Unstimulated *kek6* OE, n = 8 NMJs from 7 larvae, Shapiro-Wilk p = 0.0002. Stimulated *kek6* OE, n = 22 NMJs from 14 larvae, Shapiro-Wilk p <0.0001. Kruskal-Wallis p = 0.6849, not significant (ns).

D: Box-and-whisker plot of the number of HRP+ Ib bouton area (μm^2). *kek6* OE and optogenetic stimulation had no impact on bouton area. Unstimulated control, n = 57

boutons s from 4 larvae, Shapiro-Wilk p = 0.0003. Stimulated control, n = 114 boutons from 9 larvae, Shapiro-Wilk p <0.0001. Unstimulated *kek6* OE, n = 68 boutons from 7 larvae, Shapiro-Wilk p 0.0015. Stimulated *kek6* OE, n = 114 boutons from 14 larvae, Shaprio-Wilk p <0.0001. Kruskal-Wallis p = 0.1046, not significant (ns).

boutons following activity is lost when *kek6* is overexpressed. Interestingly however, the number of mature boutons in stimulated unstimulated *kek6* overexpression larvae were significantly greater than the unstimulated control and were not significantly different to the stimulated control (Fig. 5.12 B). In stimulated *D42>kek6-RFP, ReaChR* larvae the mean number of ghost boutons and bouton size did not change compared to the controls and unstimulated larvae of the same genotype (Fig. 5.12 C+D).

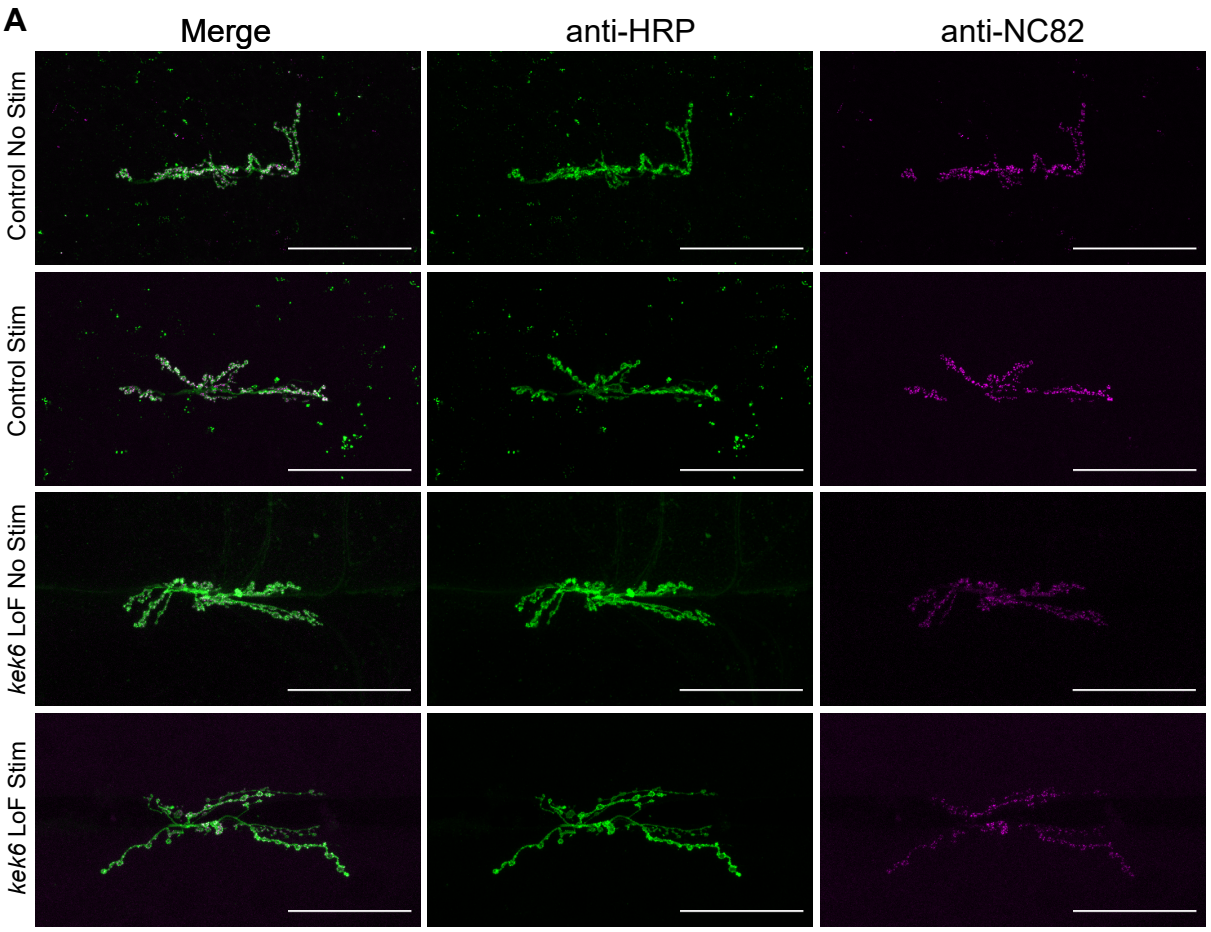
To further investigate the role of *kek6* at the NMJ following activity NMJ morphology in stimulated and unstimulated *kek6*^{35}/*kek6*^{34}*, D42>ReaChR* larvae was examined.

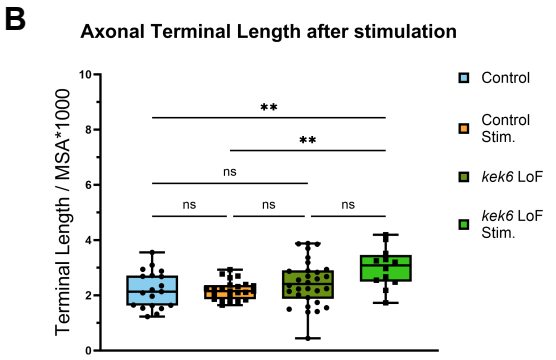
Similarly to *kek6* overexpression, stimulated *kek6* LoF larvae have significantly greater terminal length than either stimulated or unstimulated control larvae, however terminal length is not significantly different to that in unstimulated larvae of the same genotype (Fig. 5.13 B). Interestingly, terminal volume did not increase in *kek6* overexpression larvae following optogenetic stimulation, indicating that *kek6* is required for the activity-dependent outgrowth of the axonal terminal (Fig. 5.13 C).

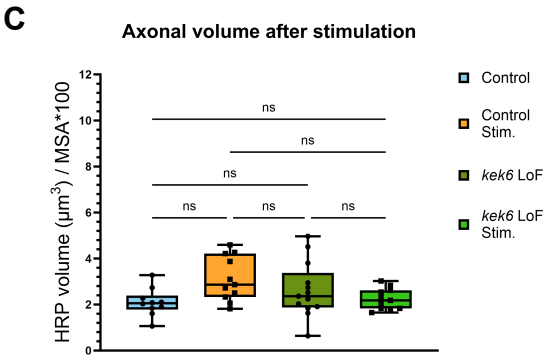
In stimulated *kek6*^{35}/*kek6*^{34}, *D42>ReaChR* larvae there was no significant increase in Brp levels compared to unstimulated larvae of the same genotype (Fig. 5.13 D+E). Additionally, there was significantly less Brp in stimulated *kek6* LoF NMJs than in those of stimulated control larvae (Fig. 5.13 D+E). These data indicate that *kek6* is required for the increase in Brp at the NMJ following activity.

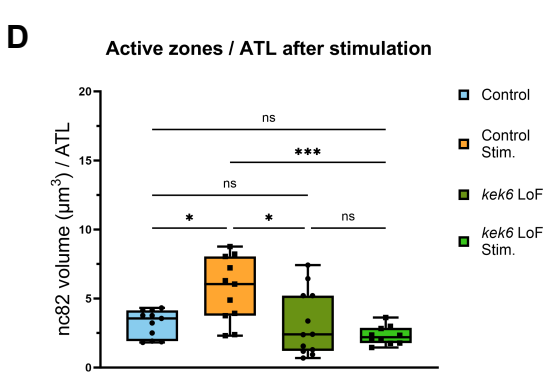
The mean number of mature boutons in stimulated *kek6* LoF larvae was not significantly different than in unstimulated larvae of the same genotype nor stimulated control larvae, and was significantly greater than in unstimulated control larvae (Fig. 5.14 B). Bouton area and the mean number of ghost boutons was unaffected by

Figure 5.13 - *kek6* is required for NMJ structural plasticity









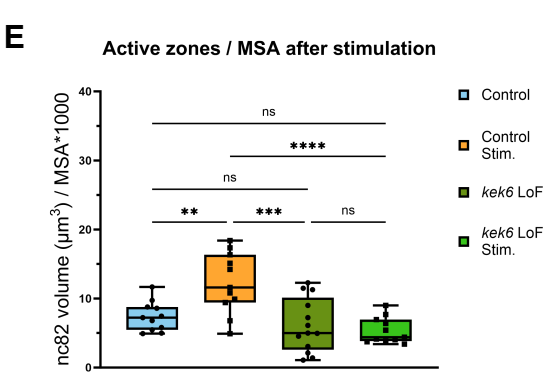


Figure 5.13 - *kek6* is required for NMJ structural plasticity

kek6 LoF is required for NMJ plasticity following optogenetic stimulation. **A:** Anti-HRP and anti-NC82 stainings of NMJ 6/7 in abdominal segment A3 from L3 larvae. Simulated control (*D42>ReaChR*) and *kek6* LoF ($kek6^{34}/kek6^{35}$; *D42>ReaChR*) larvae were stimulated via optogenetics and were allowed to recover for 24 hours before dissection. To avoid unwanted stimulation animals were reared in the dark. Unstimulated larvae did not undergo the optogenetics protocol and were reared without ChR co-factor ATR. All Scale bars = 50µm.

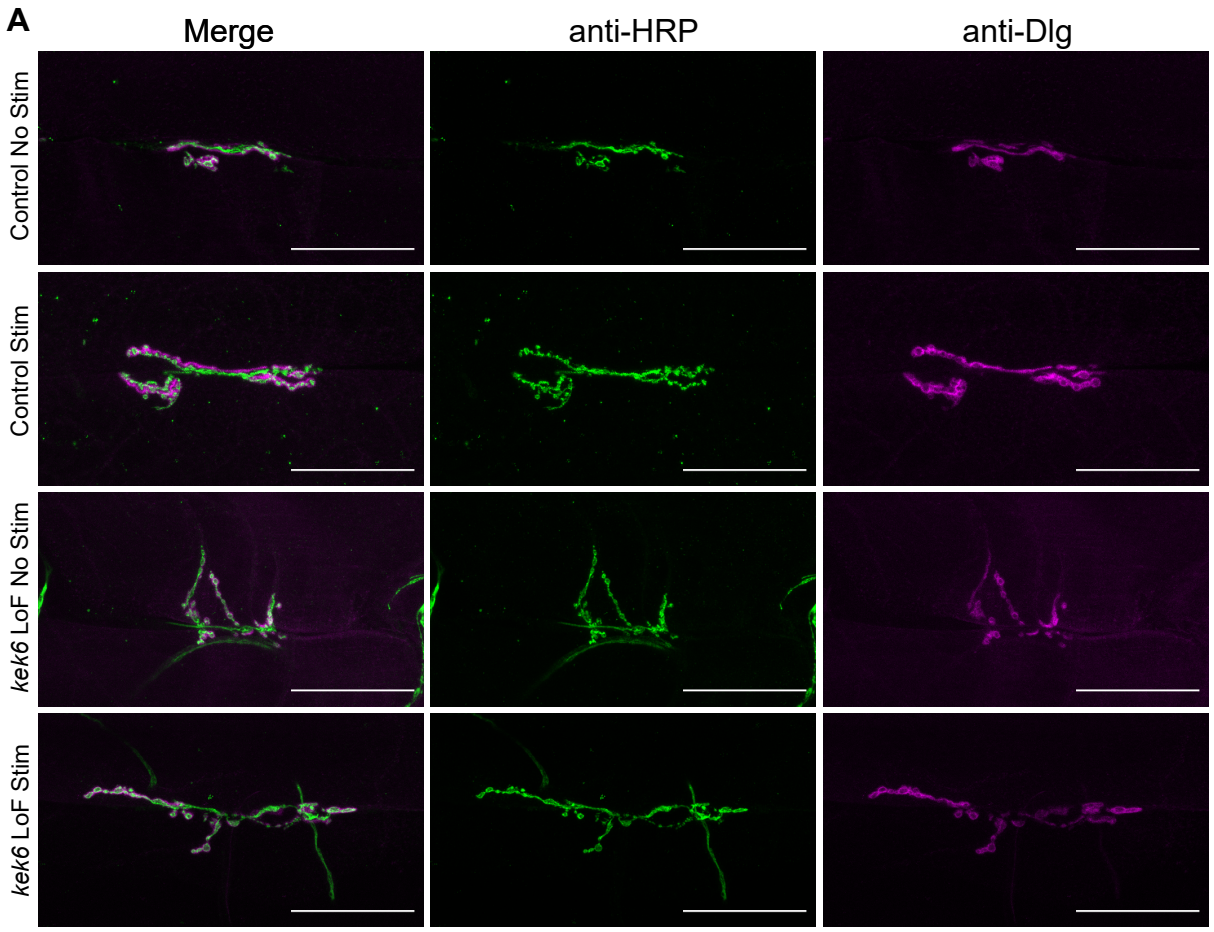
B: Box-and-whisker plot of axonal terminal length (ATL) normalised to MSA*1000. *kek6* LoF and optogenetic stimulation did not impact ATL. Unstimulated control, n = 19 NMJs from 11 larvae, Shapiro-Wilk p = 0.4319. Stimulated control, n = 23 NMJs from 16 larvae, Shapiro-Wilk p = 0.5142. Unstimulated *kek6* LoF, n = 30 NMJs from 21 larvae, Shapiro-Wilk p = 0.5978. Stimulated *kek6* LoF, n = 23 NMJs from 13 larvae, Shapiro-Wilk p = 0.9857. Ordinary one-way ANOVA p = 0.0055, significant (**), with Tukey's post-hoc comparison test: Unstimulated control vs Stimulated control p >0.9999 (ns), Unstimulated control vs Unstimulated *kek6* LoF p = 0.6061 (ns), Unstimulated control vs Stimulated *kek6* LoF p = 0.0092 (**), Stimulated control vs Unstimulated *kek6* LoF p = 0.5454 (ns), Stimulated control vs Stimulated *kek6* LoF p = 0.0062 (**), Unstimulated *kek6* LoF vs Stimulated *kek6* LoF p = 0.0782 (ns).

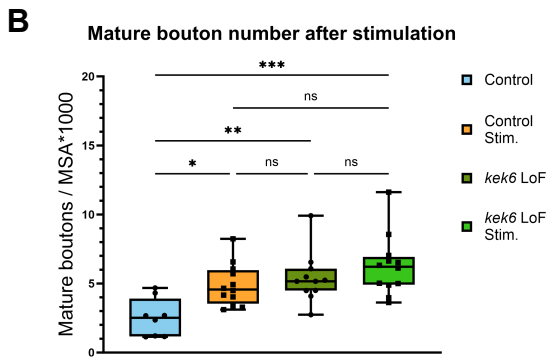
C: Box-and-whisker plot of axonal terminal volume normalised to MSA*1000. Axonal terminal volume in Stimulated *kek6* LoF was not different to unstimulated *kek6* LoF larvae. Unstimulated control, n = 11 NMJs from 7 larvae, Shapiro-Wilk p = 0.724. Stimulated control, n = 12 NMJs from 7 larvae, Shapiro-Wilk p = 0.374. Unstimulated *kek6* LoF, n = 12 NMJs from 9 larvae, Shapiro-Wilk p = 0.4552. Stimulated *kek6* LoF, n = 11 NMJs from 6 larvae, Shapiro-Wilk p = 0.502. Ordinary one-way ANOVA p = 0.0449, significant (*), with Tukey's post-hoc multiple comparisons test: Unstimulated control vs Stimulated control p = 0.0502 (ns), Unstimulated control vs Unstimulated *kek6* LoF p = 0.4825 (ns), Unstimulated control vs Stimulated *kek6* LoF p = 0.9804 (ns), Stimulated control vs Unstimulated *kek6* LoF p = 0.5213 (ns), Stimulated control vs Stimulated *kek6* LoF p = 0.1038 (ns), Unstimulated *kek6* LoF vs Stimulated *kek6* LoF p = 0.7108 (ns).

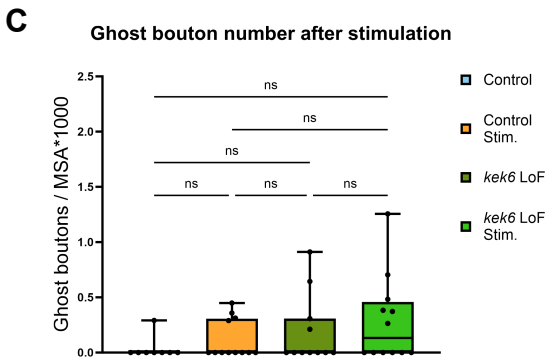
D: Ratio of Brp (anti-NC82) volume to ATL per NMJ. Brp Volume/ATL did not increase after optogenetic stimulation in *kek6* LoF larvae. Unstimulated control, n = 11 NMJs from 7 larvae, Shapiro-Wilk p = 0.0575. Stimulated control, n = 12 NMJs from 7 larvae, Shapiro-Wilk p = 0.4084. Unstimulated *kek6* LoF, n = 12 NMJs from 9 larvae, Shapiro-Wilk p = 0.0958. Stimulated *kek6* LoF, n = 11 NMJs from 6 larvae, Shapiro-Wilk p = 0.6235. Ordinary one-way ANOVA p = 0.001, significant (***), with Tukey's post-hoc multiple comparisons test: Unstimulated control vs Stimulated control p = 0.0229 (*), Unstimulated control vs Unstimulated *kek6* LoF p = 0.9982 (ns), Unstimulated control vs Stimulated *kek6* LoF p = 0.6048 (ns), Stimulated control vs Unstimulated *kek6* LoF p = 0.0125 (*), Stimulated control vs Stimulated *kek6* LoF p = 0.0009 (***), Unstimulated *kek6* LoF vs Stimulated *kek6* LoF p = 0.6906 (ns).

E: Brp volume relative to post-synaptic target area (MSA * 1000). Brp Volume/MSA did not increase after optogenetic stimulation in *kek6* LoF larvae. Unstimulated control, n = 11 NMJs from 7 larvae, Shapiro-Wilk p = 0.5108. Stimulated control, n = 12 NMJs from 7 larvae, Shapiro-Wilk p = 0.798. Unstimulated *kek6* LoF, n = 12 NMJs from 9 larvae, Shapiro-Wilk p = 0.2844. Stimulated *kek6* LoF, n = 11 NMJs from 6 larvae, Shapiro-Wilk p = 0.1106. Ordinary one-way ANOVA p <0.0001, significant (****), with Tukey's post-hoc multiple comparisons test: Unstimulated control vs Stimulated control p = 0.0066 (**), Unstimulated control vs Unstimulated *kek6* LoF p = 0.7766 (ns), Unstimulated control vs Stimulated *kek6* LoF p = 0.4741 (ns), Stimulated control vs Unstimulated *kek6* LoF p = 0.0003 (***), Stimulated control vs Stimulated *kek6* LoF p <0.0001 (****), Unstimulated *kek6* LoF vs Stimulated *kek6* LoF p = 0.9943 (ns).

Figure 5.14 - Loss of *kek6* alters Activity-dependent bouton plasticity







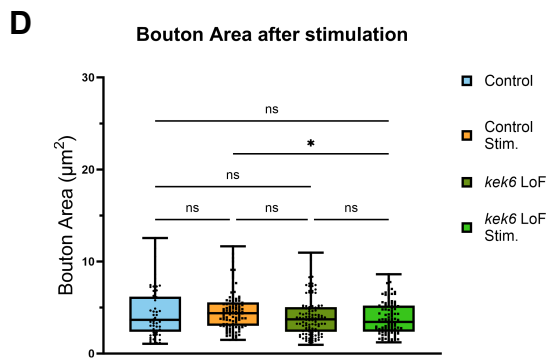


Figure 5.14 – Loss of *kek6* alters Activity-dependent bouton plasticity

kek6 LoF is required for the increase in mature bouton number following optogenetic stimulation. **A:** Anti-HRP and anti-Dlg stainings of NMJ 6/7 in abdominal segment A3 from L3 larvae. Simulated control (*D42>ReaChR*) and *kek6* LoF (*kek6*^{34}/*kek6*^{35}; *D42>ReaChR*) larvae were stimulated via optogenetics and were allowed to recover for 24 hours before dissection. To avoid unwanted stimulation animals were reared in the dark. Unstimulated larvae did not undergo the optogenetics protocol and were reared without ChR co-factor ATR. All Scale bars = 50µm.

B: Box-and-whisker plot of mature bouton number normalised to MSA*1000. Mature bouton number in *kek6* LoF larvae did not increase following optogenetic stimulation, but was greater than in unstimulated control larvae. Unstimulated control, n = 8 NMJs from 4 larvae, Shapiro-Wilk p = 0.1471. Stimulated control, n = 11 NMJs from 9 larvae, Shapiro-Wilk p = 0.3543. Unstimulated *kek6* LoF, n = 8 NMJs from 4 larvae, Shapiro-Wilk p = 0.1471. Stimulated *kek6* LoF, n = 7 NMJs from 12 larvae, Shapiro-Wilk p = 0.122. Ordinary one-way ANOVA p = 0.0005, significant (***), with Tukey's post-hoc multiple comparisons test: Unstimulated control vs Stimulated control p = 0.03 (*), Unstimulated control vs Unstimulated *kek6* LoF p = 0.0068 (**), Unstimulated control vs Stimulated *kek6* LoF p = 0.0002 (***), Stimulated control vs Unstimulated *kek6* LoF p = 0.8989 (ns), Stimulated control vs Stimulated *kek6* LoF p = 0.238 (ns), Unstimulated *kek6* LoF vs Stimulated *kek6* LoF p = 0.6426 (ns).

C: Box-and-whisker plot of the number of ghost boutons per NMJ normalised to postsynaptic target size (MSA*1000). N.B., Plot resembles a bar chart due to the high number of NMJs with 0 ghost boutons. *kek6* LoF and optogenetic stimulation had no impact on ghost bouton number. Unstimulated control, n = 8 NMJs from 4 larvae, Shapiro-Wilk p <0.0001. Stimulated control, n = 11 NMJs from 9 larvae, Shapiro-Wilk p = 0.0005. Unstimulated *kek6* LoF, n = 18 NMJs from 5 larvae, Shapiro-Wilk p <0.0001. Stimulated *kek6* LoF, n = 12 NMJs from 7 larvae, Shapiro-Wilk p = 0.0055. Kruskal-Wallis p = 0.2824, not significant (ns).

D: Box-and-whisker plot of the number of HRP+ Ib bouton area (µm^2). *kek6* LoF and optogenetic stimulation had no impact on bouton area. Unstimulated control, n = 57

boutons s from 4 larvae, Shapiro-Wilk p = 0.0003. Stimulated control, n = 114 boutons from 9 larvae, Shapiro-Wilk p <0.0001. Unstimulated *kek6* LoF, n = 88 boutons from 5 larvae, Shapiro-Wilk p <0.0001. Stimulated *kek6* LoF, n = 102 boutons from 7 larvae, Shaprio-Wilk p = 0.0003. Kruskal-Wallis p = 0.0202, significant (*), with Dunn's post-hoc multiple comparisons test: Unstimulated control vs Stimulated control p = 0.7844 (ns), Unstimulated control vs Unstimulated *kek6* LoF p >0.9999 (ns), Unstimulated control vs Stimulated *kek6* LoF p > 0.9999 (ns), Stimulated control vs Unstimulated *kek6* LoF p = 0.0854 (ns), Stimulated control vs Stimulated *kek6* LoF p = 0.228 (*), Unstimulated *kek6* LoF vs Stimulated *kek6* LoF p >0.9999 (ns). The value for Stimulated *kek6* LoF was significantly lower than that for Stimulated control larvae, however this is unlikely to be biologically relevant as neither were significantly different to the unstimulated control

stimulation. These data indicate that *kek6* is not required for mature bouton formation (Fig. 5.14 C+D).

5.7 Discussion

In this chapter I have investigated the role of *kek4* and 6 in synaptic morphology and synaptogenesis at larval NMJ 6/7 via quantifying different aspects of NMJ morphology in overexpression and loss of function genotypes, and with optogenetic stimulation, their roles in activity-dependent structural plasticity. I found that in the absence of optogenetic stimulation, *kek4* had no effect on the NMJ morphology features measured here, whereas both overexpression and loss-of-function of kek6 led to greater mature bouton numbers.

Furthermore, I established an optogenetic stimulation protocol to induce stable synaptic plasticity at NMJ 6/7, and then used this protocol to find that *kek4* overexpression could suppress activity-dependent increases to terminal volume, active zones and mature bouton number, and that *kek4* was also required for the activity-dependent growth of these features. It was also found that *kek6* overexpression did not alter bouton number, terminal volume or active zones following stimulation, but was required for the activity-dependent increases to terminal volume and active zone abundance.

The data presented in this chapter indicate that *kek4* and 6 regulate NMJ morphology and activity-dependent structural plasticity and are necessary for such plasticity to occur following activity. These findings and previous findings from this work are summarised and discussed in the context of the literature in the following chapter.

6 DISCUSSION

6.1 Summary of findings

The overarching aim of this thesis was to investigate the potential role of Kek receptors in activity-dependent structural synaptic plasticity, and to characterize the functional diversity of the *keks*. It was critical to know if *keks* are functionally diverse or are functionally redundant as this could provide insight into the role of conserved kinase-less Trk-like receptors in the nervous systems of both insects and humans.

To this end I pursued three objectives: to investigate the spatial distribution of *keks* in the nervous system (Chapter 3), to investigate the function of *keks* in Ca^{2+} dynamics (Chapter 4), and to investigate the function of *keks* in activity-dependent structural plasticity at the larval NMJ (Chapter 5).

All of the *keks* are expressed in the larval CNS, but *kek1* and *-5* are expressed in the periphery, with *kek5* being expressed in the PNS (Fig. 3.1, 3.2 and 3.8). Furthermore, Kek2 appeared to preferentially localise to dendrites, while Kek3 and -4 localised throughout the neuron, and Kek5 and -6 showing a preference for axonal terminals (Fig. 3.9 - 3.15).

All of the *keks* can modulate Ca^{2+} signalling in some way, with *kek1*, *-2*, *-3*, *-5* and *-6* altering the abundance of CaMKII and *kek1*, *-2*, *-3*, *-4* and *-6* altering Ca^{2+} dynamics following neuronal activity in presynaptic terminals (Chapter 4, Ulian-Benitez, 2018). This may occur due to an interaction with the VGCC Cacophony, as suggested by Kek6-TSTEP colocalization with Cac-sfGFP (Fig. 4.9), and supported by the observation of *kek4* and 6 overexpression leading to the clustering of Cac channels (Fig. 4.10).

Finally, *kek4* and *kek6* were found to be required for activity-dependent structural plasticity at the model synapse NMJ 6/7, and presented activity-dependent phenotypes on NMJ morphology when overexpressed (Chapter 5).

A summary of my data and previously reported findings can be found in Table 6.1. In the following sections I interpret the observations made in this work about each gene within the context of previous and recent findings of others in the field.

6.2 *kek1*

RT-PCR data showed that *kek1* is expressed in the CNS and the periphery in larvae (Fig. 3.1 and 3.2). This is consistent with previous findings showing *kek1* expression in the embryonic CNS and PNS (Musacchio et al., 1996, Bishop 2014, Ulian-Benitez et al., 2017). However, it is important to note that the resolution this experiment offers is not sufficient to distinguish expression in the muscle from expression in the PNS, or indeed elsewhere in the body wall. As *kek1* was previously found to be expressed in the embryonic PNS (Bishop 2014), these data indicate that *kek1* expression may continue in the PNS to third instar.

Kek1 has been previously reported to interact with the *Drosophila* EGF Receptor and inhibit its function (Alvarado et al., 2004a). This was found to be a unique property among the *keks*, with the other *keks* not having the ability to do this (Alvarado et al., 2004a). Despite this distinctiveness, the findings here do not further highlight any unique properties of *kek1*. In RT-PCRs, *kek1*'s expression in the CNS and periphery is similar to *kek5* (Fig. 3.1 and 3.2), when overexpressed it appears to increase CaMKII abundance similarly to *kek2* and *-5* overexpression (Fig, 4.1), and *kek1* overexpression maintains elevated Ca^{2+} levels post-stimulation like all the other

Table 6.1 – Comparison of data on the *kek* family

Gene	Chapter 3: Spatial Distribution	Chapter 4: Ca^{2+} signalling	Chapter 5: Plasticity	Previous Reports
kek1	• Expressed in CNS and periphery in L3 larvae (Fig. 3.1 and 3.2)	• *kek1* OE appears to increase CAMKII levels (Fig. 4.1) • *kek1* OE delayed Ca^{2+} decay post-stimulation (Fig. 4.2 and 4.3)	-	• Highly expressed in the embryonic CNS (Musacchio et al., 1996) and PNS (Bishop 2014). • Kek1 can bind to and inhibit EGF receptor (Alvarado et al., 2004a).
kek2	• Expressed in CNS in L3 larvae, but not in the periphery (Fig. 3.1 and 3.2) • Preferentially localises to dendrites (Fig. 3.9, 3.11 and 3.14)	• *kek2* OE appears to increase CAMKII levels (Fig. 4.1) • *kek2* OE decreased the magnitude of the initial influx of Ca^{2+} and delayed Ca^{2+} decay post-stimulation (Fig. 4.2 and 4.4)	-	• *kek2* is expressed in the embryonic CNS (Musacchio et al., 1996) and in motoneurons in larvae (Ulian-Benitez et al., 2017, Ulian-Benitez 2018). • *kek2* is regulated by neuronal activity. *kek2* is upregulated in hyperexcitable mutants but downregulated in reduced excitability mutants. (Guan et al., 2005). • Kek2 can bind DNT2 in co-IP assay (Ulian-Benitez et al., 2017) • OE and knock-down of *kek2* both reduced mature bouton number at the NMJ (Guan et al., 2005).
kek3	• Expressed in CNS in L3 larvae, but not in the periphery (Fig. 3.1 and 3.2) • Localises throughout neurons when overexpressed (Fig. 3.9, 3.12, 3.14 and 3.15).	• *kek3* OE appears to have altered the relative levels of CAMKII isoforms, with Upper isoforms being down regulated and Lower size isoforms being upregulated (Fig. 4.1). • *kek3* OE appeared to have a delayed decay in Ca^{2+} post-stimulation (Fig. 4.2 and 4.5)	-	• *kek3* not expressed in the embryonic CNS (Ulian-Benitez et al., 2017) • Kek3 does not readily bind DNT2 (Ulian-Benitez et al., 2017) • Interacts genetically with *DNT1* (Bishop, 2014)
kek4	• Expressed in CNS in L3 larvae, but not in the periphery (Fig. 3.1 and 3.2) • Localises throughout neurons when overexpressed (Fig. 3.9, 3.12, 3.14, and 3.15).	• OE appears to have altered the relative levels of CAMKII isoforms, with Lower size isoforms being down regulated (Fig. 4.1). • OE decreased the initial peak of Ca2+ and delayed Ca2+ decay post-stimulation (Fig. 4.2 and 4.6) • OE of *kek4* enhanced Cac clustering in the presynaptic side of NMJ 6/7 (Figure 4.10).	• *kek4* is required for the normal active zone formation at NMJ 6/7 and can decrease the volume of active zones when overexpressed (Fig. 5.1) • Neither OE nor loss of *kek4* impacted the size of the axonal terminal or boutons (Fig. 5.1 and 5.2). • OE of *kek4* inhibited the activity-dependent increase in active zones, terminal volume and mature boutons following stimulation (5.7 and 5.8).	• *kek4* is not expressed in the embryonic CNS (Ulian-Benitez et al., 2017) • Decreased expression in the heads of adult flies selectively bred for aggression (Dierick and Greenspan 2006). • >2 fold increase in *kek4* mRNA during developmental autophagy in the larval fat body (Juhasz et al., 2007). • Interacts genetically with *DNT1* (Bishop, 2014)

			• OE of *kek4* caused an activity-dependent gain-of-function phenotype with longer axonal terminals (Fig. 5.7). • *kek4* is required for the activity-dependent increase in axonal terminal volume, active zones, and mature boutons (Fig. 5.9 and 5.10)	
kek5	• Expressed in CNS and periphery in L3 larvae, in motoneurons, possibly in interneurons, and in a subset of PNS neurons (Fig. 3.1, 3.2, 3.7 and 3.8). • Preferentially localises to axonal terminals when overexpressed (Fig. 3.9, 3.13, 3.14, and 3.15).	• OE appears to increase CaMKII abundance (Fig. 4.1). • OE had no effect on Ca^{2+} dynamics post-stimulation (Fig. 4.2 and 4.7)	-	• Expressed in the larval CNS (Evans et al., 2009). Expressed in embryonic CNS and PNS (Ulian-Benitez et al., 2017) and in motoneurons in larvae (Ulian-Benitez et al., 2017, Ulian-Benitez 2018). • *kek5* is regulated by neuronal activity. *kek5* is downregulated in hyperexcitable mutants but unaffected in reduced excitability mutants. (Guan et al., 2005). • Can bind DNT2 in co-IP assay (Ulian-Benitez et al., 2017) • Kek5 inhibits BMP signalling (Evans et al., 2009).
kek6	• Expressed in CNS in L3 larvae, but not in the periphery (Fig. 3.1 and 3.2) • Preferentially localises to axonal terminals when overexpressed (Fig. 3.9, 3.13, 3.14 and 3.15). • At endogenous levels, localises to cell bodies in the VNC and to the axonal terminals at NMJ 6/7 (Fig. 3.21).	• OE appears to increase CAMKII levels (Fig. 4.1) • OE appears to have delayed Ca2+ decay post-stimulation, but not the initial peak (Fig. 4.2 and 4.8). • Endogenously tagged Kek6 colocalises with endogenously tagged Cac, indicating that Kek6 can localise to active zones (Fig. 4.9). • OE of *kek6* increased Cac clustering (Fig. 4.10)	• Loss of, and OE of *kek6* led to greater mature boutons at NMJ 6/7 (Fig. 5.4). • *kek6* OE did not affect the activity-dependent increase in axonal terminal volume but did inhibit the increase in active zones following stimulation (Fig. 5.11) • *kek6* OE and loss-of-function larvae lacked an activity-dependent increase in mature boutons, albeit mature bouton number was already elevated in unstimulated larvae (Fig. 5.12 and 5.14). • *kek6* is required for the activity-dependent increase in axonal terminal volume and active zones (Fig. 5.13).	• Highly expressed in the larval CNS and in motoneurons (Ulian-Benitez et al., 2017, Ulian-Benitez, 2018) • Can bind DNT1 and DNT2 in co-immunopreciptation assay. *kek6* OE can increase active zones. Kek6 is downstream of DNT2. (Ulian-Benitez et al., 2017). • Kek6 and Toll6 may work synergistically to regulate synaptic plasticity downstream of DNT2 (Ulian-Benitez et al., 2017). • Kek6 can bind and activate CAMKII (Ulian-Benitez et al., 2017).

members of the *kek* family (Fig. 4.2-4.8). These data could indicate a conserved function between the *keks*.

6.3 *kek2*

Similarly to *kek1*, *kek2* was initially reported to be expressed in the embryonic CNS (Musacchio et al., 1996, Bishop 2014, Ulian-Benitez et al., 2017). Consistent with this report and another showing *kek2* expression in larval motoneurons, I found an abundance of *kek2* mRNA in the larval CNS but not in the periphery (Fig. 3.1 and 3.2).

In the same experiment I aimed to determine if activity/temperature could regulate the expression of the *keks*. I did not detect a change in expression for any of the *keks* with temperature, which is contradictory to a previous report by Guan et al., 2005 which demonstrated that *kek2* expression was regulated by activity in hyperexcitable and reduced excitability mutants (Guan et al., 2005, Table 6.1). This discrepancy is likely due to the differences in experimental set-up. The experimental design used here (Fig. 3.1 and 3.2) was semi-quantitative and used temperature as a proxy for activity, whereas Guan et al., 2005 used microarray analysis and excitability mutants. Consequently, Guan et al., 2005's report of *kek2* being regulated by activity is more accurate.

Interestingly, Guan et al., 2005 found that *kek2* expression increased in hyperexcitable mutants but decreased in reduced excitability mutants. In this work, when overexpressed in motoneurons, *kek2* reduced the amplitude of the Ca^{2+} influx into the presynapse at the NMJ. Additionally, Guan et al., 2005 found that overexpression of *kek2* led to a decrease in the number of mature boutons at the NMJ. Taken together,

these data could indicate that *kek2* may behave in a homeostatic manner, reducing synaptic transmission and the number of available synapses.

6.4 *kek3*

Compared to the other *keks*, relatively little was known about *kek3* prior to this work (Table 6.1). It had been previously found via the use of a *kek3-GAL4* line that *kek3* may be expressed in the larval CNS (Bishop, 2014), here I have confirmed that via the detection of *kek3* transcripts in the dissected larval CNS via RT-PCR (Fig. 3.1). Furthermore, *kek3* had not appeared to be expressed in the periphery in larvae (Fig. 3.2).

Previously, *kek3* had been reported to genetically interact with *DNT1*, indicating that it may be a neurotrophin receptor (Bishop, 2014, Ulian-Benitez et al., 2017). I examined the functional properties of *kek3* within its capacity to modulate Ca^{2+} signalling (Fig. 4.1, 4.2, and 4.5), which had not been done before for *kek3*. Interpreting the data on the effect of *kek3* overexpression on the post-stimulation response in Ca^{2+} at the NMJ was made difficult due to the low sample size available for *kek3* (Fig. 4.5). This was exacerbated by the movement of the muscle upon stimulation pulling the axonal terminal out of frame and focus. Consequently, the impact of *kek3* overexpression on the amplitude of the Ca^{2+} influx post-stimulation remains unknown. It appears that, as is this case with the other *keks*, that *kek3* overexpression was able to delay the decay in Ca^{2+} post-stimulation (Fig. 4.5).

Unlike the other *keks*, however, *kek3* appears to differentially regulate the abundance of different CaMKII isoforms (Fig. 4.1). The multiple isoforms of CaMKII can be split into three groups based on their molecular weight: 60, 58 and 55kDa (Ohsako et al.,

1993), these three groups are represented on the blot as three bands (Fig. 4.1) (Takamatsu et al., 2003). The CaMKII isoforms can be differentiated by the structure of the variable domain. This variable domain is located between the catalytic and regulatory domains, and the calmodulin association domain (GuptaRoy et al., 2000). Outside of the variable domain the sequence is identical between all forms (GuptaRoy et al., 2000). Within the variable region there are two possible peptide inserts, referred to as insert 1 and insert 2. Additionally, isoforms with apparently identical molecular weights can be different due to single amino acid insertions (Ohsako et al., 1993, Griffith and Greenspan 1993). The lowest weight isoforms (~55 kDa) lack any inserts and he highest weight isoforms (~60 kDa) have all of the inserts.

CaMKII isoforms are functionally diverse, with the alternative kinases having different substrate affinities and different binding kinetics to calmodulin, even between isoforms where the only difference is a single amino acid insertion (GuptaRoy et al., 1996, GuptaRoy et al., 2000). This would allow CaMKII isoforms to differentially regulate downstream processes (GuptaRoy et al., 2000). In addition to their functional diversity, CaMKII isoform ratios change through development and likely have different spatial and temporal expression patterns (Ohsako et al., 1992).

Notably in *kek3* overexpression there appeared to be a great reduction in the levels of the Upper weight (60kDa) CaMKII isoforms and an upregulation of the lower weight (55 kDa) isoforms (Fig. 4.1). Isoform R3, which lacks any inserts, has a low affinity for potassium channel Ether-a-go-go (Eag) and transcription factor Adf-1 (GuptaRoy et al., 2000). Conversely, Isoform R6, which has all of the inserts, has a high affinity for Eag and Adf-1. R3 was more resistant to an inhibitor than R6 was, however (GuptaRoy et al., 2000).

Hypothetically, *kek3* overexpression therefore could have decreased the amount of the CaMKII isoforms with greater Eag and Adf-1 affinity and increased the isoforms with lower affinity to these substrates. However, this is likely to be more complex in reality, with different substrates having different affinities to the different CaMKII isoforms (GuptaRoy et al., 2000). Taken altogether, the data here indicate that *kek3* could differentially regulate CaMKII isoforms which have distinct functional properties.

6.5 *kek4*

As well as Kek3, Kek4 was also found to distribute throughout the neuron when overexpressed with *D42-GAL4* and *109(2)80-GAL4* (Fig. 3.9, 3.12, 3.14 and 3.15), and like *keks -2, -3* and *-6*, *kek4* was found, using RT-PCR, to be expressed in the CNS but not the periphery (Fig. 3.1 and 3.2). However, unlike all the other *keks*, overexpressed *kek4* appeared to have little impact on the abundance of CaMKII (Fig. 4.1). Indeed, the only notable potential change in abundance was a slight decrease in the 55 kDa isoforms. Due to the limitations of this experiment, chiefly sample size and precision, it is impossible to determine if the decrease in the 55 kDa isoforms is true.

On the other hand, *kek4* does appear to be capable of altering Ca^{2+} signalling (Fig. 4.2 and 4.6). Overexpression of *kek4* significantly decreased the amplitude of Ca^{2+} influx to the bouton following stimulation and delayed the decay rate of Ca^{2+} as well (Fig. 4.6). The decrease in amplitude is a feature that *kek4* shares with *kek2*, and indicated that these two *keks* are functionally similar in some ways.

Furthermore, *kek4* overexpression led to the clustering of Cac puncta at the NMJ (Fig. 4.10). The evidence that *kek4* overexpression led to Cac clustering was the data showing a significant decrease in the number of Cac puncta per bouton, the significant increase in the volume of individual Cac puncta and the increase in the intensity of Cac puncta (Fig. 4.10). These data, particularly the increase in intensity, suggest in *kek4* overexpression larvae Cac channels were being clustered, and compacted within those clusters.

Compaction of AZ proteins Brp, RBP and Cac have been demonstrated to be associated with presynaptic homeostatic potentiation (PHP) in *Drosophila* (Mrestani et al., 2021, Ghelani et al., 2023). Indeed this increase in Cac density has been reported to be functionally relevant, with the compaction being necessary for the potentiation of the presynapse resulting from short- and long-term stimulation (Ghelani et al., 2023).

The data showing the clustering of Cac in *kek4* overexpression appears, however, to be at odds with data on the impact of *kek4* overexpression on NMJ morphology, which showed that *kek4* overexpression had no effect on total Brp levels at the NMJ, nor other aspects of NMJ morphology such as mature bouton number and axonal terminal size (Fig. 5.1, 5.2). Based on the Cac clustering data, one might expect to see a likewise increase in Brp volume at the NMJ in this genotype. However, a study using super-resolution microscopy found that during PHP the amount of Brp protein at the synapse does not change (Mrestani et al., 2021). PHP is characterized by the compaction of both Cac and Brp, however the absolute amount of Cac increases at the synapse, but Brp does not change (Mrestani et al., 2021, Ghelani et al., 2023). This is consistent with *kek4* overexpression, where the total amount of Cac increases at the synapse but the amount of Brp does not (Fig. 4.10 and Fig. 5.1).

Interestingly, PHP is classically initiated via the disruption of post-synaptic glutamate receptor function (Delvendahl and Müller 2019). It could be the case that in *kek4* overexpression the release of SVs was impaired, which would be consistent with the finding of reduced initial influx of Ca^{2+} following stimulation (Fig. 4.6). Consequently, PHP, as possibly signified by Cac compaction, may have been initiated as a compensation for a reduction in synaptic transmission. This would suggest that *kek4* plays an inhibitory role with respect to synaptic growth and structure.

This would be consistent with the phenotypes observed in *kek4* overexpression and loss of function on NMJ morphology with and without optogenetic stimulation (Chapter 5). Neither *kek4* overexpression nor *kek4* knockout impacted the parameters of NMJ morphology measured here in the absence of optogenetic stimulation (Fig. 5.1 and 5.2). However, loss of *kek4* function rescued the rise in axonal terminal volume, active zones and mature bouton number phenotypes observed in the control stimulated condition, indicating *kek4* function was required for activity-dependent plasticity (Fig. 5.9 and 5.10). These data would suggest that *kek4* does not have any significant functions during development, but instead plays an important role once neurons are active, e.g. in activity-dependent processes.

Additionally, *kek4* overexpression blocked all activity-dependent changes to NMJ morphology seen in the control genotype (Fig. 5.7 and 5.8). This indicates that *kek4* may play a role in the homeostatic control of NMJ size and structure following activity. The discovery of these activity-dependent phenotypes for *kek4* warrants further investigation to decipher the possible mechanisms behind them.

6.6 *kek5*

In this work it was found that *kek5* was expressed in the larval CNS and PNS as evidenced by the presence of *kek5* transcripts in RNA extracted from dissected larvae, and from the expression pattern of *kek5-GAL4* (Fig. 3.1, 3.2, 3.7 and 3.8). This is consistent with previous reports of *kek5* expression in the larval CNS and motoneurons, and in the embryonic CNS and PNS (Evans et al., 2009, Ulian-Benitez et al., 2017, Ulian-Benitez 2018).

kek5 expression in the PNS could represent a conserved function between *keks* and *trks*. *trkA*, *B* and *C* are expressed widely in the developing and adult PNS in humans and other vertebrates including rodents and zebrafish where they are known to promote the survival of neurons and the maintenance of synapses (Lindsay 1996, Minichiello and Klien 1996, Yamamoto et al., 1993, Aragona et al., 2022).

For example, in the vertebrate dorsal root ganglia (DRG), peripheral sensory neurons are dependent on neurotrophic signalling through the Trks (Stephens et al., 2005). Distinct subpopulations of neurons in the DRG require different neurotrophin ligands for survival, and for a given population of neurons the neurotrophin that is required for survival can change through different stages in development (Mu et al., 1993, Phillips and Armanini 1996). The dependency on different neurotrophins by different subpopulations of DRG neurons is reflective of the differing targets of those subpopulations, e.g. nociceptive neurons require NGF, which is released by the skin, the target of nociceptive neuron innervation (McMahon et al., 1994, Ernfors 2001).

It could be possible, and may indeed be likely, that a similar arrangement may be true for *Drosophila* neurotrophins. *kek5* was found to be expressed in the larval PNS (Fig. 3.2 and 3.8), and *kek1* is known to be expressed in the embryonic PNS with detection

here being reported in the larval periphery (Fig. 3.2). *kek5-GAL4* drove expression in a distinct subset of PNS cells, Class II mda neurons. It could be possible that *kek1*, *kek5*, and some Toll receptors may play a conserved function in the *Drosophila* PNS, regulating the survival of peripheral neurons in a target-specific manner.

To study the role of *kek5* in the developing and adult PNS, the expression pattern of *kek5* would need to be characterised throughout development, this could be achieved with *kek5-GAL4* line generated here in flies with the genotype *kek5>Tomato*, *kek5*-GFP, as featured in Fig. 3.7 B, so that the whole neuron and the localisation of Kek5 protein could be visualised simultaneously. Additionally, this should be carried out with epistatic tests with DNT misexpression to determine neurotrophin-dependent effects.

Interestingly *kek5* appeared to increase levels of CaMKII but did not alter the Ca^{2+} levels post-stimulation when overexpressed (Fig. 4.2, 4.7), indicating that it may be different in function to its family members.

6.7 *kek6*

The endogenous tagging of Kek6 with TSTEP in this work has allowed for Kek6's spatial distribution to be visualized with greater resolution than was previously reported. Earlier work has shown that *kek6-GAL4* drives expression in the CNS and in motoneurons (Ulian-Benitez et al., 2017), but here I have been able to show that Kek6 localises to axonal terminals (Fig. 3.9, 3.13, 3.14, 3.15 and 3.21) and to active zones (Fig. 4.9). Kek6 and Toll-6 were demonstrated to function together to mediate DNT2 signalling at the NMJ, the finding here that Kek6 localises to the active zone in motoneurons is consistent with and supports this previous finding (Ulian-Benitez et al., 2017).

Ulian-Benitez et al., 2017 also found that *kek6* overexpression leads to increased activation of CaMKII, as quantified by an increase in the ratio of active phosphorylated CaMKII to the inactive unphosphorylated CaMKII. Here, I have shown that *kek6* overexpression also increases abundance of unphosphorylated CaMKII (Fig. 4.1). Taken together these data would indicate that *kek6* overexpression leads to an increase in the absolute level of both inactive and active forms of CaMKII. An increase in the abundance of CaMKII could be necessary for the increase in the number of boutons observed in *kek6* overexpression (Fig. 5.4) due to its role as a scaffold protein, and additionally may have effects on CaMKII signalling.

kek6 overexpression altered post-stimulation Ca^{2+} dynamics in manner similar to what had previously been reported, and replicated the delayed decay in Ca^{2+} (Ulian-Benitez, 2018). This delayed decay is a property shared by the other *keks*, except *kek5*, and could indicate an interaction with the Cac channel.

In support of a physical interaction with Cac I found that Kek6-TSTEP co-localises with Cac-sfGFP with a significant fair to moderate correlation (Fig. 4.9) (Akoglu, 2018). The presence of Cac puncta that lack Kek6 appear to be the reason why the correlation is not stronger. This suggests that there are two subsets of active zones: those that have Kek6 and those that do not. It appears that the Cac-sfGFP puncta with the greatest intensities consistently have Kek6-TSTEP, whereas the dimmer Cac puncta seem to consistently lack Kek6-TSTEP colocalization. However, the staining quality for Kek6-TSTEP would need to be improved to conclude this as this observation may only be due to the high amount of noise masking the dimmer Kek6-TSTEP puncta.

As has been observed here and has been previously reported, Cac-sfGFP intensity varies between puncta (Gratz et al., 2019). This heterogeneity in Cac density is

associated with the corresponding active zone's synaptic vesicle release probability (P_r), with greater Cac-sfGFP intensity being correlated with greater P_r and vice versa (Gratz et al., 2019). This would suggest, if the supposition that Kek6 associates only with the highest intensity Cac puncta is true, that Kek6 associates primarily with active zones with high P_r.

kek6 overexpression increased the size of Cac puncta but decreased their number, indicating that it was clustering Cac channels. Furthermore, *kek6* overexpression had sustained Ca^{2+} levels post-firing (Fig. 4.8), which would be consistent with accumulation of Cac at the synapse (Gratz et al., 2019). However, this recruitment of Cac was not to the same extent as with *kek4* overexpression, which also increased the density of Cac channels.

These alterations to the size and structure of the active zone in *kek6* overexpression larvae may be reflective of homeostatic synaptic scaling, where the abundance and organisation of active zone components are adaptively altered to stabilise the weight or strength of the synapse (Goel et al., 2019). Notably, with *kek6* OE the number of mature boutons increase, but the overall level of Brp across the NMJ does not increase, indicating that the same amount of active zone scaffold components are now divided across more boutons (Fig. 5.3 and 5.4). This could lead to a change in the number and size of active zones locally within boutons to compensate for the local reduction in scaffold components, a change in synaptic organisation that was observed in the reduction in Cac dot number and increase in Cac dot size (Fig. 4.10). It would therefore be expected for a there to be a local decrease in the total amount of Cac in boutons. Interestingly, however, total Cac volume stays the same locally (Fig. 4.10 E). This would indicate that *kek6* OE may be recruiting Cac to the synapse while

increasing the number of boutons, indicating that *kek6* overexpression was driving an increase in synaptic strength.

Interestingly, the *kek6* overexpression phenotype mirrored that of optogenetically-stimulated control larvae in regard to mature boutons (Fig. 5.12). Furthermore, when *kek6* overexpression larvae were stimulated in the same way, mature bouton number did not increase further, suggesting that this process reached an upper limit (Fig. 5.12).

The effect of *kek6* overexpression on active zones post-stimulation is less clear cut, as the stimulated and non-stimulated *kek6* OE larvae have similar amounts of Brp to both of the control conditions (Fig. 5.11 D+E). There is no statistical difference between the amount of Brp in stimulated and unstimulated *kek6* OE larvae, indicating that there is an impact on plasticity. However, it is unclear if plasticity has been inhibited or if a scenario similar to the effect of *kek6* overexpression on mature boutons was playing out here with Brp.

kek6 was required for the activity-dependent increase in active zones, as it was observed that this was blocked in *kek6* KO mutants (Fig. 5.13). The increase in mature boutons also observed in these mutants could have been part of a compensation effect to maintain an elevated synaptic weight. The process responsible for increasing bouton number here would be redundant with *kek6*, and may stem from Toll-6 or another Kek.

NMJ size was also impacted by *kek6* overexpression and loss of function post-stimulation. Axonal terminal length increased in stimulated *kek6* overexpression larvae compared to both control conditions. However, the difference in axonal length in stimulated and unstimulated *kek6* overexpression larvae was found to be insignificant, which makes generating definite conclusions on this phenotype difficult. Interestingly,

in *kek6* knockouts this increase in terminal length is still observed, however there is a loss in activity-dependent axonal volume. It was reported previously, on the synergistic function of Kek6 and Toll-6 in DNT2 signalling, that axonal terminal length was downstream of Toll-6 but not Kek6, and that bouton number was downstream of Kek6 but not Toll-6, and that both receptors had influence over axonal branching (Ulian-Benitez et al., 2017, Fig. 1.3). Therefore, the activity-dependent increase in terminal length might be a consequence of altered Toll-6 signalling in *kek6* misexpression, but that the activity-dependent increase in axonal terminal volume requires Kek6 function, possibly via VAP33A and CaMKII control of bouton number and axonal branching respectively (Ulian-Benitez et al., 2017).

Some of the data presented here for the effect of *kek6* overexpression and loss-of-function on NMJ morphology diverges from previous reports (Ulian-Benitez et al., 2017, Ulian-Benitez 2018). Previously, loss of *kek6* function has been demonstrated to reduce the number of mature boutons, axonal terminal length and increase the number of active zones (Ulian-Benitez et al., 2017). This is contrast to the data presented here which indicates that loss of *kek6* results in increased mature bouton numbers and little to no effect on axonal terminal length and active zones (Fig. 5.3 and 5.4).

Previously *kek6* loss of function was assessed with $kek6^{34}$ or $kek6^{35}$ hemizygous with *Df(3R)ED6361* ($kek6^{34}$/ *Df(3R)ED6361* or $kek6^{35}$/ *Df(3R)ED6361*) (Ulian-Benitez et al., 2017). Here, $kek6^{34}$/$kek6^{35}$ was used to provide loss of *kek6*. *Df(3R)ED6361* is a 469 kb deletion in the third chromosome, which contains *kek6*, along with 50 other genes or long noncoding RNAs (lncRNAs), including BMP signalling pathway protein *medea* (McCabe et al., 2004). Medea is known to be required for the development of NMJ morphology in *Drosophila* larvae (McCabe et al., 2004). The genes other than *kek6*

deleted in the *Df(3R)ED6361* line would be heterozygous with their wildtype allele so would not be total loss of functions. Potentially, however, discrepancies between the previously reported phenotypes of *kek6* loss of function and those described here could be due to previous studies using large chromosome deletions targeting a large set of genes including known regulators of NMJ morphology, and the more specific targeting of *kek6* in this work. A method to confirm this would be to examine the phenotype of *Df(3R)ED6361/+* to determine if the previously reported phenotype is still observable.

kek6 overexpression was reported to significantly increase the number of active zones (Ulian-Benitez et al., 2017). The data from this work indicated that overexpression of *kek6* had no effect on active zones. In both cases the same genotype was used. The size of samples between the previous report and this work are similar, with 35 NMJs from 10 larvae for Ulian-Benitez et al., 2017 and 28 NMJs from 9 larvae in this work.

There are differences in the experimental set up of Ulian-Benitez et al., 2017 and this work that could make the two results not fairly comparable. In this work larvae were reared in the dark with *uasReaChR* in the background to allow these samples to be used as controls for the experiments with optogenetic stimulation, which was not done previously. Additionally, Ulian-Benitez et al., 2017 analysed NMJs from abdominal sections 3 and 4, in this work only NMJs from abdominal section 3 were analysed..

Due to these reasons, the data presented here for *kek6* loss of function are likely to be more accurate than those from previous reports, with overexpression data being equally valid, possibly diverging due to differences in experimental design. In retrospect, it would have been better to demonstrate these differences prior to the generation of data that diverged from previous reports. I would have used an

experimental set up comparing *kek6*^{34} or *kek6*^{35}/ *Df(3R)ED6361* with *+/Df(3R)ED6361*, and *kek6*^{34}/*kek6*^{35} at A3+A4 vs only A3. Ideally this would have been able to replicate previous findings and experimentally demonstrate the superiority of *kek6*^{34}/*kek6*^{35} over the use of either with *Df(3R)ED6361*.

6.8 *keks* as regulators of synaptic plasticity

One of the main aims of this thesis was to investigate the function of *keks* in activity-dependent structural synaptic plasticity. In conclusion then, do *keks* function in activity-dependent structural plasticity? The evidence from this body of work and from the previous and recent research of others together indicates that at least some *keks* are important in the process of plasticity.

The data from this work supports the idea that Kek6 is a mediator of hebbian synaptic growth during activity-dependent structural plasticity. Overexpression of *kek6* resulted in a sustained elevated level of Ca^{2+} locally in presynaptic boutons post-stimulation. Elevated Ca^{2+} levels following activity is an indication of potentiation, further supported by the accumulation of Cac channels at active zones in *kek6* overexpression larvae. Additionally, it was demonstrated that Kek6 can co-localise with Cac suggesting a physical interaction. Furthermore, the *kek6* overexpression phenotype on the number of mature boutons phenocopied the stimulated control genotype. Kek6 could mediate synaptic growth at the NMJ following a high bout of activity by clustering Cac channels via a direct or indirect physical interaction to sustain Ca^{2+} levels, thereby activating CaMKII, a key plasticity signalling molecule previously described to interact with Kek6 (Ulian-Benitez et al., 2017).

Data gathered here strongly supports the idea that *kek4* is also responsible for activity-dependent structural plasticity in some capacity. Indeed, in *kek4* loss-of-function activity-dependent structural plasticity at the NMJ is blocked, there is no activity-dependent increase in the number of mature boutons, axonal terminal volume, nor in active zones. The nature and the mechanism of how *kek4* does this remains to be elucidated, however. The most likely hypothesis seems to be that the function of *kek4* in activity-dependent plasticity is homeostatic, blocking hebbian synaptic growth following activity. This is contrast to *kek6*, for which the evidence indicates that it typically behaves in a hebbian manner (Chapter 5, Ulian-Benitez et al., 2017, Ulian-Benitez, 2018).

The function of these *keks* may be context-dependent, which would be consistent with how other *Drosophila* neurotrophin receptors are known mediate signalling (Tripodi et al., 2017, Ulian-Benitez et al., 2017). Furthermore, the Kek family is capable of interacting with proteins that have been identified as being important in the regulation of synapse structure and function, such as CaMKII, the Tolls and BMPs (Evans et al., 2009, McIlroy et al., 2013, Ulian-Benitez et al., 2017). This could potentially indicate that, at least some *keks*, may function as a point of cross-talk between different molecular mechanisms of plasticity, although this is unclear at this time.

The role of the other *keks* (*kek1*, *kek2*, *kek3* and *kek5*) is difficult to determine definitively at this stage without having had the impact of their misexpression on the morphology of the NMJ assessed during activity-dependent plasticity. Functional analysis of these *keks* here, indicate that they all have features in common with each other and with *kek4* and 6. As a readout of Ca^{2+} signalling, *kek1*, *-2*, *-3* and *-5* all appeared to manipulate the abundance of CaMKII, an important effector and signalling molecule for plasticity. Additionally, overexpression of *kek1*, *-2* and *-3* all resulted in

sustained Ca^{2+} levels post-stimulation another indicator of plasticity. The combination of elevated CaMKII levels and sustained Ca^{2+} levels within presynaptic boutons suggests that these *keks* may be signalling via CaMKII to promote plasticity.

Interestingly, it was observed by the authors of Guan et al., 2005 that in both *kek2* overexpression and RNAi-knockdown there was a reduction in the number of mature boutons at the NMJ. Here, *kek2* and *kek4* overexpression had similar phenotypes on Ca^{2+} influx following stimulation, where in both cases the amplitude of Ca^{2+} had decreased (Fig. 4.10). Taken together, these data could indicate that *kek2* functions in a homeostatic role at the NMJ, potentially in a similar manner to *kek4.*

Generally, the Kek family appears to have overlapping properties with regard to Ca^{2+} signalling that could be conserved between each other and between the vertebrate Trks, and in *Drosophila* at least, these could be relevant in the context of plasticity.

The *keks* also have discrete functionalities to each other which could indicate that they may have evolved to adopt distinct but similar roles to each other through a shared familial mechanism. These distinct roles include interactions with other ligands, as is the case with Kek1 and Kek5 with EGF and BMP signalling respectively, but is also evident in their differing subcellular localisations and influence on Ca^{2+} following stimulation. These distinct but overlapping properties could allow the *keks* to tune different aspects of synapse morphology, as evidenced by their idiosyncratic effects on synapse morphology (Guan et al., 2005, This work: Fig. 5.7-14). Further investigation would be required to reveal the true nature of the *keks*, and the data presented here indicates that such investigation should be worthwhile in the pursuit of further understanding neurotrophin biology in *Drosophila*.

6.9 Limitations of experimental approach

6.9.1 Regulation of *keks* by activity

It would have been beneficial for the investigation of the role of the *keks* in plasticity to determine which *keks* are regulated by activity. This had been approached by using temperature as a proxy for activity and detecting Kek cDNA via PCR as depicted in Fig. 3.1 and 3.2. The statistical analysis of these gels did not detect any significant differences between temperature conditions, despite apparent changes in signal intensity.

The resolution of this experiment to detect differences in transcript levels was probably poor, in part due to the semi-quantitative nature of the method used. To quantify the effect of temperature on the expression of the *keks* more accurately, quantitative real-time PCR could be used. Additionally, to probe the effect of neuronal activity more specifically optogenetics could be used instead of temperature. As *kek2* and *kek5* have previously been observed to be regulated differently in neuronal activity mutants these may be found to change expression levels due to optogenetic activity (Guan et al., 2005). The inability to replicate previous findings in this case indicated a limitation with the experimental design used.

6.9.2 Overexpression of protein fusions

A drawback of using protein fusions, including all of the Kek overexpression constructs which have a C-terminal RFP protein fusion, is that the subcellular localisation may be interfered with via disrupted interactions with the PDZ domain. To work around this one would have needed antibodies specific to each Kek and stain for them directly, however no such antibodies were available.

It would have been ideal to have done a synaptic co-stain at the NMJ to determine if the observed Kek puncta (Fig. 3.14 and 3.15) are active zones, unfortunately this was not possible as the only antibody that worked to visualize the Kek-RFPs was mouse anti-mCherry and the donor animal for the anti-NC82 antibody was also mouse. Attempts were made to secure a Brp-GFP line from other labs however these were unsuccessful.

A missed opportunity for the learning about the role of *keks* at the synapse was in not quantifying NMJ morphology in the *D42>Kek-RFP* genotypes as seen in Fig. 3.14. The aim of the experiment at the time of design and execution was to determine if Keks can localise at the axonal terminal, as such it was not deemed necessary to have stringent controls for the effects of staging and abdominal section. Another consequence of this decision was a lower threshold for a satisfactory sample size than would have been required for statistical analysis. Due to these reasons it would be inappropriate to quantify NMJ morphology in these samples as they would likely be highly variable and uninformative. However, the design of this experiment was valid for the simple detection of the subcellular localisation of overexpressed Keks as observed in Fig. 3.14.

An additional caveat with much of the subcellular localisation data is that it was gathered using overexpression via GAL4, this could mean that the distributions observed is a consequence of an overabundance of a given Kek. The use of different GAL4 lines, *D42-GAL4* and *109(2)80-GAL4* offsets this somewhat, as there is a diversity in neuronal types used, and that there was consistency between them supports the findings here. Additionally, Fig. 3.14 and 3.15 lack a control for staining quality, reducing the strength of the finding. Ideally, endogenous protein fusions could be used to visualise the distribution of Keks at endogenous levels, although at the time

these did not exist for all Keks. However, *kek6-TSTEP* was generated to tackle this problem.

6.9.3 Kek6-TSTEP

Kek6-TSTEP was a valuable tool to generate and use as it allowed for the direct visualisation of endogenously expressed Kek6, previously the only data about its localisation in larvae came from overexpression constructs or the *kek6-GAL4* line.

Based on the *kek6-GAL4* data available at the time, the anticipation going into the imaging of Kek6-TSTEP was that it would be widely expressed in the VNC. This would have made morphological characterisation of individual *kek6* neurons difficult. Had this been the case, *TSTEP* would have been very useful due to the ability to change the fluorescent protein tag of the protein fusion with a GAL4 line (Fig. 3.16).

However, the low signal and small number of Kek6-TSTEP cells in the VNC meant that the intended use of the *TSTEP* cassette, the ability to swap the protein tag to GFP, was not realised. Additionally, the low signal for Kek6-TSTEP made imaging difficult. The findings of Kek6-TSTEP distributing to cell bodies and the axonal terminals of motoneurons could potentially be strengthened if the staining was more well optimized.

Due to the high background for the staining for Kek6-TSTEP the Pearson's correlation coefficient may have been falsely lower as dimmer Kek6-TSTEP puncta blended in with background noise. If this experiment were to be repeated, I would try further optimisation of the staining protocol, perhaps using a TSA kit to enhance signal. At the time of running the experiment a large amount of time had already been spent

optimizing the staining protocol to get to the quality seen in Fig. 3.21 and subsequently Fig. 4.9. Due to this completion of other experiments was prioritised.

6.9.4 *kek4* and Ca^{2+} signalling

It would have been immensely beneficial to have an endogenously tagged Kek4 protein fusion to also see if Kek4 natively colocalises with Cac, as was the case with Kek6-TSTEP. An endogenously tagged Kek4 would have been able to demonstrate the localisation of Kek4, potentially in motoneurons , clarifying the interpretation of *kek4* phenotypes. Furthermore, this tool could have demonstrated association with synaptic proteins, such as Cac. Unfortunately, at the time that the need for this tool had become apparent, an endogenously tagged Kek4 did not exist, and generating this tool was not feasible due to the time constraints of the project.

kek4 does not appear to impact the abundance of CaMKII, however it is unknown whether Kek4 can activate CaMKII as Kek6 does (Ulian-Benitez et al., 2017). Attempts were made to quantify the levels of the active phosphorylated form of CaMKII via Western blot and via immunofluorescent staining for pCaMKII in the *kek4* overexpression genotype, however in both cases I was unable to attain a sufficient level of quality in the immunostainings for pCaMKII that would have been appropriate for quantification. Theoretically, this is merely a practical issue that could be solved with sufficient troubleshooting, however further extensive troubleshooting for this dataset was determined to be not time efficient for this work.

The experimental exploration of the roles of *kek4* and 6 in Cac clustering, would have been improved by investigated *kek4* and *kek6* knockdown using RNAi. RNAi here would be preferable to KO mutants, so as to avoid phenotypes arising from the

absence of these genes during development. RNAi lines were ordered from the Vienna Drosophila Resource Center for this; however, they did not arrive on time to be useful.

Additionally, these data would have been improved by investigating *kek4* and *kek6* mutants that lack a PDZ domain to determine if it was required for the phenotypes observed. However, these did not exist at the time and would have taken too long to generate by the time the need was apparent.

A caveat with the interpretation of this experiment is that the *keks* here are overexpressed and are therefore potentially not functioning in a manner that is reflective of their normal function. For instance, as both Kek4 and -6 have PDZ ligand domains they may both appear to cluster Cac, however this may be due to increased PDZ recruitment due to artificially high levels of PDZ ligands at the synapse.

A notable result of this experiment was that bouton volume in *kek4* and *-6* overexpression larvae was significantly higher than the control genotype. This result was not replicated in the following chapter (Fig. 5.2 and 5.4). It is unclear why the result was not replicated, partially it may be due differences in the experimental set up, with samples from the Cac clustering experiment using NMJs from A3 and A4, while the plasticity experiments only used A3. Regardless of cause, the lack of reproducibility of this metric limits the credibility of the Cac clustering experiment.

Epistatic tests would have helped to determine if the *keks* are responsible for the clustering of Cac channels. It would have been interesting to see what the impact of *kek4* and *kek6* loss of function on the distribution of Cac would have been in unstimulated and stimulated larvae, and if this could be rescued by overexpression of the respective Kek. It would have been particularly interesting to have also addressed this with DNT mutants. These experiments would have helped support the hypothesis

that *keks* mediate the clustering of Cac channels following exposure to DNTs, leading to downstream Ca^{2+} signalling and plasticity.

6.9.5 Ca^{2+} imaging

The Ca^{2+} imaging with GCaMP (Fig. 4.2-8) similarly could have provided further important information on the *keks* had mutants or RNAi knockdown phenotypes had been assessed. The concern with this approach during the planning of this experiment was the suspicion that loss or knockdown of a single Kek would have been insufficient to produce a visible phenotype due to compensation by other Keks and possibly Tolls. It would be possible to knockout or down multiple *keks* at a time, however as there are six *keks* there is a large number of possible combinations. It would have been beyond what would be practically manageable to test all combinations, and there was no clear rationale for which specific combinations of *keks* to try.

A notable commonality in the results of this experiment was that most of the *keks* delay the decay in Ca^{2+} over time. This finding would be further supported by the use of a control with a genotype of *D42-GAL4* driving the expression of *uasGCaMP* and *uasRFP*. This would have the benefit of testing for an effect on Ca^{2+} dynamics stemming from the presence of RFP. It is unlikely that the RFP tag is responsible for the phenotypes observed in *kek1*, *-2*, *-3*, *-4* and *-6* however, as *kek5* also had an RFP tag but did not delay Ca^{2+} decay, and instead was similar to the control. Despite this, a *uasRFP* only control would have been beneficial for controlling for the addition of another UAS promoter, which may have diluted the effect of GAL4 in the experimental genotypes.

Generally, the Ca^{2+} imaging data could have been improved by increasing the sample size for all genotypes. This is especially the case for *kek3* overexpression which for some time points there were no usable frames for measuring GCaMP signal for any larvae. This particularly affected the time points just following stimulation as the larval muscle contracted pulling the NMJ out of focus or out of frame. As a result, interpretation of the maximum GCaMP response for *kek3* overexpression is not reliable.

A potential source of technical error in this experiment was the quality of dissection of the larvae. This would be due to the fact that the larvae begin dying from as soon as the dissection begins, and heterogenous levels of physical trauma experienced by the larvae may have impacted their longevity and therefore the consistency of the resulting data. Additionally, larvae were kept anesthetised in ice-cold water prior to dissection, larvae would have spent unequal times waiting for dissection, which could be another source of noise.

6.9.6 Western blots for CaMKII abundance

The CaMKII western blot data could have been made more robust by increasing the sample size of the number of blots (Fig. 4.1). 2 blots were used here, it would have been better to have at least 3 blots so that statistical tests could be done. Additional replicates were attempted but the effort did not yield blots with an adequate level resolution required for analysis. Due to the fact that each band corresponds to multiple isoforms of CaMKII (Takamatsu et al., 2003), it was impossible via the methods used here to delineate specifically which isoforms each Kek could be altering the abundance of. To address the question of which specific isoforms were being up or

downregulated, an RNA sequencing approach may be beneficial. In addition to identifying which isoforms may be being alternately expressed it may also identify other transcripts with altered expression levels.

For this experiment protein was extracted from adult heads with Kek overexpression being driven by *GMR-GAL4*. Larval CNS tissues may have been ideally preferable to adult heads to be consistent with other datasets however this would have likely resulted in low protein yields. *GMR-GAL4* has expressed in non-neuronal tissues in the larvae, principally the imaginal discs (Li et al., 2012, Ray and Lakhotia 2015), however a more recent study found that expression of *GMR-GAL4* in non-neuronal tissues in larvae was low (Escobedo et al., 2021). In contrast, in the adult head, *GMR-GAL4* expression was found to be specific to neuronal eye tissues, where it strongly drove expression of reporters (Escobedo et al., 2021). This indicates that the use of *GMR-GAL4* in this experiment was appropriate. Additionally, *GMR-GAL4* is a standard in the field for specifically driving expression in the eye (West et al., 2015, Escobedo et al., 2021, Deshpande et al., 2023, Brandwine et al., 2021).

6.9.7 Kek misexpression and activity-dependent structural plasticity

A limitation in the study of *kek4* at NMJ 6/7 in plasticity was the lack of knowledge on *kek4*'s expression and distribution. If *kek4* was found to be not expressed in the motoneurons that innervate muscle 6/7, then phenotypes observed here would likely be due to a developmental effect or due to an effect upstream in the neural network. Additionally, overexpression of RFP tagged Kek4 localised throughout the neuron, however it is unknown if Kek4 localises to the axonal terminal when expressed at

endogenous levels. As previously discussed, the use of two GAL4 lines indicates that this may be the case.

kek6 overexpression and loss of function had similar effects on mature bouton number, I suspected that this was due to compensation by Toll-6, consistent with previous reports on these two receptors (Ulian-Benitez et al., 2017). It would have been helpful to assess this and determine if loss of *toll-6* function with loss of *kek6* would eliminate the increase of mature boutons seen in the *kek6* mutants.

Further characterisation of the stimulated control condition could have been useful to further support the claim that the plasticity observed here is Hebbian. A notable curiosity is that with the protocol used here there is no significant change in the number of ghost boutons in any genotype or condition. Further characterisation of the effect of the stimulation protocol used here could have included AIRYSCAN or super-resolution imaging of active zones and additional time points, perhaps at 0- and 6-hours post-stimulation.

The use of 24 hours here was appropriate as the interest lied in the long-term structural changes. In this case, given the *Drosophila* life cycle, 24 hours was adequate to assess this in larvae. Furthermore the lack of ghost boutons may be unsurprising as the protocol was optimised to produce stable, mature boutons. The protocol used here to study activity-dependent structural plasticity at NMJ 6/7 also appears to be novel, as previously optogenetics as a source of stimulation has been used to quantify ghost boutons in the context of short-term plasticity (Maldonado-Díaz et al., 2021). The establishment of the protocol, troubleshooting, and the execution of the experiment as presented here constituted a substantial amount of work, and further genotypes and conditions were not considered due to the time constraints of the project.

Sources of experimental error in these experiments could include the timing of the staging, quality of the fly food, potentially the ratio of male and female larvae that were analysed, and the number of larvae in a vial. While care was taken to ensure the same number of larvae were reared in vials across the experiment, it was clear that some larvae had died soon after being transferred between containers across the experiment, thus introducing a source of technical error.

Another factor to consider for both *kek4* and *kek6* misexpression phenotypes is time. In the larvae used for the experiments with *kek4*/6 misexpression, the genes were either overexpressed or knocked out throughout development. As a result, the phenotypes observed in this chapter could be the consequence of a developmental defect.

For the overexpression genotypes this could have been remedied by the use of the temperature sensitive repressor of *GAL4*, *GAL80*. For the loss of function genotypes this would mean using RNAi alongside *GAL80ts*, instead of heteroallelic null mutants. Although this approach may have been less effective at disrupting gene function. Due to the limited number of chromosomes *Drosophila* have, and the need for being able to also do optogenetics with these tools, this would mean recombinants would have had to have been made. The additional time and risk involved to make these recombinants, and the lack of available validated RNAi lines made this approach undesirable for this project.

6.10 Future directions

The *keks* are homologs of the vertebrate Trk receptors, and the data generated here along with previous reports indicates that they may possess conserved function. The

investigation into the roles of the Keks as receptors for *Drosophila* neurotrophins and the mediation of plasticity warrants further development.

If another year of experimentation was available to continue this investigation, I would work to characterize the function of *kek4* in greater depth. Little is known about *kek4* but here I have demonstrated that is required for activity-dependent structural synaptic plasticity at the NMJ.

To this end I would generate an endogenously tagged Kek4 protein fusion to determine the expression and localisation of Kek4. For this I would use a HA tag so that the protein fusion could be visualised with other proteins with different fluorescent tags, such as Cac-sfGFP or Brp-mCherry. This would be important for establishing the presence of Kek4 in motoneurons and its endogenous subcellular localisation.

I would also attempt to identify the proteins that associate with Kek4 via pull-down assays, and confirm these findings via epistatic tests as had been done for Kek6 before (Ulian-Benitez et al., 2017). Identifying potential partners of Kek4 would be important for further understanding its function. Pull-down assays were planned to be a part of the project but were de-prioritized and delayed indefinitely due to the COVID-19 pandemic.

Interestingly, one of the top proteins identified in this study as associating with Kek6 was Nucleosome remodelling factor – 38kD (NURF-38). NURF-38 is a histone remodelling factor, that is known to act as an activator of transcription and have interactions with transcription factors (Mizuguchi et al 1997, Hamiche et al 1999, Xiao et al 2001, Badenhorst et al 2002). It was observed here that *keks* overexpression can alter the levels of CaMKII protein abundance, it would therefore be interesting to discover if other Keks associate with NURF-38, and if there is any genetic interaction

between the *keks* and *NURF-38*, as this would indicate that *keks* may alter transcription this way.

Additionally I would have designed an experiment to expand on the findings of Chapter 4 and 5 concerning the role of *kek4* and *kek6* in NMJ morphology with and without stimulation. I would expand the parameters which I had previously used to quantify NMJ morphology to include Cac distribution to understand how this is affected during plasticity elicited by my optogenetics protocol in control and misexpression larvae. Furthermore, I would have done epistatic tests with *DNT1* and *DNT2* to determine if they are required for *kek4* function and to test if and how *kek4* overexpression can rescue DNT mutant phenotypes. It would be interesting to include additional time points preceding 24 hours to further characterize the effects of the experimental conditions, which may lead to new avenues of investigation and a greater understanding of the processes at play.

It would be interesting to test the effect of *kek4* misexpression, and indeed the misexpression of the proteins that associate with it once identified, on behaviour. *kek4* had previously been found to be required for normal larval locomotion (Bishop, 2014), and was found to be downregulated in flies selectively bred for aggression (Dierick and Greenspan 2006). This would be important to connect findings at the synapse level to the behavioural level of the whole organism and underline the influence of the *keks*. I would have tested larval locomotion in *kek4* misexpression with an epistatic test involving the DNTs and downstream adaptor proteins, hopefully demonstrating the involvement of these genes in normal behaviour. Additionally, these tests could be paired with plasticity-inducing optogenetic stimulation to establish if the changes to the structure of the synapse do truly confer greater synaptic weight. I had initially planned

to do some behavioural tests of this nature, but these were set aside amid shifting priorities due to the COVID-19 pandemic.

A potential phenotype that was overlooked during this investigation was the variation in the anti-HRP staining seen in Kek overexpression boutons with AIRYSCAN microscopy (Fig. 3.15). Notably, *kek3* and *kek4* have rough and punctate anti-HRP staining which is abnormal. The same staining in *kek5* and *kek6* appears to be more consistent with wildtype anti-HRP stainings, although the lack of a suitable control makes this comparison difficult.

Notably, the antigen of the anti-HRP staining is a set of neuronal-specific glycoproteins including FasII (Snow et al., 1987). Even disregarding the other glycoproteins, FasII is an important molecule at the synapse and has been demonstrated to be important for synaptic organisation, synapse formation and stability and the regulation of plasticity (Thomas et al., 1997, Beumer et al., 2002, Schuster et al., 1996). Therefore, if I had more time to continue research in this area, it would be of immense interest to determine if an interaction between the Keks and FasII exists and what the nature of it is. This could be best explored in an epistasis experiment looking at the distribution of FasII with and without Kek function, and with and without optogenetic stimulation. I would focus on *kek4* to provide additional depth to the knowledge about this intriguing receptor.

7 BIBLIOGRAPHY

Abraham, W. C., Jones, O. D., & Glanzman, D. L. (2019). `Is plasticity of synapses the mechanism of long-term memory storage?', *NPJ science of learning*, *4*, 9. https://doi.org/10.1038/s41539-019-0048-y

Adler, J., & Parmryd, I. (2010). Quantifying colocalization by correlation: the Pearson correlation coefficient is superior to the Mander's overlap coefficient. Cytometry. Part A : the journal of the International Society for Analytical Cytology, 77(8), 733–742. https://doi.org/10.1002/cyto.a.20896

Aid, T., Kazantseva, A., Piirsoo, M., Palm, K., & Timmusk, T. (2007). `Mouse and rat BDNF gene structure and expression revisited', *Journal of neuroscience research*, *85*(3), 525–535. https://doi.org/10.1002/jnr.21139

Akoglu H. (2018). `User's guide to correlation coefficients. *Turkish journal of emergency medicine'*, *18*(3), 91–93. https://doi.org/10.1016/j.tjem.2018.08.001

Alberini C. M. (2009). `Transcription factors in long-term memory and synaptic plasticity', *Physiological reviews*, *89*(1), 121–145. https://doi.org/10.1152/physrev.00017.2008

Alderson, R. F., Curtis, R., Alterman, A. L., Lindsay, R. M., & DiStefano, P. S. (2000). `Truncated TrkB mediates the endocytosis and release of BDNF and neurotrophin-4/5 by rat astrocytes and schwann cells in vitro', *Brain research*, *871*(2), 210–222. https://doi.org/10.1016/s0006-8993(00)02428-8

Allendoerfer, K. L., Cabelli, R. J., Escandón, E., Kaplan, D. R., Nikolics, K., & Shatz, C. J. (1994). `Regulation of neurotrophin receptors during the maturation of the mammalian visual system', *The Journal of neuroscience : the official journal of the Society for Neuroscience*, *14*(3 Pt 2), 1795–1811. https://doi.org/10.1523/JNEUROSCI.14-03-01795.1994

Alvarado, D., Rice, A. H., & Duffy, J. B. (2004). `Bipartite inhibition of Drosophila epidermal growth factor receptor by the extracellular and transmembrane domains of Kekkon1', *Genetics*, *167*(1), 187–202. https://doi.org/10.1534/genetics.167.1.187

Alvarado, D., Rice, A. H., & Duffy, J. B. (2004). `Knockouts of Kekkon1 define sequence elements essential for Drosophila epidermal growth factor receptor inhibition', *Genetics*, *166*(1), 201–211. https://doi.org/10.1534/genetics.166.1.201

An, J. J., Gharami, K., Liao, G. Y., Woo, N. H., Lau, A. G., Vanevski, F., Torre, E. R., Jones, K. R., Feng, Y., Lu, B., & Xu, B. (2008). `Distinct role of long 3' UTR BDNF mRNA in spine morphology and synaptic plasticity in hippocampal neurons', *Cell*, *134*(1), 175–187. https://doi.org/10.1016/j.cell.2008.05.045

Andersen, R., Li, Y., Resseguie, M., & Brenman, J. E. (2005). `Calcium/calmodulin-dependent protein kinase II alters structural plasticity and cytoskeletal dynamics in Drosophila', *The Journal of neuroscience : the official journal of the Society for Neuroscience*, *25*(39), 8878–8888. https://doi.org/10.1523/JNEUROSCI.2005-05.2005

Anderson, K. V., Bokla, L., & Nüsslein-Volhard, C. (1985). `Establishment of dorsal-ventral polarity in the Drosophila embryo: the induction of polarity by the Toll gene product', *Cell*, *42*(3), 791–798. https://doi.org/10.1016/0092-8674(85)90275-2

Anthoney, N., Foldi, I., & Hidalgo, A. (2018). Toll and Toll-like receptor signalling in development. Development (Cambridge, England), 145(9), dev156018. https://doi.org/10.1242/dev.156018

Aponte-Santiago, N. A., & Littleton, J. T. (2020). `Synaptic Properties and Plasticity Mechanisms of Invertebrate Tonic and Phasic Neurons', *Frontiers in physiology*, *11*, 611982. https://doi.org/10.3389/fphys.2020.611982

Aponte-Santiago, N. A., Ormerod, K. G., Akbergenova, Y., & Littleton, J. T. (2020). `Synaptic Plasticity Induced by Differential Manipulation of Tonic and Phasic Motoneurons in *Drosophila*', *The Journal of neuroscience : the official journal of the Society for Neuroscience*, *40*(33), 6270–6288. https://doi.org/10.1523/JNEUROSCI.0925-20.2020

Appelbaum, L. G., Shenasa, M. A., Stolz, L., & Daskalakis, Z. (2023). `Synaptic plasticity and mental health: methods, challenges and opportunities', *Neuropsychopharmacology : official publication of the American College of Neuropsychopharmacology*, *48*(1), 113–120. https://doi.org/10.1038/s41386-022-01370-w

Aragona, M., Porcino, C., Guerrera, M. C., Montalbano, G., Laurà, R., Cometa, M., Levanti, M., Abbate, F., Cobo, T., Capitelli, G., Vega, J. A., & Germanà, A. (2022). The BDNF/TrkB Neurotrophin System in the Sensory Organs of Zebrafish. *International journal of molecular sciences*, *23*(5), 2621. https://doi.org/10.3390/ijms23052621

Ataman, B., Ashley, J., Gorczyca, M., Ramachandran, P., Fouquet, W., Sigrist, S. J., & Budnik, V. (2008). `Rapid activity-dependent modifications in synaptic structure and function require bidirectional Wnt signaling', *Neuron*, *57*(5), 705–718. https://doi.org/10.1016/j.neuron.2008.01.026

Atwood, H. L., Govind, C. K., & Wu, C. F. (1993). `Differential ultrastructure of synaptic terminals on ventral longitudinal abdominal muscles in Drosophila larvae', *Journal of neurobiology*, *24*(8), 1008–1024. https://doi.org/10.1002/neu.480240803

Autry, A. E., Adachi, M., Nosyreva, E., Na, E. S., Los, M. F., Cheng, P. F., Kavalali, E. T., & Monteggia, L. M. (2011). `NMDA receptor blockade at rest triggers rapid behavioural antidepressant responses', *Nature*, *475*(7354), 91–95. https://doi.org/10.1038/nature10130

Autry, A. E., & Monteggia, L. M. (2012). `Brain-derived neurotrophic factor and neuropsychiatric disorders', *Pharmacological reviews*, *64*(2), 238–258. https://doi.org/10.1124/pr.111.005108

Badenhorst, P., Voas, M., Rebay, I., & Wu, C. (2002). `Biological functions of the ISWI chromatin remodeling complex NURF', *Genes & development*, *16*(24), 3186–3198. https://doi.org/10.1101/gad.1032202

Ballard, S. L., Miller, D. L., & Ganetzky, B. (2014). `Retrograde neurotrophin signaling through Tollo regulates synaptic growth in Drosophila', *The Journal of cell biology*, *204*(7), 1157–1172. https://doi.org/10.1083/jcb.201308115

Baltaci, S. B., Mogulkoc, R., & Baltaci, A. K. (2019). `Molecular Mechanisms of Early and Late LTP', *Neurochemical research*, *44*(2), 281–296. https://doi.org/10.1007/s11064-018-2695-4

Baltruschat, L., Prisco, L., Ranft, P., Lauritzen, J. S., Fiala, A., Bock, D. D., & Tavosanis, G. (2021). `Circuit reorganization in the Drosophila mushroom body calyx accompanies memory consolidation', *Cell reports*, *34*(11), 108871. https://doi.org/10.1016/j.celrep.2021.108871

Barbacid M. (1994). `The Trk family of neurotrophin receptors', *Journal of neurobiology*, *25*(11), 1386–1403. https://doi.org/10.1002/neu.480251107

Barde, Y. A., Lindsay, R. M., Monard, D., & Thoenen, H. (1978). `New factor released by cultured glioma cells supporting survival and growth of sensory neurones', *Nature*, *274*(5673), 818. https://doi.org/10.1038/274818a0

Barde, Y. A., Edgar, D., & Thoenen, H. (1982). `Purification of a new neurotrophic factor from mammalian brain', *The EMBO journal*, *1*(5), 549–553. https://doi.org/10.1002/j.1460-2075.1982.tb01207.x

Barria, A., & Malinow, R. (2005). `NMDA receptor subunit composition controls synaptic plasticity by regulating binding to CaMKII', *Neuron*, *48*(2), 289–301. https://doi.org/10.1016/j.neuron.2005.08.034

Barth, M., & Heisenberg, M. (1997). `Vision affects mushroom bodies and central complex in Drosophila melanogaster', *Learning & memory (Cold Spring Harbor, N.Y.)*, *4*(2), 219–229. https://doi.org/10.1101/lm.4.2.219

Barth, M., Hirsch, H. V., Meinertzhagen, I. A., & Heisenberg, M. (1997). `Experience-dependent developmental plasticity in the optic lobe of Drosophila melanogaster', *The Journal of neuroscience : the official journal of the Society for Neuroscience*, *17*(4), 1493–1504. https://doi.org/10.1523/JNEUROSCI.17-04-01493.1997

Bartoletti, A., Cancedda, L., Reid, S. W., Tessarollo, L., Porciatti, V., Pizzorusso, T., & Maffei, L. (2002). `Heterozygous knock-out mice for brain-derived neurotrophic factor show a pathway-specific impairment of long-term potentiation but normal critical period for monocular deprivation', *The Journal of neuroscience : the official journal of the Society for Neuroscience*, *22*(23), 10072–10077. https://doi.org/10.1523/JNEUROSCI.22-23-10072.2002

Bassett, A. R., Tibbit, C., Ponting, C. P., & Liu, J. L. (2013). `Highly efficient targeted mutagenesis of Drosophila with the CRISPR/Cas9 system', *Cell reports*, *4*(1), 220–228. https://doi.org/10.1016/j.celrep.2013.06.020

Basu, J., Bousbaa, H., Logarinho, E., Li, Z., Williams, B. C., Lopes, C., Sunkel, C. E., & Goldberg, M. L. (1999). Mutations in the essential spindle checkpoint gene bub1 cause chromosome missegregation and fail to block apoptosis in Drosophila. The Journal of cell biology, 146(1), 13–28. https://doi.org/10.1083/jcb.146.1.13

Beard, N. A., Casarotto, M. G., Wei, L., Varsányi, M., Laver, D. R., & Dulhunty, A. F. (2005). `Regulation of ryanodine receptors by calsequestrin: effect of high luminal Ca2+ and phosphorylation', *Biophysical journal*, *88*(5), 3444–3454. https://doi.org/10.1529/biophysj.104.051441

Beaton, A. H., Kiss, I., Fristrom, D., & Fristrom, J. W. (1988). Interaction of the Stubble-stubbloid locus and the Broad-complex of Drosophila melanogaster. Genetics, 120(2), 453–464. https://doi.org/10.1093/genetics/120.2.453

Bellen, H. J., Tong, C., & Tsuda, H. (2010). `100 years of Drosophila research and its impact on vertebrate neuroscience: a history lesson for the future', *Nature reviews. Neuroscience*, *11*(7), 514–522. https://doi.org/10.1038/nrn2839

Berke, B., Wittnam, J., McNeill, E., Van Vactor, D. L., & Keshishian, H. (2013). `Retrograde BMP signaling at the synapse: a permissive signal for synapse maturation and activity-dependent plasticity', *The Journal of neuroscience : the official journal of the Society for Neuroscience*, *33*(45), 17937–17950. https://doi.org/10.1523/JNEUROSCI.6075-11.2013

Bertin, F., Moya-Alvarado, G., Quiroz-Manríquez, E., Ibacache, A., Köhler-Solis, A., Oliva, C., & Sierralta, J. (2022). `Dlg Is Required for Short-Term Memory and Interacts with NMDAR in the *Drosophila* Brain', *International journal of molecular sciences*, *23*(16), 9187. https://doi.org/10.3390/ijms23169187

Beumer, K., Matthies, H. J., Bradshaw, A., & Broadie, K. (2002). `Integrins regulate DLG/FAS2 via a CaM kinase II-dependent pathway to mediate synapse elaboration and stabilization during postembryonic development', *Development (Cambridge, England)*, *129*(14), 3381–3391. https://doi.org/10.1242/dev.129.14.3381

Bilz, F., Geurten, B. R. H., Hancock, C. E., Widmann, A., & Fiala, A. (2020). `Visualization of a Distributed Synaptic Memory Code in the Drosophila Brain', *Neuron*, *106*(6), 963–976.e4. https://doi.org/10.1016/j.neuron.2020.03.010

Bishop, Simon (2014). `Functional analysis of the kekkon genes in the drosophilia nervous system', University of Birmingham. Ph.D

Bliss, T. V., & Lomo, T. (1973). `Long-lasting potentiation of synaptic transmission in the dentate area of the anaesthetized rabbit following stimulation of the perforant path', *The Journal of physiology*, *232*(2), 331–356. https://doi.org/10.1113/jphysiol.1973.sp010273

Blum, R., Kafitz, K. W., & Konnerth, A. (2002). `Neurotrophin-evoked depolarization requires the sodium channel Na(V)1.9', *Nature*, *419*(6908), 687–693. https://doi.org/10.1038/nature01085

Bodmer, R., & Jan, Y. N. (1987). `Morphological differentiation of the embryonic peripheral neurons in Drosophila', *Roux's archives of developmental biology : the official organ of the EDBO*, *196*(2), 69–77. https://doi.org/10.1007/BF00402027

Böhme, M. A., McCarthy, A. W., Grasskamp, A. T., Beuschel, C. B., Goel, P., Jusyte, M., Laber, D., Huang, S., Rey, U., Petzoldt, A. G., Lehmann, M., Göttfert, F., Haghighi, P., Hell, S. W., Owald, D., Dickman, D., Sigrist, S. J., & Walter, A. M. (2019). `Rapid active zone remodeling consolidates presynaptic potentiation', *Nature communications*, *10*(1), 1085. https://doi.org/10.1038/s41467-019-08977-6

Botos, I., Segal, D. M., & Davies, D. R. (2011). `The structural biology of Toll-like receptors', *Structure (London, England : 1993)*, *19*(4), 447–459. https://doi.org/10.1016/j.str.2011.02.004

Brand, A. H., & Perrimon, N. (1993). `Targeted gene expression as a means of altering cell fates and generating dominant phenotypes', *Development (Cambridge, England)*, *118*(2), 401–415. https://doi.org/10.1242/dev.118.2.401

Brandwine, T., Ifrah, R., Bialistoky, T., Zaguri, R., Rhodes-Mordov, E., Mizrahi-Meissonnier, L., Sharon, D., Katanaev, V. L., Gerlitz, O., & Minke, B. (2021). `Knockdown of Dehydrodolichyl Diphosphate Synthase in the *Drosophila* Retina Leads to a Unique Pattern of Retinal Degeneration', *Frontiers in molecular neuroscience*, *14*, 693967. https://doi.org/10.3389/fnmol.2021.693967

Brocke, L., Chiang, L. W., Wagner, P. D., & Schulman, H. (1999). `Functional implications of the subunit composition of neuronal CaM kinase II', *The Journal of biological chemistry*, *274*(32), 22713–22722. https://doi.org/10.1074/jbc.274.32.22713

Brown, V., Jin, P., Ceman, S., Darnell, J. C., O'Donnell, W. T., Tenenbaum, S. A., Jin, X., Feng, Y., Wilkinson, K. D., Keene, J. D., Darnell, R. B., & Warren, S. T. (2001). `Microarray identification of FMRP-associated brain mRNAs and altered mRNA translational profiles in fragile X syndrome', *Cell*, *107*(4), 477–487. https://doi.org/10.1016/s0092-8674(01)00568-2

Budnik, V., Zhong, Y., & Wu, C. F. (1990). `Morphological plasticity of motor axons in Drosophila mutants with altered excitability', *The Journal of neuroscience : the official journal of the Society for Neuroscience*, *10*(11), 3754–3768. https://doi.org/10.1523/JNEUROSCI.10-11-03754.1990

Budnik, V., Gorczyca, M., & Prokop, A. (2006). `Selected methods for the anatomical study of Drosophila embryonic and larval neuromuscular junctions', *International review of neurobiology*, *75*, 323–365. https://doi.org/10.1016/S0074-7742(06)75015-2

Campos-Ortega, J. A., & Haenlin, M. (1992). Regulatory signals and signal molecules in early neurogenesis of Drosophila melanogaster. Roux's archives of developmental biology : the official organ of the EDBO, 201(1), 1–11. https://doi.org/10.1007/BF00188770

Chang, L., Jones, Y., Ellisman, M. H., Goldstein, L. S., & Karin, M. (2003). `JNK1 is required for maintenance of neuronal microtubules and controls phosphorylation of microtubule-associated proteins', *Developmental cell*, *4*(4), 521–533. https://doi.org/10.1016/s1534-5807(03)00094-7

Chen, K., & Featherstone, D. E. (2005). `Discs-large (DLG) is clustered by presynaptic innervation and regulates postsynaptic glutamate receptor subunit composition in Drosophila', *BMC biology*, *3*, 1. https://doi.org/10.1186/1741-7007-3-1

Chen, K., Merino, C., Sigrist, S. J., & Featherstone, D. E. (2005). `The 4.1 protein coracle mediates subunit-selective anchoring of Drosophila glutamate receptors to the postsynaptic actin cytoskeleton', *The Journal of neuroscience : the official journal of the Society for Neuroscience*, *25*(28), 6667–6675. https://doi.org/10.1523/JNEUROSCI.1527-05.2005

Chen, T. W., Wardill, T. J., Sun, Y., Pulver, S. R., Renninger, S. L., Baohan, A., Schreiter, E. R., Kerr, R. A., Orger, M. B., Jayaraman, V., Looger, L. L., Svoboda, K.,

& Kim, D. S. (2013). Ultrasensitive fluorescent proteins for imaging neuronal activity. Nature, 499(7458), 295–300. https://doi.org/10.1038/nature12354

Chen, X., Rahman, R., Guo, F., & Rosbash, M. (2016). `Genome-wide identification of neuronal activity-regulated genes in *Drosophila*', *eLife*, *5*, e19942. https://doi.org/10.7554/eLife.19942

Cheng, A., Coksaygan, T., Tang, H., Khatri, R., Balice-Gordon, R. J., Rao, M. S., & Mattson, M. P. (2007). `Truncated tyrosine kinase B brain-derived neurotrophic factor receptor directs cortical neural stem cells to a glial cell fate by a novel signaling mechanism', *Journal of neurochemistry*, *100*(6), 1515–1530. https://doi.org/10.1111/j.1471-4159.2006.04337.x

Chia, C. M., Winston, R. M., & Handyside, A. H. (1995). `EGF, TGF-alpha and EGFR expression in human preimplantation embryos', *Development (Cambridge, England)*, *121*(2), 299–307. https://doi.org/10.1242/dev.121.2.299

Chiba, A., Hing, H., Cash, S., & Keshishian, H. (1993). `Growth cone choices of Drosophila motoneurons in response to muscle fiber mismatch', *The Journal of neuroscience : the official journal of the Society for Neuroscience*, *13*(2), 714–732. https://doi.org/10.1523/JNEUROSCI.13-02-00714.1993

Chin, D., & Means, A. R. (2000). `Calmodulin: a prototypical calcium sensor', *Trends in cell biology*, *10*(8), 322–328. https://doi.org/10.1016/s0962-8924(00)01800-6

Cho, K. O., Wall, J. B., Pugh, P. C., Ito, M., Mueller, S. A., & Kennedy, M. B. (1991). `The alpha subunit of type II Ca2+/calmodulin-dependent protein kinase is highly conserved in Drosophila', *Neuron*, *7*(3), 439–450. https://doi.org/10.1016/0896-6273(91)90296-c

Chorna, T., & Hasan, G. (2012). The genetics of calcium signaling in Drosophila melanogaster. Biochimica et biophysica acta, 1820(8), 1269–1282. https://doi.org/10.1016/j.bbagen.2011.11.002

Cohen, S., & Levi-Montalcini, R. (1956). `A nerve growth-stimulating factor isolated from snake venom', *Proceedings of the National Academy of Sciences of the United States of America*, *42*(9), 571–574. https://doi.org/10.1073/pnas.42.9.571

Colbran R. J. (1992). `Regulation and role of brain calcium/calmodulin-dependent protein kinase II', *Neurochemistry international*, *21*(4), 469–497. https://doi.org/10.1016/0197-0186(92)90080-b

Craymer, L. (1984). Third multiple six, b structure. Drosophila Information Service, 60, 234.

Darnell, J. C., Van Driesche, S. J., Zhang, C., Hung, K. Y., Mele, A., Fraser, C. E., Stone, E. F., Chen, C., Fak, J. J., Chi, S. W., Licatalosi, D. D., Richter, J. D., & Darnell, R. B. (2011). `FMRP stalls ribosomal translocation on mRNAs linked to synaptic function and autism', *Cell*, *146*(2), 247–261. https://doi.org/10.1016/j.cell.2011.06.013

Dechant, G., Biffo, S., Okazawa, H., Kolbeck, R., Pottgiesser, J., & Barde, Y. A. (1993). `Expression and binding characteristics of the BDNF receptor chick trkB', *Development (Cambridge, England)*, *119*(2), 545–558. https://doi.org/10.1242/dev.119.2.545

Delvendahl, I., & Müller, M. (2019). `Homeostatic plasticity-a presynaptic perspective', *Current opinion in neurobiology*, *54*, 155–162. https://doi.org/10.1016/j.conb.2018.10.003

Deshpande, P., Chimata, A. V., Snider, E., Singh, A., Kango-Singh, M., & Singh, A. (2023). `N-Acetyltransferase 9 ameliorates Aβ42-mediated neurodegeneration in the Drosophila eye', *Cell death & disease*, *14*(7), 478. https://doi.org/10.1038/s41419-023-05973-z

Diao, F., Ironfield, H., Luan, H., Diao, F., Shropshire, W. C., Ewer, J., Marr, E., Potter, C. J., Landgraf, M., & White, B. H. (2015). `Plug-and-play genetic access to drosophila cell types using exchangeable exon cassettes', *Cell reports*, *10*(8), 1410–1421. https://doi.org/10.1016/j.celrep.2015.01.059

Dierick, H. A., & Greenspan, R. J. (2006). `Molecular analysis of flies selected for aggressive behavior', *Nature genetics*, *38*(9), 1023–1031. https://doi.org/10.1038/ng1864

Dong, X. X., Wang, Y., & Qin, Z. H. (2009). `Molecular mechanisms of excitotoxicity and their relevance to pathogenesis of neurodegenerative diseases', *Acta pharmacologica Sinica*, *30*(4), 379–387. https://doi.org/10.1038/aps.2009.24

Donoso, P., Sanchez, G., Bull, R., & Hidalgo, C. (2011). `Modulation of cardiac ryanodine receptor activity by ROS and RNS', *Frontiers in bioscience (Landmark edition)*, *16*(2), 553–567. https://doi.org/10.2741/3705

Dorsey, S. G., Renn, C. L., Carim-Todd, L., Barrick, C. A., Bambrick, L., Krueger, B. K., Ward, C. W., & Tessarollo, L. (2006). `In vivo restoration of physiological levels of truncated TrkB.T1 receptor rescues neuronal cell death in a trisomic mouse model', *Neuron*, *51*(1), 21–28. https://doi.org/10.1016/j.neuron.2006.06.009

Du, X., Poltorak, A., Wei, Y., & Beutler, B. (2000). `Three novel mammalian toll-like receptors: gene structure, expression, and evolution', *European cytokine network*, *11*(3), 362–371.

Egan, M. F., Kojima, M., Callicott, J. H., Goldberg, T. E., Kolachana, B. S., Bertolino, A., Zaitsev, E., Gold, B., Goldman, D., Dean, M., Lu, B., & Weinberger, D. R. (2003). `The BDNF val66met polymorphism affects activity-dependent secretion of BDNF and human memory and hippocampal function', *Cell*, *112*(2), 257–269. https://doi.org/10.1016/s0092-8674(03)00035-7

Eide, F. F., Vining, E. R., Eide, B. L., Zang, K., Wang, X. Y., & Reichardt, L. F. (1996). `Naturally occurring truncated trkB receptors have dominant inhibitory effects on brain-derived neurotrophic factor signaling', *The Journal of neuroscience : the official journal of the Society for Neuroscience*, *16*(10), 3123–3129. https://doi.org/10.1523/JNEUROSCI.16-10-03123.1996

Eldon, E., Kooyer, S., D'Evelyn, D., Duman, M., Lawinger, P., Botas, J., & Bellen, H. (1994). `The Drosophila 18 wheeler is required for morphogenesis and has striking similarities to Toll', *Development (Cambridge, England)*, *120*(4), 885–899. https://doi.org/10.1242/dev.120.4.885

Ernfors P. (2001). `Local and target-derived actions of neurotrophins during peripheral nervous system development', *Cellular and molecular life sciences : CMLS*, *58*(8), 1036–1044. https://doi.org/10.1007/PL00000918

Escobedo, S. E., Shah, A., Easton, A. N., Hall, H., & Weake, V. M. (2021). `Characterizing a gene expression toolkit for eye- and photoreceptor-specific expression in Drosophila', *Fly*, *15*(1), 73–88. https://doi.org/10.1080/19336934.2021.1915683

Eskander, M. A., Ruparel, S., Green, D. P., Chen, P. B., Por, E. D., Jeske, N. A., Gao, X., Flores, E. R., & Hargreaves, K. M. (2015). `Persistent Nociception Triggered by Nerve Growth Factor (NGF) Is Mediated by TRPV1 and Oxidative Mechanisms', The Journal of neuroscience : the official journal of the Society for Neuroscience, 35(22), 8593–8603. https://doi.org/10.1523/JNEUROSCI.3993-14.2015

Evans, T. A., Haridas, H., & Duffy, J. B. (2009). `Kekkon5 is an extracellular regulator of BMP signaling', *Developmental biology*, *326*(1), 36–46. https://doi.org/10.1016/j.ydbio.2008.10.002

Fischer, J. A., Giniger, E., Maniatis, T., & Ptashne, M. (1988). `GAL4 activates transcription in Drosophila', *Nature*, *332*(6167), 853–856. https://doi.org/10.1038/332853a0

Fitzgerald, K. A., & Kagan, J. C. (2020). `Toll-like Receptors and the Control of Immunity', *Cell*, *180*(6), 1044–1066. https://doi.org/10.1016/j.cell.2020.02.041

Foldi, I., Anthoney, N., Harrison, N., Gangloff, M., Verstak, B., Nallasivan, M. P., AlAhmed, S., Zhu, B., Phizacklea, M., Losada-Perez, M., Moreira, M., Gay, N. J., & Hidalgo, A. (2017). `Three-tier regulation of cell number plasticity by neurotrophins and Tolls in *Drosophila*', *The Journal of cell biology*, *216*(5), 1421–1438. https://doi.org/10.1083/jcb.201607098

Fouquet, W., Owald, D., Wichmann, C., Mertel, S., Depner, H., Dyba, M., Hallermann, S., Kittel, R. J., Eimer, S., & Sigrist, S. J. (2009). `Maturation of active zone assembly by Drosophila Bruchpilot', *The Journal of cell biology*, *186*(1), 129–145. https://doi.org/10.1083/jcb.200812150

Freeman M. (1996). Reiterative use of the EGF receptor triggers differentiation of all cell types in the Drosophila eye. Cell, 87(4), 651–660. https://doi.org/10.1016/s0092-8674(00)81385-9

Fukumoto, T., Morinobu, S., Okamoto, Y., Kagaya, A., & Yamawaki, S. (2001). `Chronic lithium treatment increases the expression of brain-derived neurotrophic factor in the rat brain', *Psychopharmacology*, *158*(1), 100–106. https://doi.org/10.1007/s002130100871

Ganetzky, B., & Wu, C. F. (1986). `Neurogenetics of membrane excitability in Drosophila', *Annual review of genetics*, *20*, 13–44. https://doi.org/10.1146/annurev.ge.20.120186.000305

Ganetzky, B., & Wu, C. F. (1986). `Neurogenetics of membrane excitability in Drosophila', *Annual review of genetics*, *20*, 13–44. https://doi.org/10.1146/annurev.ge.20.120186.000305

Gao, F. B., Brenman, J. E., Jan, L. Y., & Jan, Y. N. (1999). Genes regulating dendritic outgrowth, branching, and routing in Drosophila. Genes & development, 13(19), 2549–2561. https://doi.org/10.1101/gad.13.19.2549

Gao, L., Zhang, Y., Sterling, K., & Song, W. (2022). `Brain-derived neurotrophic factor in Alzheimer's disease and its pharmaceutical potential', *Translational neurodegeneration*, *11*(1), 4. https://doi.org/10.1186/s40035-022-00279-0

Gay, N. J., & Gangloff, M. (2007). `Structure and function of Toll receptors and their ligands', *Annual review of biochemistry*, *76*, 141–165. https://doi.org/10.1146/annurev.biochem.76.060305.151318

Ghelani, T., Escher, M., Thomas, U., Esch, K., Lützkendorf, J., Depner, H., Maglione, M., Parutto, P., Gratz, S., Matkovic-Rachid, T., Ryglewski, S., Walter, A. M., Holcman, D., O'Connor Giles, K., Heine, M., & Sigrist, S. J. (2023). `Interactive nanocluster compaction of the ELKS scaffold and Cacophony Ca^{2+} channels drives sustained active zone potentiation', *Science advances*, *9*(7), eade7804. https://doi.org/10.1126/sciadv.ade7804

Gideons, E. S., Lin, P. Y., Mahgoub, M., Kavalali, E. T., & Monteggia, L. M. (2017). `Chronic lithium treatment elicits its antimanic effects via BDNF-TrkB dependent synaptic downscaling', *eLife*, *6*, e25480. https://doi.org/10.7554/eLife.25480

Goel, P., Dufour Bergeron, D., Böhme, M. A., Nunnelly, L., Lehmann, M., Buser, C., Walter, A. M., Sigrist, S. J., & Dickman, D. (2019). `Homeostatic scaling of active zone scaffolds maintains global synaptic strength', *The Journal of cell biology*, *218*(5), 1706–1724. https://doi.org/10.1083/jcb.201807165

Golovin, R. M., Vest, J., Vita, D. J., & Broadie, K. (2019). `Activity-Dependent Remodeling of *Drosophila* Olfactory Sensory Neuron Brain Innervation during an Early-Life Critical Period', *The Journal of neuroscience : the official journal of the Society for Neuroscience*, *39*(16), 2995–3012. https://doi.org/10.1523/JNEUROSCI.2223-18.2019

Gorczyca, M., Augart, C., & Budnik, V. (1993). `Insulin-like receptor and insulin-like peptide are localized at neuromuscular junctions in Drosophila', *The Journal of neuroscience : the official journal of the Society for Neuroscience*, *13*(9), 3692–3704. https://doi.org/10.1523/JNEUROSCI.13-09-03692.1993

Gowda, S. B. M., Salim, S., & Mohammad, F. (2021). `Anatomy and Neural Pathways Modulating Distinct Locomotor Behaviors in *Drosophila* Larva', *Biology*, *10*(2), 90. https://doi.org/10.3390/biology10020090

Gratz, S. J., Cummings, A. M., Nguyen, J. N., Hamm, D. C., Donohue, L. K., Harrison, M. M., Wildonger, J., & O'Connor-Giles, K. M. (2013). `Genome engineering of Drosophila with the CRISPR RNA-guided Cas9 nuclease', *Genetics*, *194*(4), 1029–1035. https://doi.org/10.1534/genetics.113.152710

Gratz, S. J., Goel, P., Bruckner, J. J., Hernandez, R. X., Khateeb, K., Macleod, G. T., Dickman, D., & O'Connor-Giles, K. M. (2019). `Endogenous Tagging Reveals Differential Regulation of Ca^{2+} Channels at Single Active Zones during Presynaptic Homeostatic Potentiation and Depression', *The Journal of neuroscience : the official journal of the Society for Neuroscience*, *39*(13), 2416–2429. https://doi.org/10.1523/JNEUROSCI.3068-18.2019

Gratz, S. J., Rubinstein, C. D., Harrison, M. M., Wildonger, J., & O'Connor-Giles, K. M. (2015). `CRISPR-Cas9 Genome Editing in Drosophila', *Current protocols in*

molecular biology, *111*, 31.2.1–31.2.20. https://doi.org/10.1002/0471142727.mb3102s111

Gratz, S. J., Ukken, F. P., Rubinstein, C. D., Thiede, G., Donohue, L. K., Cummings, A. M., & O'Connor-Giles, K. M. (2014). `Highly specific and efficient CRISPR/Cas9-catalyzed homology-directed repair in Drosophila', *Genetics*, *196*(4), 961–971. https://doi.org/10.1534/genetics.113.160713

Griffith, L. C., & Budnik, V. (2006). `Plasticity and second messengers during synapse development', *International review of neurobiology*, *75*, 237–265. https://doi.org/10.1016/S0074-7742(06)75011-5

Griffith, L. C., & Greenspan, R. J. (1993). `The diversity of calcium/calmodulin-dependent protein kinase II isoforms in Drosophila is generated by alternative splicing of a single gene', *Journal of neurochemistry*, *61*(4), 1534–1537. https://doi.org/10.1111/j.1471-4159.1993.tb13650.x

Griffith, L. C., Verselis, L. M., Aitken, K. M., Kyriacou, C. P., Danho, W., & Greenspan, R. J. (1993). `Inhibition of calcium/calmodulin-dependent protein kinase in Drosophila disrupts behavioral plasticity', *Neuron*, *10*(3), 501–509. https://doi.org/10.1016/0896-6273(93)90337-q

Griffith, L. C., Wang, J., Zhong, Y., Wu, C. F., & Greenspan, R. J. (1994). `Calcium/calmodulin-dependent protein kinase II and potassium channel subunit eag similarly affect plasticity in Drosophila', *Proceedings of the National Academy of Sciences of the United States of America*, *91*(21), 10044–10048. https://doi.org/10.1073/pnas.91.21.10044

Grueber, W. B., Jan, L. Y., & Jan, Y. N. (2002). `Tiling of the Drosophila epidermis by multidendritic sensory neurons', *Development (Cambridge, England)*, *129*(12), 2867–2878. https://doi.org/10.1242/dev.129.12.2867

Grueber, W. B., Jan, L. Y., & Jan, Y. N. (2003). `Different levels of the homeodomain protein cut regulate distinct dendrite branching patterns of Drosophila multidendritic neurons', *Cell*, *112*(6), 805–818. https://doi.org/10.1016/s0092-8674(03)00160-0

Guan, Z., Saraswati, S., Adolfsen, B., & Littleton, J. T. (2005). `Genome-wide transcriptional changes associated with enhanced activity in the Drosophila nervous system', *Neuron*, *48*(1), 91–107. https://doi.org/10.1016/j.neuron.2005.08.036

GuptaRoy, B., Beckingham, K., & Griffith, L. C. (1996). `Functional diversity of alternatively spliced isoforms of Drosophila Ca2+/calmodulin-dependent protein kinase II. A role for the variable domain in activation', *The Journal of biological chemistry*, *271*(33), 19846–19851. https://doi.org/10.1074/jbc.271.33.19846

GuptaRoy, B., Marwaha, N., Pla, M., Wang, Z., Nelson, H. B., Beckingham, K., & Griffith, L. C. (2000). `Alternative splicing of Drosophila calcium/calmodulin-dependent protein kinase II regulates substrate specificity and activation', *Brain research. Molecular brain research*, *80*(1), 26–34. https://doi.org/10.1016/s0169-328x(00)00115-7

Halfon, M. S., Hashimoto, C., & Keshishian, H. (1995). `The Drosophila toll gene functions zygotically and is necessary for proper motoneuron and muscle development', *Developmental biology*, *169*(1), 151–167. https://doi.org/10.1006/dbio.1995.1134

Hall, J., Thomas, K. L., & Everitt, B. J. (2000). `Rapid and selective induction of BDNF expression in the hippocampus during contextual learning', *Nature neuroscience*, *3*(6), 533–535. https://doi.org/10.1038/75698

Hamada, F. N., Rosenzweig, M., Kang, K., Pulver, S. R., Ghezzi, A., Jegla, T. J., & Garrity, P. A. (2008). `An internal thermal sensor controlling temperature preference in Drosophila', *Nature*, *454*(7201), 217–220. https://doi.org/10.1038/nature07001

Hamiche, A., Sandaltzopoulos, R., Gdula, D. A., & Wu, C. (1999). `ATP-dependent histone octamer sliding mediated by the chromatin remodeling complex NURF', *Cell*, *97*(7), 833–842. https://doi.org/10.1016/s0092-8674(00)80796-5

Harris, K. P., & Littleton, J. T. (2015). `Transmission, Development, and Plasticity of Synapses', *Genetics*, *201*(2), 345–375. https://doi.org/10.1534/genetics.115.176529

Hartenstein, V., Spindler, S., Pereanu, W., & Fung, S. (2008). `The development of the Drosophila larval brain', *Advances in experimental medicine and biology*, *628*, 1–31. https://doi.org/10.1007/978-0-387-78261-4_1

Hasan, G., & Rosbash, M. (1992). `Drosophila homologs of two mammalian intracellular Ca(2+)-release channels: identification and expression patterns of the inositol 1,4,5-triphosphate and the ryanodine receptor genes', *Development (Cambridge, England)*, *116*(4), 967–975. https://doi.org/10.1242/dev.116.4.967

Hebb, D. O. (1949). The organization of behavior; a neuropsychological theory. Oxford, England: Wiley.

Hofer, M., Pagliusi, S. R., Hohn, A., Leibrock, J., & Barde, Y. A. (1990). `Regional distribution of brain-derived neurotrophic factor mRNA in the adult mouse brain' *The EMBO journal*, *9*(8), 2459–2464. https://doi.org/10.1002/j.1460-2075.1990.tb07423.x

Hoffmann, J. A., & Reichhart, J. M. (2002). `Drosophila innate immunity: an evolutionary perspective', *Nature immunology*, *3*(2), 121–126. https://doi.org/10.1038/ni0202-121

Holt, C. E., Martin, K. C., & Schuman, E. M. (2019). `Local translation in neurons: visualization and function', *Nature structural & molecular biology*, *26*(7), 557–566. https://doi.org/10.1038/s41594-019-0263-5

Hong, H., Zhao, K., Huang, S., Huang, S., Yao, A., Jiang, Y., Sigrist, S., Zhao, L., & Zhang, Y. Q. (2020). `Structural Remodeling of Active Zones Is Associated with Synaptic Homeostasis', *The Journal of neuroscience : the official journal of the Society for Neuroscience*, *40*(14), 2817–2827. https://doi.org/10.1523/JNEUROSCI.2002-19.2020

Horch, H. W., & Katz, L. C. (2002). `BDNF release from single cells elicits local dendritic growth in nearby neurons', *Nature neuroscience*, *5*(11), 1177–1184. https://doi.org/10.1038/nn927

Hourcade, B., Muenz, T. S., Sandoz, J. C., Rössler, W., & Devaud, J. M. (2010). `Long-term memory leads to synaptic reorganization in the mushroom bodies: a memory trace in the insect brain?', *The Journal of neuroscience : the official journal of the Society for Neuroscience*, *30*(18), 6461–6465. https://doi.org/10.1523/JNEUROSCI.0841-10.2010

Huang, E. J., & Reichardt, L. F. (2003). `Trk receptors: roles in neuronal signal transduction', *Annual review of biochemistry*, *72*, 609–642. https://doi.org/10.1146/annurev.biochem.72.121801.161629

Huang, S., Piao, C., Beuschel, C. B., Götz, T., & Sigrist, S. J. (2020). `Presynaptic Active Zone Plasticity Encodes Sleep Need in Drosophila', *Current biology : CB*, *30*(6), 1077–1091.e5. https://doi.org/10.1016/j.cub.2020.01.019

Huang, S., Piao, C., Beuschel, C. B., Zhao, Z., & Sigrist, S. J. (2022). `A brain-wide form of presynaptic active zone plasticity orchestrates resilience to brain aging in Drosophila', *PLoS biology*, *20*(12), e3001730. https://doi.org/10.1371/journal.pbio.3001730

Hubel, D. H., & Wiesel, T. N. (1970). `The period of susceptibility to the physiological effects of unilateral eye closure in kittens', *The Journal of physiology*, *206*(2), 419–436. https://doi.org/10.1113/jphysiol.1970.sp009022

Hughes, C. L., & Thomas, J. B. (2007). `A sensory feedback circuit coordinates muscle activity in Drosophila', *Molecular and cellular neurosciences*, *35*(2), 383–396. https://doi.org/10.1016/j.mcn.2007.04.001

Hummel, T., Krukkert, K., Roos, J., Davis, G., & Klämbt, C. (2000). Drosophila Futsch/22C10 is a MAP1B-like protein required for dendritic and axonal development. Neuron, 26(2), 357–370. https://doi.org/10.1016/s0896-6273(00)81169-1

Hunter, I., Coulson, B., Zarin, A. A., & Baines, R. A. (2021). `The *Drosophila* Larval Locomotor Circuit Provides a Model to Understand Neural Circuit Development and Function', *Frontiers in neural circuits*, *15*, 684969. https://doi.org/10.3389/fncir.2021.684969

Hwang, R. Y., Zhong, L., Xu, Y., Johnson, T., Zhang, F., Deisseroth, K., & Tracey, W. D. (2007). `Nociceptive neurons protect Drosophila larvae from parasitoid wasps', *Current biology : CB*, *17*(24), 2105–2116. https://doi.org/10.1016/j.cub.2007.11.029

Impey, S., McCorkle, S. R., Cha-Molstad, H., Dwyer, J. M., Yochum, G. S., Boss, J. M., McWeeney, S., Dunn, J. J., Mandel, G., & Goodman, R. H. (2004). `Defining the CREB regulon: a genome-wide analysis of transcription factor regulatory regions', *Cell*, *119*(7), 1041–1054. https://doi.org/10.1016/j.cell.2004.10.032

Inagaki, H. K., Jung, Y., Hoopfer, E. D., Wong, A. M., Mishra, N., Lin, J. Y., Tsien, R. Y., & Anderson, D. J. (2014). `Optogenetic control of Drosophila using a red-shifted channelrhodopsin reveals experience-dependent influences on courtship', *Nature methods*, *11*(3), 325–332. https://doi.org/10.1038/nmeth.2765

Ip, N. Y., Ibáñez, C. F., Nye, S. H., McClain, J., Jones, P. F., Gies, D. R., Belluscio, L., Le Beau, M. M., Espinosa, R., 3rd, & Squinto, S. P. (1992). `Mammalian neurotrophin-4: structure, chromosomal localization, tissue distribution, and receptor specificity', *Proceedings of the National Academy of Sciences of the United States of America*, *89*(7), 3060–3064. https://doi.org/10.1073/pnas.89.7.3060

Ives, P. T. (1967). New mutants report. Drosophila Information Service, 42, 39.

Juhász, G., Puskás, L. G., Komonyi, O., Erdi, B., Maróy, P., Neufeld, T. P., & Sass, M. (2007). Gene expression profiling identifies FKBP39 as an inhibitor of

autophagy in larval Drosophila fat body. Cell death and differentiation, 14(6), 1181–1190. https://doi.org/10.1038/sj.cdd.4402123

Kafitz, K. W., Rose, C. R., Thoenen, H., & Konnerth, A. (1999). `Neurotrophin-evoked rapid excitation through TrkB receptors', *Nature*, *401*(6756), 918–921. https://doi.org/10.1038/44847

KATZ, B., & MILEDI, R. (1965). 'The effect of calcium on acetylcholine release from motor nerve terminals', *Proceedings of the Royal Society of London. Series B, Biological sciences*, *161*, 496–503. https://doi.org/10.1098/rspb.1965.0017

Kawasaki, F., Felling, R., & Ordway, R. W. (2000). `A temperature-sensitive paralytic mutant defines a primary synaptic calcium channel in Drosophila', *The Journal of neuroscience : the official journal of the Society for Neuroscience*, *20*(13), 4885–4889. https://doi.org/10.1523/JNEUROSCI.20-13-04885.2000

Kawasaki, F., Zou, B., Xu, X., & Ordway, R. W. (2004). `Active zone localization of presynaptic calcium channels encoded by the cacophony locus of Drosophila', *The Journal of neuroscience: the official journal of the Society for Neuroscience*, *24*(1), 282–285. https://doi.org/10.1523/JNEUROSCI.3553-03.2004

Kim, E., & Sheng, M. (2004). `PDZ domain proteins of synapses', *Nature reviews Neuroscience*, *5*(10), 771–781. https://doi.org/10.1038/nrn1517

Klein, R., Conway, D., Parada, L. F., & Barbacid, M. (1990). `The trkB tyrosine protein kinase gene codes for a second neurogenic receptor that lacks the catalytic kinase domain', *Cell*, *61*(4), 647–656. https://doi.org/10.1016/0092-8674(90)90476-u

Koles, K., Yeh, A. R., & Rodal, A. A. (2015). `Tissue-specific tagging of endogenous loci in Drosophila melanogaster', *Biology open*, *5*(1), 83–89. https://doi.org/10.1242/bio.016089

Kowiański, P., Lietzau, G., Czuba, E., Waśkow, M., Steliga, A., & Moryś, J. (2018). `BDNF: A Key Factor with Multipotent Impact on Brain Signaling and Synaptic Plasticity', *Cellular and molecular neurobiology*, *38*(3), 579–593. https://doi.org/10.1007/s10571-017-0510-4

Kremer, M. C., Christiansen, F., Leiss, F., Paehler, M., Knapek, S., Andlauer, T. F., Förstner, F., Kloppenburg, P., Sigrist, S. J., & Tavosanis, G. (2010). Structural long-term changes at mushroom body input synapses. Current biology : CB, 20(21), 1938–1944. https://doi.org/10.1016/j.cub.2010.09.060

Krivshenko, J. D. (1959). New mutants report. Drosophila Information Service, 33, 95-96.

Kyriacou, Charalambos. (2011). Drosophila Neurobiology. A Laboratory Manual. Eds. B. Zhang, M. R. Freeman & S. Waddell. Cold Spring Harbor Laboratory Press. 2010. ISBN 9780879699055.

Lahey, T., Gorczyca, M., Jia, X. X., & Budnik, V. (1994). `The Drosophila tumor suppressor gene dlg is required for normal synaptic bouton structure', *Neuron*, *13*(4), 823–835. https://doi.org/10.1016/0896-6273(94)90249-6

Lai, F. A., Erickson, H. P., Rousseau, E., Liu, Q. Y., & Meissner, G. (1988). `Purification and reconstitution of the calcium release channel from skeletal muscle', *Nature*, *331*(6154), 315–319. https://doi.org/10.1038/331315a0

Landgraf, M., Sánchez-Soriano, N., Technau, G. M., Urban, J., & Prokop, A. (2003). Charting the Drosophila neuropile: a strategy for the standardised characterisation of genetically amenable neurites. Developmental biology, 260(1), 207–225. https://doi.org/10.1016/s0012-1606(03)00215-x

Leal, G., Bramham, C. R., & Duarte, C. B. (2017). `BDNF and Hippocampal Synaptic Plasticity', *Vitamins and hormones*, *104*, 153–195. https://doi.org/10.1016/bs.vh.2016.10.004

Lee, R., Kermani, P., Teng, K. K., & Hempstead, B. L. (2001). `Regulation of cell survival by secreted proneurotrophins', *Science (New York, N.Y.)*, *294*(5548), 1945–1948. https://doi.org/10.1126/science.1065057

Lee, T., & Luo, L. (1999). Mosaic analysis with a repressible cell marker for studies of gene function in neuronal morphogenesis. Neuron, 22(3), 451–461. https://doi.org/10.1016/s0896-6273(00)80701-1

Lemaitre, B., Nicolas, E., Michaut, L., Reichhart, J. M., & Hoffmann, J. A. (1996). `The dorsoventral regulatory gene cassette spätzle/Toll/cactus controls the potent antifungal response in Drosophila adults', *Cell*, *86*(6), 973–983. https://doi.org/10.1016/s0092-8674(00)80172-5

Lewis, E. B. (1952). New mutants report. Drosophila Information Service, 26, 66.

Li, G., Forero, M. G., Wentzell, J. S., Durmus, I., Wolf, R., Anthoney, N. C., Parker, M., Jiang, R., Hasenauer, J., Strausfeld, N. J., Heisenberg, M., & Hidalgo, A. (2020). `A Toll-receptor map underlies structural brain plasticity', *eLife*, *9*, e52743. https://doi.org/10.7554/eLife.52743

Li, W. Z., Li, S. L., Zheng, H. Y., Zhang, S. P., & Xue, L. (2012). `A broad expression profile of the GMR-GAL4 driver in Drosophila melanogaster', *Genetics and molecular research : GMR*, *11*(3), 1997–2002. https://doi.org/10.4238/2012.August.6.4

Lin J. Y. (2011). `A user's guide to channelrhodopsin variants: features, limitations and future developments', *Experimental physiology*, *96*(1), 19–25. https://doi.org/10.1113/expphysiol.2009.051961

Lin, J. Y., Knutsen, P. M., Muller, A., Kleinfeld, D., & Tsien, R. Y. (2013). `ReaChR: a red-shifted variant of channelrhodopsin enables deep transcranial optogenetic excitation', *Nature neuroscience*, *16*(10), 1499–1508. https://doi.org/10.1038/nn.3502

Lin, P. Y., Kavalali, E. T., & Monteggia, L. M. (2018). `Genetic Dissection of Presynaptic and Postsynaptic BDNF-TrkB Signaling in Synaptic Efficacy of CA3-CA1 Synapses', *Cell reports*, *24*(6), 1550–1561. https://doi.org/10.1016/j.celrep.2018.07.020

Lindsay R. M. (1996). `Role of neurotrophins and trk receptors in the development and maintenance of sensory neurons: an overview', *Philosophical transactions of the Royal Society of London. Series B, Biological sciences*, *351*(1338), 365–373. https://doi.org/10.1098/rstb.1996.0030

Lindsley, D. L. (1968). Genetic variations of Drosophila melanogaster. Carnegie Inst., 627, 472.

Lindsley, D. L., & Zimm, G. G. (2012). The genome of Drosophila melanogaster. Academic press.

Linnarsson, S., Björklund, A., & Ernfors, P. (1997). `Learning deficit in BDNF mutant mice', *The European journal of neuroscience*, *9*(12), 2581–2587. https://doi.org/10.1111/j.1460-9568.1997.tb01687.x

Lisman, J., Schulman, H., & Cline, H. (2002). `The molecular basis of CaMKII function in synaptic and behavioural memory', *Nature reviews. Neuroscience*, *3*(3), 175–190. https://doi.org/10.1038/nrn753

Liu, I. Y., Lyons, W. E., Mamounas, L. A., & Thompson, R. F. (2004). `Brain-derived neurotrophic factor plays a critical role in contextual fear conditioning', *The Journal of neuroscience : the official journal of the Society for Neuroscience*, *24*(36), 7958–7963. https://doi.org/10.1523/JNEUROSCI.1948-04.2004

Liu, Q. R., Walther, D., Drgon, T., Polesskaya, O., Lesnick, T. G., Strain, K. J., de Andrade, M., Bower, J. H., Maraganore, D. M., & Uhl, G. R. (2005). `Human brain derived neurotrophic factor (BDNF) genes, splicing patterns, and assessments of associations with substance abuse and Parkinson's Disease', *American journal of medical genetics. Part B, Neuropsychiatric genetics : the official publication of the International Society of Psychiatric Genetics*, *134B*(1), 93–103. https://doi.org/10.1002/ajmg.b.30109

Lu B. (2003). `BDNF and activity-dependent synaptic modulation', *Learning & memory (Cold Spring Harbor, N.Y.)*, *10*(2), 86–98. https://doi.org/10.1101/lm.54603

Lu, B., Pang, P. T., & Woo, N. H. (2005). `The yin and yang of neurotrophin action', *Nature reviews. Neuroscience*, *6*(8), 603–614. https://doi.org/10.1038/nrn1726

Luikart, B. W., Nef, S., Virmani, T., Lush, M. E., Liu, Y., Kavalali, E. T., & Parada, L. F. (2005). `TrkB has a cell-autonomous role in the establishment of hippocampal Schaffer collateral synapses', *The Journal of neuroscience : the official journal of the Society for Neuroscience*, *25*(15), 3774–3786. https://doi.org/10.1523/JNEUROSCI.0041-05.2005

Luo, J., Shen, W. L., & Montell, C. (2017). `TRPA1 mediates sensation of the rate of temperature change in Drosophila larvae', *Nature neuroscience*, *20*(1), 34–41. https://doi.org/10.1038/nn.4416

Lusk, J. B., Lam, V. Y., & Tolwinski, N. S. (2017). `Epidermal Growth Factor Pathway Signaling in Drosophila Embryogenesis: Tools for Understanding Cancer', *Cancers*, *9*(2), 16. https://doi.org/10.3390/cancers9020016

Ma, Z., Zang, T., Birnbaum, S. G., Wang, Z., Johnson, J. E., Zhang, C. L., & Parada, L. F. (2017). `TrkB dependent adult hippocampal progenitor differentiation mediates sustained ketamine antidepressant response', *Nature communications*, *8*(1), 1668. https://doi.org/10.1038/s41467-017-01709-8

MacLaren, C. M., Evans, T. A., Alvarado, D., & Duffy, J. B. (2004). `Comparative analysis of the Kekkon molecules, related members of the LIG

superfamily', *Development genes and evolution*, *214*(7), 360–366. https://doi.org/10.1007/s00427-004-0414-4

Maisonpierre, P. C., Belluscio, L., Squinto, S., Ip, N. Y., Furth, M. E., Lindsay, R. M., & Yancopoulos, G. D. (1990). `Neurotrophin-3: a neurotrophic factor related to NGF and BDNF', *Science (New York, N.Y.)*, *247*(4949 Pt 1), 1446–1451. https://doi.org/10.1126/science.247.4949.1446

Maldonado-Díaz, C., Vazquez, M., & Marie, B. (2021). `A comparison of three different methods of eliciting rapid activity-dependent synaptic plasticity at the Drosophila NMJ', *PloS one*, *16*(11), e0260553. https://doi.org/10.1371/journal.pone.0260553

Mandai, K., Guo, T., St Hillaire, C., Meabon, J. S., Kanning, K. C., Bothwell, M., & Ginty, D. D. (2009). `LIG family receptor tyrosine kinase-associated proteins modulate growth factor signals during neural development', *Neuron*, *63*(5), 614–627. https://doi.org/10.1016/j.neuron.2009.07.031

Marrus, S. B., Portman, S. L., Allen, M. J., Moffat, K. G., & DiAntonio, A. (2004). `Differential localization of glutamate receptor subunits at the Drosophila neuromuscular junction', *The Journal of neuroscience : the official journal of the Society for Neuroscience*, *24*(6), 1406–1415. https://doi.org/10.1523/JNEUROSCI.1575-03.2004

Matsumoto, T., Numakawa, T., Adachi, N., Yokomaku, D., Yamagishi, S., Takei, N., & Hatanaka, H. (2001). `Brain-derived neurotrophic factor enhances depolarization-evoked glutamate release in cultured cortical neurons', *Journal of neurochemistry*, *79*(3), 522–530. https://doi.org/10.1046/j.1471-4159.2001.00591.x

Matsumoto, T., Rauskolb, S., Polack, M., Klose, J., Kolbeck, R., Korte, M., & Barde, Y. A. (2008). `Biosynthesis and processing of endogenous BDNF: CNS neurons store and secrete BDNF, not pro-BDNF', *Nature neuroscience*, *11*(2), 131–133. https://doi.org/10.1038/nn2038

Matyas, J. J., O'Driscoll, C. M., Yu, L., Coll-Miro, M., Daugherty, S., Renn, C. L., Faden, A. I., Dorsey, S. G., & Wu, J. (2017). `Truncated TrkB.T1-Mediated Astrocyte Dysfunction Contributes to Impaired Motor Function and Neuropathic Pain after Spinal Cord Injury', *The Journal of neuroscience : the official journal of the Society for Neuroscience*, *37*(14), 3956–3971. https://doi.org/10.1523/JNEUROSCI.3353-16.2017

McBain, C. J., & Mayer, M. L. (1994). `N-methyl-D-aspartic acid receptor structure and function', *Physiological reviews*, *74*(3), 723–760. https://doi.org/10.1152/physrev.1994.74.3.723

McCabe, B. D., Hom, S., Aberle, H., Fetter, R. D., Marques, G., Haerry, T. E., Wan, H., O'Connor, M. B., Goodman, C. S., & Haghighi, A. P. (2004). `Highwire regulates presynaptic BMP signaling essential for synaptic growth', *Neuron*, *41*(6), 891–905. https://doi.org/10.1016/s0896-6273(04)00073-x

McCabe, B. D., Marqués, G., Haghighi, A. P., Fetter, R. D., Crotty, M. L., Haerry, T. E., Goodman, C. S., & O'Connor, M. B. (2003). `The BMP homolog Gbb provides a retrograde signal that regulates synaptic growth at the Drosophila neuromuscular junction', *Neuron*, *39*(2), 241–254. https://doi.org/10.1016/s0896-6273(03)00426-4

McCarron, M., Gelbart, W., & Chovnick, A. (1974). Intracistronic mapping of electrophoretic sites in Drosophila melanogaster: fidelity of information transfer by gene conversion. Genetics, 76(2), 289–299. https://doi.org/10.1093/genetics/76.2.289

McIlroy, G., Foldi, I., Aurikko, J., Wentzell, J. S., Lim, M. A., Fenton, J. C., Gay, N. J., & Hidalgo, A. (2013). `Toll-6 and Toll-7 function as neurotrophin receptors in the Drosophila melanogaster CNS', *Nature neuroscience*, *16*(9), 1248–1256. https://doi.org/10.1038/nn.3474

McLaughlin, C. N., Nechipurenko, I. V., Liu, N., & Broihier, H. T. (2016). `A Toll receptor-FoxO pathway represses Pavarotti/MKLP1 to promote microtubule dynamics in motoneurons', *The Journal of cell biology*, *214*(4), 459–474. https://doi.org/10.1083/jcb.201601014

McMahon, S. B., Armanini, M. P., Ling, L. H., & Phillips, H. S. (1994). `Expression and coexpression of Trk receptors in subpopulations of adult primary sensory neurons projecting to identified peripheral targets', *Neuron*, *12*(5), 1161–1171. https://doi.org/10.1016/0896-6273(94)90323-9

Melom, J. E., Akbergenova, Y., Gavornik, J. P., & Littleton, J. T. (2013). `Spontaneous and evoked release are independently regulated at individual active zones', *The Journal of neuroscience : the official journal of the Society for Neuroscience*, *33*(44), 17253–17263. https://doi.org/10.1523/JNEUROSCI.3334-13.2013

Menon, K. P., Carrillo, R. A., & Zinn, K. (2013). `Development and plasticity of the Drosophila larval neuromuscular junction', *Wiley interdisciplinary reviews. Developmental biology*, *2*(5), 647–670. https://doi.org/10.1002/wdev.108

Merriam, E. B., Lumbard, D. C., Viesselmann, C., Ballweg, J., Stevenson, M., Pietila, L., Hu, X., & Dent, E. W. (2011). `Dynamic microtubules promote synaptic NMDA receptor-dependent spine enlargement', *PloS one*, *6*(11), e27688. https://doi.org/10.1371/journal.pone.0027688

Merriam, J. R. (1969). FM7: A "new" first chromosome balancer. Dros Inf Serv, 44, 101.

Miller, S. G., & Kennedy, M. B. (1986). `Regulation of brain type II Ca2+/calmodulin-dependent protein kinase by autophosphorylation: a Ca2+-triggered molecular switch', *Cell*, *44*(6), 861–870. https://doi.org/10.1016/0092-8674(86)90008-5

Minichiello L. (2009). `TrkB signalling pathways in LTP and learning', *Nature reviews. Neuroscience*, *10*(12), 850–860. https://doi.org/10.1038/nrn2738

Minichiello, L., & Klein, R. (1996). `TrkB and TrkC neurotrophin receptors cooperate in promoting survival of hippocampal and cerebellar granule neurons', *Genes & development*, *10*(22), 2849–2858. https://doi.org/10.1101/gad.10.22.2849

Mirzoyan, Z., Sollazzo, M., Allocca, M., Valenza, A. M., Grifoni, D., & Bellosta, P. (2019). `*Drosophila melanogaster*: A Model Organism to Study Cancer', *Frontiers in genetics*, *10*, 51. https://doi.org/10.3389/fgene.2019.00051

Mizuguchi, G., Tsukiyama, T., Wisniewski, J., & Wu, C. (1997). `Role of nucleosome remodeling factor NURF in transcriptional activation of chromatin', *Molecular cell*, *1*(1), 141–150. https://doi.org/10.1016/s1097-2765(00)80015-5

Morris, E. P., & Török, K. (2001). `Oligomeric structure of alpha-calmodulin-dependent protein kinase II', *Journal of molecular biology*, *308*(1), 1–8. https://doi.org/10.1006/jmbi.2001.4584

Morris, R. G., Anderson, E., Lynch, G. S., & Baudry, M. (1986). `Selective impairment of learning and blockade of long-term potentiation by an N-methyl-D-aspartate receptor antagonist, AP5', *Nature*, *319*(6056), 774–776. https://doi.org/10.1038/319774a0

Mowla, S. J., Farhadi, H. F., Pareek, S., Atwal, J. K., Morris, S. J., Seidah, N. G., & Murphy, R. A. (2001). `Biosynthesis and post-translational processing of the precursor to brain-derived neurotrophic factor', *The Journal of biological chemistry*, *276*(16), 12660–12666. https://doi.org/10.1074/jbc.M008104200

Mrestani, A., Pauli, M., Kollmannsberger, P., Repp, F., Kittel, R. J., Eilers, J., Doose, S., Sauer, M., Sirén, A. L., Heckmann, M., & Paul, M. M. (2021). `Active zone compaction correlates with presynaptic homeostatic potentiation', *Cell reports*, *37*(1), 109770. https://doi.org/10.1016/j.celrep.2021.109770

Mu, X., Silos-Santiago, I., Carroll, S. L., & Snider, W. D. (1993). `Neurotrophin receptor genes are expressed in distinct patterns in developing dorsal root ganglia', *The Journal of neuroscience : the official journal of the Society for Neuroscience*, *13*(9), 4029–4041. https://doi.org/10.1523/JNEUROSCI.13-09-04029.1993

Muller, D. and I. Nikonenko (2013). Chapter 6 - Dendritic Spines. Neural Circuit Development and Function in the Brain. J. L. R. Rubenstein and P. Rakic. Oxford, Academic Press: ISBN 978-0-12-397267-5

Muller, H. J. (1943). A stable double X chromosome. Drosoph Inf Serv, 17, 61-62.

Musacchio, M., & Perrimon, N. (1996). `The Drosophila kekkon genes: novel members of both the leucine-rich repeat and immunoglobulin superfamilies expressed in the CNS', *Developmental biology*, *178*(1), 63–76. https://doi.org/10.1006/dbio.1996.0198

Nabavi, S., Fox, R., Proulx, C. D., Lin, J. Y., Tsien, R. Y., & Malinow, R. (2014). `Engineering a memory with LTD and LTP', *Nature*, *511*(7509), 348–352. https://doi.org/10.1038/nature13294

Nagel, G., Szellas, T., Huhn, W., Kateriya, S., Adeishvili, N., Berthold, P., Ollig, D., Hegemann, P., & Bamberg, E. (2003). `Channelrhodopsin-2, a directly light-gated cation-selective membrane channel', *Proceedings of the National Academy of Sciences of the United States of America*, *100*(24), 13940–13945. https://doi.org/10.1073/pnas.1936192100

Nairn, A. C., & Picciotto, M. R. (1994). `Calcium/calmodulin-dependent protein kinases', *Seminars in cancer biology*, *5*(4), 295–303.

Nakai, J., Ohkura, M., & Imoto, K. (2001). `A high signal-to-noise Ca(2+) probe composed of a single green fluorescent protein', *Nature biotechnology*, *19*(2), 137–141. https://doi.org/10.1038/84397

Nakamoto, M., Moy, R. H., Xu, J., Bambina, S., Yasunaga, A., Shelly, S. S., Gold, B., & Cherry, S. (2012). `Virus recognition by Toll-7 activates antiviral autophagy in Drosophila', *Immunity*, *36*(4), 658–667. https://doi.org/10.1016/j.immuni.2012.03.003

Nicoll R. A. (2017). `A Brief History of Long-Term Potentiation', *Neuron*, *93*(2), 281–290. https://doi.org/10.1016/j.neuron.2016.12.015

Nowak, L., Bregestovski, P., Ascher, P., Herbet, A., & Prochiantz, A. (1984). `Magnesium gates glutamate-activated channels in mouse central neurones', *Nature*, *307*(5950), 462–465. https://doi.org/10.1038/307462a0

Ohira, K., Homma, K. J., Hirai, H., Nakamura, S., & Hayashi, M. (2006). `TrkB-T1 regulates the RhoA signaling and actin cytoskeleton in glioma cells', *Biochemical and biophysical research communications*, *342*(3), 867–874. https://doi.org/10.1016/j.bbrc.2006.02.033

Ohsako, S., Nishida, Y., Ryo, H., & Yamauchi, T. (1993). `Molecular characterization and expression of the Drosophila Ca2+/calmodulin-dependent protein kinase II gene. Identification of four forms of the enzyme generated from a single gene by alternative splicing', *The Journal of biological chemistry*, *268*(3), 2052–2062.

Ohyama, T., Schneider-Mizell, C. M., Fetter, R. D., Aleman, J. V., Franconville, R., Rivera-Alba, M., Mensh, B. D., Branson, K. M., Simpson, J. H., Truman, J. W., Cardona, A., & Zlatic, M. (2015). `A multilevel multimodal circuit enhances action selection in Drosophila', *Nature*, *520*(7549), 633–639. https://doi.org/10.1038/nature14297

Ooi, J. Y., Yagi, Y., Hu, X., & Ip, Y. T. (2002). `The Drosophila Toll-9 activates a constitutive antimicrobial defense', *EMBO reports*, *3*(1), 82–87. https://doi.org/10.1093/embo-reports/kvf004

Orgogozo, V., & Grueber, W. B. (2005). `FlyPNS, a database of the Drosophila embryonic and larval peripheral nervous system', *BMC developmental biology*, *5*, 4. https://doi.org/10.1186/1471-213X-5-4

Oster, I. I. (1956). A new crossing-over suppressor in chromosome 2 effective in the presence of heterologous inversions. Drosophila Information Service, 30, 145.

Oswald, M. C., Brooks, P. S., Zwart, M. F., Mukherjee, A., West, R. J., Giachello, C. N., Morarach, K., Baines, R. A., Sweeney, S. T., & Landgraf, M. (2018). `Reactive oxygen species regulate activity-dependent neuronal plasticity in *Drosophila*', *eLife*, *7*, e39393. https://doi.org/10.7554/eLife.39393

Palko, M. E., Coppola, V., & Tessarollo, L. (1999). `Evidence for a role of truncated trkC receptor isoforms in mouse development', *The Journal of neuroscience : the official journal of the Society for Neuroscience*, *19*(2), 775–782. https://doi.org/10.1523/JNEUROSCI.19-02-00775.1999

Pan, L., & Broadie, K. S. (2007). `Drosophila fragile X mental retardation protein and metabotropic glutamate receptor A convergently regulate the synaptic ratio of ionotropic glutamate receptor subclasses', *The Journal of neuroscience : the official journal of the Society for Neuroscience*, *27*(45), 12378–12389. https://doi.org/10.1523/JNEUROSCI.2970-07.2007

Pang, P. T., Teng, H. K., Zaitsev, E., Woo, N. T., Sakata, K., Zhen, S., Teng, K. K., Yung, W. H., Hempstead, B. L., & Lu, B. (2004). `Cleavage of proBDNF by tPA/plasmin is essential for long-term hippocampal plasticity', *Science (New York, N.Y.)*, *306*(5695), 487–491. https://doi.org/10.1126/science.1100135

Park, H., & Poo, M. M. (2013). `Neurotrophin regulation of neural circuit development and function', *Nature reviews. Neuroscience*, *14*(1), 7–23. https://doi.org/10.1038/nrn3379

Patterson, S. L., Abel, T., Deuel, T. A., Martin, K. C., Rose, J. C., & Kandel, E. R. (1996). `Recombinant BDNF rescues deficits in basal synaptic transmission and hippocampal LTP in BDNF knockout mice', *Neuron*, *16*(6), 1137–1145. https://doi.org/10.1016/s0896-6273(00)80140-3

Pfeiffer, B. D., Ngo, T. T., Hibbard, K. L., Murphy, C., Jenett, A., Truman, J. W., & Rubin, G. M. (2010). Refinement of tools for targeted gene expression in Drosophila. Genetics, 186(2), 735–755. https://doi.org/10.1534/genetics.110.119917

Phillips, H. S., & Armanini, M. P. (1996). `Expression of the trk family of neurotrophin receptors in developing and adult dorsal root ganglion neurons', *Philosophical transactions of the Royal Society of London. Series B, Biological sciences*, *351*(1338), 413–416. https://doi.org/10.1098/rstb.1996.0036

Prokop A. (2006). `Organization of the efferent system and structure of neuromuscular junctions in Drosophila', *International review of neurobiology*, *75*, 71–90. https://doi.org/10.1016/S0074-7742(06)75004-8

Prole, D. L., & Taylor, C. W. (2019). `Structure and Function of IP_3 Receptors', *Cold Spring Harbor perspectives in biology*, *11*(4), a035063. https://doi.org/10.1101/cshperspect.a035063

Pruunsild, P., Kazantseva, A., Aid, T., Palm, K., & Timmusk, T. (2007). `Dissecting the human BDNF locus: bidirectional transcription, complex splicing, and multiple promoters', *Genomics*, *90*(3), 397–406. https://doi.org/10.1016/j.ygeno.2007.05.004

Pulver, S. R., Pashkovski, S. L., Hornstein, N. J., Garrity, P. A., & Griffith, L. C. (2009). `Temporal dynamics of neuronal activation by Channelrhodopsin-2 and TRPA1 determine behavioral output in Drosophila larvae', *Journal of neurophysiology*, *101*(6), 3075–3088. https://doi.org/10.1152/jn.00071.2009

Qin, G., Schwarz, T., Kittel, R. J., Schmid, A., Rasse, T. M., Kappei, D., Ponimaskin, E., Heckmann, M., & Sigrist, S. J. (2005). `Four different subunits are essential for expressing the synaptic glutamate receptor at neuromuscular junctions of Drosophila', *The Journal of neuroscience : the official journal of the Society for Neuroscience*, *25*(12), 3209–3218. https://doi.org/10.1523/JNEUROSCI.4194-04.2005

Rattenholl, A., Ruoppolo, M., Flagiello, A., Monti, M., Vinci, F., Marino, G., Lilie, H., Schwarz, E., & Rudolph, R. (2001). `Pro-sequence assisted folding and disulfide bond formation of human nerve growth factor', *Journal of molecular biology*, *305*(3), 523–533. https://doi.org/10.1006/jmbi.2000.4295

Ray, M., & Lakhotia, S. C. (2015). `The commonly used eye-specific sev-GAL4 and GMR-GAL4 drivers in Drosophila melanogaster are expressed in tissues other than eyes also', *Journal of genetics*, *94*(3), 407–416. https://doi.org/10.1007/s12041-015-0535-8

Reichardt L. F. (2006). `Neurotrophin-regulated signalling pathways', *Philosophical transactions of the Royal Society of London. Series B, Biological sciences*, *361*(1473), 1545–1564. https://doi.org/10.1098/rstb.2006.1894

Rodriguez-Tébar, A., Dechant, G., & Barde, Y. A. (1990). `Binding of brain-derived neurotrophic factor to the nerve growth factor receptor', *Neuron*, *4*(4), 487–492. https://doi.org/10.1016/0896-6273(90)90107-q

Rolls, A., Shechter, R., London, A., Ziv, Y., Ronen, A., Levy, R., & Schwartz, M. (2007). `Toll-like receptors modulate adult hippocampal neurogenesis', *Nature cell biology*, *9*(9), 1081–1088. https://doi.org/10.1038/ncb1629

Roote, J., & Prokop, A. (2013). `How to design a genetic mating scheme: a basic training package for Drosophila genetics', *G3 (Bethesda, Md.)*, *3*(2), 353–358. https://doi.org/10.1534/g3.112.004820

Rose, C. R., Blum, R., Pichler, B., Lepier, A., Kafitz, K. W., & Konnerth, A. (2003). `Truncated TrkB-T1 mediates neurotrophin-evoked calcium signalling in glia cells', *Nature*, *426*(6962), 74–78. https://doi.org/10.1038/nature01983

Rosenthal, A., Goeddel, D. V., Nguyen, T., Martin, E., Burton, L. E., Shih, A., Laramee, G. R., Wurm, F., Mason, A., & Nikolics, K. (1991). `Primary structure and biological activity of human brain-derived neurotrophic factor', *Endocrinology*, *129*(3), 1289–1294. https://doi.org/10.1210/endo-129-3-1289

Rutherford, L. C., Nelson, S. B., & Turrigiano, G. G. (1998). `BDNF has opposite effects on the quantal amplitude of pyramidal neuron and interneuron excitatory synapses', *Neuron*, *21*(3), 521–530. https://doi.org/10.1016/s0896-6273(00)80563-2

Saarelainen, T., Hendolin, P., Lucas, G., Koponen, E., Sairanen, M., MacDonald, E., Agerman, K., Haapasalo, A., Nawa, H., Aloyz, R., Ernfors, P., & Castrén, E. (2003). `Activation of the TrkB neurotrophin receptor is induced by antidepressant drugs and is required for antidepressant-induced behavioral effects', *The Journal of neuroscience : the official journal of the Society for Neuroscience*, *23*(1), 349–357. https://doi.org/10.1523/JNEUROSCI.23-01-00349.2003

Safir, S. R. (1913). A new eye color mutation in Drosophila and its mode of inheritance. The Biological Bulletin, 25(1), 45-51.

Sapranauskas, R., Gasiunas, G., Fremaux, C., Barrangou, R., Horvath, P., & Siksnys, V. (2011). `The Streptococcus thermophilus CRISPR/Cas system provides immunity in Escherichia coli', *Nucleic acids research*, *39*(21), 9275–9282. https://doi.org/10.1093/nar/gkr606

Schmid, A., Hallermann, S., Kittel, R. J., Khorramshahi, O., Frölich, A. M., Quentin, C., Rasse, T. M., Mertel, S., Heckmann, M., & Sigrist, S. J. (2008). `Activity-dependent site-specific changes of glutamate receptor composition in vivo', *Nature neuroscience*, *11*(6), 659–666. https://doi.org/10.1038/nn.2122

Scholich, K., Pierre, S., & Patel, T. B. (2001). `Protein associated with Myc (PAM) is a potent inhibitor of adenylyl cyclases', *The Journal of biological chemistry*, *276*(50), 47583–47589. https://doi.org/10.1074/jbc.M107816200

Schulman, H., & Greengard, P. (1978). `Stimulation of brain membrane protein phosphorylation by calcium and an endogenous heat-stable protein', *Nature*, *271*(5644), 478–479. https://doi.org/10.1038/271478a0

Schuster, C. M., Davis, G. W., Fetter, R. D., & Goodman, C. S. (1996). `Genetic dissection of structural and functional components of synaptic plasticity. I. Fasciclin II

controls synaptic stabilization and growth', *Neuron*, *17*(4), 641–654. https://doi.org/10.1016/s0896-6273(00)80197-x

Schweigreiter R. (2006). `The dual nature of neurotrophins', *BioEssays : news and reviews in molecular, cellular and developmental biology*, *28*(6), 583–594. https://doi.org/10.1002/bies.20419

Shearin, H. K., Dvarishkis, A. R., Kozeluh, C. D., & Stowers, R. S. (2013). Expansion of the gateway multisite recombination cloning toolkit. PloS one, 8(10), e77724. https://doi.org/10.1371/journal.pone.0077724

Shearn, A., Rice, T., Garen, A., & Gehring, W. (1971). Imaginal disc abnormalities in lethal mutants of Drosophila. Proceedings of the National Academy of Sciences of the United States of America, 68(10), 2594–2598. https://doi.org/10.1073/pnas.68.10.2594

Shelton, D. L., Sutherland, J., Gripp, J., Camerato, T., Armanini, M. P., Phillips, H. S., Carroll, K., Spencer, S. D., & Levinson, A. D. (1995). `Human trks: molecular cloning, tissue distribution, and expression of extracellular domain immunoadhesins', *The Journal of neuroscience : the official journal of the Society for Neuroscience*, *15*(1 Pt 2), 477–491. https://doi.org/10.1523/JNEUROSCI.15-01-00477.1995

Sheng, M., Thompson, M. A., & Greenberg, M. E. (1991). `CREB: a Ca(2+)-regulated transcription factor phosphorylated by calmodulin-dependent kinases', *Science (New York, N.Y.)*, *252*(5011), 1427–1430. https://doi.org/10.1126/science.1646483

Shimazu, K., Zhao, M., Sakata, K., Akbarian, S., Bates, B., Jaenisch, R., & Lu, B. (2006). `NT-3 facilitates hippocampal plasticity and learning and memory by regulating neurogenesis', *Learning & memory (Cold Spring Harbor, N.Y.)*, *13*(3), 307–315. https://doi.org/10.1101/lm.76006

Sidorov, M. S., Auerbach, B. D., & Bear, M. F. (2013). `Fragile X mental retardation protein and synaptic plasticity', *Molecular brain*, *6*, 15. https://doi.org/10.1186/1756-6606-6-15

Siegal, M. L., & Hartl, D. L. (2000). Application of Cre/loxP in Drosophila. Site-specific recombination and transgene coplacement. Methods in molecular biology (Clifton, N.J.), 136, 487–495. https://doi.org/10.1385/1-59259-065-9:487

Sigrist, S. J., Reiff, D. F., Thiel, P. R., Steinert, J. R., & Schuster, C. M. (2003). `Experience-dependent strengthening of Drosophila neuromuscular junctions', *The Journal of neuroscience: the official journal of the Society for Neuroscience*, *23*(16), 6546–6556. https://doi.org/10.1523/JNEUROSCI.23-16-06546.2003

Sigrist, S. J., & Schmitz, D. (2011). `Structural and functional plasticity of the cytoplasmic active zone', *Current opinion in neurobiology*, *21*(1), 144–150. https://doi.org/10.1016/j.conb.2010.08.012

Sigrist, S. J., Thiel, P. R., Reiff, D. F., Lachance, P. E., Lasko, P., & Schuster, C. M. (2000). `Postsynaptic translation affects the efficacy and morphology of neuromuscular junctions', *Nature*, *405*(6790), 1062–1065. https://doi.org/10.1038/35016598

Silva, A. J., Paylor, R., Wehner, J. M., & Tonegawa, S. (1992). `Impaired spatial learning in alpha-calcium-calmodulin kinase II mutant mice', *Science (New York, N.Y.)*, *257*(5067), 206–211. https://doi.org/10.1126/science.1321493

Silva, A. J., Stevens, C. F., Tonegawa, S., & Wang, Y. (1992). `Deficient hippocampal long-term potentiation in alpha-calcium-calmodulin kinase II mutant mice', *Science (New York, N.Y.)*, *257*(5067), 201–206. https://doi.org/10.1126/science.1378648

Silva, B., Niehage, C., Maglione, M., Hoflack, B., Sigrist, S. J., Wassmer, T., Pavlowsky, A., & Preat, T. (2020). `Interactions between amyloid precursor protein-like (APPL) and MAGUK scaffolding proteins contribute to appetitive long-term memory in *Drosophila melanogaster*' *Journal of neurogenetics*, *34*(1), 92–105. https://doi.org/10.1080/01677063.2020.1712597

Simpson, J. H., & Looger, L. L. (2018). `Functional Imaging and Optogenetics in *Drosophila*', *Genetics*, *208*(4), 1291–1309. https://doi.org/10.1534/genetics.117.300228

Singhania, A., & Grueber, W. B. (2014). `Development of the embryonic and larval peripheral nervous system of Drosophila', *Wiley interdisciplinary reviews. Developmental biology*, *3*(3), 193–210. https://doi.org/10.1002/wdev.135

Skaper S. D. (2012). The neurotrophin family of neurotrophic factors: an overview. Methods in molecular biology (Clifton, N.J.), 846, 1–12. https://doi.org/10.1007/978-1-61779-536-7_1

Smith, L. A., Wang, X., Peixoto, A. A., Neumann, E. K., Hall, L. M., & Hall, J. C. (1996). `A Drosophila calcium channel alpha1 subunit gene maps to a genetic locus associated with behavioral and visual defects', *The Journal of neuroscience : the official journal of the Society for Neuroscience*, *16*(24), 7868–7879. https://doi.org/10.1523/JNEUROSCI.16-24-07868.1996

Snow, P. M., Patel, N. H., Harrelson, A. L., & Goodman, C. S. (1987). `Neural-specific carbohydrate moiety shared by many surface glycoproteins in Drosophila and grasshopper embryos', *The Journal of neuroscience : the official journal of the Society for Neuroscience*, *7*(12), 4137–4144. https://doi.org/10.1523/JNEUROSCI.07-12-04137.1987

Sone, M., Suzuki, E., Hoshino, M., Hou, D., Kuromi, H., Fukata, M., Kuroda, S., Kaibuchi, K., Nabeshima, Y., & Hama, C. (2000). `Synaptic development is controlled in the periactive zones of Drosophila synapses', *Development (Cambridge, England)*, *127*(19), 4157–4168. https://doi.org/10.1242/dev.127.19.4157

Srinivasan, M., Edman, C. F., & Schulman, H. (1994). `Alternative splicing introduces a nuclear localization signal that targets multifunctional CaM kinase to the nucleus', *The Journal of cell biology*, *126*(4), 839–852. https://doi.org/10.1083/jcb.126.4.839

Stephens, H. E., Belliveau, A. C., Gupta, J. S., Mirkovic, S., & Kablar, B. (2005). `The role of neurotrophins in the maintenance of the spinal cord motor neurons and the dorsal root ganglia proprioceptive sensory neurons', *International journal of developmental neuroscience : the official journal of the International Society for Developmental Neuroscience*, *23*(7), 613–620. https://doi.org/10.1016/j.ijdevneu.2005.07.002

Stevens C. F. (1998). `A million dollar question: does LTP = memory?', *Neuron*, *20*(1), 1–2. https://doi.org/10.1016/s0896-6273(00)80426-2

Steward, O., & Levy, W. B. (1982). `Preferential localization of polyribosomes under the base of dendritic spines in granule cells of the dentate gyrus', *The Journal of neuroscience : the official journal of the Society for Neuroscience*, *2*(3), 284–291. https://doi.org/10.1523/JNEUROSCI.02-03-00284.1982

Stocker, B., Bochow, C., Damrau, C., Mathejczyk, T., Wolfenberg, H., Colomb, J., Weber, C., Ramesh, N., Duch, C., Biserova, N. M., Sigrist, S., & Pflüger, H. J. (2018). `Structural and Molecular Properties of Insect Type II Motor Axon Terminals', *Frontiers in systems neuroscience*, *12*, 5. https://doi.org/10.3389/fnsys.2018.00005

Stoilov, P., Castren, E., & Stamm, S. (2002). `Analysis of the human TrkB gene genomic organization reveals novel TrkB isoforms, unusual gene length, and splicing mechanism', *Biochemical and biophysical research communications*, *290*(3), 1054–1065. https://doi.org/10.1006/bbrc.2001.6301

Stollewerk, A., & Seyfarth, E. A. (2008). `Evolutionary changes in sensory precursor formation in arthropods: embryonic development of leg sensilla in the spider Cupiennius salei', *Developmental biology*, *313*(2), 659–673. https://doi.org/10.1016/j.ydbio.2007.11.003

Sturtevant, A. H. (1915). Experiments on sex recognition and the problem of sexual selection in Drosophilia. Journal of Animal Behavior, 5(5), 351.

Südhof T. C. (2012). `Calcium control of neurotransmitter release', *Cold Spring Harbor perspectives in biology*, *4*(1), a011353. https://doi.org/10.1101/cshperspect.a011353

Sullivan, K. M., Scott, K., Zuker, C. S., & Rubin, G. M. (2000). `The ryanodine receptor is essential for larval development in Drosophila melanogaster', *Proceedings of the National Academy of Sciences of the United States of America*, *97*(11), 5942–5947. https://doi.org/10.1073/pnas.110145997

Suslak, T. J., Watson, S., Thompson, K. J., Shenton, F. C., Bewick, G. S., Armstrong, J. D., & Jarman, A. P. (2015). `Piezo Is Essential for Amiloride-Sensitive Stretch-Activated Mechanotransduction in Larval Drosophila Dorsal Bipolar Dendritic Sensory Neurons', *PloS one*, *10*(7), e0130969. https://doi.org/10.1371/journal.pone.0130969

Sutcliffe, B., Forero, M. G., Zhu, B., Robinson, I. M., & Hidalgo, A. (2013). `Neuron-type specific functions of DNT1, DNT2 and Spz at the Drosophila neuromuscular junction', *PloS one*, *8*(10), e75902. https://doi.org/10.1371/journal.pone.0075902

Sweatt J. D. (1999). `Toward a molecular explanation for long-term potentiation', *Learning & memory (Cold Spring Harbor, N.Y.)*, *6*(5), 399–416. https://doi.org/10.1101/lm.6.5.399

Takamatsu, Y., Kishimoto, Y., & Ohsako, S. (2003). `Immunohistochemical study of Ca2+/calmodulin-dependent protein kinase II in the Drosophila brain using a specific monoclonal antibody', *Brain research*, *974*(1-2), 99–116. https://doi.org/10.1016/s0006-8993(03)02562-9

Takeshima, H., Iino, M., Takekura, H., Nishi, M., Kuno, J., Minowa, O., Takano, H., & Noda, T. (1994). `Excitation-contraction uncoupling and muscular degeneration in

mice lacking functional skeletal muscle ryanodine-receptor gene', *Nature*, *369*(6481), 556–559. https://doi.org/10.1038/369556a0

Takeuchi, T., Duszkiewicz, A. J., & Morris, R. G. (2013). `The synaptic plasticity and memory hypothesis: encoding, storage and persistence', *Philosophical transactions of the Royal Society of London. Series B, Biological sciences*, *369*(1633), 20130288. https://doi.org/10.1098/rstb.2013.0288

Tauszig, S., Jouanguy, E., Hoffmann, J. A., & Imler, J. L. (2000). `Toll-related receptors and the control of antimicrobial peptide expression in Drosophila', *Proceedings of the National Academy of Sciences of the United States of America*, *97*(19), 10520–10525. https://doi.org/10.1073/pnas.180130797

Thomas, U., Kim, E., Kuhlendahl, S., Koh, Y. H., Gundelfinger, E. D., Sheng, M., Garner, C. C., & Budnik, V. (1997). `Synaptic clustering of the cell adhesion molecule fasciclin II by discs-large and its role in the regulation of presynaptic structure', *Neuron*, *19*(4), 787–799. https://doi.org/10.1016/s0896-6273(00)80961-7

Thurmond, J., Goodman, J. L., Strelets, V. B., Attrill, H., Gramates, L. S., Marygold, S. J., Matthews, B. B., Millburn, G., Antonazzo, G., Trovisco, V., Kaufman, T. C., Calvi, B. R., & FlyBase Consortium (2019). `FlyBase 2.0: the next generation', *Nucleic acids research*, *47*(D1), D759–D765. https://doi.org/10.1093/nar/gky1003

Timmusk, T., Palm, K., Metsis, M., Reintam, T., Paalme, V., Saarma, M., & Persson, H. (1993). `Multiple promoters direct tissue-specific expression of the rat BDNF gene', *Neuron*, *10*(3), 475–489. https://doi.org/10.1016/0896-6273(93)90335-o

Tombes, R. M., Faison, M. O., & Turbeville, J. M. (2003). `Organization and evolution of multifunctional Ca(2+)/CaM-dependent protein kinase genes', *Gene*, *322*, 17–31. https://doi.org/10.1016/j.gene.2003.08.023

Tripodi, M., Evers, J. F., Mauss, A., Bate, M., & Landgraf, M. (2008). `Structural homeostasis: compensatory adjustments of dendritic arbor geometry in response to variations of synaptic input', *PLoS biology*, *6*(10), e260. https://doi.org/10.1371/journal.pbio.0060260

Tsubouchi, A., Caldwell, J. C., & Tracey, W. D. (2012). `Dendritic filopodia, Ripped Pocket, NOMPC, and NMDARs contribute to the sense of touch in Drosophila larvae', *Current biology: CB*, *22*(22), 2124–2134. https://doi.org/10.1016/j.cub.2012.09.019

Turrel, O., Ramesh, N., Escher, M. J. F., Pooryasin, A., & Sigrist, S. J. (2022). `Transient active zone remodeling in the Drosophila mushroom body supports memory', *Current biology : CB*, *32*(22), 4900–4913.e4. https://doi.org/10.1016/j.cub.2022.10.017

Ugur, B., Chen, K., & Bellen, H. J. (2016). `Drosophila tools and assays for the study of human diseases', *Disease models & mechanisms*, *9*(3), 235–244. https://doi.org/10.1242/dmm.023762

Ulian Benitez, Suzana (2018). Function of Kek-6 and DNT2 in structural synaptic plasticity in *Drosophila*. University of Birmingham. Ph.D.

Ulian-Benitez, S., Bishop, S., Foldi, I., Wentzell, J., Okenwa, C., Forero, M. G., Zhu, B., Moreira, M., Phizacklea, M., McIlroy, G., Li, G., Gay, N. J., & Hidalgo, A. (2017).

`Kek-6: A truncated-Trk-like receptor for Drosophila neurotrophin 2 regulates structural synaptic plasticity', *PLoS genetics*, *13*(8), e1006968. https://doi.org/10.1371/journal.pgen.1006968

Ultanir, S. K., Kim, J. E., Hall, B. J., Deerinck, T., Ellisman, M., & Ghosh, A. (2007). `Regulation of spine morphology and spine density by NMDA receptor signaling in vivo', *Proceedings of the National Academy of Sciences of the United States of America*, *104*(49), 19553–19558. https://doi.org/10.1073/pnas.0704031104

Ultsch, A., Schuster, C. M., Laube, B., Betz, H., & Schmitt, B. (1993). `Glutamate receptors of Drosophila melanogaster. Primary structure of a putative NMDA receptor protein expressed in the head of the adult fly', *FEBS letters*, *324*(2), 171–177. https://doi.org/10.1016/0014-5793(93)81387-f

Van Petegem F. (2012). `Ryanodine receptors: structure and function', *The Journal of biological chemistry*, *287*(38), 31624–31632. https://doi.org/10.1074/jbc.R112.349068

Van Vactor, D., & Sigrist, S. J. (2017). `Presynaptic morphogenesis, active zone organization and structural plasticity in Drosophila', *Current opinion in neurobiology*, *43*, 119–129. https://doi.org/10.1016/j.conb.2017.03.003

Venkatasubramanian, L., & Mann, R. S. (2019). `The development and assembly of the Drosophila adult ventral nerve cord', *Current opinion in neurobiology*, *56*, 135–143. https://doi.org/10.1016/j.conb.2019.01.013

Voelzmann, A., Okenve-Ramos, P., Qu, Y., Chojnowska-Monga, M., Del Caño-Espinel, M., Prokop, A., & Sanchez-Soriano, N. (2016). Tau and spectraplakins promote synapse formation and maintenance through Jun kinase and neuronal trafficking. eLife, 5, e14694. https://doi.org/10.7554/eLife.14694

Wan, H. I., DiAntonio, A., Fetter, R. D., Bergstrom, K., Strauss, R., & Goodman, C. S. (2000). `Highwire regulates synaptic growth in Drosophila', *Neuron*, *26*(2), 313–329. https://doi.org/10.1016/s0896-6273(00)81166-6

Wang, C. S., Kavalali, E. T., & Monteggia, L. M. (2022). `BDNF signaling in context: From synaptic regulation to psychiatric disorders', *Cell*, *185*(1), 62–76. https://doi.org/10.1016/j.cell.2021.12.003

Wang, J., Renger, J. J., Griffith, L. C., Greenspan, R. J., & Wu, C. F. (1994). `Concomitant alterations of physiological and developmental plasticity in Drosophila CaM kinase II-inhibited synapses', *Neuron*, *13*(6), 1373–1384. https://doi.org/10.1016/0896-6273(94)90422-7

Wang Z. W. (2008). Regulation of synaptic transmission by presynaptic CaMKII and BK channels. Molecular neurobiology, 38(2), 153–166. https://doi.org/10.1007/s12035-008-8039-7

Wasser, M., & Chia, W. (2003). The Drosophila EAST protein associates with a nuclear remnant during mitosis and constrains chromosome mobility. Journal of cell science, 116(Pt 9), 1733–1743. https://doi.org/10.1242/jcs.00379

West, R. J., Lu, Y., Marie, B., Gao, F. B., & Sweeney, S. T. (2015). `Rab8, POSH, and TAK1 regulate synaptic growth in a Drosophila model of frontotemporal dementia', *The Journal of cell biology*, *208*(7), 931–947. https://doi.org/10.1083/jcb.201404066

Whitlock, J. R., Heynen, A. J., Shuler, M. G., & Bear, M. F. (2006). `Learning induces long-term potentiation in the hippocampus', *Science (New York, N.Y.)*, *313*(5790), 1093–1097. https://doi.org/10.1126/science.1128134

WIESEL, T. N., & HUBEL, D. H. (1963). `Effects of visual deprivation on morphology and physiology of cells in the cats lateral geniculate body', *Journal of neurophysiology*, *26*, 978–993. https://doi.org/10.1152/jn.1963.26.6.978

Wiesel, T. N., & Hubel, D. H. (1965). `Comparison of the effects of unilateral and bilateral eye closure on cortical unit responses in kittens', *Journal of neurophysiology*, *28*(6), 1029–1040. https://doi.org/10.1152/jn.1965.28.6.1029

Woll, K. A., & Van Petegem, F. (2022). `Calcium-release channels: structure and function of IP_3 receptors and ryanodine receptors', *Physiological reviews*, *102*(1), 209–268. https://doi.org/10.1152/physrev.00033.2020

Xia, S., Miyashita, T., Fu, T. F., Lin, W. Y., Wu, C. L., Pyzocha, L., Lin, I. R., Saitoe, M., Tully, T., & Chiang, A. S. (2005). `NMDA receptors mediate olfactory learning and memory in Drosophila', *Current biology : CB*, *15*(7), 603–615. https://doi.org/10.1016/j.cub.2005.02.059

Xiang, Y., Yuan, Q., Vogt, N., Looger, L. L., Jan, L. Y., & Jan, Y. N. (2010). `Light-avoidance-mediating photoreceptors tile the Drosophila larval body wall', *Nature*, *468*(7326), 921–926. https://doi.org/10.1038/nature09576

Xiao, H., Sandaltzopoulos, R., Wang, H. M., Hamiche, A., Ranallo, R., Lee, K. M., Fu, D., & Wu, C. (2001). `Dual functions of largest NURF subunit NURF301 in nucleosome sliding and transcription factor interactions', *Molecular cell*, *8*(3), 531–543. https://doi.org/10.1016/s1097-2765(01)00345-8

Yacoubian, T. A., & Lo, D. C. (2000). `Truncated and full-length TrkB receptors regulate distinct modes of dendritic growth', *Nature neuroscience*, *3*(4), 342–349. https://doi.org/10.1038/73911

Yamamoto, M., Sobue, G., Mutoh, T., Li, M., Doyu, M., Mitsuma, T., & Kimata, K. (1993). `Gene expression of high- (p140trk) and low-affinity nerve growth factor receptor (LNGFR) in the adult and aged human peripheral nervous system', *Neuroscience letters*, *158*(1), 39–43. https://doi.org/10.1016/0304-3940(93)90607-m

Yan, Q., Rosenfeld, R. D., Matheson, C. R., Hawkins, N., Lopez, O. T., Bennett, L., & Welcher, A. A. (1997). `Expression of brain-derived neurotrophic factor protein in the adult rat central nervous system', *Neuroscience*, *78*(2), 431–448. https://doi.org/10.1016/s0306-4522(96)00613-6

Yan, X., Liu, J., Ye, Z., Huang, J., He, F., Xiao, W., Hu, X., & Luo, Z. (2016). `CaMKII-Mediated CREB Phosphorylation Is Involved in Ca2+-Induced BDNF mRNA Transcription and Neurite Outgrowth Promoted by Electrical Stimulation', *PloS one*, *11*(9), e0162784. https://doi.org/10.1371/journal.pone.0162784

Yan, Z., Zhang, W., He, Y., Gorczyca, D., Xiang, Y., Cheng, L. E., Meltzer, S., Jan, L. Y., & Jan, Y. N. (2013). `Drosophila NOMPC is a mechanotransduction channel subunit for gentle-touch sensation', *Nature*, *493*(7431), 221–225. https://doi.org/10.1038/nature11685

Yasuda, R., Hayashi, Y., & Hell, J. W. (2022). CaMKII: a central molecular organizer of synaptic plasticity, learning and memory. Nature reviews. Neuroscience, 23(11), 666–682. https://doi.org/10.1038/s41583-022-00624-2

Yeh, E., Gustafson, K., & Boulianne, G. L. (1995). Green fluorescent protein as a vital marker and reporter of gene expression in Drosophila. Proceedings of the National Academy of Sciences of the United States of America, 92(15), 7036–7040. https://doi.org/10.1073/pnas.92.15.7036

Yeh, F. C., Kao, C. F., & Kuo, P. H. (2015). `Explore the Features of Brain-Derived Neurotrophic Factor in Mood Disorders', *PloS one*, *10*(6), e0128605. https://doi.org/10.1371/journal.pone.0128605

Yu, Z., Ren, M., Wang, Z., Zhang, B., Rong, Y. S., Jiao, R., & Gao, G. (2013). `Highly efficient genome modifications mediated by CRISPR/Cas9 in Drosophila', *Genetics*, *195*(1), 289–291. https://doi.org/10.1534/genetics.113.153825

Zarin, A. A., Mark, B., Cardona, A., Litwin-Kumar, A., & Doe, C. Q. (2019). `A multilayer circuit architecture for the generation of distinct locomotor behaviors in *Drosophila*', *eLife*, *8*, e51781. https://doi.org/10.7554/eLife.51781

Zhang, W., Ge, W., & Wang, Z. (2007). `A toolbox for light control of Drosophila behaviors through Channelrhodopsin 2-mediated photoactivation of targeted neurons', *The European journal of neuroscience*, *26*(9), 2405–2416. https://doi.org/10.1111/j.1460-9568.2007.05862.x

Zhang, Y. Q., Bailey, A. M., Matthies, H. J., Renden, R. B., Smith, M. A., Speese, S. D., Rubin, G. M., & Broadie, K. (2001). `Drosophila fragile X-related gene regulates the MAP1B homolog Futsch to control synaptic structure and function', *Cell*, *107*(5), 591–603. https://doi.org/10.1016/s0092-8674(01)00589-x

Zhou, Y., Takahashi, E., Li, W., Halt, A., Wiltgen, B., Ehninger, D., Li, G. D., Hell, J. W., Kennedy, M. B., & Silva, A. J. (2007). `Interactions between the NR2B receptor and CaMKII modulate synaptic plasticity and spatial learning', *The Journal of neuroscience : the official journal of the Society for Neuroscience*, *27*(50), 13843–13853. https://doi.org/10.1523/JNEUROSCI.4486-07.2007

Zhu, B., Pennack, J. A., McQuilton, P., Forero, M. G., Mizuguchi, K., Sutcliffe, B., Gu, C. J., Fenton, J. C., & Hidalgo, A. (2008). `Drosophila neurotrophins reveal a common mechanism for nervous system formation', *PLoS biology*, *6*(11), e284. https://doi.org/10.1371/journal.pbio.0060284

Zwart, M. F., Randlett, O., Evers, J. F., & Landgraf, M. (2013). `Dendritic growth gated by a steroid hormone receptor underlies increases in activity in the developing Drosophila locomotor system', *Proceedings of the National Academy of Sciences of the United States of America*, *110*(40), E3878–E3887. https://doi.org/10.1073/pnas.1311711110

APPENDIX I: BASIC GENETICS PROTOCOLS

Figure A1.1 - 2nd and 3rd combinations protocol

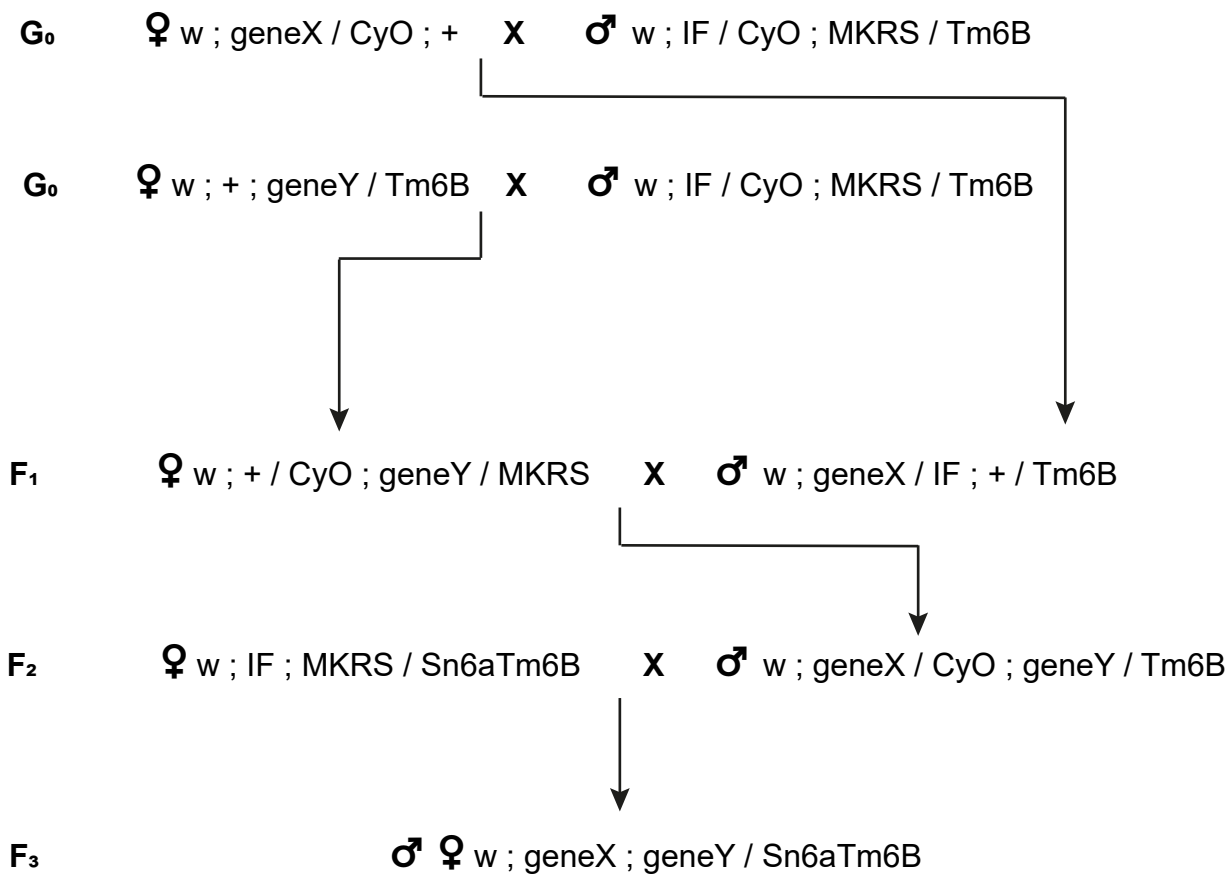


Figure A1.2 - X and 3rd combinations protocol

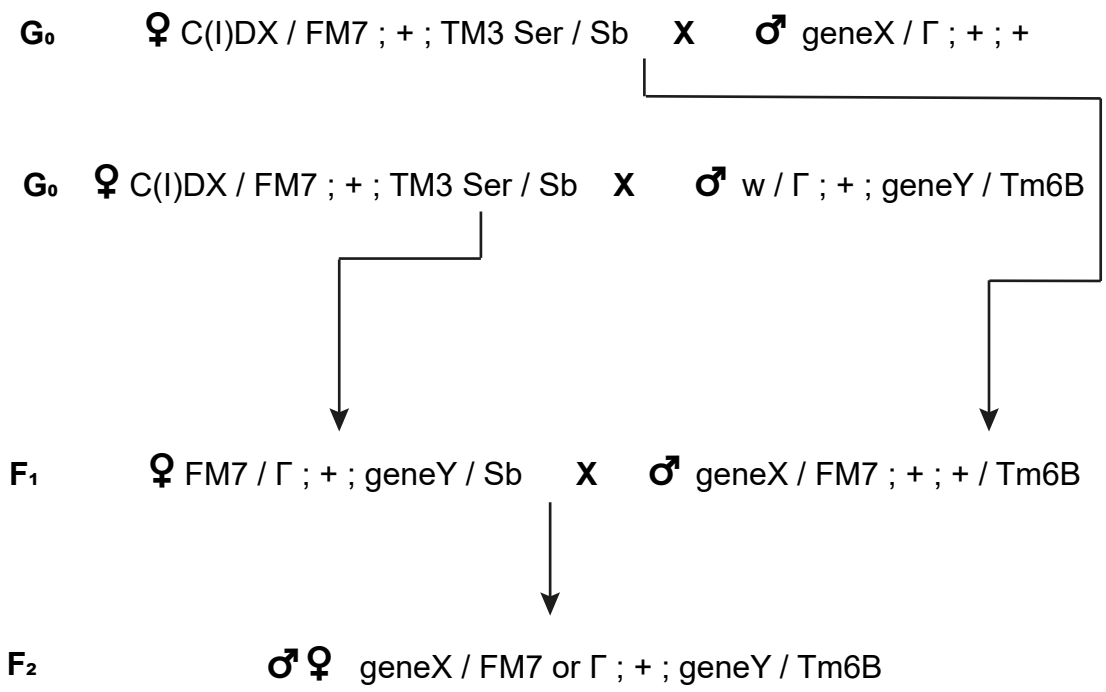
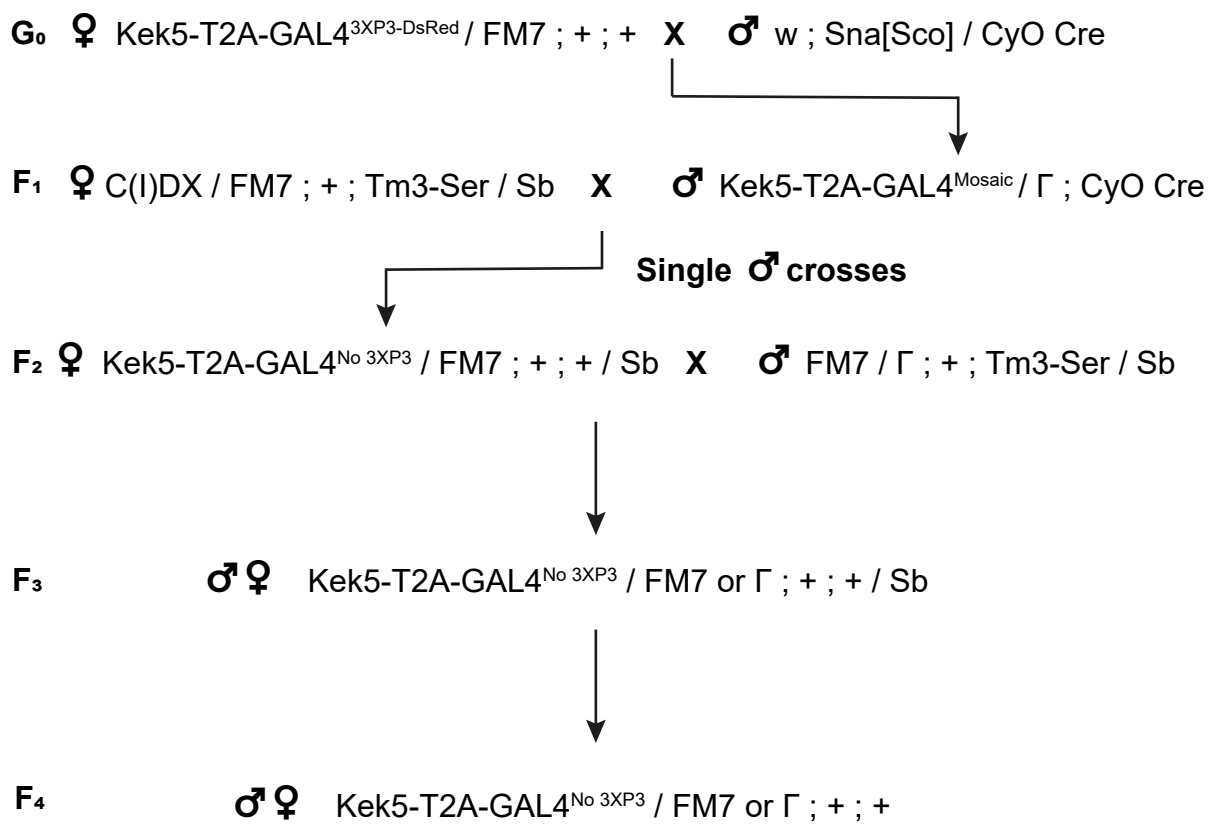


Figure A1.3 - Removal of 3XP3-DsRed from Kek5-T2A-GAL4



APPENDIX II: STATISICAL INFORMATION

Chapter 3: Spatial distribution of *keks*

FIGURE		SAMPLE TYPE	GENOTYPE/ CONDITION	SAMPLE SIZE		NORMALITY TESTS			TEST	p value	POST-HOC TEST & MULTIPLE COMPARISONS		
				Larvae	Replicates	TEST	DISTRIBUTION	p value			TEST	SAMPLES COMPARED	Adjusted p value
3.1	a'	Gel intensity of PCR product from larval CNS cDNA	Kek1 - 18oC	10	4	Shapiro-Wilk	Normal	0.851	Ordinary one-way ANOVA	0.2543			
			Kek1 - 25oC	10			Normal	0.7867					
			Kek1 - 30oC	10			Normal	0.2576					
	b'		Kek2 - 18oC	10	5	Shapiro-Wilk	Normal	0.8476	Ordinary one-way ANOVA	0.5635			
			Kek2 - 25oC	10			Normal	0.1793					
			Kek2 - 30oC	10			Normal	0.9334					
	c'		Kek3 - 18oC	10	5	Shapiro-Wilk	Normal	0.1056	Ordinary one-way ANOVA	0.7043			
			Kek3 - 25oC	10			Normal	0.462					
			Kek3 - 30oC	10			Not Normal	0.0425					
	d'		Kek4 - 18oC	10	5	Shapiro-Wilk	Normal	0.9727	Ordinary one-way ANOVA	0.4904			
			Kek4 - 25oC	10			Normal	0.8564					
			Kek4 - 30oC	10			Normal	0.1787					
	e'		Kek5 - 18oC	10	5	Shapiro-Wilk	Normal	0.4223	Ordinary one-way ANOVA	0.1543			
			Kek5 - 25oC	10			Normal	0.5506					
			Kek5 - 30oC	10			Normal	0.8235					
	f'		Kek6 - 18oC	10	5	Shapiro-Wilk	Normal	0.5188	Ordinary one-way ANOVA	0.3959			
			Kek6 - 25oC	10			Normal	0.9628					
			Kek6 - 30oC	10			Not Normal	0.0361					
	a'		Kek1 - 18oC	5	4	Shapiro-Wilk	Normal	0.696	Ordinary one-way ANOVA	0.5033			
			Kek1 - 25oC	5			Normal	0.4871					
			Kek1 - 30oC	5			Normal	0.3723					
	b'		Kek2 - 18oC	5	5	Shapiro-Wilk	Not Normal	0.0001	Kruskal-Wallis	>0.9999			
			Kek2 - 25oC	5			Not Normal	0.0001					
			Kek2 - 30oC	5			Not Normal	0.0001					
	c'	Gel intensity	Kek3 - 18oC	5	5	Shapiro-Wilk	Not Normal	0.0001	Kruskal-Wallis	>0.9999			
			Kek3 - 25oC	5			Not Normal	0.0001					

3.2		of PCR product from larval BW cDNA	Kek3 - 30oC	5			Not Normal	0.0001					
	d'		Kek4 - 18oC	5			Not Normal	0.032					
			Kek4 - 25oC	5	5	Shapiro-Wilk	Normal	0.4345	Ordinary one-way ANOVA	0.9501			
			Kek4 - 30oC	5			Normal	0.0854					
	e'		Kek5 - 18oC	5			Normal	0.1747					
			Kek5 - 25oC	5	5	Shapiro-Wilk	Normal	0.5429	Ordinary one-way ANOVA	0.3386			
			Kek5 - 30oC	5			Normal	0.2222					
	f'		Kek6 - 18oC	5			Not Normal	0.0273					
			Kek6 - 25oC	5	5	Shapiro-Wilk	Not Normal	0.0302	Kruskal-Wallis	0.9956			
			Kek6 - 30oC	5			Not Normal	0.045					

Chapter 4: Differential regulation of calcium signalling by *keks*													
FIGURE		SAMPLE TYPE	GENOTYPE	SAMPLE SIZE		NORMALITY TESTS			TEST	p value	POST-HOC TEST & MULTIPLE COMPARISONS		
				Larvae	Boutons	TEST	DISTRIBUTION	p value			TEST	SAMPLES COMPARED	Adjusted p value
4.3	B	Max intensity Stimulation 1	Control (D42>ReaChR, GCAMP)	6	14	Shapiro-Wilk	Not Normal	0.0475	Unpaired student's t-test	0.097			
			Kek1 OE (D42>ReaChR, GCAMP, Kek1)	6	12		Normal	0.3042					
	B'	Max intensity Stimulation 2	Control (D42>ReaChR, GCAMP)	6	14	Shapiro-Wilk	Normal	0.2936	Unpaired student's t-test	0.0733			
			Kek1 OE (D42>ReaChR, GCAMP, Kek1)	5	10		Normal	0.8458					
	C	Min intensity Stimulation 1	Control (D42>ReaChR, GCAMP)	6	14	Shapiro-Wilk	Normal	0.1603	Unpaired student's t-test	0.0093			
			Kek1 OE (D42>ReaChR, GCAMP, Kek1)	6	12		Normal	0.0978					
	C'	Min intensity Stimulation 2	Control (D42>ReaChR, GCAMP)	6	14	Shapiro-Wilk	Normal	0.2412	Unpaired student's t-test	0.1403			
			Kek1 OE (D42>ReaChR, GCAMP, Kek1)	5	10		Normal	0.3579					
	B	Max intensity Stimulation 1	Control (D42>ReaChR, GCAMP)	6	14	Shapiro-Wilk	Not Normal	0.0475	Mann-Whitney	0.2297			
			Kek2 OE (D42>ReaChR, GCAMP, Kek2)	6	17		Not Normal	0.0023					

4.4	B'	Max intensity Stimulation 2	Control (D42>ReaChR, GCAMP)	6	14	Shapiro-Wilk	Normal	0.2936	Unpaired student's t-test	0.0129			
			Kek2 OE (D42>ReaChR, GCAMP, Kek2)	6	17		Not Normal	0.0005					
	C	Min intensity Stimulation 1	Control (D42>ReaChR, GCAMP)	6	14	Shapiro-Wilk	Normal	0.1603	Unpaired student's t-test	<0.0001			
			Kek2 OE (D42>ReaChR, GCAMP, Kek2)	6	17		Normal	0.3188					
	C'	Min intensity Stimulation 2	Control (D42>ReaChR, GCAMP)	6	14	Shapiro-Wilk	Normal	0.2412	Unpaired student's t-test	0.0007			
			Kek2 OE (D42>ReaChR, GCAMP, Kek2)	6	17		Normal	0.0775					
4.5	B	Max intensity Stimulation 1	Control (D42>ReaChR, GCAMP)	6	14	Shapiro-Wilk	Not Normal	0.0475	Unpaired student's t-test	0.102			
			Kek3 OE (D42>ReaChR, GCAMP, Kek3)	3	5		Normal	0.9002					
	B'	Max intensity Stimulation 2	Control (D42>ReaChR, GCAMP)	6	14	Shapiro-Wilk	Normal	0.2936	Unpaired student's t-test	0.4663			
			Kek3 OE (D42>ReaChR, GCAMP, Kek3)	3	5		Normal	0.4481					
	C	Min intensity Stimulation 1	Control (D42>ReaChR, GCAMP)	6	14	Shapiro-Wilk	Normal	0.1603	Unpaired student's t-test	0.3976			
			Kek3 OE (D42>ReaChR, GCAMP, Kek3)	3	5		Normal	0.6434					

	C'	Min intensity Stimulation 2	Control (D42>ReaChR, GCAMP)	6	14	Shapiro-Wilk	Normal	0.2412	Unpaired student's t-test	0.0296			
			Kek3 OE (D42>ReaChR, GCAMP, Kek3)	3	5		Normal	0.0845					
4.6	B	Max intensity Stimulation 1	Control (D42>ReaChR, GCAMP)	6	14	Shapiro-Wilk	Not Normal	0.0475	Unpaired student's t-test	0.0134			
			Kek4 OE (D42>ReaChR, GCAMP, Kek4)	7	10		Normal	0.1163					
	B'	Max intensity Stimulation 2	Control (D42>ReaChR, GCAMP)	6	14	Shapiro-Wilk	Normal	0.2936	Unpaired student's t-test	0.0105			
			Kek4 OE (D42>ReaChR, GCAMP, Kek4)	7	10		Normal	0.2013					
	C	Min intensity Stimulation 1	Control (D42>ReaChR, GCAMP)	6	14	Shapiro-Wilk	Normal	0.1603	Unpaired student's t-test	0.0739			
			Kek4 OE (D42>ReaChR, GCAMP, Kek4)	7	10		Normal	0.2743					
	C'	Min intensity Stimulation 2	Control (D42>ReaChR, GCAMP)	6	14	Shapiro-Wilk	Normal	0.2412	Unpaired student's t-test	0.0029			
			Kek4 OE (D42>ReaChR, GCAMP, Kek4)	7	10		Normal	0.5419					
	B	Max intensity Stimulation 1	Control (D42>ReaChR, GCAMP)	6	14	Shapiro-Wilk	Not Normal	0.0475	Unpaired student's t-test	0.5044			
			Kek5 OE (D42>ReaChR, GCAMP, Kek5)	7	14		Normal	0.3574					

4.7	B'	Max intensity Stimulation 2	Control (D42>ReaChR, GCAMP)	6	14	Shapiro-Wilk	Normal	0.2936	Unpaired student's t-test	0.3494			
			Kek5 OE (D42>ReaChR, GCAMP, Kek5)	7	14		Normal	0.4497					
	C	Min intensity Stimulation 1	Control (D42>ReaChR, GCAMP)	6	14	Shapiro-Wilk	Normal	0.1603	Unpaired student's t-test	0.5635			
			Kek5 OE (D42>ReaChR, GCAMP, Kek5)	7	14		Normal	0.093					
	C'	Min intensity Stimulation 2	Control (D42>ReaChR, GCAMP)	6	14	Shapiro-Wilk	Normal	0.2412	Unpaired student's t-test	0.3286			
			Kek5 OE (D42>ReaChR, GCAMP, Kek5)	7	14		Normal	0.0534					
4.8	B	Max intensity Stimulation 1	Control (D42>ReaChR, GCAMP)	6	14	Shapiro-Wilk	Not Normal	0.0475	Unpaired student's t-test	0.6524			
			Kek6 OE (D42>ReaChR, GCAMP, Kek6)	8	23		Normal	0.5949					
	B'	Max intensity Stimulation 2	Control (D42>ReaChR, GCAMP)	6	14	Shapiro-Wilk	Normal	0.2936	Unpaired student's t-test	0.4427			
			Kek6 OE (D42>ReaChR, GCAMP, Kek6)	8	23		Normal	0.5398					
	C	Min intensity Stimulation 1	Control (D42>ReaChR, GCAMP)	6	14	Shapiro-Wilk	Normal	0.1603	Unpaired student's t-test	0.0163			
			Kek6 OE (D42>ReaChR, GCAMP, Kek6)	8	23		Normal	0.3576					

	C'	Min intensity Stimulation 2	Control (D42>ReaChR, GCAMP)	6	14	Shapiro-Wilk	Normal	0.2412	Unpaired student's t-test	0.013			
			Kek6 OE (D42>ReaChR, GCAMP, Kek6)	8	23		Normal	0.9528					
				Larvae	NMJ 6/7 (A3/4)								
4.9	B	Pearson's correlation coefficient	Background	3	6	Shapiro-Wilk	Normal	0.2902	Unpaired student's t-test	0.0026			
			Axonal Terminal	3	6		Normal	0.7132					
				Larvae	Boutons (Cac dots)								
	B	No. of Cac dots / Bouton volume	Control (cac-sfGFP;D42-GAL4/+)	4	15	Shapiro-Wilk	Not Normal	0.0019	Kruskal-Wallis	0.0015	Dunn's	-	-
			Kek4 OE (cac-sfGFP;D42>Kek4)	7	16		Not Normal	0.0039				Control vs Kek4 OE	0.0065
			Kek6 OE (cac-sfGFP;D42>Kek6)	6	20		Normal	0.1075				Control vs Kek6 OE	0.0016
	C	Mean Volume of Cac dots	Control (cac-sfGFP;D42-GAL4/+)	4	15	Shapiro-Wilk	Not Normal	<0.0001	Kruskal-Wallis	0.0006	Dunn's	-	-
			Kek4 OE (cac-sfGFP;D42>Kek4)	7	16		Not Normal	0.0005				Control vs Kek4 OE	0.0002
			Kek6 OE (cac-sfGFP;D42>Kek6)	6	20		Not Normal	0.0001				Control vs Kek6 OE	0.0487
	D	Cac intensity	Control (cac-sfGFP;D42-GAL4/+)	4	15 (146)	Shapiro-Wilk	Not Normal	<0.0001	Kruskal-Wallis	<0.0001	Dunn's	-	-
			Kek4 OE (cac-sfGFP;D42>Kek4)	7	16 (213}		Not Normal	<0.0001				Control vs Kek4 OE	<0.0001

4.10			Kek6 OE (cac-sfGFP;D42>Kek6)	6	20 (141)		Not Normal	<0.0001				Control vs Kek6 OE	0.6785
	E	Total Cac volume / Bouton volume	Control (cac-sfGFP;D42-GAL4/+)	4	15	Shapiro-Wilk	Normal	0.0544	Kruskal-Wallis	0.0038	Dunn's	-	-
			Kek4 OE (cac-sfGFP;D42>Kek4)	7	16		Not Normal	0.0016				Control vs Kek4 OE	0.0099
			Kek6 OE (cac-sfGFP;D42>Kek6)	6	20		Not Normal	0.013				Control vs Kek6 OE	>0.9999
	F	Bouton volume	Control (cac-sfGFP;D42-GAL4/+)	4	15	Shapiro-Wilk	Normal	0.0897	Kruskal-Wallis	0.0001	Dunn's	-	-
			Kek4 OE (cac-sfGFP;D42>Kek4)	7	16		Not Normal	0.0128				Control vs Kek4 OE	<0.0001
			Kek6 OE (cac-sfGFP;D42>Kek6)	6	20		Not Normal	0.0041				Control vs Kek6 OE	0.0375
	G	Mean Cac dot volume / Bouton volume	Control (cac-sfGFP;D42-GAL4/+)	4	15	Shapiro-Wilk	Not Normal	0.0056	Kruskal-Wallis	0.909			
			Kek4 OE (cac-sfGFP;D42>Kek4)	7	16		Not Normal	<0.0001					
			Kek6 OE (cac-sfGFP;D42>Kek6)	6	20		Not Normal	<0.0001					

Chapter 5: *keks* modulate NMJ morphology and activity-dependent structural plasticity													
FIGURE		SAMPLE TYPE	GENOTYPE/ CONDITION	SAMPLE SIZE		NORMALITY TESTS			TEST	p value	POST-HOC TEST & MULTIPLE COMPARISONS		
				Larvae	NMJ 6/7 (A3 only)	TEST	DISTRIBUTION	p value			TEST	SAMPLES COMPARED	Adjusted p value
5.1	B	Axonal terminal length / MSA*1000	Control (D42>ReaChR) No Stim	11	19	Shapiro-Wilk	Normal	0.4319	Ordinary one-way ANOVA	0.1966			
			Kek4 OE (D42>ReaChR, Kek4) No Stim	22	36	Shapiro-Wilk	Normal	0.9989					
			Kek4 KO (D42>ReaChR, kek4[20]/kek4[23]), No Stim	11	19	Shapiro-Wilk	Normal	0.8593					
	C	Axonal volume / MSA*1000	Control (D42>ReaChR) No Stim	7	11	Shapiro-Wilk	Normal	0.724	Ordinary one-way ANOVA	0.0104	Tukey's	Control No Activity vs. Kek4 OE No Activity	0.1175
			Kek4 OE (D42>ReaChR, Kek4) No Stim	12	20	Shapiro-Wilk	Normal	0.3744				Control No Activity vs. Kek4 LoF No Activity	0.6303
			Kek4 KO (D42>ReaChR, kek4[20]/kek4[23]), No Stim	5	9	Shapiro-Wilk	Normal	0.6471				Kek4 OE No Activity vs. Kek4 LoF No Activity	0.0125
	D	nc82 volume / Terminal Length	Control (D42>ReaChR) No Stim	7	11	Shapiro-Wilk	Normal	0.0575	Ordinary one-way ANOVA	0.2811			
			Kek4 OE (D42>ReaChR, Kek4) No Stim	12	20	Shapiro-Wilk	Normal	0.7794					

			Kek4 KO (D42>ReaChR, kek4[20]/kek4[23]), No Stim	5	9	Shapiro-Wilk	Normal	0.3793					
	E	nc82 volume / MSA*1000	Control (D42>ReaChR) No Stim	7	11	Shapiro-Wilk	Normal	0.5108	Ordinary one-way ANOVA	0.0913	Tukey's	Control No Activity vs. Kek4 OE No Activity	0.1222
			Kek4 OE (D42>ReaChR, Kek4) No Stim	12	20	Shapiro-Wilk	Normal	0.9454				Control No Activity vs. Kek4 LoF No Activity	0.9538
			Kek4 KO (D42>ReaChR, kek4[20]/kek4[23]), No Stim	5	9	Shapiro-Wilk	Normal	0.5226				Control No Activity vs. Kek4 LoF No Activity	0.1401
	B	Mature bouton number / MSA*1000	Control (D42>ReaChR) No Stim	4	8	Shapiro-Wilk	Normal	0.1471	Ordinary one-way ANOVA	0.5166			
			Kek4 OE (D42>ReaChR, Kek4) No Stim	10	16	Shapiro-Wilk	Normal	0.6503					
			Kek4 KO (D42>ReaChR, kek4[20]/kek4[23]), No Stim	6	10	Shapiro-Wilk	Not Normal	0.0342					
	C	Ghost bouton number / MSA*1000	Control (D42>ReaChR) No Stim	4	8	Shapiro-Wilk	Not Normal	<0.0001	Kruskal-Wallis	0.7314			
5.2			Kek4 OE (D42>ReaChR, Kek4) No Stim	10	16	Shapiro-Wilk	Not Normal	<0.0001					

			Kek4 KO (D42>ReaChR, kek4[20]/kek4[23]), No Stim	6	10	Shapiro-Wilk	Not Normal	<0.0001					
				Larvae	Boutons								
	D	Bouton Area (um^2)	Control (D42>ReaChR) No Stim	4	57	Shapiro-Wilk	Not Normal	0.0003	Kruskal-Wallis	0.3345			
			Kek4 OE (D42>ReaChR, Kek4) No Stim	10	220	Shapiro-Wilk	Not Normal	<0.0001					
			Kek4 KO (D42>ReaChR, kek4[20]/kek4[23]), No Stim	6	137	Shapiro-Wilk	Not Normal	<0.0001					
				Larvae	NMJs								
	B	Axonal terminal length / MSA*1000	Control (D42>ReaChR) No Stim	11	19	Shapiro-Wilk	Normal	0.4319	Ordinary one-way ANOVA	0.3698			
			Kek6 OE (D42>ReaChR, Kek6) No Stim	14	19	Shapiro-Wilk	Normal	0.592					
			Kek6 KO (D42>ReaChR, kek6[35]/kek6[34]) No Stim	21	30	Shapiro-Wilk	Normal	0.5978					
	C	Axonal volume / MSA*1000	Control (D42>ReaChR) No Stim	7	11	Shapiro-Wilk	Normal	0.724	Ordinary one-way ANOVA	0.2188			
			Kek6 OE (D42>ReaChR, Kek6) No Stim	7	11	Shapiro-Wilk	Normal	0.2492					

5.3			Kek6 KO (D42>ReaChR, kek6[35]/kek6[34]) No Stim	9	12	Shapiro-Wilk	Normal	0.4552					
	D	nc82 volume / Terminal Length	Control (D42>ReaChR) No Stim	7	11	Shapiro-Wilk	Normal	0.0575	Ordinary one-way ANOVA	0.4174			
			Kek6 OE (D42>ReaChR, Kek6) No Stim	7	11	Shapiro-Wilk	Normal	0.131					
			Kek6 KO (D42>ReaChR, kek6[35]/kek6[34]) No Stim	9	12	Shapiro-Wilk	Normal	0.0958					
	E	nc82 volume / MSA*1000	Control (D42>ReaChR) No Stim	7	11	Shapiro-Wilk	Normal	0.5108	Ordinary one-way ANOVA	0.0482	Tukey's	Control No Activity vs. Kek6 OE No Activity	0.2382
			Kek6 OE (D42>ReaChR, Kek6) No Stim	7	11	Shapiro-Wilk	Not Normal	0.0477				Kek6 OE No Activity vs. Kek6 LoF No Activity	0.0401
			Kek6 KO (D42>ReaChR, kek6[35]/kek6[34]) No Stim	9	12	Shapiro-Wilk	Normal	0.2844				Control No Activity vs. Kek6 LoF No Activity	0.6853
	B	Mature bouton number / MSA*1000	Control (D42>ReaChR) No Stim	4	8	Shapiro-Wilk	Normal	0.1471	Ordinary one-way ANOVA	0.0023	Tukey's	Control No Activity vs. Kek6 OE No Activity	0.0036
			Kek6 OE (D42>ReaChR, Kek6) No Stim	7	8	Shapiro-Wilk	Normal	0.4319				Kek6 OE No Activity vs. Kek6 LoF No Activity	0.9313

			Kek6 KO (D42>ReaChR, kek6[35]/kek6[34]) No Stim	12	18	Shapiro-Wilk	Normal	0.078				Control No Activity vs. Kek6 LoF No Activity	0.0069
5.4	C	Ghost bouton number / MSA*1000	Control (D42>ReaChR) No Stim	4	8	Shapiro-Wilk	Not Normal	<0.0001	Kruskal-Wallis		0.4581		
			Kek6 OE (D42>ReaChR, Kek6) No Stim	7	8	Shapiro-Wilk	Not Normal	0.0002					
			Kek6 KO (D42>ReaChR, kek6[35]/kek6[34]) No Stim	5	18	Shapiro-Wilk	Not Normal	0.0003					
				Larvae	Boutons								
	D	Bouton Area (um^2)	Control (D42>ReaChR) No Stim	4	57	Shapiro-Wilk	Not Normal	0.0003	Kruskal-Wallis		0.5346		
			Kek6 OE (D42>ReaChR, Kek6) No Stim	7	68	Shapiro-Wilk	Not Normal	0.0015					
			Kek6 KO (D42>ReaChR, kek6[35]/kek6[34]) No Stim	5	88	Shapiro-Wilk	Not Normal	<0.0001					
				Larvae	NMJs								
	B	Axonal terminal length / MSA*1000	Control (D42>ReaChR) No Stim	11	19	Shapiro-Wilk	Normal	0.4319	Unpaired student's t-test	0.9769			
			Control (D42>ReaChR) Stim	16	23	Shapiro-Wilk	Normal	0.5142					

5.5	C	Axonal volume / MSA*1000	Control (D42>ReaChR) No Stim	7	11	Shapiro-Wilk	Normal	0.724	Unpaired student's t-test	0.009			
			Control (D42>ReaChR) Stim	7	12	Shapiro-Wilk	Normal	0.374					
	D	nc82 volume / Terminal Length	Control (D42>ReaChR) No Stim	7	11	Shapiro-Wilk	Normal	0.0575	Unpaired student's t-test	0.0079			
			Control (D42>ReaChR) Stim	7	12	Shapiro-Wilk	Normal	0.4084					
	E	nc82 volume / MSA*1000	Control (D42>ReaChR) No Stim	7	11	Shapiro-Wilk	Normal	0.5108	Unpaired student's t-test	0.0036			
			Control (D42>ReaChR) Stim	7	12	Shapiro-Wilk	Normal	0.798					
	B	Mature bouton number / MSA*1000	Control (D42>ReaChR) No Stim	4	8	Shapiro-Wilk	Normal	0.1471	Unpaired student's t-test	0.0025			
			Control (D42>ReaChR) Stim	9	11	Shapiro-Wilk	Normal	0.3543					

5.6	C	Ghost bouton number / MSA*1000	Control (D42>ReaChR) No Stim	4	8	Shapiro-Wilk	Not Normal	<0.0001	Mann-Whitney	0.3064				
			Control (D42>ReaChR) Stim	9	11	Shapiro-Wilk	Not Normal	0.0005						
				Larvae	Boutons									
	D	Bouton Area (um^2)	Control (D42>ReaChR) No Stim	4	57	Shapiro-Wilk	Not Normal	0.0003	Mann-Whitney	0.1914				
			Control (D42>ReaChR) Stim	9	114	Shapiro-Wilk	Not Normal	<0.0001						
				Larvae	NMJs									
	B	Axonal terminal length / MSA*1000	Control (D42>ReaChR) No Stim	11	19	Shapiro-Wilk	Normal	0.4319	Ordinary one-way ANOVA	<0.0001	Tukey's	Control No Activity vs. Control Activity	>0.9999
												Control No Activity vs. Kek4 OE No Activity	0.9719
			Control (D42>ReaChR) Stim	16	23	Shapiro-Wilk	Normal	0.5142				Control No Activity vs. Kek4 OE Activity	<0.0001
												Control Activity vs. Kek4 OE No Activity	0.9728
			Kek4 OE (D42>ReaChR, Kek4) No Stim	22	36	Shapiro-Wilk	Normal	0.9989				Control Activity vs. Kek4 OE Activity	<0.0001

			Kek4 OE (D42>ReaChR, Kek4) Stim	20	33	Shapiro-Wilk	Normal	0.3839				Kek4 OE No Activity vs. Kek4 OE Activity	<0.0001
	C	Axonal volume / MSA*1000	Control (D42>ReaChR) No Stim	7	11	Shapiro-Wilk	Normal	0.724	Ordinary one-way ANOVA	0.0184	Tukey's	Control No Activity vs. Control Activity	0.0128
												Control No Activity vs. Kek4 OE No Activity	0.2212
			Control (D42>ReaChR) Stim	7	12	Shapiro-Wilk	Normal	0.374				Control No Activity vs. Kek4 OE Activity	0.4408
												Control Activity vs. Kek4 OE No Activity	0.2212
			Kek4 OE (D42>ReaChR, Kek4) No Stim	12	20	Shapiro-Wilk	Normal	0.3744				Control Activity vs. Kek4 OE Activity	0.151
			Kek4 OE (D42>ReaChR, Kek4) Stim	8	12	Shapiro-Wilk	Normal	0.0931				Kek4 OE No Activity vs. Kek4 OE Activity	0.5879
5.7													
			Control (D42>ReaChR) No Stim	7	11	Shapiro-Wilk	Normal	0.0575				Control vs. Control Activity	0.0025
												Control vs. Kek4 OE	0.6612

	D	nc82 volume / Terminal Length	Control (D42>ReaChR) Stim	7	12	Shapiro-Wilk	Normal	0.4084	Ordinary one-way ANOVA	<0.0001	Tukey's	Control vs. Kek4 OE Activity	0.2678
												Control Activity vs. Kek4 OE	<0.0001
			Kek4 OE (D42>ReaChR, Kek4) No Stim	12	20	Shapiro-Wilk	Normal	0.7794				Control Activity vs. Kek4 OE Activity	<0.0001
			Kek4 OE (D42>ReaChR, Kek4) Stim	8	12	Shapiro-Wilk	Normal	0.1122				Kek4 OE vs. Kek4 OE Activity	0.7941
	E	nc82 volume / MSA*1000	Control (D42>ReaChR) No Stim	7	11	Shapiro-Wilk	Normal	0.5108	Ordinary one-way ANOVA	<0.0001	Tukey's	Control vs. Control Activity	0.0061
												Control vs. Kek4 OE	0.5232
			Control (D42>ReaChR) Stim	7	12	Shapiro-Wilk	Normal	0.798				Control vs. Kek4 OE Activity	0.9891
												Control Activity vs. Kek4 OE	<0.0001
			Kek4 OE (D42>ReaChR, Kek4) No Stim	12	20	Shapiro-Wilk	Normal	0.9454				Control Activity vs. Kek4 OE Activity	0.0019

			Kek4 OE (D42>ReaChR, Kek4) Stim	8	12	Shapiro-Wilk	Normal	0.0689				Kek4 OE vs. Kek4 OE Activity	0.721
	B	Mature bouton number / MSA*1000	Control (D42>ReaChR) No Stim	4	8	Shapiro-Wilk	Normal	0.1471	Kruskal-Wallis	0.0056	Dunn's	Control No Activity vs. Control Activity	0.0145
												Control No Activity vs. Kek4 OE No Activity	>0.9999
			Control (D42>ReaChR) Stim	9	11	Shapiro-Wilk	Normal	0.3543				Control No Activity vs. Kek4 OE Activity	0.1497
												Control Activity vs. Kek4 OE No Activity	0.0387
			Kek4 OE (D42>ReaChR, Kek4) No Stim	10	16	Shapiro-Wilk	Normal	0.6503				Control Activity vs. Kek4 OE Activity	>0.9999
			Kek4 OE (D42>ReaChR, Kek4) Stim	13	24	Shapiro-Wilk	Not normal	0.0088				Kek4 OE No Activity vs. Kek4 OE Activity	0.4718
			Control (D42>ReaChR) No Stim	4	8	Shapiro-Wilk	Not Normal	<0.0001					

5.8	C	Ghost bouton number / MSA*1000	Control (D42>ReaChR) Stim	9	11	Shapiro-Wilk	Not Normal	0.0005	Kruskal-Wallis	0.5453			
			Kek4 OE (D42>ReaChR, Kek4) No Stim	10	16	Shapiro-Wilk	Not Normal	<0.0001					
			Kek4 OE (D42>ReaChR, Kek4) Stim	13	24	Shapiro-Wilk	Not Normal	<0.0001					
				Larvae	Boutons								
	D	Bouton Area (um^2)	Control (D42>ReaChR) No Stim	4	57	Shapiro-Wilk	Not Normal	0.0003	Kruskal-Wallis	0.2648			
			Control (D42>ReaChR) Stim	9	114	Shapiro-Wilk	Not Normal	<0.0001					
			Kek4 OE (D42>ReaChR, Kek4) No Stim	9	114	Shapiro-Wilk	Not Normal	<0.0001					

			Kek4 OE (D42>ReaChR, Kek4) Stim	9	253	Shapiro-Wilk	Not Normal	<0.0001					
				Larvae	NMJs								
	B	Axonal terminal length / MSA*1000	Control (D42>ReaChR) No Stim	11	19	Shapiro-Wilk	Normal	0.4319	Ordinary one-way ANOVA	0.0977			
			Control (D42>ReaChR) Stim	16	23	Shapiro-Wilk	Normal	0.5142					
			Kek4 KO (D42>ReaChR, kek4[20]/kek4[23]), No Stim	11	19	Shapiro-Wilk	Normal	0.8593					
			Kek4 KO (D42>ReaChR, kek4[20]/kek4[23]), Stim	8	14	Shapiro-Wilk	Normal	0.5232					
			Control (D42>ReaChR) No Stim	7	11	Shapiro-Wilk	Normal	0.724				Control No Activity vs. Control Activity	0.0088
												Control No Activity vs. Kek4 LoF No Activity	0.8265

5.9	C	Axonal volume / MSA*1000	Control (D42>ReaChR) Stim	7	12	Shapiro-Wilk	Normal	0.374	Ordinary one-way ANOVA	0.0009	Tukey's	Control No Activity vs. Kek4 LoF Activity	0.9999
												Control Activity vs. Kek4 LoF No Activity	0.0011
			Kek4 KO (D42>ReaChR, kek4[20]/kek4[23]), No Stim	5	9	Shapiro-Wilk	Normal	0.6471				Control Activity vs. Kek4 LoF Activity	0.0336
			Kek4 KO (D42>ReaChR, kek4[20]/kek4[23]), Stim	4	8	Shapiro-Wilk	Normal	0.3823				Kek4 LoF No Activity vs. Kek4 LoF Activity	0.8488
	D	nc82 volume / Terminal Length	Control (D42>ReaChR) No Stim	7	11	Shapiro-Wilk	Normal	0.0575	Ordinary one-way ANOVA	0.0006	Tukey's	Control vs. Control Activity	0.006
												Control vs. Kek4 LoF	0.8333
			Control (D42>ReaChR) Stim	7	12	Shapiro-Wilk	Normal	0.4084				Control vs. Kek4 LoF Activity	0.9925
												Control Activity vs. Kek4 LoF	0.0019
			Kek4 KO (D42>ReaChR, kek4[20]/kek4[23]), No Stim	5	9	Shapiro-Wilk	Normal	0.3793				Control Activity vs. Kek4 LoF Activity	0.0063

			Kek4 KO (D42>ReaChR, kek4[20]/kek4[23]), Stim	4	8	Shapiro-Wilk	Normal	0.8612				Kek4 LoF vs. Kek4 LoF Activity	0.9486
	E	nc82 volume / MSA*1000	Control (D42>ReaChR) No Stim	7	11	Shapiro-Wilk	Normal	0.5108	Ordinary one-way ANOVA	<0.0001	Tukey's	Control vs. Control Activity	0.0029
												Control vs. Kek4 LoF	0.4713
			Control (D42>ReaChR) Stim	7	12	Shapiro-Wilk	Normal	0.798				Control vs. Kek4 LoF Activity	0.3946
												Control Activity vs. Kek4 LoF	<0.0001
			Kek4 KO (D42>ReaChR, kek4[20]/kek4[23]), No Stim	5	9	Shapiro-Wilk	Normal	0.5226				Control Activity vs. Kek4 LoF Activity	<0.0001
			Kek4 KO (D42>ReaChR, kek4[20]/kek4[23]), Stim	4	8	Shapiro-Wilk	Normal	0.4137				Kek4 LoF vs. Kek4 LoF Activity	0.9981
			Control (D42>ReaChR) No Stim	4	8	Shapiro-Wilk	Normal	0.1471				Control No Activity vs. Control Activity	0.0239
												Control No Activity vs. Kek4 LoF No Activity	0.7718

	B	Mature bouton number / MSA*1000	Control (D42>ReaChR) Stim	9	11	Shapiro-Wilk	Normal	0.3543	Ordinary one-way ANOVA	0.0293	Tukey's	Control No Activity vs. Kek4 LoF Activity	0.6638
												Control Activity vs. Kek4 LoF No Activity	0.1357
			Kek4 KO (D42>ReaChR, kek4[20]/kek4[23]), No Stim	6	10	Shapiro-Wilk	Not Normal	0.0342				Control Activity vs. Kek4 LoF Activity	0.4384
			Kek4 KO (D42>ReaChR, kek4[20]/kek4[23]), Stim	4	6	Shapiro-Wilk	Normal	0.4397				Kek4 LoF No Activity vs. Kek4 LoF Activity	0.9863
5.1	C	Ghost bouton number / MSA*1000	Control (D42>ReaChR) No Stim	4	8	Shapiro-Wilk	Not Normal	<0.0001	Kruskal-Wallis	0.6084			
			Control (D42>ReaChR) Stim	9	11	Shapiro-Wilk	Not Normal	0.0005					
			Kek4 KO (D42>ReaChR, kek4[20]/kek4[23]), No Stim	6	10	Shapiro-Wilk	Not Normal	<0.0001					

			Kek4 KO (D42>ReaChR, kek4[20]/kek4[23]), Stim	4	6	Shapiro-Wilk	Not Normal	0.0058					
				Larvae	Boutons								
	D	Bouton Area (um^2)	Control (D42>ReaChR) No Stim	4	57	Shapiro-Wilk	Not Normal	0.0003	Kruskal-Wallis	0.1286			
			Control (D42>ReaChR) Stim	9	114	Shapiro-Wilk	Not Normal	<0.0001					
			Kek4 KO (D42>ReaChR, kek4[20]/kek4[23]), No Stim	6	137	Shapiro-Wilk	Not Normal	<0.0001					
			Kek4 KO (D42>ReaChR, kek4[20]/kek4[23]), Stim	4	68	Shapiro-Wilk	Not Normal	<0.0001					
				Larvae	NMJs								
			Control (D42>ReaChR) No Stim	11	19	Shapiro-Wilk	Normal	0.4319				Control No Activity vs. Control Activity	>0.9999
												Control No Activity vs. Kek6 OE No Activity	0.3462

	B	Axonal terminal length / MSA*1000	Control (D42>ReaChR) Stim	16	23	Shapiro-Wilk	Normal	0.5142	Ordinary one-way ANOVA	0.0029	Tukey's	Control No Activity vs. Kek6 OE Actvity	0.0105
												Control Activity vs. Kek6 OE No Activity	0.2935
			Kek6 OE (D42>ReaChR, Kek6) No Stim	14	19	Shapiro-Wilk	Normal	0.592				Control Activity vs. Kek6 OE Actvity	0.006
			Kek6 OE (D42>ReaChR, Kek6) Stim	23	39	Shapiro-Wilk	Normal	0.8428				Kek6 OE No Activity vs. Kek6 OE Actvity	0.4611
	C	Axonal volume / MSA*1000	Control (D42>ReaChR) No Stim	7	11	Shapiro-Wilk	Normal	0.724	Ordinary one-way ANOVA	<0.0001	Tukey's	Control No Activity vs. Control Activity	0.0118
												Control No Activity vs. Kek6 OE No Activity	0.9854
			Control (D42>ReaChR) Stim	7	12	Shapiro-Wilk	Normal	0.374				Control No Activity vs. Kek6 OE Actvity	<0.0001
												Control Activity vs. Kek6 OE No Activity	0.0106
			Kek6 OE (D42>ReaChR, Kek6) No Stim	7	11	Shapiro-Wilk	Normal	0.2492				Control Activity vs. Kek6 OE Actvity	0.2857

5.11			Kek6 OE (D42>ReaChR, Kek6) Stim	9	17	Shapiro-Wilk	Normal	0.0927				Kek6 OE No Activity vs. Kek6 OE Actvity	<0.0001
	D	nc82 volume / Terminal Length	Control (D42>ReaChR) No Stim	7	11	Shapiro-Wilk	Normal	0.0575	Ordinary one-way ANOVA	0.0366	Tukey's	Control vs. Control Activity	0.0235
												Control vs. Kek6 OE	0.7307
			Control (D42>ReaChR) Stim	7	12	Shapiro-Wilk	Normal	0.4084				Control vs. Kek6 OE Actvity	0.6357
												Control Activity vs. Kek6 OE	0.2266
			Kek6 OE (D42>ReaChR, Kek6) No Stim	7	11	Shapiro-Wilk	Normal	0.131				Control Activity vs. Kek6 OE Actvity	0.1735
			Kek6 OE (D42>ReaChR, Kek6) Stim	9	17	Shapiro-Wilk	Normal	0.0673				Kek6 OE vs. Kek6 OE Actvity	>0.9999
			Control (D42>ReaChR) No Stim	7	11	Shapiro-Wilk	Normal	0.5108				Control vs. Control Activity	0.0212
												Control vs. Kek6 OE	0.3635

	E	nc82 volume / MSA*1000	Control (D42>ReaChR) Stim	7	12	Shapiro-Wilk	Normal	0.798	Ordinary one-way ANOVA	0.0266	Tukey's	Control vs. Kek6 OE Actvity	0.0767
												Control Activity vs. Kek6 OE	0.5277
			Kek6 OE (D42>ReaChR, Kek6) No Stim	7	11	Shapiro-Wilk	Not Normal	0.0477				Control Activity vs. Kek6 OE Actvity	0.836
			Kek6 OE (D42>ReaChR, Kek6) Stim	9	17	Shapiro-Wilk	Normal	0.4984				Kek6 OE vs. Kek6 OE Actvity	0.9096
	B	Mature bouton number / MSA*1000	Control (D42>ReaChR) No Stim	4	8	Shapiro-Wilk	Normal	0.1471	Kruskal-Wallis	0.0055	Dunn's	Control No Activity vs. Control Activity	0.0289
												Control No Activity vs. Kek6 OE No Activity	0.0044
			Control (D42>ReaChR) Stim	9	11	Shapiro-Wilk	Normal	0.3543				Control No Activity vs. Kek6 OE Actvity	0.0375
												Control Activity vs. Kek6 OE No Activity	>0.9999
			Kek6 OE (D42>ReaChR, Kek6) No Stim	7	8	Shapiro-Wilk	Normal	0.4319				Control Activity vs. Kek6 OE Actvity	>0.9999

			Kek6 OE (D42>ReaChR, Kek6) Stim	14	22	Shapiro-Wilk	Normal	0.3088				Kek6 OE No Activity vs. Kek6 OE Actvity	>0.9999
5.12	C	Ghost bouton number / MSA*1000	Control (D42>ReaChR) No Stim	4	8	Shapiro-Wilk	Not Normal	<0.0001	Kruskal-Wallis	0.6849			
			Control (D42>ReaChR) Stim	9	11	Shapiro-Wilk	Not Normal	0.0005					
			Kek6 OE (D42>ReaChR, Kek6) No Stim	7	8	Shapiro-Wilk	Not Normal	0.0002					
			Kek6 OE (D42>ReaChR, Kek6) Stim	14	22	Shapiro-Wilk	Not Normal	<0.0001					
				Larvae	Boutons								
			Control (D42>ReaChR) No Stim	4	57	Shapiro-Wilk	Not Normal	0.0003					

	D	Bouton Area (um^2)	Control (D42>ReaChR) Stim	9	114	Shapiro-Wilk	Not Normal	<0.0001	Kruskal-Wallis	0.1046			
			Kek6 OE (D42>ReaChR, Kek6) No Stim	7	68	Shapiro-Wilk	Not Normal	0.0015					
			Kek6 OE (D42>ReaChR, Kek6) Stim	14	114	Shapiro-Wilk	Not Normal	<0.0001					
				Larvae	NMJs								
	B	Axonal terminal length / MSA*1000	Control (D42>ReaChR) No Stim	11	19	Shapiro-Wilk	Normal	0.4319	Ordinary one-way ANOVA	0.0055	Tukey's	Control No Activity vs. Control Activity	>0.9999
												Control No Activity vs. Kek6 LoF No Activity	0.6061
			Control (D42>ReaChR) Stim	16	23	Shapiro-Wilk	Normal	0.5142				Control No Activity vs. Kek6 LoF Activity	0.0092
												Control Activity vs. Kek6 LoF No Activity	0.5454
			Kek6 KO (D42>ReaChR, kek6[35]/kek6[34]) No Stim	21	30	Shapiro-Wilk	Normal	0.5978				Control Activity vs. Kek6 LoF Activity	0.0062

			Kek6 KO (D42>ReaChR, kek6[35]/kek6[34]) Stim	13	23	Shapiro-Wilk	Normal	0.9857				Kek6 LoF No Activity vs. Kek6 LoF Activity	0.0782
	C	Axonal volume / MSA*1000	Control (D42>ReaChR) No Stim	7	11	Shapiro-Wilk	Normal	0.724	Ordinary one-way ANOVA	0.0449	Tukey's	Control No Activity vs. Control Activity	0.0502
												Control No Activity vs. Kek6 LoF No Activity	0.4825
			Control (D42>ReaChR) Stim	7	12	Shapiro-Wilk	Normal	0.374				Control No Activity vs. Kek6 LoF Activity	0.9804
												Control Activity vs. Kek6 LoF No Activity	0.5213
			Kek6 KO (D42>ReaChR, kek6[35]/kek6[34]) No Stim	9	12	Shapiro-Wilk	Normal	0.4552				Control Activity vs. Kek6 LoF Activity	0.1038
			Kek6 KO (D42>ReaChR, kek6[35]/kek6[34]) Stim	6	11	Shapiro-Wilk	Normal	0.502				Kek6 LoF No Activity vs. Kek6 LoF Activity	0.7108
5.13													
			Control (D42>ReaChR) No Stim	7	11	Shapiro-Wilk	Normal	0.0575				Control vs. Control Activity	0.0229
												Control vs. Kek6 LoF	0.9982

	D	nc82 volume / Terminal Length	Control (D42>ReaChR) Stim	7	12	Shapiro-Wilk	Normal	0.4084	Ordinary one-way ANOVA	0.001	Tukey's	Control vs. Kek6 LoF Activity	0.6048
												Control Activity vs. Kek6 LoF	0.0125
			Kek6 KO (D42>ReaChR, kek6[35]/kek6[34]) No Stim	9	12	Shapiro-Wilk	Normal	0.0958				Control Activity vs. Kek6 LoF Activity	0.0009
			Kek6 KO (D42>ReaChR, kek6[35]/kek6[34]) Stim	6	11	Shapiro-Wilk	Normal	0.6235				Kek6 LoF vs. Kek6 LoF Activity	0.6906
	E	nc82 volume / MSA*1000	Control (D42>ReaChR) No Stim	7	11	Shapiro-Wilk	Normal	0.5108	Ordinary one-way ANOVA	<0.0001	Tukey's	Control vs. Control Activity	0.0066
												Control vs. Kek6 LoF	0.7766
			Control (D42>ReaChR) Stim	7	12	Shapiro-Wilk	Normal	0.798				Control vs. Kek6 LoF Activity	0.4741
												Control Activity vs. Kek6 LoF	0.0003
			Kek6 KO (D42>ReaChR, kek6[35]/kek6[34]) No Stim	9	12	Shapiro-Wilk	Normal	0.2844				Control Activity vs. Kek6 LoF Activity	<0.0001

			Kek6 KO (D42>ReaChR, kek6[35]/kek6[34]) Stim	6	11	Shapiro-Wilk	Normal	0.1106				Kek6 LoF vs. Kek6 LoF Activity	0.9433
	B	Mature bouton number / MSA*1000	Control (D42>ReaChR) No Stim	4	8	Shapiro-Wilk	Normal	0.1471	Ordinary one-way ANOVA	0.0005	Tukey's	Control No Activity vs. Control Activity	0.03
												Control No Activity vs. Kek6 LoF No Activity	0.0068
			Control (D42>ReaChR) Stim	9	11	Shapiro-Wilk	Normal	0.3543				Control No Activity vs. Kek6 LoF Activity	0.0002
												Control Activity vs. Kek6 LoF No Activity	0.8989
			Kek6 KO (D42>ReaChR, kek6[35]/kek6[34]) No Stim	12	18	Shapiro-Wilk	Normal	0.078				Control Activity vs. Kek6 LoF Activity	0.238
			Kek6 KO (D42>ReaChR, kek6[35]/kek6[34]) Stim	7	12	Shapiro-Wilk	Normal	0.122				Kek6 LoF No Activity vs. Kek6 LoF Activity	0.6426
			Control (D42>ReaChR) No Stim	4	8	Shapiro-Wilk	Not Normal	<0.0001					

5.14	C	Ghost bouton number / MSA*1000	Control (D42>ReaChR) Stim	9	11	Shapiro-Wilk	Not Normal	0.0005	Kruskal-Wallis				
			Kek6 KO (D42>ReaChR, kek6[35]/kek6[34]) No Stim	5	18	Shapiro-Wilk	Not Normal	0.0003					
			Kek6 KO (D42>ReaChR, kek6[35]/kek6[34]) Stim	7	12	Shapiro-Wilk	Not Normal	0.0055					
				Larvae	Boutons								
	D	Bouton Area (um^2)	Control (D42>ReaChR) No Stim	4	57	Shapiro-Wilk	Not Normal	0.0003	Kruskal-Wallis	0.0202	Dunn's	Control No Activity vs. Control Activity	0.7844
												Control No Activity vs. Kek6 LoF No Activity	>0.9999
			Control (D42>ReaChR) Stim	9	114	Shapiro-Wilk	Not Normal	<0.0001				Control No Activity vs. Kek6 LoF Activity	>0.9999
												Control Activity vs. Kek6 LoF No Activity	0.0854
			Kek6 KO (D42>ReaChR, kek6[35]/kek6[34]) No Stim	5	88	Shapiro-Wilk	Not Normal	<0.0001				Control Activity vs. Kek6 LoF Activity	0.0228

			Kek6 KO (D42>ReaChR, kek6[35]/kek6[34]) Stim	7	102	Shapiro-Wilk	Not Normal	0.0003				Kek6 LoF No Activity vs. Kek6 LoF Activity	>0.9999